Technical University of Crete
School of Chemical and Environmental Engineering

Lab of Biochemical Engineering & Environmental Biotechnology

HELLENIC REPUBLIC
National and Kapodistrian University of Athens
EST. 1837

Technical University of Crete

School of Chemical and Environmental Engineering

Biochemical Engineering and Environmental Biotechnology Laboratory

Oxygen-Nanobubble Biotechnology To Enhance Physiologic Wound Healing and Tissue Regeneration *in Vivo*

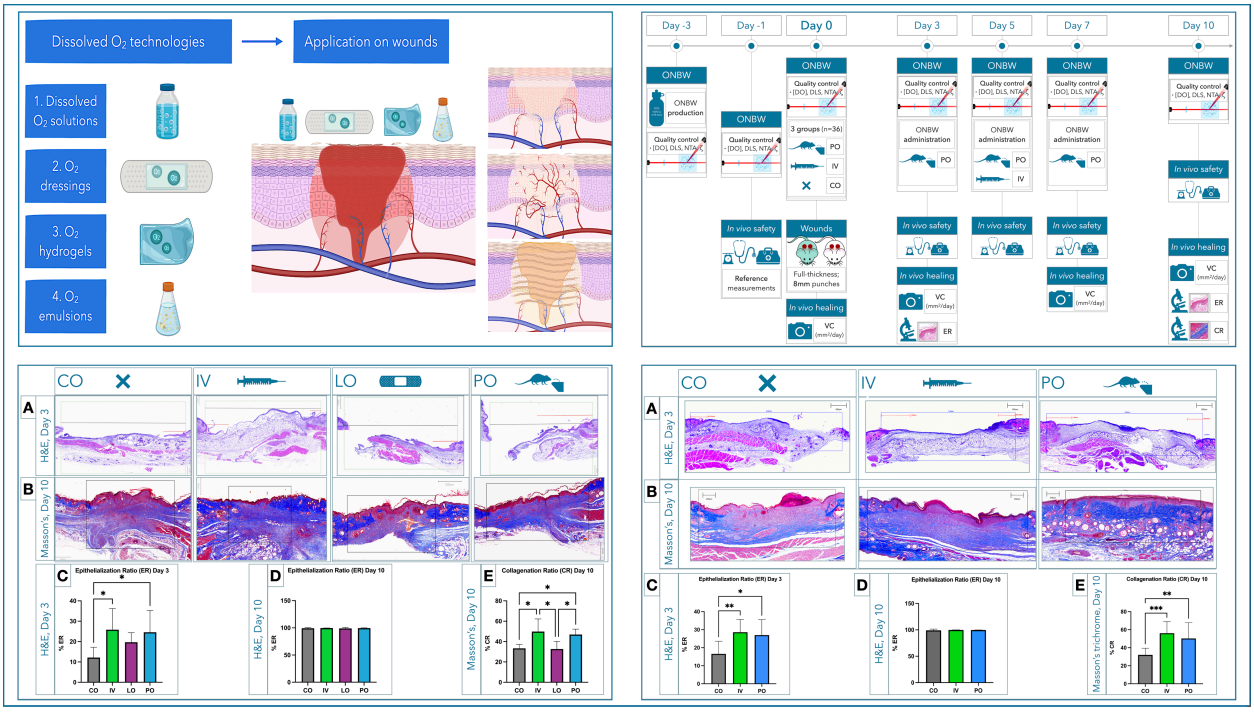

Dimitrios Ntentakis

Doctor of Medicine, MD

October 2024

Oxygen-Nanobubble Biotechnology To Enhance Physiologic Wound Healing and Tissue Regeneration *in Vivo*

Βιοτεχνολογία Νανοφυσαλίδων Οξυγόνου Για Την Ενίσχυση Του Μηχανισμού Επούλωσης Τραυμάτων Και Ιστικής Αναγέννησης *In Vivo*

This research received financial support by the Hellenic Foundation for Research and Innovation (H.F.R.I.), under the 2nd call of the H.F.R.I. in support of PhD candidates (Grant No 940), and by the GSRI's ERA-MIN2 project "nanoBT".

School of Chemical and Environmental Engineering

Technical University of Crete, Chania, Greece

Examination committee

Nicolas Kalogerakis (Supervisor)

Professor Emeritus
School of Chemical and Environmental Engineering
Technical University of Crete, Chania, Greece

Nikolaos Arkadopoulos (Advisory Committee)

Professor
Department of Medicine, School of Health Sciences
National and Kapodistrian University of Athens, Athens, Greece

Danae Venieri (Advisory Committee)

Professor
School of Chemical and Environmental Engineering
Technical University of Crete, Chania, Greece

Tryfon Daras

Associate Professor
School of Chemical and Environmental Engineering
Technical University of Crete, Chania, Greece

Michail Fountoulakis

Associate Professor
School of Chemical and Environmental Engineering
Technical University of Crete, Chania, Greece

Mihalis Lazaridis

Professor

School of Chemical and Environmental Engineering

Technical University of Crete, Chania, Greece

Vanessa Mitsialis

Instructor

Harvard Medical School

Harvard University, Boston, Massachusetts, United States of America

Acknowledgments

There are many people who have helped me during this journey, and to whom I owe my deepest gratitude and recognition. First, I would like to thank my supervisor Dr. Nicolas Kalogerakis, for his tutoring, mentorship, unwavering support of my progress, and for believing in me as a person, and in my ideas at every step of this journey. Even though I had no background as an engineer, he trusted me with this Ph.D. opportunity, and has always been willing to share his experience, immense knowledge, as well as his thought process; which, for me, have been priceless. Also, I would like to extend my gratitude to the other two members of my Dissertation Advisory Committee, Dr. Danae Venieri and Dr. Nikolaos Arkadopoulos. With her multidimensional background and deep knowledge in topics related to biology and medicine, our discussions with Dr. Venieri have always been inspiring and insightful, not only from a research perspective but also in topics related to education, productivity, and academic affairs. This has also been the case with Dr. Arkadopoulos, whom I have had the pleasure of knowing since Medical School. His constructive feedback has been instrumental in overcoming key obstacles I encountered during my Ph.D., while his optimism and perseverance have always been a point of reference in my professional life. Moreover, I would like to thank the other members of my examination committee, Dr. Michail Fountoulakis, Dr. Tryfon Daras, Dr. Mihalis Lazaridis, and Dr. Vanessa Mitsialis, for their willingness to evaluate this dissertation despite their demanding schedules.

Also, I would like to thank all the great teachers, professors, and mentors whom I have been lucky to have met and learn from, throughout my life; because they have all contributed to where I am today. From the Technical University of Crete, I would like to wholeheartedly acknowledge Dr. Tryfon Daras, for being the exceptional teacher and human being that he is, and for making me rediscover my passion for mathematics and data analysis. From my time as a medical student, I feel deeply grateful to have worked with the world-renowned pioneer in robotic surgery Dr. Konstantinos M. Konstantinidis, and for the outstanding achievements and beautiful life memories we shared together. Among other things, Dr. Konstantinidis taught me to think out of the box as a doctor, to not hesitate to deviate from the majority, and to carve my own path in the quest for true innovation; therefore, my interaction with him has been instrumental in my decision to pursue my Ph.D. studies at an engineering school.

Furthermore, I would like to thank the people I have worked with the most during these years. First, I am wholeheartedly grateful to Dr. Petroula Seridou, currently a postdoctoral researcher at the Technical University of Crete, for her astonishing work, amazing personality, and our excellent collaboration. Her engineering background and skills have been pivotal for the successful execution of my Ph.D. research, while her scientific integrity and commendable dedication make her an ideal colleague. Also, the technical assistant from our laboratory, Ariadne Pantidou, whose positive perspective and hard work makes everything possible for all of us, daily. Moreover, my colleague and friend, Dr. Georgina Calypso Kalogerakis, for encouraging me to proceed with this Ph.D. from the beginning, and for supporting me with her insightful feedback and kind advice ever since. Meanwhile, I would like to underline the contributions of Dr. Dimitrios Kletsas, Dr. Lykourgos Klamarias, Ioannis Zafiropoulos, and Georgios Doulgeridis, to the execution of our *in vivo* experiments at the National Center for Scientific Research "Demokritos"; and particularly, Zoe Kollia, an exceptional animal technician and character, whose input and skills have been invaluable throughout my experiments.

Last but not least, I would like to extend my gratitude to the significant people in my personal life. My parents, Panagiotis and Konstantina, to whom I owe everything and who deserve every praise for my upbringing and accomplishments. The true friends that life has blessed me with, and who, regardless of the geographic distance, continue to be a huge part of my life. My beloved wife, Eleni, for her unwavering encouragement, commitment, and intellectual insights, as well as our baby daughter, Elina, for adding a new, meaningful purpose in our lives. Ms. Aspasia, for emerging as the grandmother I never had. My sister, Anastasia Maria, who has been voluntarily working with me with remarkable dedication and efficacy throughout my Ph.D. journey, and is, now, preparing to pursue a Ph.D. of her own at the Technical University of Crete, to expand our research in animal models simulating human diseases; to put it simply, no brother ever had a better sister. Finally, this dissertation is dedicated to the memory of my grandfather, Dimitrios Melakis (Melas); a courageous and authentic Cretan, who has been my greatest role model and source of inspiration in this world.

Oxygen-nanobubble biotechnology to enhance physiologic wound healing and tissue regeneration *in vivo*

Abstract

Physiologically, the healing mechanism operates as an orchestrated continuum of molecular responses, organized in 4 stages: 1) hemostasis, 2) acute inflammation, 3) tissue proliferation, and 4) remodeling. There is evidence indicating that, disruptions in the most upstream biological pathways in this continuum of normal healing, are strong prognosticators of downstream wound chronicity and pertinent complications. Clinical and epidemiological interest in wound healing is increasing on a global scale, due to a combination of the following factors: the rising prevalence in systemic vasculopathies predisposing to peripheral ischemia, tissue hypoxia, and suboptimal healing, such as diabetes mellitus, the aging world population, and the questionable capacity of the available management and prevention strategies to confront a potentially generalized surge in complicated wounds.

Administration of gaseous oxygen (O_2) has consistently demonstrated beneficial outcomes in cutaneous wounds, reflecting the pivotal role of O_2 in physiologic healing. A characteristic example is hyperbaric O_2 therapy, which has become an established management strategy for diabetic wounds, alongside multiple clinical indications. Yet, an important limitation lies in the short-lived efficacy of O_2 when administered in its gaseous form, as a result of passive diffusion through biological tissues in response to local O_2 pressure gradients. Thereby, technologies supplying dissolved oxygen (DO) within aqueous solutions, namely DO solutions (DOS), are currently investigated as a novel approach to enhancing wound oxygenation. By enabling O_2 to become gradually bioavailable in the liquid medium, a DOS can theoretically supply high oxygen amounts for longer periods compared to gas-based O_2 therapies. However, sustaining DO levels without using potentially toxic artificial surfactants and complex chemical additives, remains one of the biggest challenges in the field.

The research described herein, aims to document the capacity to manufacture a DOS by exclusively leveraging the physics of the gas-liquid interphase, in the absence of chemical surfactants or additives, and to incorporate the cutting-edge technology of

O_2 nanobubbles in formulations that are suitable for biomedical applications in wound healing and cutaneous regeneration. First, we conduct a comprehensive analysis of the existing technologies that can be used for supplying DO to healing tissues, with the aim to identify the most promising technological category for further investigation. Via a systematic co-evaluation of engineering principles, oxygenating effects, biomechanics of DO delivery, safety parameters, and healing-related efficacy for all technologies, we highlight the benefits of using a DOS containing no exogenous chemicals, and discuss the potential of O_2 nanobubble technology in this approach. Concurrently, we introduce an original classification system for the DO technologies tested in healing applications.

Then, we discuss the design, scientific rationale, and implementation of a novel *in vivo* protocol, aiming to facilitate the clinical translation of biotechnologies developed for healing applications, such as DO-supplying therapies. By simulating the design of early-stage clinical trials, and incorporating standardized methodological components from previous protocols, we enable a holistic examination of engineering fundamentals, quality-control requirements, biological safety, and a preliminary assessment of healing efficacy for new biotechnologies in the field. Of note, the experimental manipulations in the proposed protocol have been selected to maximize simplicity and reproducibility; to account for the fact that, a growing number of relevant research projects are carried out primarily by biochemical and biomedical engineers nowadays.

Next, we implement the aforementioned *in vivo* protocol to study a “plain” DOS containing no physical enhancements to sustain DO delivery, which was manufactured via infusion of high-purity (>99.9%) O_2 into sterile normal saline (N/S; 0.9% NaCl) under predetermined conditions, without chemical additives. Our aim is the collection of preliminary data on the *in vivo* administration of a DOS with the aforementioned characteristics, including the magnitude and sustainability of DO levels in the final formulation, the best routes of administration, optimal dosing parameters, biological safety, and healing outcomes in full-thickness excisional wounds on healthy SKH1 mice. Our findings suggest that the plain DOS can deliver high DO concentrations consistently and sustainably for at least 14 days, while being safe for *in vivo* administration intravenously, locally, and *per os*. Also, we show a promising effect of intravenous and *per os* administration of plain DOS in physiologic wound healing, macroscopically and histopathologically.

Finally, we implement the proposed *in vivo* protocol to evaluate a DOS manufactured by employing the cutting-edge technology of O_2 nanobubbles, while also eschewing the use of exogenous chemicals; which we refer to as oxygen nanobubble-enriched water solution (ONBW). Our findings show that the ONBW maintains high DO concentrations throughout a 14-day evaluation period, and is completely safe *in vivo* for systemic administration, either intravenously or *per os*. Furthermore, by monitoring full-thickness excisional wounds on healthy SKH1 mice, we extend our observations to show that, independently, two intravenous injections and *per os* intake of the ONBW can accelerate wound closure macroscopically, and improve epithelial regeneration and collagen deposition histopathologically.

Βιοτεχνολογία νανοφυσαλίδων οξυγόνου για την ενίσχυση του μηχανισμού επούλωσης τραυμάτων και ιστικής αναγέννησης *in vivo*

Περίληψη

Κατά τη φυσιολογία, ο μηχανισμός επούλωσης τραυμάτων λειτουργεί ως ένα καλά ενορχηστρωμένο και συνεχές μονοπάτι κυτταρικών αντιδράσεων, το οποίο διαρθρώνεται σε 4 στάδια: 1) αιμόσταση, 2) οξεία φλεγμονή, 3) ιστικός πολλαπλασιασμός και 4) ιστική αναδιαμόρφωση. Μάλιστα, υπάρχουν επιστημονικά δεδομένα τα οποία υποδεικνύουν ότι, διαταραχές στις βιολογικές οδούς που εξελίσσονται στα πιο πρώιμα στάδια αυτού του συνεχούς μονοπατιού της φυσιολογικής επούλωσης, αποτελούν ισχυρούς προγνωστικούς παράγοντες για κλινική επιδείνωση σε επιπλεγμένη επούλωση και χρόνια τραύματα. Ταυτόχρονα, το κλινικό και επιδημιολογικό ενδιαφέρον με επίκεντρο την επούλωση τραυμάτων εκτοξεύεται παγκοσμίως, λόγω του συνδυασμού των ακόλουθων παραγόντων: της αυξανόμενης επίπτωσης συστηματικών αγγειοπαθειών που προδιαθέτουν σε περιφερική ισχαιμία, ιστική υποξία και προβληματική επούλωση, όπως ο σακχαρώδης διαβήτης, της γήρανσης του παγκόσμιου πληθυσμού και της αμφίβολης ικανότητας των διαθέσιμων θεραπευτικών επιλογών να αντιμετωπίσουν μια ολοένα και πιθανότερη, γενικευμένη έξαρση των επιλεγμένων τραυμάτων.

Η χορήγηση οξυγόνου σε αέρια μορφή (O_2), έχει αποδειχθεί συστηματικά ότι οδηγεί σε ευεργετικά αποτελέσματα σε δερματικά τραύματα, αντικατοπτρίζοντας τον κεντρικό ρόλο του O_2 στη φυσιολογική επούλωση. Το πλέον χαρακτηριστικό παράδειγμα είναι η θεραπεία με υπερβαρικό O_2, η οποία έχει καθιερωθεί μεταξύ των αποτελεσματικότερων στρατηγικών αντιμετώπισης για τα διαβητικά τραύματα, καθώς επίσης και σε πολλές άλλες κλινικές ενδείξεις. Ωστόσο, ένας σημαντικός περιορισμός έγκειται στη βραχύβια αποτελεσματικότητα του O_2 όταν χορηγείται σε αέρια μορφή, ως αποτέλεσμα της παθητικής διάχυσης διαμέσου των βιολογικών ιστών σε συνάρτηση με τις κατά τόπους βαθμιδώσεις στη μερική πίεση του O_2. Στο πλαίσιο αυτό, νεότερες τεχνολογίες με τη δυνατότητα να παρέχουν διαλυμένο οξυγόνο (Dissolved O_2, DO) μέσα σε υδατικά διαλύματα, γνωστά ως διαλύματα διαλυμένου οξυγόνου (Dissolved O_2 solutions, DOS), διερευνώνται ως μια καινοτόμος τεχνολογική προσέγγιση για τη

βελτιστοποίηση των θεραπειών οξυγόνωσης των τραυμάτων. Πράγματι, επιτρέποντας στο O_2 να καθίσταται σταδιακά βιοδιαθέσιμο μέσα στο υδάτινο μέσο, ένα διάλυμα DOS μπορεί, θεωρητικά, να παρέχει υψηλές ποσότητες οξυγόνου για μεγαλύτερο χρονικό διάστημα σε σύγκριση με τις θεραπείες που χορηγούν O_2 στην αέρια φάση. Ωστόσο, η μακρόχρονη διατήρηση υψηλών επιπέδων DO χωρίς τη χρήση δυνητικά τοξικών επιφανειοδραστικών παραγόντων και πολύπλοκων χημικών ενώσεων, παραμένει μία από τις μεγαλύτερες προκλήσεις στο συγκεκριμένο επιστημονικό πεδίο.

Η έρευνα που εκπονείται στην παρούσα διδακτορική διατριβή, μελετά τη δυνατότητα παραγωγής ενός διαλύματος DOS αξιοποιώντας αποκλειστικά τις αρχές της Φυσικής που διέπουν την αλληλεπίδραση μεταξύ υγρών και αερίων, χωρίς τη χρήση χημικών επιφανειοδραστικών παραγόντων ή άλλων προσθέτων, καθώς και την αξιοποίηση της τεχνολογίας αιχμής των νανοφυσαλίδων O_2 σε βιοϊατρικές εφαρμογές για την επούλωση τραυμάτων και την αναγέννηση δερματικού ιστού. Αρχικά, διεξάγουμε μια ενδελεχή ανάλυση των διαθέσιμων τεχνολογιών με τη δυνατότητα να χρησιμοποιηθούν για παροχή DO σε ιστούς που επουλώνονται, στοχεύοντας στην ανάδειξη της πλέον υποσχόμενης τεχνολογικής κατηγορίας προς περαιτέρω διερεύνηση. Μέσω συστηματικής συναξιολόγησης του μηχανικού υπόβαθρου, του δυναμικού οξυγόνωσης, των μηχανισμών παροχής DO στου ιστούς, των παραμέτρων ασφαλείας και της αποτελεσματικότητας ως προς την αναγέννηση δερματικού ιστού για όλες τις τεχνολογίες, αναδεικνύουμε τα συγκριτικά πλεονεκτήματα της χρήσης διαλυμάτων DOS που παρασκευάζονται χωρίς χημικά πρόσθετα, και υπογραμμίζουμε τις δυνατότητες της τεχνολογίας νανοφυσαλίδων O_2 στη συγκεκριμένη τεχνολογική κατηγορία. Παράλληλα, εισάγουμε ένα πρωτότυπο σύστημα ταξινόμησης για τις τεχνολογίες DO που μελετώνται σε εφαρμογές σχετικές με την επούλωση τραυμάτων.

Στη συνέχεια, παρουσιάζουμε τον ερευνητικό σχεδιασμό, την επιστημονική τεκμηρίωση και την πρακτική εφαρμογή ενός νέου *in vivo* πρωτοκόλλου, που αποσκοπεί στην επιτάχυνση της ανάπτυξης νέων βιοτεχνολογιών στον τομέα της επούλωσης τραυμάτων, όπως οι τεχνολογίες παροχής DO, και της ενσωμάτωσής τους στην κλινική πράξη. Προσομοιάζοντας το σχεδιασμό κλινικών δοκιμών αρχικού σταδίου, και ενσωματώνοντας εγκεκριμένες μεθοδολογίες από προηγούμενα πρωτόκολλα, το προτεινόμενο πρωτόκολλο παρέχει ένα λεπτομερή οδηγό για την ολιστική αξιολόγηση των βασικών αρχών μηχανικής, των απαιτούμενων ελέγχων ποιότητας, της βιολογικής

ασφάλειας και της θεραπευτικής αποτελεσματικότητας στην επούλωση τραυμάτων για όλες τις νέες βιοτεχνολογίες που αναπτύσσονται στο συγκεκριμένο τομέα. Σημειώνεται ότι, οι πειραματικοί χειρισμοί στο προτεινόμενο πρωτόκολλο έχουν επιλεγεί με γνώμονα την απλότητα και τη βέλτιστη επαναληψιμότητα, λαμβάνοντας υπόψιν και το γεγονός ότι, στην εποχή μας, ολοένα και αυξάνονται τα ερευνητικά έργα στο συγκεκριμένο πεδίο τα οποία εκτελούνται στο μεγαλύτερο ποσοστό τους από βιοχημικούς και βιοϊατρικούς μηχανικούς.

Στη συνέχεια, εφαρμόζουμε το προαναφερόμενο *in vivo* πρωτόκολλο για να μελετήσουμε ένα «απλό» διάλυμα DOS (plain DOS), το οποίο δεν περιέχει κανένα παράγοντα ικανό να ενισχύσει τα επίπεδα DO ούτε με χημικά πρόσθετα, αλλά ούτε και με φυσικό τρόπο. Το διάλυμα αυτό παρασκευάζεται μέσω έγχυσης O_2 υψηλής καθαρότητας (>99,9%) σε αποστειρωμένο διάλυμα φυσιολογικού ορού (0.9% NaCl), υπό προκαθορισμένες συνθήκες. Στόχος μας είναι η συλλογή προκαταρκτικών *in vivo* δεδομένων σχετικά με τη χορήγηση ενός διαλύματος DOS με τα προαναφερθέντα χαρακτηριστικά, συμπεριλαμβανομένου του μεγέθους και του χρόνου παραμονής των επιπέδων DO στο προκύπτον διάλυμα, των βέλτιστων οδών χορήγησης, των παραμέτρων δοσολογίας, της βιολογικής ασφάλειας και της αποτελεσματικότητας σε τραύματα πλήρους εκτομής σε υγιή ποντίκια SKH1. Τα ευρήματά μας υποδεικνύουν ότι το διάλυμα plain DOS μπορεί να παρέχει υψηλές συγκεντρώσεις DO συστηματικά, για τουλάχιστον 14 ημέρες, ενώ είναι ασφαλές για *in vivo* χορήγηση ενδοφλεβίως, τοπικά και από το στόμα. Επίσης, τα δεδομένα μας υποστηρίζουν ότι τόσο η ενδοφλέβια, όσο και η από του στόματος χορήγηση του διαλύματος plain DOS έχει πολλά υποσχόμενα αποτελέσματα ως προς την ενίσχυση της φυσιολογικής επούλωσης, μακροσκοπικά και ιστοπαθολογικά.

Τέλος, εφαρμόζουμε το προτεινόμενο *in vivo* πρωτόκολλο για να αξιολογήσουμε ένα διάλυμα DOS που παρασκευάστηκε αξιοποιώντας την τεχνολογία αιχμής των νανοφυσαλίδων O_2, αποφεύγοντας ταυτόχρονα τη χρήση εξωγενών χημικών ουσιών, το οποίο αναφέρουμε ως “διάλυμα εμπλουτισμένο με νανοφυσαλίδες O_2” (O_2 nanobubble-enriched water, ONBW). Τα ευρήματά μας αποδεικνύουν ότι το διάλυμα ONBW διατηρεί υψηλές συγκεντρώσεις DO καθ' όλη τη διάρκεια της περιόδου αξιολόγησης των 14 ημερών, ενώ είναι απόλυτα ασφαλές για συστηματική χορήγηση *in vivo*, είτε ενδοφλεβίως είτε από το στόμα. Επιπλέον, μελετώντας τραύματα πλήρους

δερματικής εκτομής σε υγιή ποντίκια SKH1, επεκτείνουμε τις παρατηρήσεις μας δείχνοντας ότι, ανεξάρτητη χορήγηση με δύο ενδοφλέβιες ενέσεις ή με από του στόματος λήψη του διαλύματος ONBW, μπορεί να επιταχύνει τη μακροσκοπική σύγκλειση των τραυμάτων και να βελτιώσει την επιθηλιακή αναγέννηση και την εναπόθεση κολλαγόνου ιστοπαθολογικά.

Table of Contents

List of Figures

List of Tables

List of Abbreviations

Abbreviation	Definition
AEs	Adverse events (severe)
ANOVA	Analysis of variance
CO	Controls (negative controls)
CR	Collagenation ratio
DFP	Decafluoropentane
DLS	Dynamic light scattering
DM	Diabetes mellitus
DO	Dissolved oxygen
DOS	Dissolved oxygen solutions
ECMO	Extracorporeal membranous oxygenation
ER	Epithelialization ratio
H&E	Hematoxylin and eosin staining
H_2O_2	Hydrogen peroxide
HBOT	Hyperbaric oxygen therapy
IP	Intraperitoneally
IQR	Interquartile range
IV	Intravenous administration
LO	Local administration
MACF	Methacrylamide chitosan modified with perfluorocarbon chains
N/A	Not applicable
N/S	Normal saline (0.9% NaCl)
NADPH	Nicotinamide adenine dinucleotide phosphate
NTA	Nanoparticle tracking analysis
O_2	Oxygen (in gaseous form)
OLNDs	O_2-loaded nanodroplets
OMBs	Oxygen micro-bubbles
ONBW	Oxygen nanobubble-enriched water

Abbreviation	Definition
OUBs	Oxygen ultra-fine bubbles
OUPs	O_2-loaded ultra-fine particles
OWS_x	Open wound surface at a time-point x
pDOS	Plain dissolved oxygen solution
PFCs	Perfluorocarbons
PFP	Perfluoropentane
PO	Per os intake
PO_2	Partial pressure of oxygen
PRN	Per needed
ROS	Reactive oxygen species
SD	Standard deviation
VC	Velocity of wound closure (mm^2/days)
VEGF	Vascular endothelial growth factor

1 | Introduction

1.1 | Overview of the healing mechanism

The healing mechanism, alternately referred to as the “healing response”, “healing process”, or “healing cascade” in the literature, represents a constellation of molecular pathways whose orchestrated function enables multicellular organisms to repair tissues having undergone trauma, typically as a consequence of an acute insult [Gurtner et al., 2008]. It is noteworthy that, evolutionarily, this particular ability of multicellular organisms has been highly conserved, with only minor, sporadic variations among the different phyla that typically stem from histologic differences. Although currently, the aforementioned terms are typically used to describe cutaneous wound healing, it warrants emphasis that the individual pathways involved, as well as the stages comprising the healing mechanism, are universally encountered across immunologic responses and human diseases; thus, expanding the biomedical and clinical significance of this mechanism beyond skin disruptions and superficial wounds. Nevertheless, to remain consistent with the literature in the field, the following paragraphs delve further into the healing mechanism by adhering to the example of cutaneous wounds.

Physiologically, the healing mechanism can be divided in 4 sequential stages or phases: 1) hemostasis, 2) acute inflammation, 3) tissue proliferation, and 4) tissue remodeling [Singer and Clark, 1999; Schreml et al., 2010; Rodrigues et al., 2019]. Hemostasis is regarded, by some researchers, as part of the acute inflammatory response; regardless, both these stages are considered to begin immediately post-wounding [Singer and Clark, 1999; Gurtner et al., 2008]. Incoming platelets, which are recruited via the activation of the coagulation cascade during hemostasis, contribute to the successful initiation of the healing mechanism not only by minimizing blood loss and microorganism invasion, but also by also secreting chemotactic factors and molecular mediators for the subsequent healing stages [Singer and Clark, 1999; Gurtner et al., 2008]. During acute inflammation, which is considered to extend until day 3 post-wounding [Figure 1.1], the predominant cellular type is the neutrophil. Neutrophils are indispensable for removing any invading microorganisms and foreign bodies, while stimulating phagocytosis [Dahlgren and Karlsson, 1999; Kurahashi and Fujii, 2015]. In turn, effective phagocytosis entails the cornerstone of normal wound

healing, as it coordinates both the associated immune responses and the subsequent tissue formation and regeneration [Dahlgren and Karlsson, 1999].

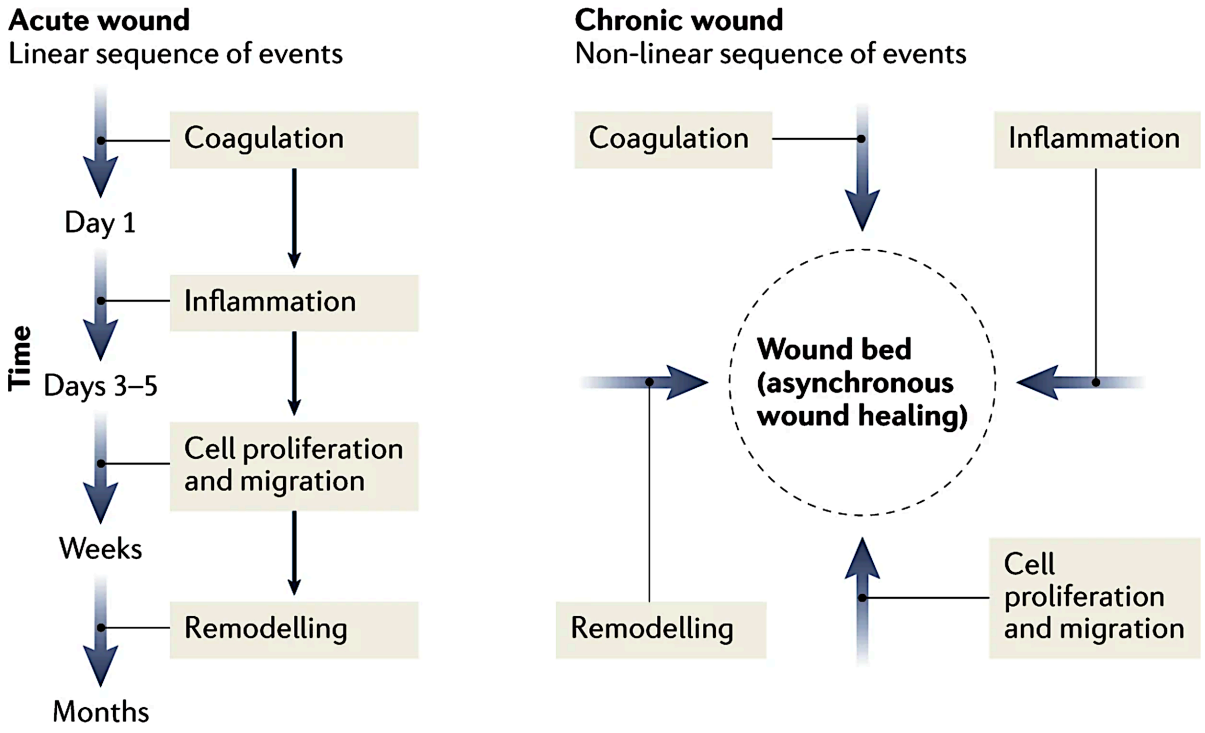

Figure 1.1: Overview of wound healing progression in acute versus chronic wounds. Illustrative comparison of healing processes in acute versus chronic wounds. Acute wounds follow a linear sequence of the recognized healing stages (left), while chronic wounds (right) experience irregular progression, with phases occurring unpredictably and lacking a defined timeline. Different sections of a chronic wound may be in distinct stages of healing simultaneously, complicating treatment as varying parts may require different or individualized therapeutic strategies. Adapted from *Falanga et al., 2022.* All rights reserved.

New tissue formation, or proliferation, is the third stage in the healing mechanism, starting approximately between days 2 and 3 post-wounding with an estimated total duration of 10 days [Gurtner et al., 2008; Falanga et al., 2022]. In cutaneous wounds, the proliferative stage involves the following biological processes: 1) re-epithelialization of the wound bed, subsequently to the migration of keratinocytes across the damaged dermis and their gradual maturation, 2) angiogenesis, to replace any damaged blood vessels and increase blood flow and nutrients to the area of tissue damage, 3) granulation tissue formation by macrophages and migrating fibroblasts, and 4) collagen synthesis by fibroblasts and myofibroblasts, which will serve as the foundation of the permanent scar [Opalenik and Davidson, 2005; Werner et al., 2007].

Ultimately, the stage of tissue remodeling begins, approximately two to three weeks post-wounding, while its total duration may exceed 12 months. In this stage, the previously-activated pathways gradually subside; for instance, vascular endothelial cells, macrophages, and myofibroblasts undergo apoptosis or migrate outside the wound bed, leaving an acellular matrix abundant with temporary (type III) collagen and extracellular-matrix proteins [Singer and Clark, 1999; Gurtner et al., 2008]. The remodeling of temporary (type III) collagen to type I collagen also occurs during this stage, catalyzed by matrix metalloproteinases [Lovvorn et al., 1999].

A pictorial overview of the aforementioned stages of the healing mechanism is presented in Figure 1.2. It should be pointed out that, in the absence of additional stressors or risk factors with the capacity to compromise tissue repair, these stages progress in a synchronized and well-organized sequence, with a degree of dynamic overlapping, as illustrated in Figure 1.1 [Singer and Clark, 1999; Rodrigues et al., 2019; Falanga et al., 2022]. Figure 1.1 also schematizes the linear and orderly healing response as expected in uncomplicated, acute wounds, in contrast to the disorganized natural history of complicated, chronic wounds. Of note, in the previous decades, the majority of our understanding of the healing stages and the significance of individual pathways, such as acute inflammation, was based on the interpretation of experimental data from rodents. Yet lately, with the evolution of advanced sequencing technologies, newer studies have corroborated the key components of our conceptualization of the healing mechanism, while strengthening our knowledge into the specific pathways and molecular mechanisms involved in each stage [Falanga et al., 2022].

Additionally, there are two, potentially overlooked, characteristics of the healing mechanism that warrant acknowledgement, due to their clinical relevance. Interestingly, the majority of molecular pathways implicated in the healing mechanism are associated with innate immunity; which is the primary, non-specific, and evolutionally primitive part of the immune system, functioning as the first line of defense against tissue trauma and invading pathogens. The most illustrative example is the stage of acute inflammation, one of the earliest responses activated in the healing mechanism [MacLeod and Mansbridge, 2016]. In humans, acute inflammation is activated upon first encounter with an external stressor or via the initial manifestation of an internal pathology, with the aim to contain the primary insult while allowing the organism enough time to

orchestrate an antigen-specific response, which is part of the more evolutionally-advanced, adaptive immunity [Arenas Gómez et al., 2020; Weavers and Martin, 2020].

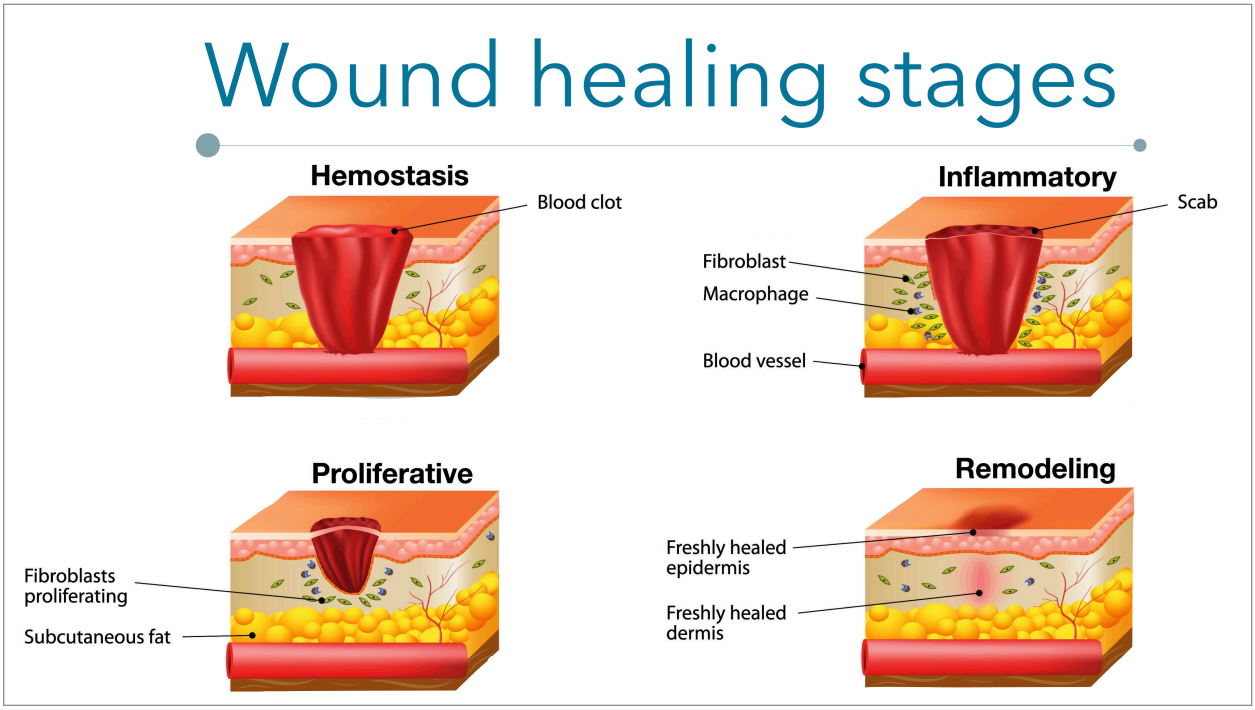

Figure 1.2: Synoptic overview of the stages of normal wound healing: Of note, the four stages/phases of the healing mechanism in eukaryotes, as illustrated on this schematic, are evolutionarily preserved across multicellular organisms.

The multifaceted role of acute inflammation in the healing mechanism, and the importance of its successful completion to the ultimate healing outcome, is summarized in Figure 1.3. Despite its upstream position in the linearly-organized pathway of normal healing, a failure during the acute inflammatory stage will impede progression towards tissue proliferation and remodeling, which, in turn, predisposes to chronicity of both the inflammatory response, and the wound itself. This aligns with the argument of some investigators in the field, supporting that upstream abnormalities in the earliest healing stages are the most crucial prognosticators of subsequent wound complications and chronicity [Fowler, 1990; Singh et al., 2004]. Importantly, beyond cutaneous wounds, a chronic and unresolved inflammatory response can be identified as the primary pathology of multiple human diseases, particularly as the main pathway preceding tissue degeneration and, eventually, atrophy.

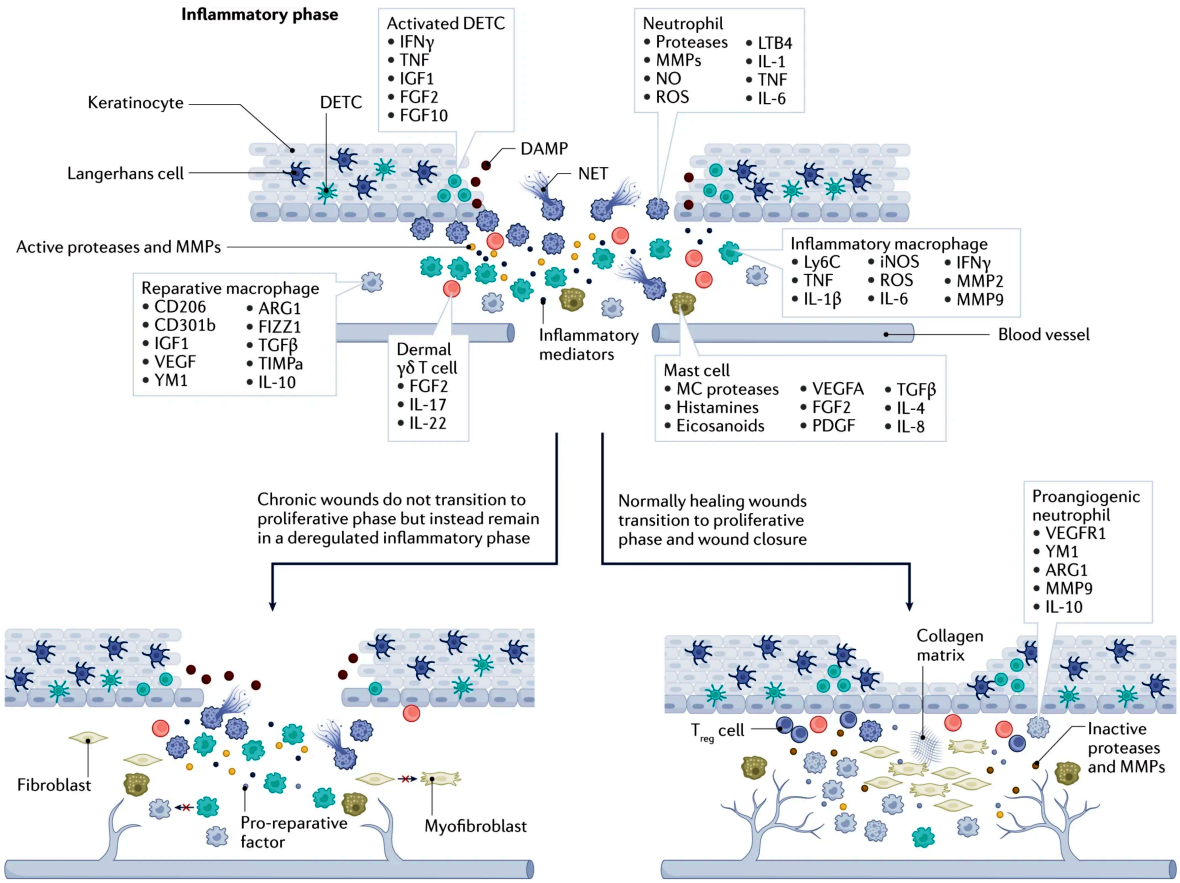

Figure 1.3: Inflammatory response in normal and chronic wound healing. In normal wound healing, the inflammatory phase transitions smoothly into the proliferative phase, characterized by immune cells shifting toward anti-inflammatory and tissue-repair functions (bottom right panel). In contrast, chronic wounds exhibit a prolonged inflammatory phase, where local inflammation persists uncontrolled, preventing progression to tissue repair and leaving the wound stuck in a disordered healing process (bottom left panel). **Abbreviations**: DAMP, damage-associated molecular pattern; DETC, dendritic epidermal T cell; MC, mastcell; MMP, matrix metalloproteinase; NET, neutrophil extracellular trap; NO, nitric oxide; ROS, reactive oxygen species; T_{reg} cell, regulatory T cell. Adapted from *Falanga et al., 2022.* All rights reserved.

The second noteworthy characteristic of the healing mechanism, is that it has been highly conserved across multicellular organisms, evolutionarily. Even in sponges, simple organisms not consisting of a body axis, multiple cell layers, or distinct tissues [Nichols et al., 2006], it has been shown that soluble mediators contributing to mammalian healing, such as transforming growth factor-β (TGF-β), regulate the three-dimensional orientation of sponge cells as well [Adamska et al., 2007]; a process which, by definition, is required for successful migration and proliferation of cells contributing to the healing mechanism. Similarly, in *Drosophila melanogaster*, pivotal

morphological events that occur during development, such as dorsal closure and tracheal fusion [Woolner et al., 2005; Samakovlis et al., 1996], resemble not only the wound healing response found in the same insects [Wood et al., 2002], but also the equivalent mechanism in humans. In turn, amphibians such as salamanders, have been more extensively studied over the years, due to their closer evolutionary relationship with mammals along with their extraordinary capacity to entirely regenerate amputated limbs; the latter have been described to sprout from a characteristic mass of undifferentiated cells in these organisms, called blastema [Kumar et al., 2007]. Interestingly, while the healing response in mammals shares a lot of similarities with the amphibians, the mammalian tissue-regenerating potential is believed to have been sacrificed *in lieu* of the deposition of fibrous tissue. In studies evaluating spinal-cord injuries in mice, neuronal regeneration does occur in the beginning, though rapidly counteracted by the compensatory migration of glial cells at the injury site, and physically limited by the subsequent production and intercalation of scar tissue; instead, functional neuronal recovery is possible when scar formation is inhibited [Klapka and Müller, 2006; Stichel and Müller, 1998]. In theory, the evolutional advantage of scar tissue lies in enhancing mechanical stability by rapidly filling tissue gaps, while reducing the risk of potentially-fatal infections by invading microorganisms. Collectively, despite the differences in skin histology among the different phyla and species, schematically illustrated in Figure 1.4, the universality of the healing mechanism is a remarkable phenomenon which can, and will continue to, be leveraged in multidimensional topics of academic and biomedical interest.

1.2 | Role of oxygen in the wound healing mechanism

1.2.1 | Contributions of oxygen to the wound healing mechanism

At a molecular level, oxygen (O_2) has been documented to play a pivotal role in the majority of stages and molecular pathways contributing to normal wound healing. Of note, early in the acute inflammation stage, the rate-limiting enzyme of phagocytosis called nicotinamide adenine dinucleotide phosphate (NADPH) oxidase, uses molecular O_2 as its substrate in the following oxidation-reduction pathway, which yields reactive oxygen species (ROS):

$$\mathbf{NADPH + 2O_2 \leftrightarrow NADP^+ + 2O_2^- + H^+}$$

Specifically, the majority of ROS generated via the aforementioned reaction are converted to hydrogen peroxide (H_2O_2). A fraction of this H_2O_2 is directly utilized for the production of highly toxic hypochlorous anion ($HClO^-$) that contributes to phagocytosis. In turn, the remaining H_2O_2 acts as a molecular regulator in the subsequent process of angiogenesis; it also functions as a chemotactic mediator, attracting crucial biological substrates and cellular types that participate in the tissue proliferation and regeneration phases [Dahlgren and Karlsson, 1999; Kurahashi and Fujii, 2015]. A schematic overview of those chemical reactions, and their biological implications, is presented in Figure 1.5.

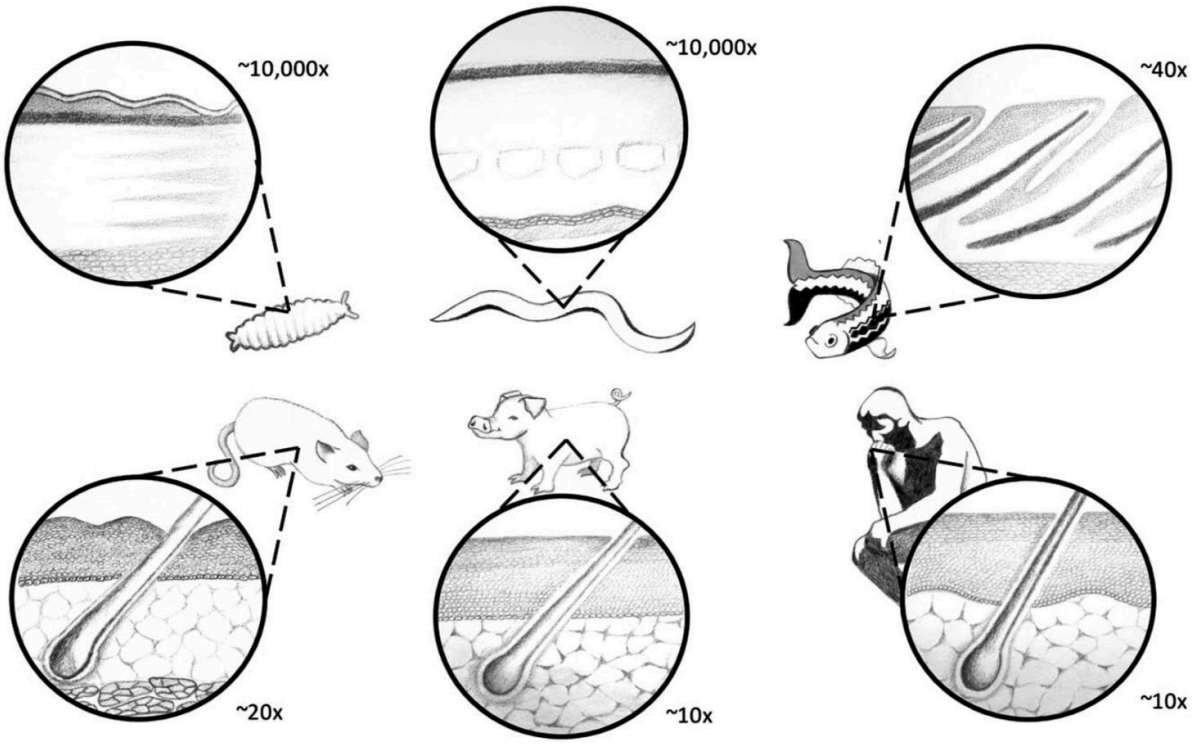

Figure 1.4: Skin histology in different animals used in wound healing research, versus human skin. *Drosophila melanogaster* larvae (above, left), *Caenorhabditis elegans* (above, center), zebrafish (above, right), mouse (below, left), pig (below, center), and human (below, right). Note that swine (pig) skin has the closest histologic resemblance to human skin. Adapted from *Boyko et al., 2017.* All rights reserved.

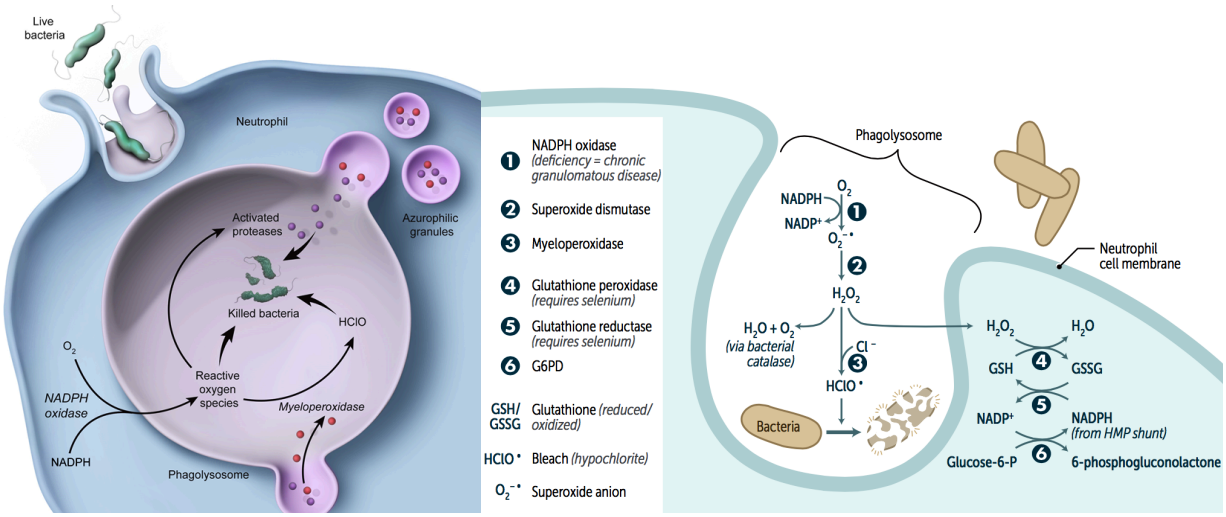

Figure 1.5: Role of oxygen in NADPH oxidase activation and reactive oxygen species production in wound healing. **(A)** NADPH oxidase acts as a rate-limiting enzyme during the phagocytosis process, playing a key role in phase 2 of eukaryotic wound healing. **(B)** Once NADPH oxidase is activated, it triggers a self-regulating sequence of reactions that lead to the production of reactive oxygen species, including hydrogen peroxide (H_2O_2), which are essential for oxidative defense mechanisms. Adapted from USMLE World and *FA for the USMLE Step 1, 2016.* All rights reserved.

Furthermore, the pivotal role of O_2 is elucidated by studying specific molecular pathways contributing to the normal healing stages. There is substantial evidence that O_2 contributes to neutrophil chemotaxis [Klyubin et al., 1996], the respiratory burst [Babior, 1978], decreased infection rates [Greif et al., 2000; Belda et al., 2005], enhanced re-epithelialization [Said et al., 2005], angiogenesis [Berthod et al., 2006; Knighton et al., 1983; Sen et al., 2002; Roy et al., 2006], collagen formation [Kivisaari et al., 1975], collagen maturation [Eyre et al., 1984], and the overall tensile strength of the regenerated tissue [Stephens and Hunt, 1971]. Also, O_2 is known for supply the necessary energy required throughout tissue repair; which, by definition, constitutes an energy-demanding process [Kivisaari et al., 1975; Vihersaari et al., 1974]. Interestingly, detailed data on the O_2 requirements for unopposed progression of particular pathways in the healing mechanism also point towards the same conclusion regarding the role of O_2. For example, NADPH oxidase reaches half its maximum efficacy during ROS production at a partial pressure of O_2 (PO_2) range of 45-80mmHg [Allen et al., 1997]. Meanwhile, at lower values, the bactericidal activity of neutrophils is significantly

impaired [Edwards et al., 1984; Jonsson et al., 1984], reflecting the downstream impact of decreased NADPH oxidase activity on the healing outcome. For the rate-limiting hydroxylases catalyzing collagen synthesis, half maximum efficacy has been shown to be achieved at a PO_2 of 25mmHg [Myllylä et al., 1977]. Collagen deposition by fibroblasts also occurs at a minimum PO_2 range of 30-40mmHg [Myllylä et al., 1977; Hutton et al., 1967]. Of note, NADPH oxidase and collagen hydroxylases have demonstrated a dose-dependent relationship with PO_2, before reaching their maximum efficacy at approximately 250 and 300mmHg, respectively [Allen et al., 1997; Myllylä et al., 1977]. Albeit limited, there is also clinical evidence supporting the benefits of adequate O_2 supply in wound healing. In a double-blind randomized controlled trial of 500 patients undergoing colonic resection, a 50% increase in inspired O_2 concentration was accompanied by an equivalent decrease in surgical wound infections [Greif et al., 2000]. Also, collagen synthesis has been found to be proportional to local perfusion and ensuing PO_2 in subcutaneous wounds treated postoperatively [Jonsson et al., 1991].

Considering the aforementioned evidence, along with the significance of the physiologic completion of the most upstream healing stages as a prerequisite for normal and successful progression of the entire healing mechanism, as discussed in the precious section of this Chapter, we can advocate that O_2 is fundamental for both the successful initiation and the unopposed progression of normal wound healing.

1.2.2 | Wound healing under hypoxic conditions

In turn, inadequate O_2 supply has been documented itself as a major culprit of chronic wounds. Interestingly, it has been hypothesized that the longer hypoxia lasts, the more pronounced are its inhibitory effects in tissue repair [Siddiqui et al., 1996]. Over the years, numerous *in vitro* and *in vivo* studies have reported a strongly negative correlation between the duration of hypoxia, and the physiological activity of multiple pathways mediating wound restoration [Hohn et al., 1976; Edwards et al., 1984; Jönsson et al., 1988; Siddiqui et al., 1996; Allen et al., 1997; Hopf et al., 2005]. Particular examples in specific pathways, where prolonged hypoxia has been shown to impact crucial steps in the healing mechanism, include ROS formation [Edwards et al., 1984; Allen et al., 1997], neutrophil chemotaxis and phagocytosis [Hohn et al., 1976;

Jönsson et al., 1988], angiogenesis [Hopf et al., 2005], and granulation tissue formation [Sano and Ichioka, 2015]. Meanwhile, vasculature disruptions can be irreversible under hypoxia, as indicated by the lack of response to external angiogenic factors [Hopf et al., 2005]. Also, failure to functionally restore tissues under hypoxic conditions has been verified *in vivo* [Sano and Ichioka, 2015; Shandall et al., 1985], as well as in human studies on the natural history of anastomotic leakage [Sheridan et al., 1987].

1.3 | The emerging global-health issue implicating wound healing

Complications in wound healing, and non-healing wounds in particular, are considered an emerging global health issue. Within the decade from 2000 to 2010, annual healthcare expenditures dedicated to wound healing increased from $14 billion worldwide [Walmsley, 2002], to $25 billion in the United States alone [Sen et al., 2009]. According to more recent evidence, the latter has further increased up to approximately $50 billion in the United States [Fife and Carter, 2012; Nussbaum et al., 2018; Rodrigues et al., 2019]. Among the multiple potential etiologies associated with complicated wound healing and chronic wounds, such as burn injuries, surgical incisions, genetic disorders, and traumatic lacerations [Leavitt et al., 2016; Wang et al., 2024], the rate at which wound-related costs are rising closely resembles the escalating prevalence of systemic vascular comorbidities and risk factors predisposing to problematic wound healing.

Among the latter, epidemiological awareness is particularly raised towards type 2 diabetes mellitus (DM). Indeed, its global prevalence is estimated to exceed 642 million cases by 2040 [International Diabetes Federation, 2015], a quarter (25%) of which are considered high-risk for developing persisting wounds during their lifetime [International Working Group on the Diabetic Foot, 2003]. The most characteristic example of diabetic wounds involves diabetic foot ulcers, which account for the majority of non-healing wounds and for approximately 80% of non-traumatic limb amputations, both on a global scale [International Working Group on the Diabetic Foot, 2003; Serena, 2014]. Moreover, the concurrent population aging not only correlates positively with type 2 DM rates [International Diabetes Federation, 2015], but may also serve as an independent risk factor for abnormal wound healing and chronicity [Wu et al., 1999; Gottrup, 2004]. Despite the availability of numerous management strategies

introduced to enhance the healing mechanism over the years [Figure 1.6], the epidemiological concern persists due to the questionable efficacy of the existing management options and the lack of gold-standard treatments, especially for complicated wounds [Das and Baker, 2016].

1.4 | Limitations of the available technological approaches to enhancing wound oxygenation

Based on the pivotal role of O_2 in wound healing, numerous technologies have been proposed over the years, as a means to optimize healing outcomes by enhancing wound O_2 levels [de Smet et al., 2017]. The most characteristic example is hyperbaric O_2 therapy (HBOT), which has become an established management strategy for complicated wounds in patients with diabetes mellitus, alongside other clinical indications [Wang et al., 2003; de Smet et al., 2017]. Devices supplying topical O_2 therapy have also been successfully introduced, enabling continuous local application on wounds in the home setting [Sayadi et al., 2018]. However, none of these approaches has been applied as definite treatment to date. Mainly, this can be attributed to technical limitations when superfluous O_2 is administered in its gaseous form; which, in turn, lead to extremely short-lived biological effects, as a result of passive diffusion within tissues in response to local O_2 pressure gradients.

Meanwhile, the FDA-approved HBOT requires expensive infrastructure and daily hospitalizations for several hours. Therefore, apart from cost-effectiveness, the ensuing high rates of patient non-compliance, as a consequence of the demanding treatment schedule, can compromise the otherwise well-documented healing benefits [de Smet et al., 2017; Wang et al., 2003]. Furthermore, HBOT has numerous adverse effects and contraindications, mostly due to the fact that it employs prolonged lung ventilation in a pressurized chamber of 2-3 atmospheres, under unnaturally-high pressures. Examples include systemic O_2 toxicity [Narkowicz et al., 1993], respiratory comorbidities, diseases of the ear and sinuses, claustrophobia, hyperthermia, congenital spherocytosis, and pregnancy [Kindwall, 1999; Broussard, 2004]. Regarding topical O_2 therapy, which is typically administered via wound-attaching devices supplying O_2 at atmospheric pressures, this approach can overcome many of the limitations inherent

in HBOT [Gordillo and Sen, 2003]. Yet, physical restrictions needed for continuous local application, and the possibility of fire accidents remain two important issues with the portable equipment used. Thereby, novel technologies with the capacity to establish both increased and prolonged wound oxygenation, are actively tested worldwide [Sayadi et al., 2018].

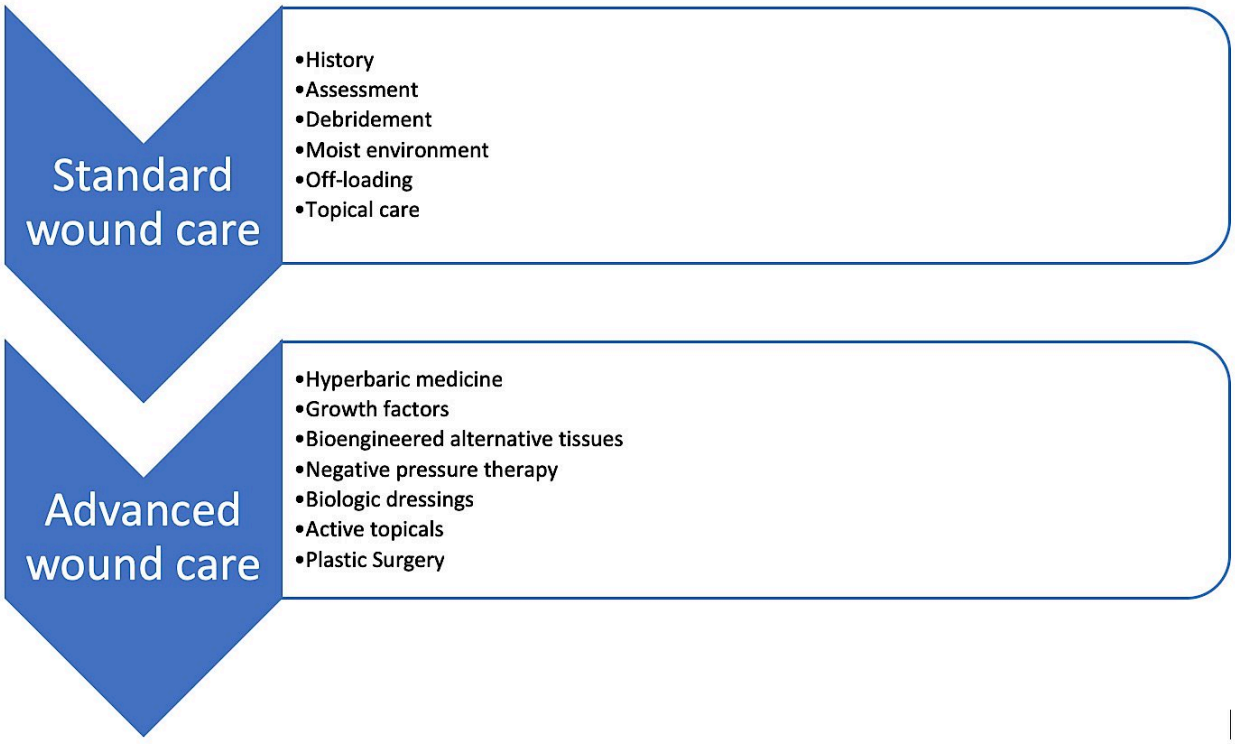

Figure 1.6: **Schematic diagram summarizing the available management options for wound healing, as documented by clinical availability in the United States**. Graphical synopsis of the available therapeutic interventions in standard and advanced wound care units in the United States of America, highlighting the vastly unmet clinical need for safe, effective, consistent, and affordable wound management worldwide. Adapted from *Das et al. 2016.* All rights reserved.

1.5 | The promising potential of novel technologies supplying dissolved oxygen

In this setting, biotechnologies supplying dissolved O_2 (DO) within the aqueous phase, may introduce a breakthrough in the ongoing quest for novel approaches to increased and prolonged wound oxygenation. Given the liquid microenvironment surrounding the cells in living tissues, namely the extracellular fluid, a DO approach

could theoretically enhance O_2 supplementation safely and efficiently [Androjna et al., 2008]. In fact, the enabling effects of DO have been quantified by comparing gaseous O_2 to DO delivery *in vitro*; cutaneous oxygenation via the latter was significantly more efficient in both speed and magnitude [Roe et al., 2010]. Also, DO technologies enhance clinical flexibility in routes of administration, with a broad range from localized applications via wound dressings [Roe et al., 2010], to intravascular uses [Kheir et al., 2012], and even liquid-ventilation applications [Legband et al., 2014]. In terms of topical wound treatment in particular, air exposure has been proven inadvisable in early stages [Hinman and Maibach, 1963]; meanwhile, there are indications that the entire healing mechanism can be substantially up-regulated in the presence of a moist/wet wound bed, provided that it remains non-infected [Junker et al., 2013]. Although a comparative study evaluating the costs of gas-based versus DO-based treatments is pending, it can be hypothesized that in terms of manufacturing, operational, and healthcare expenditure, DO technologies might offer a more balanced cost-effectiveness relationship, since no life-threatening infrastructure is involved.

1.6 | Research objectives

Given the documented contributions of O_2 to the healing mechanism, the rising need for novel technologies to broaden the clinical implementation of enhanced wound oxygenation, and the promising yet largely unexplored potential of DO administration in wound healing and actively-regenerating tissues, collectively discussed throughout this Chapter, this dissertation has the following research objectives:

- To identify and comprehensively study the available technologies that can be leveraged for DO administration in healing wounds and actively-regenerating tissues, via a systematic analysis and critical co-evaluation of their engineering fundamentals, oxygenating effects, biomechanics of DO delivery to tissues, safety parameters, and healing-related efficacy

- To pinpoint the technological approach with the most promising cost-effectiveness projection, among the available technologies enabling DO supply to healing tissues, for subsequent biomedical testing

- To design and introduce a comprehensive *in vivo* protocol, encompassing a spherical investigation of the engineering fundamentals, quality-control processes, biological safety, and preliminary healing efficacy for DO technologies explored in wound healing applications, with the aim to standardize procedural parameters, facilitate experimental execution, and ultimately accelerate the biomedical translation of novel, technologically-relevant treatment factors in the field of wound healing and cutaneous regeneration

- To successfully implement the proposed *in vivo* protocol to independently study two DO-supplying technologies, manufactured by leveraging the physics of the gas-liquid interphase without chemical surfactants or exogenous additives, with the following secondary objectives:

    - identification of the most efficient routes of administration *in vivo*
    - description of the manufacturing and quality-control fundamentals for the DO-supplying technologies tested
    - validation of their biological safety *in vivo*, and
    - assessment of their healing efficacy *in vivo*

2 | Dissolved oxygen technologies in wound healing and tissue regeneration

The contents of this chapter also appear in *Wound Repair and Regeneration* as:

Ntentakis, D. P., Ntentaki, A. M., Delavogia, E., Kalomoiris, L., Venieri, D., Arkadopoulos, N., & Kalogerakis, N. (2021). Dissolved oxygen technologies as a novel strategy for non-healing wounds: A critical review. *Wound repair and regeneration: official publication of the Wound Healing Society [and] the European Tissue Repair Society*, *29*(6), 1062–1079. https://doi.org/10.1111/wrr.12972

2.1 | Background information

Complications in the healing mechanism, and the associated prevalence of non-healing wounds, are expected to rise exponentially in the upcoming decades [Walmsley, 2002; Sen et al., 2009]; alongside the increasing rates of systemic vascular comorbidities, predominantly type 2 diabetes [International Diabetes Federation, 2015], which keep escalating in the aging world population. Epidemiological concern is further exacerbated by the lack of gold-standard treatments in the field, especially for high-risk wounds, and the questionable capacity of the existing treatment approaches to counterbalance the projected increase in wound prevalence. Notably, these concerns persist despite the availability of numerous management strategies introduced over the years [Das and Baker, 2016].

Among the latter, technologies supplying gaseous oxygen to enhance wound healing, such as hyperbaric oxygen therapy (HBOT) and topical oxygen therapy, have been accompanied by substantial clinical benefits [Wang et al., 2003; de Smet et al., 2017], enabled by the established role of adequate wound oxygenation on the successful completion of the healing mechanism [Tandara and Mustoe, 2004; Rodriguez et al., 2008]. Yet, their clinical applications are far from becoming broadly generalized, mainly due to technical limitations and pertinent complications; the most important of which, is the extremely short half-life of gaseous oxygen when administered in living tissues, as it succumbs to the principles of passive diffusion via the lipid bilayers of cell membranes. To overcome this limitation, aqueous solutions enriched with dissolved oxygen (DO) are investigated as a novel and highly-promising technological alternative to enhancing wound oxygenation. At this stage though, a collective and comparative analysis of the available technologies for supplying DO to healing tissues, has not been systematically conducted.

In this Chapter, we systematically study the technological approaches enabling DO administration for wound healing and tissue-regenerating applications. For each of the technological approaches we identified, we evaluate its technical fundamentals, oxygenating effects, the biomechanics underlying DO supply, and the ensuing healing-related outcomes, as presented in the existing literature. Also, via a collective and critical interpretation of the aforementioned engineering and biological parameters, we

introduce an original classification system for the DO technologies that are being, or have been, tested in healing applications. Subsequently, we discuss pivotal aspects for the practical implementation of these technologies in real-life biomedical applications, such as the optimal timing of DO administration, dosing requirements, and potential safety concerns. Finally, we pinpoint crucial limitations in the existing literature, that should be addressed by future research in the field. Ultimately, the points presented in this work could contribute to an easier integration of DO technologies in the biomedical and clinical setting. To our knowledge, this is the first systematic analysis and classification of DO technologies investigated for healing applications in the literature.

2.2 | Methods

2.2.1 | Literature search

A systematic literature search was designed and conducted according to the Preferred Reporting Items for Systematic Reviews and Meta-analyses (PRISMA) statement [Moher et al., 2009; Figure 2.1] and the Population, Intervention, Comparison, Outcomes, and Study design (PICOS) framework [Petticrew and Roberts, 2006]. The following databases were systematically searched: EMBASE, Medline, Web of Science, Cochrane, PubMed as supply by the publisher, Scopus, and Google Scholar. Of the 457 articles originally identified, 450 remained after removal of duplicates.

2.2.2 | Data selection

A total of 450 articles were carefully reviewed, using Endnote X9 for reference management. All clinical and experimental studies evaluating DO technologies in wound healing were included. For the scope of this work, our search was restricted to aqueous solutions enhancing oxygenation via DO, excluding articles testing artificial O_2 carriers. Letters to the editor, congress abstracts, and articles published in a language other than English were not considered. A total of 40 articles met met the aforementioned eligibility criteria, in the process illustrated on the PRISMA flow diagram in Figure 2.1.

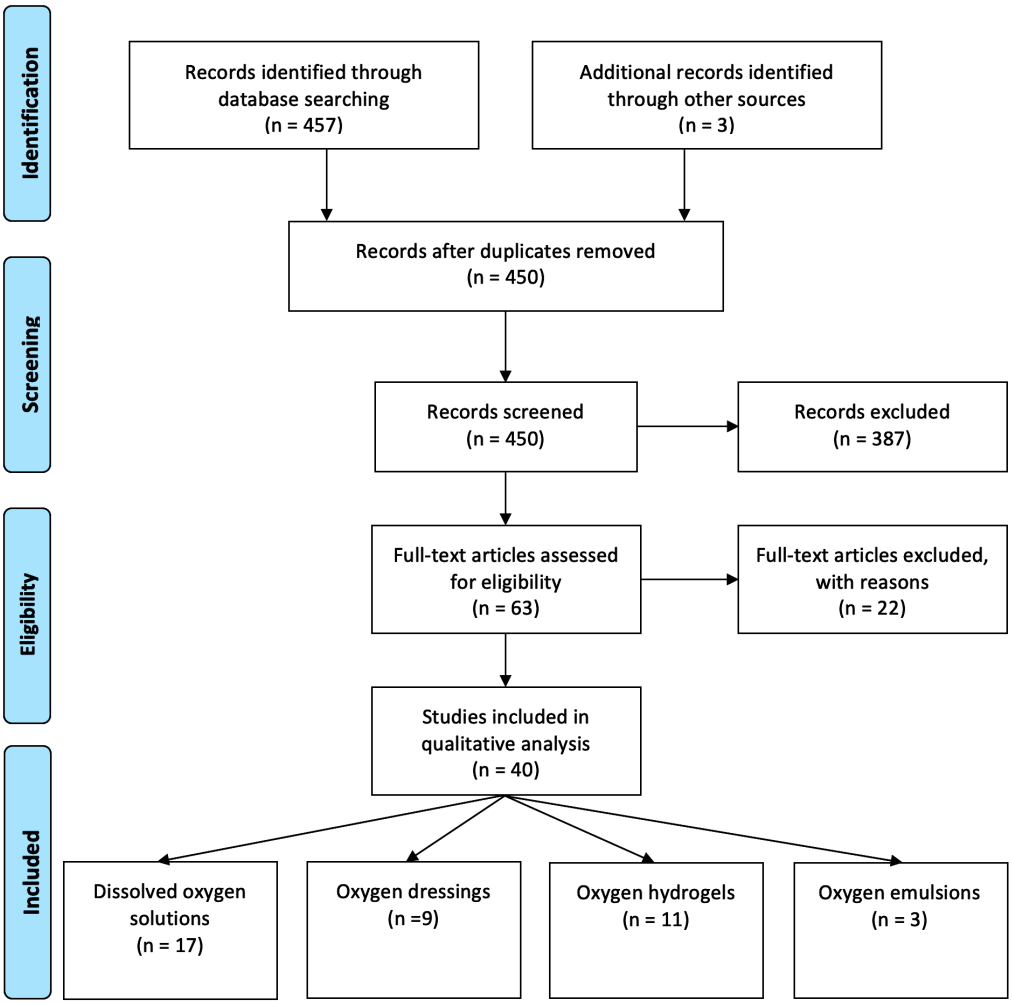

Figure 2.1: **Flow diagram summarizing the literature search conducted according to the PRISMA guidelines** [35]. Via the implementation of the PRISMA guidelines [Moher et al., 2009], combined with the systematic criteria applied during data extraction and organization (section 2.3.3 in this Chapter), our methodology enabled the effective categorization of all DO-supplying technologies that are being, or have been, tested for applications related to wound healing and tissue regeneration, into distinct categories based on their engineering background, manufacturing process, and DO-supplying parameters. **Abbreviations**: PRISMA, preferred reporting items for systematic reviews and meta-analyses; DO, dissolved oxygen.

2.2.3 | Data extraction and organization

Our stepwise analysis sequentially focussed on each study's methodology, the healing endpoints assessed, the statistically significant outcomes, and the engineering fundamentals for each DO technology tested. For every original article, the following

parameters were collectively recorded in Table S.1: first author, year of publication, level of evidence (LoE), subject (cell cultures, animal species, or humans), number of subjects/sample size (n), wound duration (acute if wounds were followed for <6 weeks, or chronic if either infected, ischemic, or simply evaluated for over 6 weeks), wound model (wound etiology; partial or full thickness when applicable), treatment timeline (duration; frequency), follow-up duration, treatment groups, control groups, measured endpoints, and positive outcomes (significant if $p<0.05$, non-significant if $p>0.05$). LoE was identified according to the Oxford Centre for Evidence-Based Medicine [Howick et al., 2011].

DO technologies were further analyzed based on the manufacturing fundamentals establishing their enhanced O_2 content. The following technical details were recorded per technological group in Table S.2: manufacturing and application parameters, O_2 supply/origin during the manufacturing process and additional materials apart from O_2 (core materials, coating materials and extra solutes). Resulting O_2 levels (*in vitro*, *in vivo*, or clinically) and the physical parameters during O_2 administration (pressure and temperature) are presented with the corresponding healing data in Tables S.3 – S.6.

2.3 | Classification of technological approaches enabling dissolved oxygen supply *in vivo*

To our knowledge, this is the first classification of DO technologies evaluated for applications pertinent to wound healing and tissue regeneration. Based on the rationale described in section 2.3 of this Chapter, all original studies meeting the predetermined inclusion criteria (40) were classified among the following 4 technological approaches: DO solutions (17), oxygenating (O_2) dressings (9), oxygenating (O_2) hydrogels (11), and oxygenating (O_2) emulsions (3), respectively. The healing outcomes pertaining to each technological group are presented separately, preceded by a paragraph summarizing the engineering fundamentals of the DO-supplying technology used.

In this section, we focus on statistically significant results; a complete list of methodological details per study is included in Tables S.1 and S.2, for qualitative comparisons. An overview of the significant healing outcomes achieved with each DO

technology is provided in Figure 2.2. Healing endpoints and outcomes are presented in Tables S.3 – S.6, in correlation with the oxygenation parameters of biomedical interest. Statistical comparisons were impeded by the methodological variability even among studies evaluating the same technology; these are summarized in section 2.4 of this Chapter.

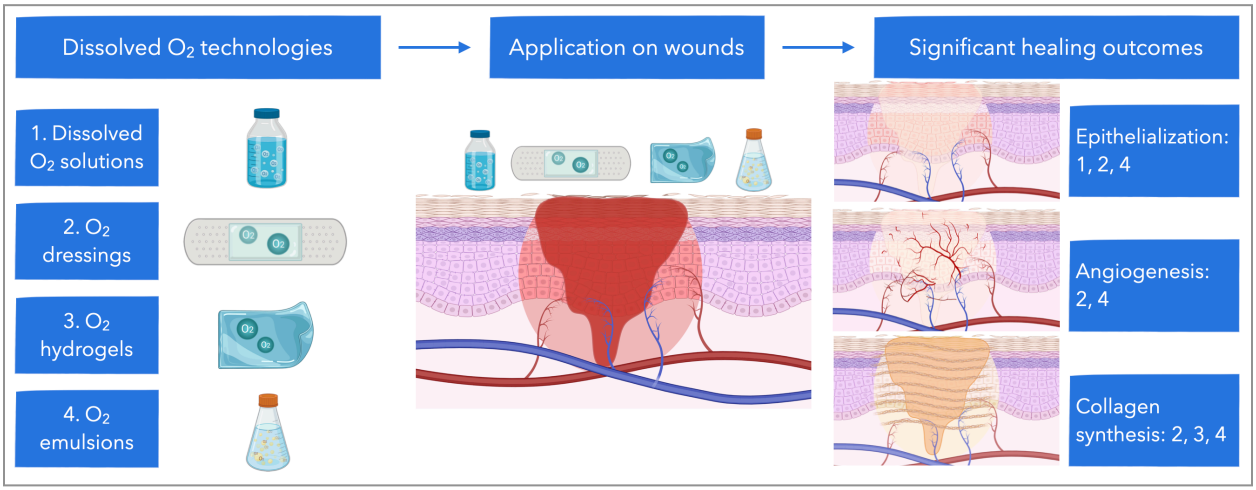

Figure 2.2: **Overview of the 4 main categories of DO technologies identified, along with their outcomes on three key pathways of wound healing: epithelialization, angiogenesis, and collagen synthesis**. Evaluation of dissolved oxygen (DO) technologies in wound healing. Four main technological approaches were identified: 1. DO solutions, 2. Oxygen (O_2) dressings, O_2 hydrogels, and O_2 emulsions. Wound oxygenation was significantly enhanced with the majority of these DO technologies. Effects on key healing pathways, such as epithelialization, angiogenesis, and collagen synthesis were characterized by higher degree of variability.

2.3.1 | Dissolved oxygen solutions

In this approach, O_2 gas was directly dissolved in water-based solutions aiming for gradual release upon administration. Further classification in Table S.2 and S.3 highlights the distinct engineering approaches investigated for healing applications. Initially, molecular O_2 was equilibrated with normal saline leading to O_2-saturated solutions. Although significant, their oxygenating effect was relatively short-lived; thus, they have been mainly used as control treatments, in studies testing more complicated oxygenating technologies [Magnetto et al., 2014; Khadjavi et al., 2015; Prato et al., 2015; Gulino et al., 2015; Basilico et al., 2015]. In a series of 3 cases evaluating this approach after plastic surgery, cosmetic and healing benefits were restricted to the

short timeframe of daily administration; furthermore, mixture with multiple constituents and the subjectivity of photographic evaluation did not favor larger-scale clinical testing [Onouye et al., 2000]. Upon electrolysis, a similar saline formula can be enriched with both O_2 and chloride free radicals, whose antibacterial effect has been shown to overall enhance the healing process in diabetic patients [Paola et al., 2006].

In the pursuit of increased and prolonged O_2 delivery however, research has recently emphasized on O_2-loaded ultra-fine particles (OUPs). Despite technical and physical variations, all OUP designs aim for maximum O_2 content per unit size. Such highly-pressurized O_2 would favor instantaneous collapse in aqueous solutions, according to Laplace's law. Yet clinically significant oxygenation mandates improved OUP stability, for a long-lasting effect. To decelerate O_2 diffusion in water, artificial coating materials have been tested. Via high-speed centrifugation, OUPs can be engulfed by complex carbohydrates such as chitosan [Magnetto et al., 2014, Khadjavi et al., 2015; Bisazza et al., 2008; Cavalli et al., 2009a] or dextran [Prato et al., 2015; Gulino et al., 2015; Basilico et al., 2015; Cavalli et al., 2009b]. Alternatively, phospholipid coatings are formed via sonication-driven emulsification with O_2, at the beginning of each solution's preparation [Feshitan et al., 2014; Fiala et al., 2020]. To enhance O_2 content, some researchers added O_2-binding perfluorocarbons (PFCs) to the OUP core; mainly perfluoropentane (PFP) and decafluoropentane (DFP). Core materials determine OUP nomenclature and physical state at body temperature. For example, homogenization with gaseous PFP yields O_2 ultra-fine bubbles (PFP-OUBs) [Magnetto et al., 2014; Prato et al., 2015; Bisazza et al., 2008; Cavalli et al., 2009a; Cavalli et al., 2009b], whereas a liquid DFP core forms O_2-loaded nanodroplets (OLNDs) at 25 ^{o}Celsius [Magnetto et al., 2014; Khadjavi et al., 2015; Prato et al., 2015; Gulino et al., 2015; Basilico et al., 2015].

Recently, OUBs manufactured without any additional materials achieved oxygenation of remarkable magnitude and duration [Matsuki et al., 2012; Matsuki et al., 2014; Ebina et al., 2013; Noguchi et al., 2017; Matsuoka et al., 2018]. By applying Bernoulli's hydrodynamic principle, cylindrical water acceleration produces a centrifugal pressure gradient that enables mixture with 100% O_2 from a different inlet. In the common outlet, shearing forces from abrupt pressure and temperature changes generate O_2 micro-bubbles (OMBs) [Tsuge, 2014]. Shortly, OMBs collapse to create

stable OUBs with a potential lifespan of 70 days and mean diameters of less than 10μm [Ebina et al., 2013; Noguchi et al., 2017; Matsuoka et al., 2018]. Stability of these "plain" OUBs is founded upon electrochemical phenomena almost exclusive to the nanoscale. In fact, the latter mostly pertain to the OUB surface charge, the liquid medium, and the manufacturing process rather than the enclosed gas itself [Tsuge, 2014].

Following mixture with hypoxic saline, PFP-OUB solutions restored normoxic DO concentration within 24 hours [Bisazza et al., 2008; Cavalli et al., 2009a; Cavalli et al., 2009b]. Although mostly down-regulated [Bisazza et al., 2008; Cavalli et al., 2009a], hypoxia-inducible factor 1-alpha (HIF-1α) expression may vary depending on oxidative stress intensity [Bisazza et al., 2008]. *In vitro*, chitosan-OLNDs achieved significantly higher DO concentration after ultrasound application [Magnetto et al., 2014]. O_2 skin penetration was also enhanced by sonication [Magnetto et al., 2014]; illustrated as ΔDO in Table S.3. *In vitro* administration of similar OLNDs under hypoxia normalized the ratio of matrix metalloproteinases to their tissue-specific inhibitors (MMPs/TIMPs) [Khadjavi et al., 2015]. Subsequent studies evaluated dextran-OLNDs in human cell lines playing a fundamental role in cutaneous healing; such as keratinocytes [Prato et al., 2015], monocytes [Gulino et al., 2015], and endothelium [Basilico et al., 2015]. Outcomes were similar in terms of DO increase [Prato et al., 2015], O_2 penetration [Prato et al., 2015], and MMP/TIMP equilibrium [Gulino et al., 2015; Basilico et al., 2015] over 24 hours. In the majority of *in vitro* experiments, oxygenating effects were significantly more pronounced in severe hypoxia [Magnetto et al., 2014; Khadjavi et al., 2015; Prato et al., 2015; Gulino et al., 2015; Basilico et al., 2015; Cavalli et al., 2009a; Cavalli et al., 2009b]. Highest efficiency in O_2 release was achieved when OUPs were dissolved in an aqueous environment, compared to similar gel formulations [Magnetto et al., 2014; Prato et al., 2015].

Versus untreated controls, OLNDs increased transcutaneous O_2 partial pressure ($TcPO_2$) and oxidized hemoglobin (OxyHb) in healthy mice for 15 minutes [Magnetto et al., 2014; Prato et al., 2015]. Brief sonication (10-135min *in vitro*, 10min *in vivo*) increased both the duration and the magnitude of O_2 delivery [Magnetto et al., 2014; Prato et al., 2015; Cavalli et al., 2009a; Cavalli et al., 2009b], sometimes in a time-dependent manner *in vitro* [Cavalli et al., 2009a; Cavalli et al., 2009b]. The enabling

effect of ultrasound was concurrently investigated in all *in vitro* study groups [Magnetto et al., 2014; Prato et al., 2015; Cavalli et al., 2009a; Cavalli et al., 2009b]; yet *in vivo* statistical comparisons included OLNDs and negative controls only [Magnetto et al., 2014; Prato et al., 2015]. Phosphate-buffered saline containing phospholipid-coated OMBs successfully abrogated systemic hypoxia following acute lung trauma in rats [Feshitan et al., 2014; Fiala et al., 2020]. Both continuous and intermittent intra-peritoneal infusion improved survival in pneumothorax [Feshitan et al., 2014] and acute respiratory distress syndrome [Fiala et al., 2020] protocols respectively, over a maximum period of 48 hours. However, clinical and histological markers of lung trauma were inconsistently affected [Feshitan et al., 2014; Fiala et al., 2020].

"Plain" OUB solutions demonstrated a dose-dependent oxygenating effect in healing -related protocols both *in vitro* and *in vivo* [Matsuki et al., 2012; Matsuki et al., 2014; Noguchi et al., 2017; Matsuoka et al., 2018]. Among fluid-resuscitation constituents, normal saline (0.9% NaCl) was verified as the ideal microenvironment to combine optimal OUB stability with efficient O_2 delivery [Matsuki et al., 2012; Matsuki et al., 2014]. OUB-enriched water significantly promoted physical growth in healthy developing mice per os [Ebina et al., 2013]. Such an anabolic status simulates accelerated tissue regeneration during proliferative healing [Ebina et al., 2013]. Notably, *in vitro* application of similarly-engineered ultra-fine bubbles containing air (21% O_2) yielded analogous outcomes [Ebina et al., 2013]. Peripheral nerve regeneration [Matsuoka et al., 2018] and osteoclast inhibition [Noguchi et al., 2017] were also found proportional to OUB concentration, in subsequent *in vitro* experiments by the same group. *In vivo*, the aforementioned solutions enhanced not only the regeneration of fully-transected sciatic nerve [Matsuoka et al., 2018], but also bone sustainability under osteoclastic stimulation [Noguchi et al., 2017]. Expression of healing-related growth factors was also significantly up-regulated *in vitro* [Matsuoka et al., 2018]. OUBs were not only detectable, but could also maintain their oxygenating effect for nearly 70 days post-production at 4 degrees Celsius [Ebina et al., 2013].

Furthermore, ultrasound application varied substantially among the DO technological subgroups. For phospholipid-coated OMBs, sonication energy was used to emulsify the gas-liquid interphase with the covering material, at the beginning of the manufacturing process [Feshitan et al., 2014; Fiala et al., 2020]. Brief ultrasound

application (~30 seconds) facilitated the rupture of larger-diameter bubbles in “plain” OUB solutions [Matsuki et al., 2012; Matsuki et al., 2014; Ebina et al., 2013; Noguchi et al., 2017; Matsuoka et al., 2018]. Regarding core-enhanced OUP solutions, O_2 delivery was enhanced by the sonication-driven OUP oscillation [Magnetto et al., 2014; Khadjavi et al., 2015; Prato et al., 2015; Gulino et al., 2015; Basilico et al., 2015].

2.3.2 | Oxygenating dressings

Over the years, wound dressings have been classified by multiple criteria including main function [Purna and Babu, 2000], predominant material [Queen et al., 2004], physical form [Falabella, 2006], and attachment to healing surface [van Rijswijk, 2006]. In our analysis, oxygenating (O_2) dressings are further sub-categorized to facilitate the association between different biotechnologies and healing outcomes [Table S.4]. A considerable number of researchers used H_2O_2 as an O_2-releasing intermediate [Tur et al., 1995; Chandra et al., 2015; Harrison et al., 2007; Wright et al., 2003]. H_2O_2 is typically generated via oxidation of implantable biomaterials such as sodium percarbonate and calcium peroxide [Chandra et al., 2015; Harrison et al., 2007]; alternatively, it can be exogenously administered through the overlying dressing for intermittent control of wound O_2 [Wright et al., 2003], or integrated in a cream [Tur et al., 1995]. Other dressings come pre-loaded with O_2 using proprietary technologies [Lairet et al., 2014; Zellner et al., 2015; Gueldner et al., 2017; Kellar et al., 2013]. The latter are typically encased by a polymer O_2-binding matrix, in either foam [Zellner et al., 2015; Kellar et al., 2013] or powder configurations [Gueldner et al., 2017]. Interestingly, the cutting-edge technology of microfluidics can also be incorporated in bandages to provide dynamic wound oxygenation [Lo et al., 2013]. Although this design required continuous connection to an O_2 tank, it enabled accelerated O_2 equilibration in the 60-second range [Lo et al., 2013]. Such real-time monitoring and supply might be applied for individualized wound care, meeting each tissue’s O_2 demands at every healing stage. Table S.2 provides an overview of technical and O_2-releasing parameters for the aforementioned dressings; the ensuing oxygenation outcomes are presented in Table S.4.

Detailed healing endpoints and outcomes are presented in Table S.1. In rodent models of acute [Tur et al., 1995; Harrison et al., 2007] and chronic [Wright et al., 2003] wounds, the effect of H_2O_2-based dressings on wound closure remains inconclusive. Enhanced re-epithelialization [Harrison et al., 2007; Wright et al., 2003] was accompanied by improved flap survival [Harrison et al., 2007], preservation of skin histology [Harrison et al., 2007], and local anti-bacterial defense [Wright et al., 2003]. On the other hand, wound closure was not noticeably benefited despite a dose-dependent increase in local perfusion upon macroscopic evaluation; this effect was most evident on days 2 and 15 post-trauma, and became insignificant after the first 20 days [Tur et al., 1995]. Via H_2O_2, Chandra et al. achieved continuous O_2 supply for 3-4 days before requiring dressing replacement [Chandra et al., 2015]. In their porcine protocol of acute surgical wounds, pivotal steps such as wound re-epithelialization, collagen deposition, and angiogenesis were significantly enhanced [Chandra et al., 2015].

Although promising, experimental data on pre-loaded O_2 dressings also exhibit variable O_2 delivery. *In vitro*, poly-oxygenated aluminum hydroxide (Ox66™) improved cellular viability, proliferation, and migration on scratch assays; yet, significant effects were restricted to specific dose ranges [Gueldner et al., 2017]. In a full-thickness porcine model, healing outcomes were benefited by an oxygenated foam dressing both macroscopically and histologically [Zellner et al., 2015]. However, the most distal quarters of the wound flap demonstrated increased subcutaneous necrosis and fibrosis, compared to control flaps on the same animal [Zellner et al., 2015]. Even more contradictory are the available clinical data, from small case series with diverging methodologies [Lairet et al., 2014; Kellar et al., 2013]. Cutaneous hydration and expression of structural proteins were increased by application of the “OxygeneSys" foam dressing on healthy skin; meanwhile, inflammatory and toxicity markers were significantly down-regulated [Kellar et al., 2013]. In a small randomized study, healing and cosmetic results were favorable; yet additional limitations related to follow-up variability and subjectivity of macroscopic evaluations impact clinical significance [Lairet et al., 2014]. Microfluidic dressings enhanced O_2 delivery *in vitro* throughout

a14-day evaluation [Lo et al., 2013]. With the exception of collagen maturation though, no significant healing benefits were recorded in diabetic mice [Lo et al., 2013].

2.3.3 | Oxygenating hydrogels

Oxygenating (O_2) hydrogels are composed of synthetic (methacrylates, polyvinylpyrrolidone) or natural (alginate) polymers, integrated in a water-dominant gelatinous phase by 70-90% [Boateng et al., 2008]. They have been designed for topical wound treatments via three distinct approaches, each incorporating a different oxygenating technology. Once the hydrogel core has been finalized [Table S.2], it can be directly saturated with atmospheric air [Patil et al., 2016] or 100% O_2 for 10 to 30 minutes at 5PSI [Patil et al., 2016; Patil et al., 2018; Patil et al., 2019; Wijekoon et al., 2013; Akula et al., 2017; Almeleh, 2013; Moen et al., 2018]. In this scenario, the most extensively tested polymer is a methacrylamide chitosan modified with perfluorocarbon chains (MACF) [Patil et al., 2016; Patil et al., 2018; Patil et al., 2019; Wijekoon et al., 2013; Akula et al., 2017; Almeleh, 2013]. It is synthesized via a sequence of chitosan modifications including fluorination, freeze-drying, polymerization under ultraviolet radiation (for 20 minutes), and mixture with exogenous chemicals [Table S.2]. MACF-based O_2 hydrogels (2% w/v) are directly applied on the wound.

Alternatively, O_2 is produced upon contact with the wound surface [Queen et al., 2007; Ivins et al., 2007; Moffatt et al., 2014; Chen et al., 2020]. Hydrogels are embedded in two separate sheets of a specialized dressing containing glucose and glucose oxidase, respectively. The latter interact for the first time once applied to the wound, and O_2 is instantly released via a hydrogen peroxide (H_2O_2) intermediate [Queen et al., 2007; Ivins et al., 2007; Moffatt et al., 2014]. Such an oxidative reaction mimics H_2O_2 generation during leukocyte respiratory burst. Lesser amounts of molecular iodine (<0.04%) are also produced, probably contributing to local bactericidal conditions [Queen et al., 2007; Ivins et al., 2007; Moffatt et al., 2014]. A secondary dressing, for example a gauge, is concurrently attached to secure physical coverage in most hydrogel technologies. Recently, Chen et al. presented a novel approach to O_2-generating hydrogels, evaluated in cell cultures and animal protocols [Chen et al., 2020]. In this design, O_2 is produced via photosynthesis and respiration by microalgae pre-embedded in the hydrogel sheets [Chen et al., 2020].

Variability in oxygenation magnitude and healing parameters are presented in Table S.5. *In vitro*, MACF hydrogels established elevated O_2 levels for up to 5 days [Wijekoon et al., 2013]. O_2-loading capacity, duration and magnitude of O_2 release, cellularity, and metabolic activity increased with the addition of fluorine residues, especially in a chain conformation [Wijekoon et al., 2013]. Although less pronounced, analogous effects were observed on biosynthetic pathways of neonatal fibroblasts and keratinocytes under hypoxia [Akula et al., 2017]. In this case, oxygenation peaked within 2 hours of hydrogel application, and gradually dropped to control levels by 20 hours [Akula et al., 2017]. *In vivo* though, the outcomes of MACF O_2 hydrogels in full-thickness wound models have been largely inconsistent. For example, epithelialization showed no significant difference between O_2- and air-saturated (21% O_2) hydrogels [Patil et al., 2016], nor in comparison to the MACF hydrogel core before saturation with 100% O_2 [Patil et al., 2018; Patil et al., 2019]. Improvements in collagen synthesis might be more reproducible [Patil et al., 2016; Patil et al., 2018; Patil et al., 2019]; similarly though, significant differences were only recorded in comparison to a non-oxygenating control dressing, rather than the MACF hydrogel core prior to O_2 saturation [Patil et al., 2018; Patil et al., 2019]. Scarce clinical data from three case series and one randomized comparative trial focussed on chronic venous ulcers [Almeleh, 2013; Queen et al., 2007; Ivins et al., 2007; Moffatt et al., 2014] and hydrogel cost-effectiveness [Moffatt et al., 2014]. Yet, small samples and lack of untreated controls in these studies preclude clinically applicable conclusions [Almeleh, 2013; Queen et al., 2007; Ivins et al., 2007; Moffatt et al., 2014]. Superiority of DO in terms of skin penetration was also reproduced with microalgae hydrogels, versus topical gas O_2 [Chen et al., 2020]. These hydrogels achieved favorable outcomes in DO production, healing-related parameters, and associated immunoreactivity both *in vitro* and *in vivo*; however, the necessity for light exposure and additional constituents that include living microorganisms might generate cost-effectiveness concerns, especially in large-scale clinical testing [Chen et al., 2020].

2.3.4 | Oxygenating emulsions

Oxygenating (O_2) emulsions were manufactured in cream format for topical wound treatment [Davis et al., 2007; Li et al., 2013; Li et al., 2015]. In these immiscible

formulations, O_2 supersaturation is achieved via the addition of miniature PFC droplets and a surfactant oil. PFCs enable superior O_2 transfer than hemoglobin, mediated by linear gas-exchange kinetics proportional to PFC concentration [Riess and Le Blanc, 1982]. Yet they are practically insoluble in water; thus, droplet diameters are kept in the low micrometer scale [Riess and Le Blanc, 1982], while the hydrophilic surfactant is required for cohesion in a continuous aqueous state [Davis et al., 2007; Li et al., 2013; Li et al., 2015; Spears, 2002]. To prevent rapid outgassing and premature O_2 dissolution, these emulsions are stored under high pressure [Table S.2]. When topically applied on wounds, the high O_2-carrying capacity of PFCs is represented by a slow yet prolonged oxygenating effect.

In porcine partial-thickness wounds, O_2 emulsions significantly enhanced epithelialization [Davis et al., 2007; Li et al., 2013; Li et al., 2015], granulation tissue formation [Li et al., 2013; Li et al., 2015], collagen synthesis [Li et al., 2013; Li et al., 2015], and angiogenesis [Li et al., 2013; Li et al., 2015] in terms of speed and efficacy [Table S.6]. For the majority of healing outcomes, maximum benefits from additional O_2 were recorded on day 4 post-trauma; with the exception of VEGF production and subsequent angiogenesis, which peaked on day 7 [Li et al., 2013; Li et al., 2015]. Initial O_2 content was 2ml per ml of emulsion prior to dispensation, which could surpass the O_2-dissolving capacity of regular water by up to twenty times [Davis et al., 2007; Li et al., 2013; Li et al., 2015]. Most partial-thickness wounds were fully epithelialized before day 14 [Davis et al., 2007; Li et al., 2013]. Detailed follow-up duration and treatment intervals are presented on Table S.1. All treatment groups were compared to non-treated controls, plus another group where the emulsion vehicle (PFC + surfactant) was administered without adding O_2. Notably, the aforementioned healing pathways were also benefited in the vehicle-only groups; although to a significantly lesser magnitude than O_2 emulsions could enable.

2.4 | Discussion

DO technologies introduce a highly promising strategy for efficient, persistent, and affordable wound oxygenation. Our qualitative analysis verifies our original hypothesis, and supports further investigation in the management of non-healing wounds. Statistical comparisons were impeded by technical and methodological

variations, even among similar technological approaches. Instead, the following paragraphs are dedicated to research gaps that require further attention, focusing specifically on DO technologies. We anticipate that once properly addressed, the ensuing data shall facilitate integration of such biotechnologies in routine healthcare.

2.4.1 | The promising potential of oxygen ultra-fine bubble technology

From our perspective, “plain” OUB solutions entail the strongest potential for healing applications. This technology has already been tested in agricultural and environmental settings, achieving unprecedented oxygenation outcomes [Agarwal et al., 2011; Etchepare et al., 2017]. The latter are attributed to the unique physical properties demonstrated by OUBs in water solutions, as a result of their miniature size. In the articles we reviewed, mean OUB diameter was reported lower than 2μm [Matsuki et al., 2012; Matsuki et al., 2014; Ebina et al., 2013; Noguchi et al., 2017; Matsuoka et al., 2018]. At this size range, O_2 dissolution is substantially up-regulated by a higher pressure gradient though the OUB shell, according to Laplace’s law [Matsuki et al., 2012; Tsuge, 2014]. Apart from magnitude, oxygenating effects are concurrently enhanced in duration. OUB rising velocity is exponentially decreased by their smaller radius, favoring longevity in aqueous solutions; in the available literature, OUBs were detected for up to 70 days after production [Ebina et al., 2013]. Additional OUB stability is forged by repulsive electrochemical phenomena almost exclusive to the nanoscale, collectively described by zeta (ζ) potential [Tsuge, 2014]. In contradiction to regular physics of the gas-liquid interface, hydrodynamics of buoyancy, coalescence, and dissolution appear to work synergistically to the benefit of oxygenation.

Besides the technical background, biomedical parameters further support “plain” OUBs for wound healing. Nanometer diameters not only ensure vascular patency, but also permit unobstructed movement through fenestrated capillaries. For comparison purposes, the filter pores in extracorporeal membranous oxygenation (ECMO) devices are measured in the 28–40μm range [Barak and Katz, 2005]. Clinical safety is also reinforced by the manufacturing process; a multi-step mixture of O_2 and water, that does not require exogenous materials. Meanwhile, normal saline has already been documented as the most ideal microenvironment for OUBs [Matsuki et al., 2012; Matsuki et al., 2014]. Since this is the typical formulation for fluid resuscitation in

medicine, clinical integration of such OUB solutions could be expedited. Furthermore, this approach also permits intravascular administration; the latter may expand therapeutic applications towards systemic O_2 delivery. Flexibility in isotope selection without compromising their oxygenating effects [Ebina et al., 2013] also broadens clinical utility, especially for disinfection. In our categorization of DO solutions, "plain" OUB technology achieved the most consistent outcomes in both oxygenation and healing [Table S.3].

2.4.2 | Potential safety concerns with surfactant materials and chemical reactions

Meanwhile, alternative DO formulations raise multifaceted safety concerns. In part, the latter are associated with inherent toxicity of constituents other than O_2 and water. Among these chemicals [Table S.2], PFCs are the most frequently encountered despite their hydrophobic nature; indeed, they have been included in core-enhanced OUP solutions [Magnetto et al., 2014; Prato et al., 2015; Gulino et al., 2015; Basilico et al., 2015; Bisazza et al., 2008; Cavalli et al., 2009a; Cavalli et al., 2009b], O_2 emulsions [Davis et al., 2007; Li et al., 2013; Li et al., 2015], and the majority of O_2 hydrogels [Patil et al., 2016; Patil et al., 2018; Patil et al., 2019; Wijekoon et al., 2013; Akula et al., 2017; Almeleh, 2013]. Extensive environmental exposure predisposes to dose-related hepatotoxicity [Butenhoff et al., 2002], and gestational DM [Zhang et al., 2015]; both these conditions can independently impair healing via coagulation and microvascular disorders, respectively. Equally concerning is the high risk of long-term accumulation in the lungs, even after 12 months of PFC administration [Nosé, 2004]. Similarly, chitosan cytotoxicity has been reported in human keratinocytes [Wiegand et al., 2010], lung fibroblasts, and endothelium [Je et al., 2006]. Such effects may progress unpredictably *in vivo*, as they seem to strongly correlate with the degree of chitosan de-acetylation [Je et al., 2006]. Certain surfactants from O_2 emulsions have been associated with life-threatening pro-inflammatory [Lowe, 1999] and hemodynamic [Castro and Briceno, 2010] adverse events; in this setting, an FDA-approved hydrogel for salvage of ischemic myocardium during percutaneous coronary angioplasty (PCA) was recently withdrawn [F-D-C Reports, 1990]. Interestingly, substances like polyvinylpyrrolidone (PVP) and emulsion vehicles may exert an inhibitory effect on O_2 kinetics [Cavalli et al., 2009b] and the healing mechanism [Eaglstein and Mertz, 1980]. In an aging and largely

vasculopathic global population, such lipids and complex carbohydrates might not represent the ideal constituents for oxygenating formulations.

A similar verdict can be reached with a projected risk-benefit assessment. Via the aforementioned technologies, O_2 delivery and healing outcomes have been rather inconsistent [Table S.1]. Within dressings for example, O_2 is frequently released by oxidative reactions that simulate bactericidal respiratory burst [Tur et al., 1995; Chandra et al., 2015; Harrison et al., 2007]. Such a strategy possibly entails both local and systemic toxicities, secondary to chemical byproducts, pH disruptions, and exothermic heat generation. It may also propagate a vicious cycle of repetitive trauma and incomplete healing.; this might be worsened by frequent dressing replacements, especially in the case of adhesive products. Regarding O_2 emulsions, additional complications pertain to frozen shipping, storage, and specialized conditions prior to liquified administration [Castro and Briceno, 2010]. In turn, hydrogels have been associated with decreased patient compliance, as their elasticity can complicate daily manipulations [Morgan, 1999].

Generally, healing benefits from enhanced oxygenation should be maximized in an adequately moisturized microenvironment [Androjna et al., 2008; Roe et al., 2010]. In our analysis, this was reflected on the inconsistent healing outcomes among indirect approaches to DO, such as O_2 dressings and O_2 hydrogels [Tables S.4 and S.5]. In OUP technologies, comparisons between gel and aqueous formulations also verified a statistically significant benefit for O_2 dissolution in liquid media [Magnetto et al., 2014; Prato et al., 2015]. Meanwhile, *in vivo* oxygenation was significantly improved only after ultrasound application; an effect that was maintained for maximum 15 minutes [Magnetto et al., 2014; Prato et al., 2015]. Effective duration should obviously be prolonged before such technologies can be considered for actual patients. Notably, sonication was administered at the highest therapeutic doses for humans [Table S.2]; this may not only impact patient compliance, but could also raise safety concerns related to membrane permeability and intracellular H_2O_2 accumulation [Juffermans et al., 2006].

2.4.3 | Optimal timing to enhance wound oxygenation

To ensure maximum efficacy, the timing of wound oxygenation should also be investigated. Normally, healing progresses via four universal stages: hemostasis, acute inflammation, proliferation, and remodeling [Singer and Clark, 1999; Gurtner et al., 2008]. Although sequential, these phases are characterized by variable overlapping in terms of participating cellular types [Gurtner et al., 2008]; for this reason, healing experiments are preferably designed *in vivo* to better simulate the actual mechanism, when possible [Boyko et al., 2017]. Successful completion of all the implicated pathways is founded upon adequate O_2 supply. In fact, O_2 contributes to neutrophil chemotaxis [Klyubin et al., 1996], respiratory burst [Babior, 1978], decreased infections [Greif et al., 2000; Belda et al., 2005], enhanced re-epithelialization [Said et al., 2005], angiogenesis [Berthod et al., 2006; Knighton et al., 1983; Sen et al., 2002; Roy et al., 2006], and successful collagen deposition [Kivisaari et al., 1975; Eyre et al., 1984; Stephens and Hunt, 1971]; it also provides sufficient energy throughout tissue repair [Kivisaari et al., 1975; Vihersaari et al., 1974]. In this setting, additional oxygenation could be beneficial regardless of the healing stage. Over the years, this argument has been supported by multiple studies on the healing outcomes of O_2-based therapies, regardless of the technology used [de Smet et al., 2017; Wang et al., 2003]. However, specific effects per healing stage are yet to be fully clarified.

It is widely believed that hypoxia (1-2% O_2) acts beneficially within the first hours following trauma. This was based on its up-regulating effects on dermal fibroblast proliferation [Siddiqui et al., 1996; Falanga and Kirsner, 1993], mobility [Mogford et al., 2002; O'Toole et al., 1997], as well as the expression of transforming growth factor-beta 1 (TGF-1) [Falanga et al., 1991], procollagen [Falanga et al., 1993], collagen [Falanga et al., 2002], platelet-derived growth factor (PDGF) by endothelial cells [Kourembanas et al., 1990], and vascular endothelial growth factor (VEGF) by various implicated cell types [Shweiki et al., 1992]. While the aforementioned data were obtained *in vitro*, they have not been reproduced *in vivo*; in fact, they are substantially blunted *in vivo* to the point of being insignificant to the healing outcome. For example, induction of VEGF expression by hypoxia was significantly lower than the effect of vascular trauma itself [Corral et al., 1999]. Thus, hypoxia was not required to stimulate angiogenesis *in vivo* [Corral et al., 1999]. Variability between *in vitro* and *in vivo* observations can be attributed to multiple parameters affecting normal healing.

Probably the one with the highest clinical relevance, is the subject's age. *In vitro* enhancement of TGF-1, PDGF, and VEGF expression by hypoxia was not reproduced neither in aged wound models *in vivo* [Wu et al., 1999; Corral et al., 1999; Brucker et al., 1996], nor in aged human cell lines [Mogford et al., 2002; Xia et al., 2001]. Since most systemic comorbidities predisposing to non-healing wounds affect older patients, even transient hypoxia might not enhance tissue repair.

From our analysis, early hypoxia should not be over-stressed when applying O_2-based healing therapies. Maximum benefits from O_2 emulsions were recorded until day 4 post-trauma; with the only exception of VEGF production and subsequent angiogenesis, which peaked on day 7 [Li et al., 2013; Li et al., 2015]. Tissue survival was significantly improved only at days 2 and 3 from application of the H_2O_2 dressing by Harrison et al. [Harrison et al., 2007]. Additional data suggest a detrimental effect of hypoxia on hemostasis [Görlach et al., 2000], energy supply [Knighton et al., 1981; Gupta and Raghubir, 2005], and bacterial killing both *in vitro* [Allen et al., 1997] and *in vivo* [Edwards et al., 1984; Niethammer et al., 2009]. These molecular pathways start within the first hours post-trauma. On the other hand, chronic hypoxia is notorious for its catastrophic consequences on the healing process, as summarized in the Introduction section. In combination with the overlapping among healing stages, such data may advocate the necessity of adequate oxygenation as early as possible. Further research in the field is warranted, especially in the *in vivo* and clinical settings.

2.4.4 | Quantification of oxygen requirements for safe and effective healing applications

Furthermore, we should specify the amount of supplementary O_2 permitting uncomplicated healing. Clinically, $TcPO_2$ measurements are already applied as prognostic markers in high-risk wounds [Padberg et al., 1996]. Normal $TcPO_2$ approximates 40mmHg for the subcutaneous, in a 30-40mmHg range; pressures lower than 30mmHg are frequently encountered in acute cutaneous wounds [Chang et al., 1983]. Chronic wounds are typically classified as severely hypoxic, and local O_2 tension (PO_2) fluctuates below the 20mmHg cutoff [Sheffield, 1988; Shah, 2011]. O_2 demands are accentuated by the hyper-metabolic state in all healing tissues; by nature, this energy expenditure is preferentially covered via oxidative phosphorylation [Gupta and

Raghubir, 2005; Matsuda et al., 1987]. Appropriate PO_2 is highlighted by the Km values of key enzymes in the healing mechanism. For example, NADPH oxidase reaches half its maximum efficacy during ROS production at a range of 45-80mmHg [Allen et al., 1997]. At lower values, bactericidal activity of neutrophils is significantly impaired [Edwards et al., 1984; Jonsson et al., 1984], reflecting the downstream effect of decreased NADPH oxidase activity. For the rate-limiting hydroxylases in collagen synthesis, Km is achieved at a PO_2 of 25mmHg [Myllylä et al., 1977]. Collagen deposition by fibroblasts also occurs at a minimum O_2 range of 30-40mmHg. [Myllylä et al., 1977; Hutton et al., 1967]. In fact, both NADPH oxidase and collagen hydroxylases demonstrate a dose-dependent relationship with PO_2, before reaching their maximum effect at approximately 250 and 300mmHg, respectively [Allen et al., 1997; Myllylä et al., 1977]. In a double-blind randomized controlled trial of 500 patients undergoing colonic resection, 50% increase in inspired O_2 concentration was accompanied by an equivalent decrease in surgical wound infections [Greif et al., 2000]. Furthermore, collagen synthesis was directly proportional to local perfusion and ensuing PO_2 in subcutaneous wounds postoperatively [Jonsson et al., 1991]. Angiogenesis may also demonstrate a similar dose-dependent relationship with O_2 [Hopf et al., 2005]. In the experiments by Matsuoka et al., VEGF and PDGF expression showed a linear correlation to O_2 levels, after mixture with “plain” OUB solutions [Matsuoka et al., 2018].

In order for universal clinical applications, an ideal 40mmHg PO_2 cutoff should be maintained efficiently and safely. Duration is determined by physical form, route of administration, wound accessibility, and O_2 consumption in each particular tissue. For example, systemic delivery is limited in cases of local vasculature disruption; such treatments require higher initial doses, so that the resulting O_2 gradient can uniformly supply the entire wound surface. In our analysis, O_2 levels in OUP-enriched gels were substantially lower than in aqueous solutions with the same OUP content [Magnetto et al., 2014; Prato et al., 2015]. Despite the lack of statistical comparisons, O_2 dressings and O_2 hydrogels demonstrated significant inconsistency in healing outcomes [Patil et al., 2016; Patil et al., 2018]. Safety entails manufacturing parameters, as well as adverse sequelae from potential O_2 redundancy [Bert, 1943]. Integration of hyperoxia-

induced biomarkers [Roy et al., 2006] and regular follow-up may ultimately prevent or compensate for hyperoxia risk in healing tissues.

2.4.5 | Methodological variability in the wound healing literature

Methodological variability is an established limitation in the healing literature, and studies evaluating O_2-enhancing treatments are no exception [de Smet et al., 2017]. In our analysis, inconsistencies ranged from the timepoints of endpoint evaluation, the assessment techniques, the absence of control groups, the frequency and dosage of DO technologies, to the wound models themselves. For example, oxygenating outcomes after applying a DO formula have been reported as PO_2, ΔPO_2 (sometimes without the independent numerical measurements), DO concentration, or as ΔDO. Statistical comparisons were sometimes impossible even among similar technologies testing the same endpoint. For example, PO_2 achieved after 15 minutes of ultrasound application on chitosan OLNDs solution [Magnetto et al., 2014] cannot be compared to ΔPO_2 values from dextran OLNDs solutions after 60min [Prato et al., 2015]. Since DO technologies comprise a novel approach towards wound oxygenation, the majority of available data are experimental. Instead of actual wound models, many studies simulated universal healing conditions *in vitro*, typically hypoxia. Thus, clinical translation is currently decelerated by the low LoE of available data. Detailed methodological inconsistencies in the studies we analyzed are collectively illustrated on Table S.1.

2.4.6 | Conclusions and future research needs

From our perspective, systematic analyses like the one presented herein (Chapter 2 of this dissertation) should suggest specific solutions to address the current literature limitations. In order for comparable data and reproducible protocols, worldwide experts need to reach a consensus specifying the basic endpoints in all wound models, as well as the techniques and timepoints for their evaluation; particularly when it comes to healing efficacy, and healing speed. Meanwhile, the following *in vivo* experiments are required prior to extensively testing DO technologies in clinical practice. First, we need a comparative study evaluating “plain” OUBs containing no chemical surfactants, versus OUP solutions in terms of magnitude and

duration of O_2 delivery. All formulations should be applied under identical ambient conditions, with and without brief sonication. A complete experimental design shall incorporate both positive and negative control groups for every healing parameter assessed; all data should be recorded at the same pre-designated timepoints for every group. If properly executed, such a protocol can provide substantial evidence for the most promising DO formulation in wound healing. A subsequent study shall address the optimal route of administration, as well as treatment intervals for the preferred technology. Minimum PO_2 target in the wound bed should be set at 40mmHg, and dosage timeline will be determined by O_2 half-life in the formula applied. Finally, another protocol should be dedicated to the effects of DO during each of the healing phases independently. Such a design will not only validate the true role of acute hypoxia, but also highlight its potential downstream impact on the healing mechanism. Ideally, these experiments should be performed in the same rodent wound model at standardized conditions. Clinical translation would be significantly accelerated if the observed outcomes could be reproduced in a swine model; swine tissue repair is the closest resemblance to human healing [Sullivan et al., 2001]. If still promising, such safety and efficacy data shall expedite randomized clinical trials in the field. Ultimately, bioengineered aqueous formulations may provide a definite solution against a constantly expanding global health issue.

In conclusion, DO-supplying technologies should be further investigated in terms of their clinical potential in enhancing wound oxygenation. “Plain” OUB solutions manufactured without chemical surfactants or exogenous additives, entail a highly-promising approach among the available DO technologies, as they have the technical capacity to establish the appropriate O_2 levels for effective wound oxygenation, with the longest duration, and the best possible safety profile, at least theoretically at this point. Therefore, at this early stage of research and clinical development on this topic, additional and targeted experimental data are required to introduce DO technologies as treatment factors in the rapidly-expanding cohort of complicated wounds globally.

3 | Experimental design and methodology

Parts of the contents of this chapter are also represented in the following submission to *Journal of the American College of Surgeons*:

Dimitrios Ntentakis, Anastasia Maria Ntentaki, Eleni Delavogia, Petroula Seridou, Zoi Kollia, Nikolaos Sfakianos, Victor San Martin Carvalho Corrêa, Patroklos Katafygiotis, Danae Venieri, Nikolaos Arkadopoulos, Nicolas Kalogerakis. Dissolved oxygen and O_2-nanobubble biotechnologies enhance physiologic wound healing and cutaneous regeneration *in vivo*. (2024) *Submitted at Journal of the American College of Surgeons*.

3.1 | Background information

Over the years, numerous experimental protocols have been introduced for evaluating aspects of the healing mechanism, either *in vitro* or *in vivo*. Yet, currently, no consensus has been reached regarding which particular protocol should be prioritized according to the objectives of each research project, nor gold-standard guidelines exist to guide investigators during protocol selection. As a consequence, the literature in the field of wound healing is characterized by notable methodological variability, not only in basic-science but also in clinical protocols. In the systematic analysis of the particular subset of studies testing DO technologies in healing applications, presented in Chapter 2 of this dissertation, we pinpoint the methodological inconsistencies most interesting from an academic perspective, and discuss their role in decelerating, and sometimes even impeding, the clinical translation of novel biotechnologies in wound healing. Also, we highlight another pertinent parameter associated with the same outcome, which is the relative scarcity in data evaluating the healing outcomes of DO technologies *in vivo*, compared to *in vitro* data. However, the inherent complexity of the healing mechanism, which relies on the orchestrated interplay of multiple cellular types and molecular pathways [Gurtner et al., 2008], makes it quite challenging to simulate and accurately evaluate it *in vitro*. Furthermore, to our knowledge, there is no *in vivo* protocol designed to enable a comprehensive investigation of the translational potential of novel biotechnologies in wound healing; which, from our perspective, should include a concurrent examination of engineering fundamentals, quality-control requirements, concerns for biological safety, and a preliminary assessment of healing efficacy.

To collectively address those limitations, in this Chapter we describe the design and rationale behind the construction of an *in vivo* protocol encompassing all the aforementioned components. This protocol was designed as an analogy to early-stage clinical trials, with equal emphasis on the validation of safety for each novel treatment factor tested, along with the evaluation of key endpoints indicating healing efficacy. It comprises a synthesis of standardized methodologies from previous studies, with optimizations as deemed appropriate for the scope of this work. Furthermore, our protocol design prioritizes practicality and simplicity, to the benefit of feasibility and reproducibility; parameters which we consider pivotal for the successful development and testing of novel biotechnologies in particular, as these projects are frequently

carried out by multidisciplinary teams led by biochemical and biomedical engineers, instead of biologists or physician scientists.

For the scope of this dissertation, the proposed protocol has been tailored for the evaluation of two biotechnologies from the category of dissolved oxygen solutions (DOS), manufactured without chemical surfactants or exogenous additives, in terms of their potential benefits in wound healing and cutaneous-regenerating applications. To provide an illustrative example of the minor adjustments that may considered during the concurrent testing of more than one treatment factors, even when they originate from the same technological category, our experimental design has been divided into two sequential phases, Phase 1 and Phase 2. Each phase was conducted independently, and was dedicated to a single DOS biotechnology from the ones tested in this dissertation. A chronological synopsis of this protocol, illustrating key time-points in the DOS manufacturing and quality-control processes, the *in vivo* wound model, and the assessments of biological safety and healing efficacy, is presented in Figure 3.1. All the procedures described herein were conducted under completely sterile conditions, and following sterilization of the equipment used.

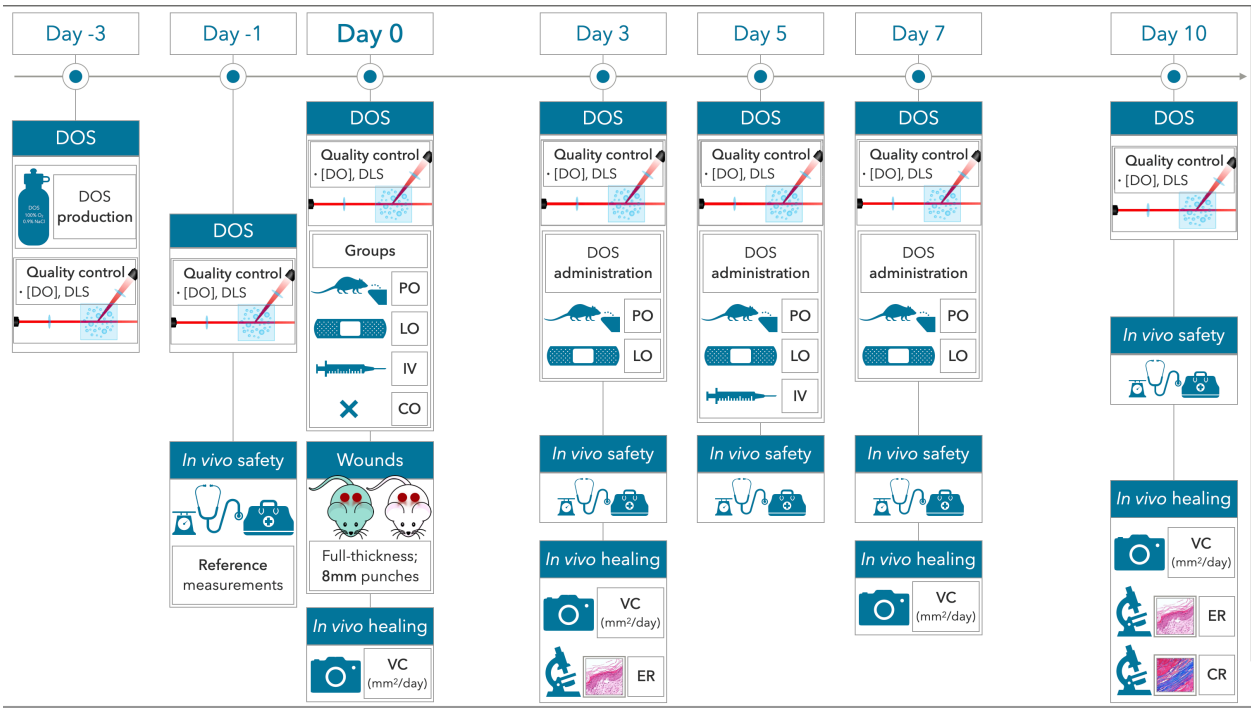

Figure 3.1: **Graphical synopsis of the protocol design of this study, illustrating the key time-points for the production of each DOS biotechnology, the quality-control processes, and the *in vivo* assessments of biological safety and healing efficacy, on a chronological order**. Day -3 marks the time-point when each of the two DOS biotechnologies evaluated in this study, the plain DOS in Phase 1 and the ONBW in Phase 2, were manufactured. Quality control processes were conducted daily and prior to any *in vivo* use, based on the physical parameters specific to each DOS formulation; for instance, [DO] monitoring and DLS screening for the presence of large-diameter (≥28μm) bubbles, were performed daily in both Phases 1 and 2. Additional nanoparticle tracking analyses and zeta-potential recording were conducted exclusively during Phase 2 experiments, to monitor the characteristics of OUBs within the ONBW. To enhance safety prior to any *in vivo* use, detection of at least one bubble with diameter ≥28μm led to exclusion of the corresponding sample from all further experiments. At day 0, two full-thickness cutaneous wounds were simultaneously excised with an 8mm surgical punch per mouse dorsum, under general anesthesia with ketamine (100mg/kg) and xylazine (5mg/kg). Postoperatively, the SKH1 mice were randomly divided to equally-populated, sex-matched experimental groups, according to DOS administration; Phase 1 included 32 mice divided into 4 groups of plain DOS administration (PO, LO, IV, CO), and Phase 2 included 36 mice divided into 3 groups of ONBW administration (PO, IV, CO). IV administration was performed retro-orbitally at days 0 and 5. LO administration was performed via irrigation directly on each wound surface with a syringe, daily, in Phase 1. Mice in the PO group consumed each DOS *ad libitum*. *In vivo* safety was monitored daily, based on severe adverse events and standardized safety and tolerability measures. VC (in mm2/day) was calculated from macroscopic photographs for all the timeframes among days 0, 3, 7, and 10. ER (hematoxylin & eosin) was assessed on days 3 and 10, by dividing the length of re-epithelialization to the length of each wound bed on the horizontal axis. CR (Masson's trichrome) was evaluated on Day 10, by dividing the area of

Figure 3.1 (continued): blue-stained collagen pixels to the total area corresponding to each wound bed. All pertinent methodological details are discussed in the subsequent sections of the main text of this Chapter. **Abbreviations**: DOS, dissolved oxygen solution; [DO], dissolved oxygen concentration in mg/L; DLS, dynamic light scattering; PO, per os intake; LO, local administration; IV, intravenous administration; CO, negative controls; VC, macroscopic velocity of wound closure; ER, histopathologic epithelialization ratio; CR, histopathologic collagenation ratio; ONBW, oxygen nanobubble-enriched water; OUBs, oxygen ultra-fine bubbles.

3.2 | Manufacturing, storage, and quality control of dissolved oxygen solutions

In this dissertation, two distinct engineering approaches for manufacturing a DOS were sequentially employed and tested, both excluding the use of exogenous chemicals and surfactants and conducted under completely sterile conditions. For both formulations, sterile normal saline solution (N/S; 0.9% NaCl) was consistently used as the aqueous medium. The latter was selected because of its non-polarity, the additional flexibility it introduces while testing potential routes of administration *in vivo*, along with preexisting data demonstrating its superiority for manufacturing O_2 super-saturated fluids among the liquid formulations most frequently used clinically [Matsuki et al., 2012; Matsuki et al., 2014]. Collectively, each manufacturing process was repeated at least three times for standardization purposes, at the Laboratory of Biochemical and Environmental Engineering of the School of Chemical and Environmental Engineering of the Technical University of Crete (Chania, Crete, Greece). All the equipment utilized during the manufacturing and quality control processes for each DOS biotechnology had been fully sterilized prior to the start of each experiment, and all the procedures described herein were also conducted under sterile conditions.

The DOS biotechnology studied in Phase 1, is an original formulation containing no physical enhancements to sustain DO concentrations; which is referred to as “plain” DOS, according to our proposed classification system for the DOS biotechnologies being investigated for healing applications, presented in Chapter 2 of this dissertation. At day -3 of our protocol design [Figure 3.1], twenty eight, 500mL, borosilicate (Boro 3.3) glass bottles (IVYX Scientific, Seattle, WA, USA), designed with high anti-corrosive properties and thermal resistance (140^{o}C), were autoclaved at 121^{o}C for 20 minutes, and then filled with sterile N/S. Subsequently, the plain DOS was aseptically produced

via infusion of oxygen gas (O_2) with purity higher than 99.9% into each bottle, via an air diffuser, at a flow rate of 7 L/min, for 10 minutes, under controlled temperature and pressure conditions. The bottles containing the plain DOS were tightly sealed with open-topped screw caps provided by the manufacturer, each integrating a semi-transparent impermeable silicone septum to prevent pressure fluctuations. An additional period of 30 minutes was allowed for effective equilibration of the O_2 gas molecules within the liquid medium. To replace any atmospheric air entrapped within each bottle's headspace, additional infusion of high-purity (>99.9%) O_2 was performed by inserting the sterile 30-gauge needle of an O_2-filled 10mL syringe, through the cap's silicone septum. Then, the caps were encased in laboratory film (Parafilm M; Pechiney Plastic Packaging, Chicago, IL, USA), and all bottles were stored at room temperature and atmospheric pressure. During storage, the 28 identical bottles containing plain DOS were grouped in pairs. Each pair of bottles was randomly assigned to one of the 14 consecutive days in our protocol design [Figure 3.1]. One bottle from each pair was designated to be used for all *in vivo* administrations on each corresponding protocol day. Meanwhile, the duplicate bottle was kept for independent monitoring of DO concentrations and gas-bubble formation for quality-control purposes, on that same protocol day.

The DOS biotechnology tested in Phase 2, was an oxygen nanobubble-enriched water (ONBW) formulation. At protocol day -3 [Figure 3.1], 160 liters of sterile N/S were filtered through 0.2μm pore filters in an isolated tank, which was subsequently connected to a commercially-available device (MK2 Nanobubbler; Fine Bubble Technologies Pty Ltd., Cape Town, South Africa) that generates O_2 ultra-fine bubbles (OUBs). Concurrently, high-purity (>99.9%) O_2 was infused through a different inlet on the same device, at a flow rate of 22L/min, for 30 minutes, resulting in a 10% air/liquid mixture. ONBW was manufactured by continuously recirculating the sterile N/S reservoir through the aforementioned O_2-enriched environment, using a multiphase pump (PBU 201 E10; EDUR, Germany) than enabled high-speed centrifugations within the device. A schematic illustration of the ONBW manufacturing process is presented in Figure 3.2. All the subsequent steps including packaging in sterile glass bottles, time for gas-liquid equilibration, replacement of any atmospheric air within the bottles, storage in pairs, and random assignment of paired bottles to each protocol day, were

performed identically to plain DOS manufacturing in Phase 1, as described in the previous paragraph.

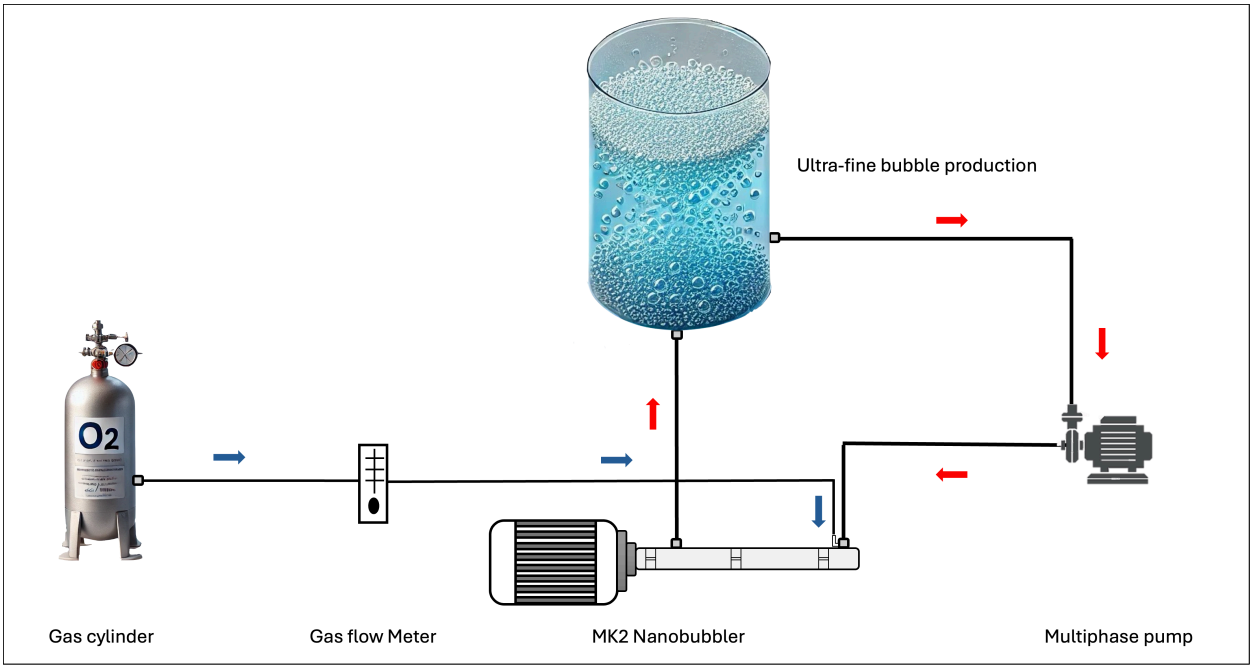

Figure 3.2: **Schematic illustration of the manufacturing process yielding the ONBW, the DOS biotechnology evaluated in experimental Phase 2**. The ONBW was manufactured using a commercially-available device (MK2 Nanobubbler; Fine Bubble Technologies Pty Ltd., Cape Town, South Africa). The latter generates O_2 ultra-fine bubbles (OUBs) by continuously recirculating 160 liters of sterile N/S with high-purity (>99.9%) O_2, infused from a different inlet at a flow rate of 22L/min, via a patented high-speed centrifugation device, for a period of 30 minutes. **Abbreviations**: DOS, dissolved oxygen solution; ONBW, oxygen nanobubble-enriched water.

In both Phases 1 and 2, quality control processes were focussed on ensuring that each DOS biotechnology could achieve enhanced DO concentrations, with appropriate sustainability for biomedical applications, while being safe for *in vivo* use. DO concentrations, expressed in mg/L, were recorded in each DOS biotechnology, daily. For comparison purposes, DO measurements were also performed in samples of regular N/S containing no additional O_2, which were stored in similar 500mL glass bottles and under the same conditions as the corresponding DOS biotechnology tested. The aforementioned measurements were obtained using a standardized optical DO probe (HQ30d Portable Meter Kit; Hack, Düsseldorf, Germany), also fitted with

pressure and temperature sensors. Regarding safety, dynamic light scattering (DLS) analyses were conducted daily (SALD-7500nano; Shimadzu Corporation, Columbia, MD, USA), to screen for larger-diameter bubbles (≥28μm) as a prognosticator of the potential risk of gas embolism from any naturally-forming bubbles. The 28μm-diameter cutoff was adopted from the minimum acceptable size specifications of the filter pores used in clinical-grade extracorporeal membranous oxygenation (ECMO) devices [Barak and Katz, 2005]. Detection of even a single large-diameter bubble (≥28μm) was considered unacceptable, and the corresponding sample was excluded from further experiments.

Also, the following quality-control procedures were exclusively conducted in the ONBW during Phase 2, as they pertain to the physics specifically characterizing OUB-enriched solutions. Mean OUB concentration, diameter, and size distribution were measured every other day via nanoparticle tracking analysis (Nanosight, Malvern, UK), and were evaluated as additional safety indicators. Also, the zeta potential was monitored every other day due to its documented correlation with OUB physical stability within aqueous solutions [Tsuge, 2014], using an electrophoresis instrument (Zetasizer Nano ZS90; Malvern, UK).

3.3 | Animal model

In vivo wound-healing experiments were conducted in SKH1 hairless mice, as in previous studies [Lim et al., 2006; Benavides et al., 2009]; animal characteristics were wild type, aged between 8 and 12 weeks, with a female to male ratio of one to one (sex-matched). The hairless SKH1 mouse strain was selected due to its naturally atrophic hair follicles, which eliminate the necessity for skin shaving prior to wound excision and, thus, any associated cutaneous irritations causing additional stress to the animals. Also, an equal number of female and male mice was consistently used, to neutralize any potentially-confounding effects associated with gender-related differences in the healing outcomes [Ashcroft, 2004; Gilliver et al., 2008; Grada et al., 2018]. All the mice used in this study were born and raised in the same certified facility (National Center for Scientific Research (NCSR) Demokritos; Athens, Greece), to minimize external confounders. Since their birth, and throughout the duration of each *in vivo* experiment, the mice were housed in a temperature-controlled environment

(22-25°C), on a 12:12 hour light-dark cycle, and provided with food and water *ad libitum*.

Prior to the start of each *in vivo* experiment, mice of the same sex were housed in groups of three to five. From protocol day 0 [Figure 3.1], when the excisional wounds were created, and throughout the period of *in vivo* testing and data collection for each DOS biotechnology, every mouse was housed separately to decrease the risk of post-operative infections. The aforementioned living conditions, and all the procedures described in the following subsections, were pre-approved by the Institutional Animal Care and Use Committee of the NCSR Demokritos, as well as the Decentralized Administration of Attica, Greece in accordance with the Directive 2010/63/EU of the European Parliament on the Protection of Animals Used for Scientific Purposes [European Parliament, 2010].

3.4 | *In vivo* wound model

Surgical procedures for cutaneous wound excision were based on standardized protocols for evaluating the healing mechanism in mice [Wang et al., 2013; Chen et al., 2015], with occasional adaptations according to the specific objectives of this work. At protocol day 0, the dorsal skin surface of each mouse was sequentially disinfected with 10% povidone iodine solution (wt/vol; #40000-040; Cardinal Health, Dublin, OH, USA), and 70% ethanol solution (vol/vol; #40000-040; Pharmco; Greenfield Global Inc., Shelbyville, KY, USA), applied sequentially. General anesthesia was induced with an intra-peritoneal (IP) injection of a solution containing ketamine (100 mg/kg) and xylazine (5 mg/kg), using a dose of 10μL per gram of body mass [Zhao et al., 2016]. Subsequently, two full-thickness cutaneous wounds were simultaneously excised with an 8mm biopsy punch (Acu-Punch; Acuderm, Ft. Lauderdale, FL, USA) per mouse dorsum, at approximately 3mm below the shoulder blades, as previously described [Wang et al., 2013; Chen et al., 2015]. In the immediate post-operative period, the wounds were covered with a sterile transparent dressing (Tegaderm; 3M, St. Paul, MN, USA) [Wang et al., 2013; Chen et al., 2015] to minimize the risk of infection, and each mouse was monitored until complete recovery from surgery and general anesthesia. All wounds were evaluated on a daily basis, throughout the remaining duration of each *in vivo* experiment, until protocol day 10 [Figure 3.1]. The procedures were performed at

the certified facility of the NCSR Demokritos, under standardized and sterile conditions. A stepwise guide, including technical and procedural details involved in the excision and monitoring of the wounds, is presented in Table 3.4 at the final section of this Chapter.

For the research objectives of this dissertation, in accordance with the rationale of this protocol, an acute wound model was preferred to assess the biological safety and preliminary healing efficacy of both the plain DOS and the ONBW. Of note, it has been suggested that, disruptions in any of the earliest physiological stages implicated in the healing response, namely inflammation, proliferation, and remodeling, can be considered among the strongest predictors of downstream wound chronicity, recurrence, and relevant complications [Fowler, 1990; Singh et al., 2004]. Therefore, while experimental testing of the aforementioned DOS biotechnologies in chronic wounds is pending, the translational relevance of the data extracted using this protocol is not necessarily affected by the non-complicated natural history of the wounds.

Furthermore, the splinting manipulation described in the established protocol by Wang and colleagues [Wang et al., 2013], with overlaid silicone rings sutured in healthy skin along the wound perimeter, was omitted. This decision was based on more recent insights regarding the role of contraction in rodent cutaneous healing [Chen et al., 2015; Park et al., 2015], the increasing adoption of a similar non-splinting approach by numerous recent studies in the field [Lim et al., 2006; Valacchi et al., 2011; Tiganescu et al., 2014; Öri et al., 2017; Seo et al., 2021; Yampolsky et al., 2024], and our strong emphasis on animal well-being. Indeed, the described protocol eliminates the additional surgical manipulations and physical stress associated with the splinting process, thus significantly reducing total surgical time, general anesthesia duration, and dosing. Therefore, it aligns with the principles of the 3Rs (Replacement, Reduction, Refinement) for *in vivo* experiments, as designated by the European Regulations [Russell and Burch, 1959; European Parliament, 2010], without compromising the validity of the experimental data referring to the healing mechanism [Chen et al., 2015; Park et al., 2015; Yampolsky et al., 2024]. A representative wound created with the aforementioned protocol on the dorsum of an SKH1 mouse, also illustrating the macroscopic image scale, is presented in Figure 3.3.

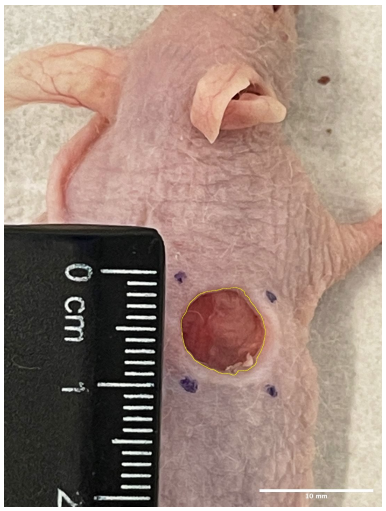

Figure 3.3: **A representative wound created with the described protocol, photographed in the immediate postoperative period, at Day 0.**

3.5 | Experimental groups and treatment administration

Identifying the most appropriate routes of administration, based on the collective interpretation of data on biological safety, tolerability, and healing efficacy is a pivotal step during the development of any novel treatment factor. Thereby, the route of DOS administration was the only criterion applied to determine the different experimental groups, in both Phases 1 and 2. In Phase 1, 32 SKH1 mice (wild type, 8-12 weeks old, 1:1 female:male), were randomly divided to four treatment groups based on plain DOS administration: intravenous (IV), local (LO), per os (PO), and negative controls (CO). Analogously, in Phase 2, 36 SKH1 mice (wild type, 8-12 weeks old, 1:1 female:male), were randomly assigned to three treatment groups according to ONBW administration: IV, PO, and CO.

For IV administration, each mouse was injected 150μL of plain DOS (Phase 1) or ONBW (Phase 2) in the retro-bulbar sinus, using a sterile 1mL syringe and a 30-gauge needle, according to a standardized protocol for retro-orbital injections [Yardeni et al., 2011]. As illustrated on Figure 3.1, two injections were administered per mouse in the IV group of each experiment: the first at day 0, under the general anesthesia that had already been induced preoperatively, and the second at day 5, under general anesthesia with 2% isoflurane gas. The 150μL IV dose was considered safe, according to mammal body water homeostasis; and was verified by approximating the intra-

vascular volume of a 25g mouse as a function of extra-cellular fluid (ECF) volume and body mass, by adapting the following equation from human physiology [Goljan, 2013]:

$$ECF(ml) = 20/100 * (BodyMass) = 20/100 * 25g = 5ml$$

For LO administration (Phase 1), 500μL of plain DOS were directly irrigated on each wound surface, with a sterile 1mL syringe. A 30-gauge needle was used to tangentially approach the wound bed, by carefully sliding through an opening created between the healthy skin surrounding each wound, and the transparent wound dressing (Tegaderm; 3M, USA). LO administration was performed on a daily basis, under general anesthesia with either ketamine and xylazine at day 0, or with 2% isoflurane gas during protocol days 1-9. In the PO groups, either plain DOS (Phase 1) or ONBW (Phase 2) was directly used *in lieu* of drinking water, and the mice consumed it *ad libitum* throughout the duration of each *in vivo* experiment, from day 0 to day 10. The volume of fluid intake was systematically recorded for all mice in the PO groups, daily. Finally, mice in the CO groups received no treatment; with the exception of local washing of the wound surface with sterile N/S, as needed.

3.6 | *In vivo* safety assessment

As in the case of every novel treatment factor tested clinically, our protocol was designed to thoroughly assess the biological safety and tolerability of the two DOS biotechnologies containing no exogenous chemicals, the plain DOS and the ONBW. For this purpose, we carefully selected and evaluated standardized endpoints that could accurately represent the health status and well-being of the mice used in our experiments [Bachmanov et al., 2002]. Those are collectively presented in Table 3.1, alongside the precise criteria, schedule, and grading systems employed to evaluate each corresponding safety/tolerability endpoint: body weight, food and water intake, burrowing behavior, spontaneous behavior, posture, breathing, behavior after provocation/weighing, movement after provocation/weighing, as well as the condition of the coat, body, eyes, and wounds [Deacon, 2006; Arras et al., 2007; National Research Council, 2009; Hohlbaum et al., 2018].

Furthermore, incidence of any of the following 7 complications was considered as a severe adverse event (AE) in our protocol: 1) death, 2) local inflammation/infection persisting for more than 24 hours, 3) occurrence of non-healing cutaneous wounds/ulcers, 4) hemorrhage from any orifice that was unresponsive to treatment, 5) water consumption less than 5mL for more than 24 hours, 6) decrease in body mass equal or higher than 15% of the original measurement recorded at day 0, and 7) combination of abnormalities in physical appearance and behavior [Table 3.1]. A pictorial overview of the endpoints used to assess animal safety, tolerability, and the incidence of AEs is presented in Figure 3.4.

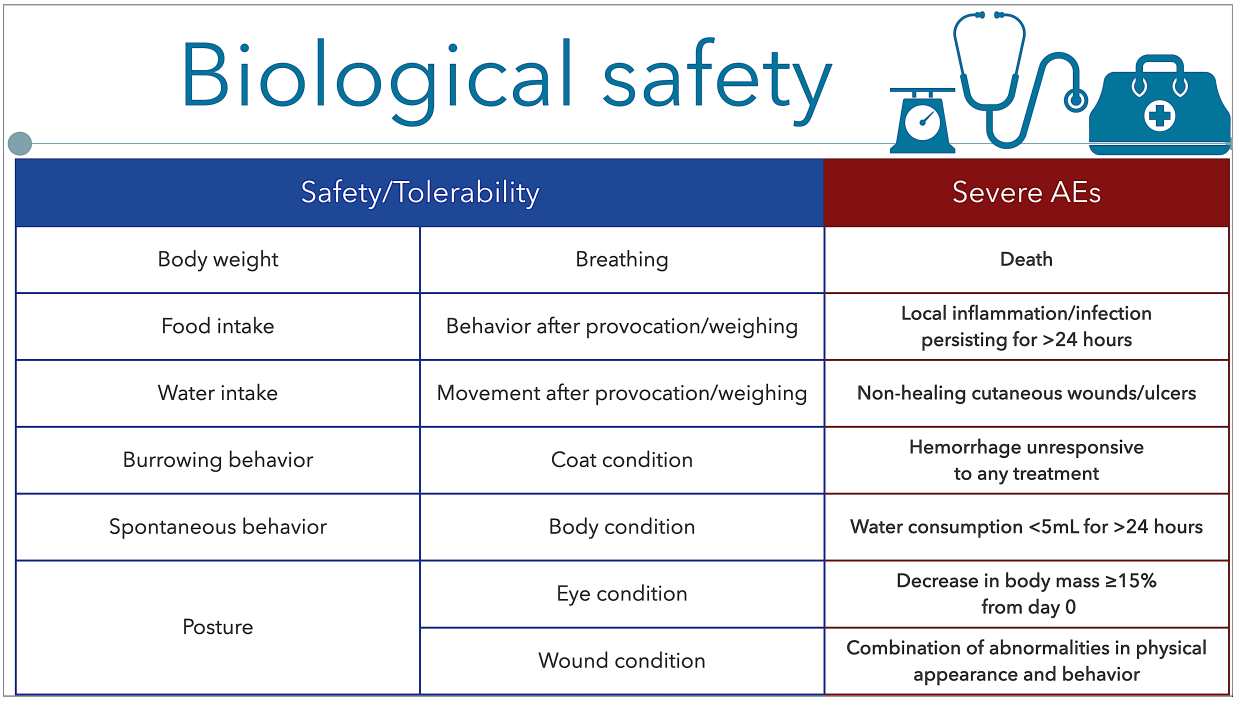

Figure 3.4: **Pictorial overview of the endpoints used to comprehensively assess animal safety, tolerability, and the incidence of severe adverse events.**

In both Phases 1 and 2, daily monitoring of the aforementioned safety and tolerability outcomes was conducted by two investigators independently, by filling predetermined checklists containing the scoring systems for grading each outcome, as summarized in Table 3.1. All safety assessments were consistently performed prior to any *in vivo* experiment scheduled for that same protocol day.

Table 3.1: Systematic criteria for the evaluation of *in vivo* safety, tolerability, and severe adverse-event rates following either plain DOS or ONBW administration during Phase 1 or Phase 2 experiments, respectively.

	Evaluation methods	Time-points	Grading/scoring/ documentation
Well-being & tolerability parameters			
Body weight	Recorded in g	Day 0 (pre-operatively); Day 3; Day 10	N/A
Food intake [1]	Recorded in g; expressed in g of food intake per 30g of body weight	24h before each corresponding body weight measurement (Day -1; Day 2; Day 9)	N/A
Water intake [1]	Recorded in mL; expressed in mL of water intake per 30g of body weight	24h before each corresponding body weight measurement (Day -1; Day 2; Day 9)	N/A
Burrowing behavior [2]	Observation in a clean cage, 2h after placing a standardized burrow filled with 200g of food pellets; expressed as the percentage (%) of food pellets displaced from the burrow after 2h	48h prior to excisional wound creation (Day -2), and each experimental day involving administration of anesthesia (Day 0; Day 3; Day 7)	**Normal**: Approximately 60g of food pellets burrowed/displaced
Spontaneous behavior [3]	Observation, recorded in a blinded manner by 3 examiners	Daily, between 7:30 and 8:30am	**Score 0**: Sudden movements, backwards movements, transient involuntary muscular contraction of any body part, kicking with hind paws, licking/biting the wound **Score 1**: Sleeping, resting, digging, running, walking, rearing, climbing, eating, drinking, grooming, sniffing;

	Evaluation methods	Time-points	Grading/scoring/ documentation
Posture [3]	Observation, recorded in a blinded manner by 3 examiners	Daily, between 7:30 and 8:30am	**Score 0**: Hunched, arched back, crouched **Score 1**: Lying, sitting, moving;
Breathing [3]	Observation, recorded in a blinded manner by 3 examiners	Daily, between 7:30 and 8:30am	**Score 0**: Exerted, irregular **Score 1**: Undisturbed, regular;
Behavior after provocation/ weighing [3]	Observation, recorded in a blinded manner by 3 examiners	Daily, between 7:30 and 8:30am	**Score 0**: Apathetic, sedated, highly aggressive, increased vocalization **Score 1**: Alert, ready to take flight;
Movement after provocation/ weighing [3]	Observation, recorded in a blinded manner by 3 examiners	Daily, between 7:30 and 8:30am	**Score 0**: Decelerated/slowed, crawling, immobile, lameness, tiptoe gait **Score 1**: No aberration in moving pattern;
Coat condition [3]	Observation, recorded in a blinded manner by 3 examiners	Daily, between 7:30 and 8:30am	**Score 0**: Ruffled, dirty, unkempt, piloerection, hair loss (alopecia) **Score 1**: Clean, smooth, well-groomed;
Body condition [3]	Observation, recorded in a blinded manner by 3 examiners	Daily, between 7:30 and 8:30am	**Score 0**: Sunken flanks, swollen areas, ascites **Score 1**: Good, unchanged as judged from external appearance;
Eye condition [3]	Observation, recorded in a blinded manner by 3 examiners	Daily, between 7:30 and 8:30am	**Score 0**: Discharge **Score 1**: Clear, bright;
Wound condition [3]	Observation, recorded in a blinded manner by 3 examiners	Daily, between 7:30 and 8:30am	**Score 0**: Dirty, bloody, uncleaned, signs of self-injury, signs of inflammation/necrosis, i.e., unusual color (e.g., red, pale) or swollen **Score 1**: Clean, dry, smooth;
Severe adverse events			

	Evaluation methods	Time-points	Grading/scoring/ documentation
Death [4]	Observation and physical examination	Daily, throughout each experimental day	Adverse event recorded upon incidence of **≥1 case**
Local inflammation/ infection for >24h [4]	Observation of redness, swelling, signs of pain/ discomfort; reported in a blinded manner by 3 examiners	Daily, between 7:30 and 8:30am	Adverse event recorded upon incidence of **≥1 case**
Non-healing cutaneous wounds/ulcers	Observation, reported in a blinded manner by 3 examiners	Daily, between 7:30 and 8:30am	Adverse event recorded upon incidence of **≥1 case**
Hemorrhage from any orifice, unresponsive to treatment [4]	Observation, reported in a blinded manner by 3 examiners	Daily, between 7:30 and 8:30am	Adverse event recorded upon incidence of **≥1 case**
Water consumption <5mL for >24h	Observation, reported in a blinded manner by 3 examiners	Daily, between 7:30 and 8:30am	Adverse event recorded upon incidence of **≥1 case**
Decrease in body mass ≥15% of day 0 measurement [4]	Observation, reported in a blinded manner by 3 examiners	Daily, between 7:30 and 8:30am	Adverse event recorded upon incidence of **≥1 case**

	Evaluation methods	Time-points	Grading/scoring/ documentation
Abnormal physique & behavior [4]	Observation, reported in a blinded manner by 3 examiners	Daily, between 7:30 and 8:30am	Adverse event recorded upon incidence of **≥1 case** of the following **combination**: 1) poor physical appearance (hair, posture, grunting); 2); abnormal behavior (mobility, unconsciousness, unsolicited vocalizations, self-mutilation); 3) abnormal/exaggerated responses to external stimuli

Table 3.1 Notes: For the safety and tolerability criteria that were not assessed daily, the evaluation time-points correspond to the protocol days designated in our experimental design, applying to both Phases 1 and 2; for reference, Day 0 is the time-point when all cutaneous wounds were excised, and thus, the starting point of each *in vivo* experiment. Assessments for severe adverse events were conducted daily, by documenting the absolute number of cases corresponding to each event, per time-point. Water consumption was also monitored daily, due to the presence of PO-treated mice in both Phases 1 and 2, which consumed each corresponding DOS tested *ad libitum*. [1], evaluation methods, time-points, and grading/scoring systems adapted from *Hohlbaum et al., 2018*; [2], evaluation methods, time-points, and grading/scoring systems adapted from *Deacon, 2006(a)*; [3], evaluation methods, time-points, and grading/scoring systems adapted from *Arras et al., 2007*; [4], evaluation methods, time-points, and grading/scoring systems adapted from the *National Research Council, Humane Endpoints for Animals in Pain, 2009*. **Abbreviations**: DOS, dissolved oxygen solution; ONBW, oxygen nanobubble-enriched water; g, grams; h, hours; mL, milliliters; N/A, not applicable.

3.7 | Macroscopic quantification of the velocity of wound closure

To evaluate the velocity of wound closure (VC) macroscopically, both wounds of each mouse were photographed (iPhone 12 Pro Max, Wide 5.1mm lens [26mm equivalent], f/1.6, 5.6x zoom), at a set distance (25cm), under standardized lighting conditions, using a dedicated photography station. Photographs were taken at four time-points: at day 0 postoperatively, under the general anesthesia induced with ketamine and xylazine prior to wound excision, and at days 3, 7, and 10 under general anesthesia with 2% isoflurane gas, for 45-60 seconds [Wang et al., 2013]. At each time-point, three photographs were taken per mouse, for reference: the first illustrated both wounds symmetrically, the second focussed on the right-sided wound, and the third focussed on the left-sided wound. The transparent wound dressing (Tegaderm;

3M, USA) was not removed for photography, unless it was substantially deformed or detached; in which cases, photographs were taken before and after complete removal of the old dressing, as well as following the placement of a new dressing, up to day 7. At days 7 and 10, all photographs were taken without dressings, as the majority of them had been almost entirely removed by the animals. With this approach, standardized photographs from all the wounds, with or without the dressing, were available at each time-point; thus reducing variability, and the potentially confounding effect from the presence of the dressings on the subsequent statistical analyses.

The photographs were analyzed using the open-source Fiji software [Schindelin et al., 2012]. The stepwise mathematical process for calculating VC is illustrated in Figure 3.5. First, open wound surface at a time-point x (OWS_x), expressed in square millimeters, was measured manually with the Fiji freehand tool, and automatically using a custom Fiji macro. Each OWS value represented the wound surface area not covered by macroscopically visible epithelium, at a specific time-point in our experimental design [Figure 3.1]. The automated measurements were only used as a tool to externally validate the wound measurements recorded manually; with the latter considered more accurate in general, as they do not rely exclusively on image segmentation and color difference. Unless there was a difference ≥10% in the OWS measurements of the same wound in the photograph illustrating both wounds from that mouse symmetrically, versus the photograph focussing on that particular wound, the OWS value kept for further analyses was from the photograph illustrating both wounds symmetrically, to enhance standardization among all wounds. Similarly, the OWS measurements analyzed further were the ones recorded manually with the Fiji freehand tool, unless there was a ≥10% difference from the automatic OWS measurement of the same wound; in which cases, the average of the 2 measurements (manual and automatic) for that particular wound was recorded, and used for all subsequent calculations. In the second step, the absolute value of wound closure was calculated for each wound, as the difference in the OWS values (ΔOWS) between two specific time-points in our protocol, as previously described [Wang et al., 2013; Park et al., 2015]. Finally, the velocity of wound closure (VC; mm^2/days) was determined by dividing the wound closure values to each corresponding timeframe, between two of

the four time-points in our protocol design (days 0, 3, 7, 10) [Figure 3.1], using the following equation:

$$VC = \Delta OWS / \Delta t$$

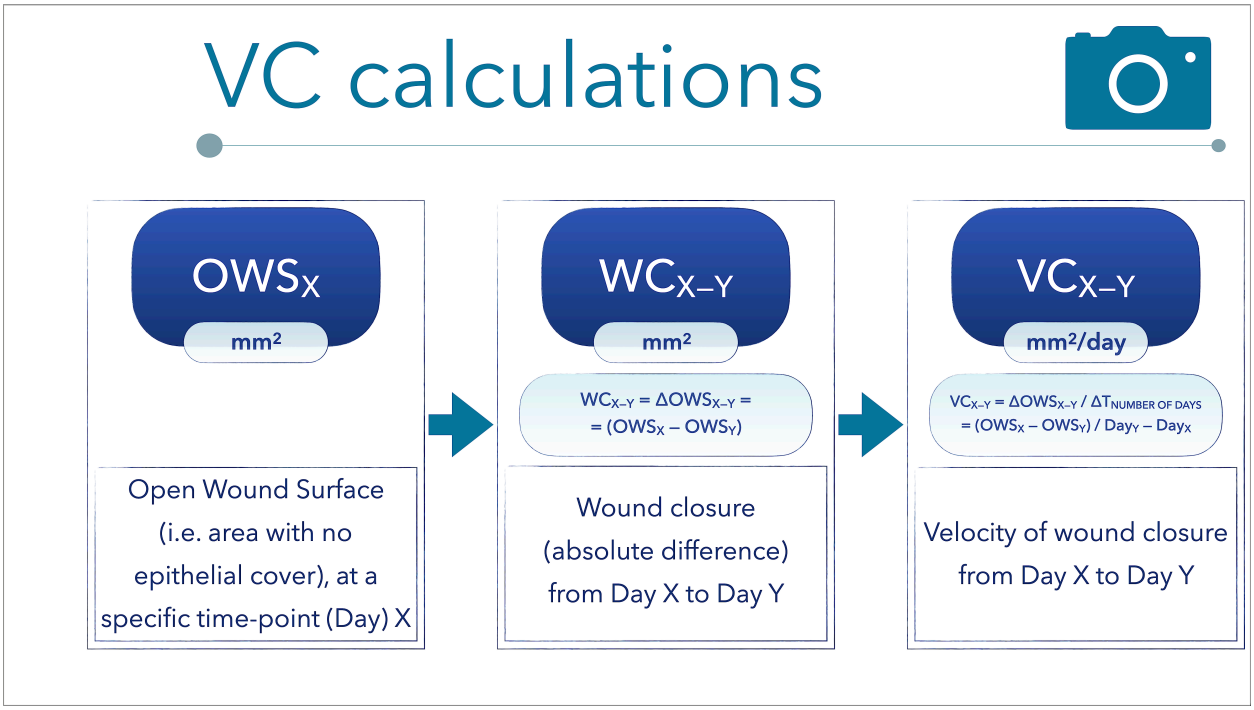

Figure 3.5: **The stepwise mathematical equations for calculating macroscopic velocity of wound closure (VC), as an endpoint for preliminarily assessing healing efficacy**. Macroscopic velocity of wound closure (VC), expressed in mm²/day, was determined based on measurements of open wound surface at each protocol day x (OWSx, mm²). The difference (ΔOWSx-y, mm²) between days x and y represented the area of wound closure during the corresponding timeframe between days x and z. This difference was then divided by the corresponding timeframe (Δtx-y, days) to calculate VC (VC = ΔOWSx-y/Δtx-y, mm²/days).

3.8 | Tissue harvesting and processing for histopathology studies

Specimens for histopathological analyses were collected at two time-points, day 3 and day 10 [Wang et al., 2013]. At day 3, an equal number of female and male mice from each experimental group were randomly selected to be euthanized via IP injection of a lethal dose (50μL/g) from the ketamine/xylazine solution used for preoperative anesthesia [section 3.4 *In vivo* wound model], followed by cervical dislocation. The number of animals sacrificed at protocol day 3 represented half of the total number of animals from each experimental group; for example, in Phase 1 experiments, 2 female

mice and 2 male mice were randomly euthanized from each group (PO, LO, IV, CO) at day 3, which originally included 8 mice at day 0 (4 females and 4 males). Then, upon careful detachment of the transparent dressing when applicable, a rectangular cutaneous flap surrounding the original wound areas with approximately 5-10mm uninjured margins at each direction, was excised with a sterile No. 11 surgical blade. Each flap contained both cutaneous wounds from each mouse, as well as the underlying subcutaneous and *panniculus carnosus* layers. Immediately after excision, each specimen was placed on the crude surface of qualitative filter paper (Whatman Qualitative Filter Paper; Sigma-Aldrich, Inc., St. Louis, MO, USA), so that it could retain its original horizontal configuration. The next step was fixation in 10% formalin solution (37% formaldehyde) for 48 hours; then, the specimens were stored in 70% ethanol solution, until they were embedded in paraffin. The process was supervised by our team's pathologist (PK), and remained blinded to the other investigators. At day 10, the same process was repeated for the remaining mice in each experimental group. The subsequent embedding, sectioning, and staining processes were performed by an external collaborator (iHisto, Inc., Salem, MA, USA).

3.9 | Histopathologic quantification of epithelialization and collagenation

Paraffin-embedded, 5μm-thick sections were stained with hematoxylin and eosin (H&E) or Masson's trichrome according to established protocols [Schrementi et al., 2008; Chen et al., 2013; Zhao et al., 2016], for histopathologic evaluation of two fundamental pathways in the cutaneous healing mechanism, epithelialization and collagenation, respectively. Whole slide imaging (Bright-field; MoticEasyScan Infinity 60; Motic Hong Kong Limited, Kowloon, Hong Kong) was performed by an external collaborator (iHisto, Inc., USA), to produce digital slides which integrate continuous optical magnification up to the equivalent of a 40x objective lens. The digital slides were initially evaluated using the open-source QuPath software [Bankhead et al., 2017], and high-resolution static images were exported for further analyses with Fiji [Schindelin et al., 2012], at a magnification scale of 200-500μm, similarly to slide photomicrography. The wound margins were determined based on the established anatomical landmarks for SKH1 mouse skin [Öri et al., 2017; Seo et al., 2021], and

independently verified by a pathologist. A rectangle shape was drawn to demarcate each wound area.

Epithelialization was quantified with H&E staining at two time-points, days 3 and 10. For each wound, the epithelialization ratio was determined by measuring the length of the epithelialized wound bed (El), represented by a horizontal red line on each slide, which was divided by the length of the original wound area (Wl), represented by a different black (Phase 1)/dark blue (Phase 2) line on the same slide, using Fiji. The following equation was used:

$$Epithelialization = El/Wl$$

Collagenation was quantified with Masson's trichrome staining at day 10, as it represents a more advanced healing stage compared to epithelialization [Gurtner et al., 2008]. The amount of blue-stained collagen deposited in each wound bed was measured using Fiji, in a two-step process. First, we demarcated the entire wound bed using the Fiji freehand tool, and measured the total number of pixels. Then, we applied contrast and color thresholds to precisely isolate blue-stained pixels exclusively within the wound bed, using an preexisting Fiji plugin and a custom Fiji command line (macro available upon request). The collagenation ratio was determined by the number of blue pixels (Cp) divided by the total number of pixels (Wp) in each wound bed, using the following equation:

$$Collagenation = Cp/Wp$$

All the aforementioned quantifications of epithelialization and collagenation were performed in a blinded manner with regards to the experimental group, by two investigators. By definition, image scale was eliminated as a variable from all our histopathological analyses, as the numbers used for the calculation of each ratio originated from the same image, and were obtained under the exact same magnification.

3.10 | Statistical analyses

As previously recommended for studies evaluating novel treatment factors, sample size was calculated based on the law of diminishing returns for Phase 1 experiments, [Festing and Altman, 2002], and using g*power analysis for Phase 2 experiments (available upon request) based on the healing-related data extracted from Phase 1; because the two treatment factors evaluated in this work belong to the same biotechnological category, as described in Chapter 2 of this dissertation. Normality of distribution and homogeneity of variance were studied with the Kolmogorov-Smirnov, Shapiro-Wilk, and Levene's tests, using IBM SPSS Statistics (Version 27) and Prism (GraphPad 9.0, San Diego, CA, USA). Subsequent statistical analyses and graphical illustrations were conducted using Prism.

Daily measurements of DO concentrations were compared between each DOS biotechnology and a regular N/S solution, using the independent-samples t-test or the Mann–Whitney U test, according to each sample's distribution. *In vivo* safety and tolerability data were qualitatively evaluated, based on standardized outcome measures and categorical scoring systems collectively summarized in Table 3.1 [Arras et al., 2007; National Research Council, 2009; Hohlbaum et al., 2018]. DOS route of administration served as the only independent variable in the analyses of all *in vivo* data. Investigators were blinded to experimental groups during the analyses of all data pertaining to healing outcomes. Of the two excisional wounds per mouse dorsum, one was randomly selected to be analyzed as a biological replicate. Data referring to macroscopic and histopathologic assessments of healing efficacy (VC, ER, CR) were described as mean ± standard deviation (SD) or mean ranks, depending on each dataset's normality of distribution. Normally distributed data were analyzed using one-way analysis of variance (ANOVA) followed by Tukey's honest significant difference (HSD) test, or Brown-Forsythe and Welch ANOVA followed by Dunnett's T3 test, depending on each sample's homogeneity of variance. Non-normally distributed data were analyzed using the non-parametric version of one-way ANOVA on ranks (Kruskal-Wallis H test), followed by Dunn's multiple comparisons test. Each set of VC comparisons referred to a specific timeframe between two of the predesignated time-points in our experimental design, namely days 0, 3, 7, and 10 [Figure 3.1]. Analyses of the histopathologic outcomes, ER and CR, were specific to each corresponding time-point (day 3, day 10). The cutoff for statistical significance was defined as $p<0.05$.

3.11 | Procedural guides

This section presents a collection of stepwise procedural guides, formatted as tables, each dedicated to one of the main experimental manipulations required to successfully conduct the described protocol. The enclosed tables can be used as a surgical/procedural checklist by researchers using this protocol, to ensure that all experimental steps are executed in the appropriate sequence while also having immediate access to important technical details.

Table 3.2: Distribution and number of SKH1 mice per experimental group during Experimental Phase 1.

Experimental Groups (Experimental Phase 1)	Route of plain DOS administration	Dosing frequency of plain DOS	Initial sample size per group (n_0)	Sample size at the time of the 1st biopsy (n_3)	Sample size at the time of the 2nd biopsy (n_{10})
1.I (LO)	Local administration of 1mL of plain DOS to each wound surface	Daily	8	8	4
1.II (IV)	Intravascular injection of 0.15mL retro-orbitally	1) Day 0 2) Day 5 (1 injection every 5 days, beginning on day 0)	8	8	4
1.III (PO)	Per os intake *ad libitum*, plain DOS *in lieu* of drinking water	Daily (*ad libitum*)	8	8	4
1.IV (CO)	N/A (rinsed with N/S PRN)	N/A	8	8	4

Abbreviations: DOS, dissolved oxygen solution; n_0, number of laboratory animals on day 0; n_3, number of laboratory animals on postoperative day 3; n_{10}, number of laboratory animals on postoperative day 10; N/A, not applicable; N/S, normal saline solution NaCl 0.9%; PRN, per needed.

Table 3.3: Distribution and number of SKH1 mice per experimental group during Experimental Phase 2.

Experimental Groups (Experimental Phase 2)	Route of ONBW administration	Dosing frequency of ONBW	Initial sample size per group (n_0)	Sample size at the time of the 1st biopsy (n_3)	Sample size at the time of the 2nd biopsy (n_{10})
2.I (IV)	Intravascular injection of 0.15mL retro-orbitally	1) Day 0 2) Day 5 (1 injection every 5 days, beginning on day 0)	12	12	6
2.II (PO)	Per os intake *ad libitum*, ONBW *in lieu* of drinking water	Daily (*ad libitum*)	12	12	6
2.III (CO)	N/A (rinsed with N/S PRN)	N/A	12	12	6

Abbreviations: ONBW, oxygen nanobubble-enriched water; n_0, number of laboratory animals on day 0; n_3, number of laboratory animals on postoperative day 3; n_{10}, number of laboratory animals on postoperative day 10; N/A, not applicable; N/S, normal saline solution NaCl 0.9%; PRN, per needed.

Table 3.4: Surgical procedures on day 0 and parameters of the excisional wound model implementation across experimental Phases 1 and 2.

Surgical Procedures (day 0)	Implementation in the Proposed Protocol
Wound Model	Full-thickness excision wound model on the dorsal skin of the mouse
Anesthetic Solution for General Anesthesia	In a total volume of 5 mL, 4.25 mL of sterile N/S is mixed with 0.5 mL of ketamine solution (100 mg/mL) and 0.25 mL of xylazine solution (10 mg/mL). In the resulting 5 mL anesthetic solution, the concentration of ketamine is 10 mg/mL and that of xylazine is 0.5 mg/mL.

Surgical Procedures (day 0)	Implementation in the Proposed Protocol
Induction of General Anesthesia	Using a 1mL syringe, 0.1mL of the anesthetic solution (N/S solution containing 10mg/mL ketamine and 0.5mg/mL xylazine) will be administered IP per 10g of body weight. Each mouse will receive a dose of 100mg/kg ketamine and 5mg/kg xylazine. The depth of anesthesia will be monitored based on the response to the pedal reflex.
Preoperative Surgical Site Preparation	1) povidone-iodine solution 2) 70% (vol/vol) ethanol
Number of Wounds per Mouse	2 per mouse (created simultaneously using a skin punch biopsy)
Wound Diameter	8mm (punch biopsy diameter: Acu Punch, Acuderm, Ft. Lauderdale, FL)
Splinting (Suturing of Silicone Rings)	N/A
Hemostasis	Local application of light pressure PRN
Postoperative Surgical Site Disinfection	70% (vol/vol) ethanol application around the wounds
Postoperative Analgesia	1) 20ml bupivacaine 0.25% w/v (immediately after surgery, and PRN on days 1-14) 2) carprofen 0.005mg/g SC (for additional analgesia PRN, on days 1-14)
Wound Coverage	Sterile transparent dressing (Tegaderm; 3M, St. Paul, MN, USA)
Antibiotic Administration	PRN, only in cases of postoperative infections (after day 0), in consultation with the facility's veterinary team
Anesthesia recovery	1) Monitoring well-being and recovery for the first 40 minutes postoperatively 2) Heating pads PRN, for the first 20-40 minutes postoperatively
Monitoring	Daily monitoring of animal safety and tolerability parameters, and the incidence of severe AEs throughout each Experimental Phase (days 0-10), as detailed in **Table 3.1**

Abbreviations: N/S, normal saline solution NaCl 0.9%; IP, intraperitoneal administration; N/A, not applicable; PRN, per needed; SC, subcutaneous injection; AEs, adverse events.

Table 3.5: Steps followed for each route of administration of plain DOS (Phase 1) and ONBW (Phase 2) in animal models.

Route of DOS Administration	Execution Steps
Local Irrigation to the Wound Surface	1) If the mouse is not already anesthetized—> induce anesthesia with 2% isoflurane gas 2) Carefully position the needle of a 1 mL syringe tangentially between the transparent wound dressing (Tegaderm; 3M, USA) covering the wounds and the mouse's skin 3) Using a 1 mL syringe, irrigate each wound with 1 mL of plain DOS (Phase 1), maintaining a smooth injection flow without applying high pressure
Intravascular Administration (retro-orbitally)	1) Immobilize the mouse following the procedure used for IP injections (stabilize the mouse by grasping the dorsal skin and pulling toward the midline → in the case of retro-orbital injections, this handling should expose part of the mouse's orbit) 2) Inject 0.15mL plain DOS (Phase 1) or ONBW (Phase 2) retro-orbitally per mouse using a 1 mL syringe
Per Os Intake (ad libitum)	Plain DOS (Phase 1) or ONBW (Phase 2) will be provided *in lieu* of drinking water in the respective cages, and the mice will consume it *ad libitum* daily throughout the duration of the *in vivo* experiment, from day 0 to day 10

Abbreviations: DOS, dissolved oxygen solution; ONBW, oxygen nanobubble-enriched water; IP, intraperitoneal administration.

Table 3.6: Steps for performing euthanasia and subsequent specimen collection at the time-points specified for each experimental Phase.

Experimental Procedures	Execution Steps
Euthanasia	1) Using a 2 mL syringe, administer IP a lethal dose (50µL/g) from the anesthetic solution used for preoperative anesthesia on day 0 (N/S solution containing 10mg/mL ketamine and 0.5mg/mL xylazine) 2) Assess the pedal reflex 60 seconds after IP administration of the anesthetic solution 3) Complete the euthanasia by cervical dislocation → carefully ensuring no pressure is applied to the wounds under study.

Experimental Procedures	Execution Steps
Biopsy Sampling	1) Collect a rectangular cutaneous flap, extending to the subcutaneous and *panniculus carnosus* layers, containing both wounds with approximately 5-10mm uninjured margins at each direction, with a sterile No. 11 surgical blade 2) Place the specimen on the crude surface of qualitative filter paper (Whatman Qualitative Filter Paper; Sigma-Aldrich, Inc., St. Louis, MO, USA), to retain its original horizontal configuration 3) Fix the tissue sample in 10% (vol/vol) formalin solution for 48h; then submerge the specimen in 70% (vol/vol) ethanol solution until histopathological processing

Abbreviations: IP, intraperitoneal administration; N/S, normal saline solution NaCl 0.9%.

Table 3.7: Sequential steps for the macroscopic assessment of wound healing in animal models, at the time-points specified for each experimental Phase.

Macroscopic Assessment	Execution Steps
Wound Photography (days 0, 3, 7, 10)	1) Anesthesia a. On day 0 mice will already be anesthetized with preoperative administration of 0.1mL of the anesthetic solution (N/S solution containing 10mg/mL ketamine and 0.5mg/mL xylazine) per 10g of body weight IP b. For mice that will undergo euthanasia for biopsy collection —> using a 2 mL syringe, administer IP a lethal dose (50μL/g) from the anesthetic solution used for preoperative anesthesia on day 0 (N/S solution containing 10mg/mL ketamine and 0.5mg/mL xylazine) c. For mice that will not undergo euthanasia at the given time-point —> induce anesthesia with 2% isoflurane gas 2) Pedal reflex assessment to determine the depth of anesthesia 3) At days 0 and 3—> photographs were taken without removal of the transparent wound dressing (Tegaderm; 3M, USA); in case it was substantially deformed or detached, photographs were taken before and after complete removal of the old dressing, and following the placement of a new dressing. At days 7 and 10—> photographs were taken without dressings (almost entirely removed by the animals). 4) Capture the wounds from a set distance (25cm) under standardized lighting conditions, using the same device and settings (iPhone 12 Pro Max, Wide 5.1mm lens [26mm equivalent], f/1.6, 5.6x zoom) at a dedicated photography station. Take three photographs per mouse at each time-point: one illustrating both wounds symmetrically, one focussing on the right-sided wound, and one focussing on the left-sided wound. 5) Completion of the Procedure a. For mice that will undergo euthanasia for biopsy collection → proceed with euthanasia and biopsy collection b. For mice that will not undergo euthanasia at the given time-point → return the mouse to its cage and monitor for anesthesia recovery

Macroscopic Assessment	Execution Steps
Collection of Macroscopic Data & Evaluation of Primary Endpoints	1) **ΔOWSx-y (mm²)**: Using Fiji software, calculate OWS open wound surface at each time-point x (OWSx, mm²) for all wounds. Then, the absolute value of wound closure between two specific time-points x and y is calculated as the difference in the OWS values on these time-points (ΔOWSx-y), following the formulas illustrated in **Figure 3.5** —> assessment of the speed and efficacy of the healing mechanism 2) **VCx-y (mm²/days)**: Calculate by dividing the absolute value of wound closure between time-points x and y (ΔOWSx-y, mm²) by the corresponding timeframe (Δtx-y, days) , following the formulas illustrated in **Figure 3.5** —> assessment of the speed and efficacy of the healing mechanism

Abbreviations: N/S, normal saline solution NaCl 0.9%; IP, intraperitoneal administration; ΔOWSx-y, change in open wound surface (OWS, mm²), calculated as the difference between OWSy and OXSx values measured on the corresponding y and x time-points; OWS, open wound surface, expressed in mm²; VCx-y, velocity of wound closure during the timeframe Δty-x= Day y - Day x, calculated based on the ΔOWSx-y during the corresponding timeframe; Δtx-y, timeframe calculated as Day y - Day x, expressed in days.

Table 3.8: Experimental procedures per day of Experimental Phases 1 and 2.

Time-point	Experimental Procedures

Day 0	• Weigh each animal and assess for well-being parameters
	• Surgically induce wounds on the dorsal skin of the mice [excisional wound model, no splinting, coverage with transparent wound dressing (Tegaderm; 3M, St. Paul, MN, USA)] → under general anesthesia
	• Wound Photography
	• Plain DOS (Phase 1) or ONBW (Phase 2) administration via the route of administration designated for each experimental group in the respective Experimental Phase, following the steps presented on **Table 3.5**
	  • local irrigation
	  • intravascular
	  • per os (*ad libitum*, *in lieu* of drinking water)
	• Monitoring of anesthesia recovery for each animal
	• Place the animals in cages (1 mouse/cage to reduce the risk of wound infections)

Time-point	Experimental Procedures

Day 1	• Safety and well-being assessment of each animal
	• Record and treat any postoperative complications (e.g., pain, infection)
	• Plain DOS (Phase 1) or ONBW (Phase 2) administration via the route of administration designated for each experimental group in the respective Experimental Phase, following the steps presented on **Table 3.5**
	  • local irrigation
	  • per os (Plain DOS or ONBW provided is replaced with sealed plain DOS or ONBW, respectively)

Day 2	• Safety and well-being assessment of each animal
	• Record and treat any postoperative complications (e.g., pain, infection)
	• Plain DOS (Phase 1) or ONBW (Phase 2) administration via the route of administration designated for each experimental group in the respective Experimental Phase, following the steps presented on **Table 3.5**
	  • local irrigation
	  • per os (Plain DOS or ONBW provided is replaced with sealed plain DOS or ONBW, respectively)

Day 3	• Safety and well-being assessment of each animal
	• Record and treat any postoperative complications (e.g., pain, infection)
	• Wound Photography (**Table 3.7**)
	• Plain DOS (Phase 1) or ONBW (Phase 2) administration via the route of administration designated for each experimental group in the respective Experimental Phase, following the steps presented on **Table 3.5**
	  • local irrigation
	  • per os (Plain DOS or ONBW provided is replaced with sealed plain DOS or ONBW, respectively)
	  • Euthanasia and biopsy collection (**Table 3.6**)

Day 4	• Safety and well-being assessment of each animal
	• Record and treat any postoperative complications (e.g., pain, infection)
	• Plain DOS (Phase 1) or ONBW (Phase 2) administration via the route of administration designated for each experimental group in the respective Experimental Phase, following the steps presented on **Table 3.5**
	  • local irrigation
	  • per os (Plain DOS or ONBW provided is replaced with sealed plain DOS or ONBW, respectively)

Day 5	• Safety and well-being assessment of each animal
	• Record and treat any postoperative complications (e.g., pain, infection)
	• Plain DOS (Phase 1) or ONBW (Phase 2) administration via the route of administration designated for each experimental group in the respective Experimental Phase, following the steps presented on **Table 3.5**
	  • local irrigation
	  • intravascular
	  • per os (Plain DOS or ONBW provided is replaced with sealed plain DOS or ONBW, respectively)

Time-point	Experimental Procedures

Day 6	• Safety and well-being assessment of each animal
	• Record and treat any postoperative complications (e.g., pain, infection)
	• Plain DOS (Phase 1) or ONBW (Phase 2) administration via the route of administration designated for each experimental group in the respective Experimental Phase, following the steps presented on **Table 3.5**
	  • local irrigation
	  • per os (Plain DOS or ONBW provided is replaced with sealed plain DOS or ONBW, respectively)

Day 7	• Safety and well-being assessment of each animal
	• Record and treat any postoperative complications (e.g., pain, infection)
	• Wound Photography (**Table 3.7**)
	• Plain DOS (Phase 1) or ONBW (Phase 2) administration via the route of administration designated for each experimental group in the respective Experimental Phase, following the steps presented on **Table 3.5**
	  • local irrigation
	  • per os (Plain DOS or ONBW provided is replaced with sealed plain DOS or ONBW, respectively)

Day 8	• Safety and well-being assessment of each animal
	• Record and treat any postoperative complications (e.g., pain, infection)
	• Plain DOS (Phase 1) or ONBW (Phase 2) administration via the route of administration designated for each experimental group in the respective Experimental Phase, following the steps presented on **Table 3.5**
	  • local irrigation
	  • per os (Plain DOS or ONBW provided is replaced with sealed plain DOS or ONBW, respectively)

Day 9	• Safety and well-being assessment of each animal
	• Record and treat any postoperative complications (e.g., pain, infection)
	• Plain DOS (Phase 1) or ONBW (Phase 2) administration via the route of administration designated for each experimental group in the respective Experimental Phase, following the steps presented on **Table 3.5**
	  • local irrigation
	  • per os (Plain DOS or ONBW provided is replaced with sealed plain DOS or ONBW, respectively)

Day 10	• Safety and well-being assessment of each animal • Record and treat any postoperative complications (e.g., pain, infection) • Wound Photography (**Table 3.7**) • Euthanasia and biopsy collection (**Table 3.6**)

Abbreviations: DOS, dissolved oxygen solution; ONBW, oxygen nanobubble-enriched water.

4 | Plain dissolved oxygen solution (DOS) biotechnology for excisional wounds *in vivo*

The contents of this chapter are also represented in the following submission to *Journal of the American College of Surgeons*:

Dimitrios Ntentakis, Anastasia Maria Ntentaki, Eleni Delavogia, Petroula Seridou, Zoi Kollia, Nikolaos Sfakianos, Victor San Martin Carvalho Corrêa, Patroklos Katafygiotis, Danae Venieri, Nikolaos Arkadopoulos, Nicolas Kalogerakis. Dissolved oxygen and O_2-nanobubble biotechnologies enhance physiologic wound healing and cutaneous regeneration *in vivo*. (2024) *Submitted at Journal of the American College of Surgeons*.

4.1 | Background information

Non-healing wounds comprise an insidious yet burgeoning global health issue, underlined by the rapid increase in pertinent healthcare costs [Walmsley, 2002; Sen et al., 2009]. Their etiopathogenesis and prognosis have been consistently linked to tissue hypoxia [Shandall et al., 1985; Sheridan et al., 1987; Sano and Ichioka, 2015], highlighting the established role of adequate oxygenation in the successful completion of the healing mechanism [Tandara and Mustoe, 2004; Rodriguez et al., 2008]. Interestingly, numerous *in vitro* and *in vivo* studies have described a strongly negative correlation between the duration of hypoxia, and the physiological activity of multiple pathways mediating wound restoration [Hohn et al., 1976; Edwards et al., 1984; Jönsson et al., 1988; Siddiqui et al., 1996; Allen et al., 1997; Hopf et al., 2005]. Meanwhile, any disruption in the pathways defining the most upstream healing stages, namely inflammation, proliferation, and remodeling, can be considered as a strong predictor of downstream wound chronicity, recurrence, and relevant complications [Fowler, 1990; Singh et al., 2004]. Epidemiological urgency is associated with the rising prevalence in systemic vasculopathies predisposing to peripheral ischemia and suboptimal healing, such as diabetes [International Working Group on the Diabetic Foot, 2003; International Diabetes Federation, 2015], the aging world population [Wu et al. 1999; Gottrup, 2004], along with the questionable capacity of current management and prevention strategies to confront a generalized escalation in persisting wounds [Das and Baker, 2016].

To address the anticipated escalation in clinical demands, biotechnologies supplying dissolved oxygen (DO) are currently investigated as novel management strategies. Apart from enhancing wound oxygenation, what makes DO use particularly intriguing in healing applications is the potential to significantly improve treatment intervals, safety, and patient compliance compared to the clinically-established technologies supplying gaseous oxygen (O_2), such as hyperbaric O_2 therapy (HBOT) [Wang et al., 2003; de Smet et al., 2017]. However, achieving a biologically significant outcome without using potentially toxic chemical surfactants to prolong DO half-life remains one of the biggest challenges in the DO field.

Hence, in this Chapter, we study an O_2-saturated, aqueous-based DO solution (DOS), which we refer to as plain DOS, since it contains no physical enhancements to sustain DO levels. We discuss the technical and quality-control fundamentals for the plain DOS, manufactured by employing the principles of the gas-liquid interphase while eschewing the use of chemical additives. Subsequently, we evaluate its suitability for biomedical applications by daily monitoring DO concentrations and the diameter of any naturally-forming gas bubbles, over a consecutive fourteen-day period. Also, we analyze macroscopic and histopathological endpoints to characterize its safety profile, and to preliminarily assess its healing efficacy in full-thickness excisional mouse wounds, while identifying the most effective routes of administration. Collectively, our findings suggest that a plain DOS with the described specifications can deliver high DO concentrations consistently and sustainably, while being safe for *in vivo* administration and showing promising efficacy in physiologic wound healing.

4.2 | Methods

This section provides an overview of the experimental design and methodology followed while conducting this work, which corresponds to the experimental Phase 1 discussed in Chapter 3 of this dissertation. Extended description of the manufacturing and quality control processes employed for producing the plain DOS, along the *in vivo* wound model, our endpoint selection for evaluating safety and healing efficacy, and our analytical methods accompanied by the underlying scientific rationale, per case, are detailed in Chapter 3 of this dissertation. A graphical timeline of the protocol design, encompassing all the endpoints assessed along with the main time-points corresponding to each assessment, is illustrated in Figure 4.1. A pictorial overview of key methodological parameters implicated in the experiments of Phase 1 is presented in Figure 4.2.

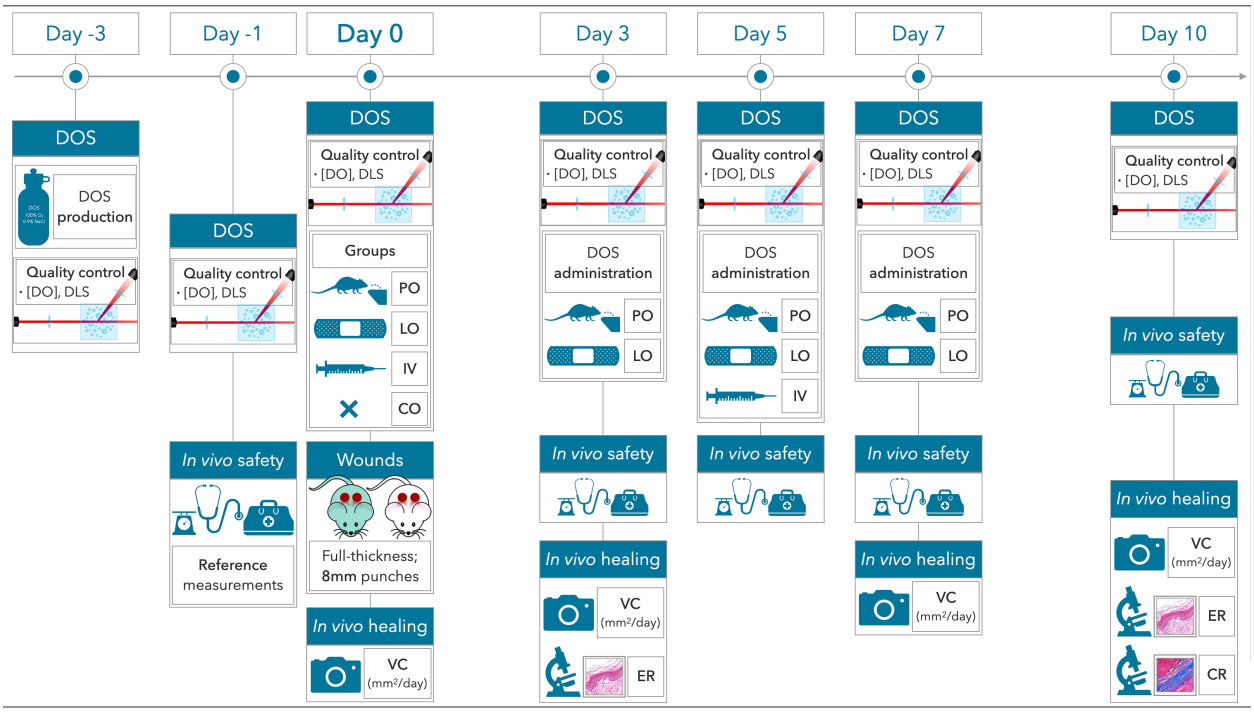

Figure 4.1: **Graphical synopsis of the protocol design of experimental Phase 1, illustrating the key timepoints corresponding to the production of the plain DOS biotechnology, the quality-control processes, and the *in vivo* assessments of biological safety and healing efficacy, on a chronological order**. Plain DOS was manufactured on day -3 of the protocol timeline, followed by quality-control processes which were conducted daily and prior to any *in vivo* use. The latter included daily [DO] measurements (in mg/L), and DLS screening for the presence of large-diameter (≥28μm) bubbles; detection of at least one bubble with diameter ≥28μm led to exclusion of the corresponding plain DOS sample from all further experiments. At day 0, two full-thickness cutaneous wounds were simultaneously excised with an 8mm surgical punch per mouse dorsum, under general anesthesia with ketamine (100mg/kg) and xylazine (5mg/kg). Postoperatively, the SKH1 mice were randomly divided to 4 equally-populated, sex-matched experimental groups (PO, LO, IV, CO), according to plain DOS administration starting from day 0. IV administration was performed retro-orbitally, at days 0 and 5. LO administration was performed via irrigation directly on each wound surface with a syringe, daily. Mice in the PO group consumed the plain DOS *in lieu* of drinking water, *ad libitum*. The mice in the negative control (CO) group received no treatment, as there is no gold-standard treatment intervention for wound healing clinically. *In vivo* safety was monitored daily, based on severe adverse events and standardized safety and tolerability measures. VC (in mm^2/day) was calculated from macroscopic photographs for all the timeframes among days 0, 3, 7, and 10. ER (hematoxylin & eosin) was assessed on days 3 and 10, by dividing the length of re-epithelialization to the length of each wound bed on the horizontal axis. CR (Masson's trichrome) was evaluated on Day 10, by dividing the area of blue-stained collagen pixels to the total area corresponding to each wound bed. All pertinent methodological details are detailed in Chapter 3 of this dissertation, whereas key points are summarized in section 4.2 of this Chapter. **Abbreviations**: DOS, dissolved oxygen solution; [DO], dissolved oxygen concentration in mg/L; DLS, dynamic light scattering; PO, per os intake; LO, local administration; IV, intravenous administration; CO, negative controls;

Figure 4.1 (continued): VC, macroscopic velocity of wound closure; ER, histopathologic epithelialization ratio; CR, histopathologic collagenation ratio; ONBW, oxygen nanobubble-enriched water; OUBs, oxygen ultra-fine bubbles.

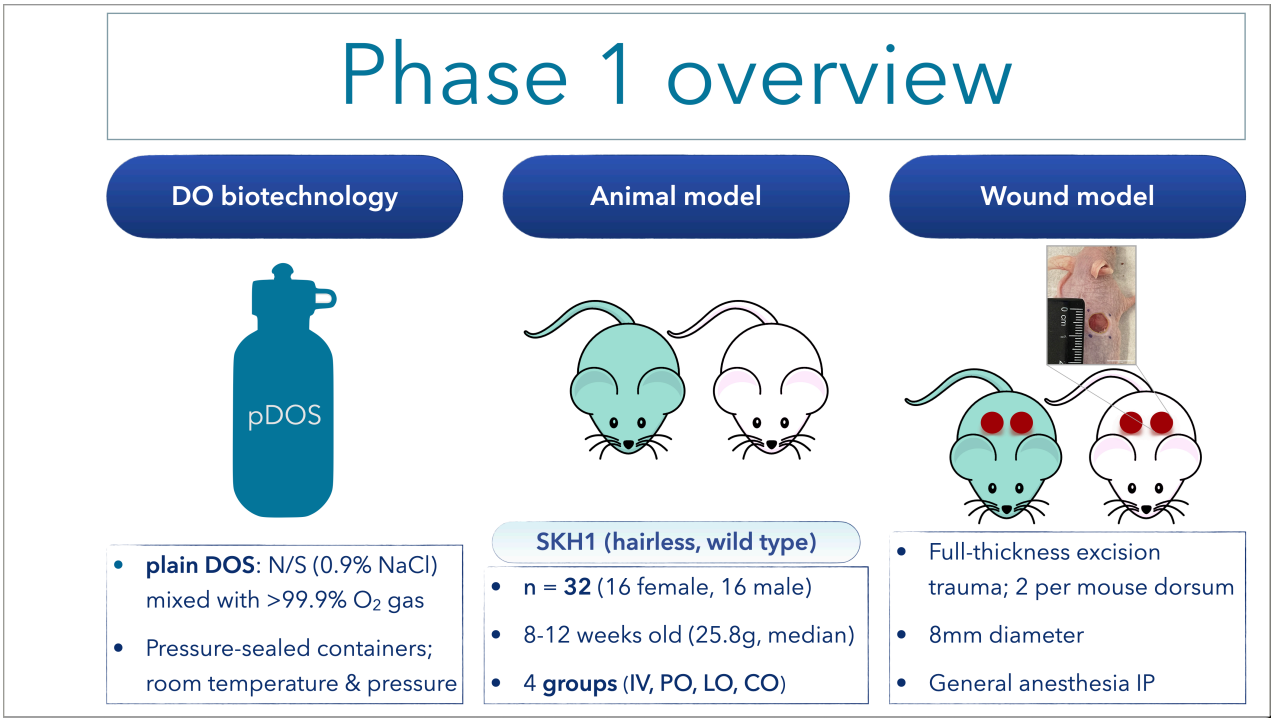

Figure 4.2: **Synoptic overview of the DOS biotechnology, the animal parameters, and the wound model used in experimental Phase 1**. **Abbreviations**: DO, dissolved oxygen; DOS, dissolved oxygen solution; pDOS, plain dissolved oxygen solution; N/S, normal saline (0.9% NaCl); PO, per os intake; LO, local administration; IV, intravenous administration; CO, negative controls; IP, intraperitoneally.

4.2.1 | Study approval

Plain DOS manufacturing and quality-control processes were approved by the Laboratory of Biochemical Engineering and Environmental Biotechnology of the School of Chemical and Environmental Engineering, at the Technical University of Crete (Technical University of Crete; Chania, Greece). Animal procedures and experiments were approved by the Institutional Animal Care and Use Committee of the National Center for Scientific Research (NCSR) Demokritos (NCSR Demokritos; Athens, Greece), and the Decentralized Administration of Attica, Greece, in accordance with the Directive 2010/63/EU of the European Parliament on the Protection of Animals Used for Scientific Purposes [European Parliament, 2010].

4.2.2 | Manufacturing, storage, and monitoring of the plain DOS

The DOS biotechnology studied in experimental Phase 1 contained no physical enhancements to sustain DO concentrations, while excluding the use of exogenous chemicals and surfactants *a priori*; thereby, it was referred to as "plain" DOS, according to our proposed classification system analyzed in Chapter 2 of this dissertation. At protocol day -3 [Figure 4.1], the plain DOS was aseptically produced via infusion of high-purity (>99.9%) O_2 into sterile normal saline solution (N/S; 0.9% NaCl), at a flow rate of 7 L/min, for 10 minutes, under controlled temperature and pressure conditions.

Regarding quality control, the plain DOS was packaged in tightly-sealed, autoclaved, 500mL, borosilicate glass bottles (IVYX Scientific, Seattle, WA, USA) to minimize oxygen losses from contact with atmospheric air, and stored at room temperature and pressure. DO concentrations, expressed in mg/L, were recorded daily for the plain DOS and a regular N/S solution used for comparisons, under identical physical parameters, using standardized equipment (HQ30d Portable Meter Kit; Hack, Düsseldorf, Germany). Also, dynamic light scattering (DLS) analyses were conducted daily (SALD-7500nano; Shimadzu Corporation, Columbia, MD, USA), to screen for larger-diameter bubbles (≥28μm) as a prognosticator of the potential risk of gas embolism from any naturally-forming bubbles.

4.2.3 | Animals and *in vivo* wound model

Thirty two SKH1 hairless mice (wild type, 1:1 female:male), with a median weight of 25.31g (8-12 weeks old), were randomly divided to four treatment groups according to plain DOS administration: intravenous (IV), local (LO), per os (PO), and negative controls (CO). At day 0, two full-thickness cutaneous wounds were simultaneously excised with an 8mm biopsy punch (Acu-Punch; Acuderm, Ft. Lauderdale, FL, USA) per mouse dorsum, under general anesthesia with ketamine (100 mg/kg) and xylazine (5 mg/kg), as previously described [Wang et al., 2013; Chen et al., 2015]. Postoperatively, the wounds were covered with a sterile transparent dressing (Tegaderm; 3M, St. Paul, MN, USA) to minimize the risk of infection, and each mouse was monitored until complete recovery from surgery and anesthesia. In each treatment group, the plain DOS was administered after successful recovery from surgery and

anesthesia at day 0, and then prior to the daily assessments of biological safety until protocol day 10 [Figure 4.1]. All wounds were daily evaluated throughout the remaining duration of each *in vivo* experiment, until day 10 [Figure 4.1].

4.2.4 | Experimental groups and plain DOS treatment administration

IV administration was performed in the retro-bulbar sinus, using a standardized technique [Yardeni et al., 2011]. Each mouse was injected 150μL of plain DOS, twice in total during experimental Phase 1: once at day 0, and then at day 5, under general anesthesia. For LO administration, 500μL of plain DOS were directly irrigated on each wound surface underneath the transparent dressing, under general anesthesia, daily. In the PO group, the plain DOS was used *in lieu* of drinking water, which the mice consumed *ad libitum* throughout the duration of each experiment [Figure 4.1]. Mice in the CO groups received no treatment.

4.2.5 | *In vivo* safety and healing endpoints

All mice were monitored for their safety and well-being daily, based on standardized scoring systems characterizing tolerability and adverse events (AEs) [Arras et al., 2007; National Research Council, 2009; Hohlbaum et al., 2018; Supplement S.6]. Specifically, 13 well-being parameters were evaluated: body weight, food and water intake, burrowing behavior, spontaneous behavior, posture, breathing, behavior after provocation/weighing, movement after provocation/weighing, as well as the condition of the coat, body, eyes, and wounds [Deacon, 2006; Arras et al., 2007; National Research Council, 2009; Hohlbaum et al., 2018]. Additionally, the occurrence of the following 7 conditions, characterized as severe AEs, was cautiously monitored: 1) death, 2) local inflammation/infection persisting for more than 24 hours, 3) occurrence of non-healing cutaneous wounds/ulcers, 4) hemorrhage from any orifice that was unresponsive to treatment, 5) water consumption less than 5mL for more than 24 hours, 6) decrease in body mass equal or higher than 15% of the original measurement recorded at day 0, and 7) combination of abnormalities in physical appearance and behavior. Collectively, the aforementioned endpoints used to assess animal safety, tolerability, and the incidence of AEs, alongside the criteria, timeline, and

grading systems applied for evaluating each of them, are presented in Table 3.1 and Figure 3.4 of Chapter 3 of this dissertation.

Regarding healing efficacy, all wounds were photographed at days 0, 3, 7, and 10, under standardized conditions. The macroscopic velocity of wound closure (VC, in mm^2/days) was assessed from measurements of the wound surface area obtained from these photographs, in correlation with each of the timeframes among days 0, 3, 7, and 10, the key predetermined time-points of this protocol. Furthermore, wound specimens containing the mouse skin and subcutaneous in healthy margins were collected at days 3 and 10, for histopathological analyses of epithelialization (Hematoxylin/eosin; day 3, day 10) and collagenation (Masson's trichrome; day 10) ratios.

4.2.6 | Statistics

Statistical analyses and graphical illustrations were conducted using IBM SPSS Statistics (Version 27) and Prism (GraphPad 9.0, San Diego, CA, USA). DO concentrations were compared between the plain DOS biotechnology and regular N/S, using the independent-samples t-test. Route of administration of the plain DOS served as the only independent variable in the analyses of *in vivo* data. *S*afety and tolerability data were qualitatively evaluated, based on standardized outcome measures and categorical scoring systems [Arras et al., 2007; National Research Council, 2009; Hohlbaum et al., 2018]. Investigators were blinded to experimental groups during the analyses of all data pertaining to healing outcomes. Of the two excisional wounds per mouse dorsum, one was randomly selected to be analyzed as a biological replicate. Data assessing healing outcomes (VC, ER, CR) were described as mean ± standard deviation (SD) or mean ranks, according to each sample's distribution; subsequently, they were analyzed using one-way analysis of variance (ANOVA) followed by Tukey's honest significant difference (HSD) test, or the non-parametric version of one-way ANOVA on ranks (Kruskal-Wallis H test) followed by Dunn's multiple comparisons test, respectively. Each set of macroscopic VC comparisons referred to a specific timeframe between two of the predesignated timepoints in our experimental design, namely days 0, 3, 7, and 10 [Figure 4.1]. Histopathological comparisons were specific to each corresponding timepoint (day 3, day 10). The cutoff for statistical significance was defined as $p<0.05$.

4.3 | Results

4.3.1 | Enhanced DO concentrations are maintained in the plain DOS consistently for 14 days

Given the established role of oxygen as a prerequisite for physiological wound healing [Tandara and Mustoe, 2004; Rodriguez et al., 2008], we evaluated both the magnitude and the sustainability of DO concentrations in the plain DOS. Mean DO concentrations were significantly higher in the plain DOS versus the regular N/S solution used as comparator (22.87mg/L versus 6.78mg/L, $p<0.001$), upon daily measurements for 14 consecutive days under identical physical parameters [Table 4.1]. Moreover, DO concentrations remained consistently enhanced in the plain DOS throughout the duration of *in vivo* experiments, for 14 days [Figure 4.3]. The corresponding graph plotting DO concentrations in the plain DOS versus time, in Figure 4.3, can be divided in three segments; an initial segment spanning the first 6 protocol days, which showed an anticipated decline in DO concentrations based on the principles determining gas dissolution, a second segment where DO concentrations appeared to reach a plateau close to the median DO concentration at approximately 21.27mg/L on protocol day 7, at one week since plain DOS production, and a final segment with slowly-declining DO levels until protocol day 10. Based on these data, we hypothesized that the plain DOS would be capable of effectively supplying DO to tissues throughout our *in vivo* experiments, and, secondarily, contribute to the healing mechanism.

Table 4.1: **Consecutive measurements of DO concentrations in the plain DOS and the control saline solution per protocol day, along with the corresponding physical conditions of temperature and pressure, and an overview of the subsequent statistical analysis**.

Time-point	[DO] in pDOS (mg/L)	[DO] in control N/S (mg/L)	Temperature (°C)	Pressure
Day -3	30.76	7.23	25.4	Atmospheric
Day -2	25.84	7.11	26.1	Atmospheric
Day -1	26.78	6.88	25.9	Atmospheric
Day 0	25.56	6.97	26.3	Atmospheric

Time-point	[DO] in pDOS (mg/L)	[DO] in control N/S (mg/L)	Temperature (°C)	Pressure
Day 1	25.19	6.83	26.0	Atmospheric
Day 2	23.77	6.79	25.5	Atmospheric
Day 3	21.27	6.75	25.1	Atmospheric
Day 4	21.67	6.72	26.2	Atmospheric
Day 5	21.72	6.74	25.9	Atmospheric
Day 6	21.69	6.75	26.1	Atmospheric
Day 7	20.78	6.67	25.0	Atmospheric
Day 8	19.62	6.63	25.4	Atmospheric
Day 9	18.53	6.54	25.7	Atmospheric
Day 10	17.07	6.41	25.2	Atmospheric
Median (IQR)	**21.71 (4.57)**	**6.75 (0.19)**	**25.8 (0.7)**	N/A
Mean ± SD	**22.87 ± 3.66**	**6.78 ± 0.21**	**25.7 (0.42)**	N/A
p value	**p<0.001**		N/A	N/A

Table 4.1 Notes: The plain DOS was manufactured at the beginning of protocol day -3, whereas day 0 represents the time-point when all excisional wounds were created *in vivo*. [DO] measurements were recorded for three days prior to any *in vivo* administration, to verify the plain DOS's suitability for further biological testing, and subsequently throughout the duration of each *in vivo* experiment, on a daily basis. An independent-samples t-test was performed to compare the mean [DO] values between the plain DOS (22.87mg/L, n=14) and the control solution (6.78mg/L, n=14), showing a statistically significant difference ($p<0.001$), with a large effect size (Cohen's d=6.21). The [DO] measurements were recorded under temperature- and pressure-controlled conditions, consistently maintaining atmospheric pressure; meanwhile, median temperature was 25.8°C (IQR, 0.7). Detailed data from the statistical analyses are included in the Table S.7. **Abbreviations**: DO, dissolved oxygen; pDOS, plain dissolved oxygen solution; [DO], dissolved oxygen concentration in mg/L; N/S, normal saline solution 0.9% NaCl; N/A, not applicable; IQR, interquartile range; SD, standard deviation.

4.3.2 | Plain DOS treatment is safe and well-tolerated in healthy SKH1 mice regardless of intravenous, local, or *per os* administration

Next, we performed a stepwise investigation of safety and tolerability for each of the IV, LO, and PO groups receiving the plain DOS treatment, in comparison to the CO group. Daily, and prior to any *in vivo* use, consecutive DLS analyses confirmed the

absence of large-diameter bubbles (≥28μm) from all DOS samples (data not shown, available upon request), thus minimizing the possibility of microvascular gas embolism. Subsequently, and throughout the duration of *in vivo* experiments, the absolute number of life-threatening or severe AEs recorded was zero [Table S.8]. Analogously, no substantial abnormalities were found in any of the dedicated well-being and tolerability measures evaluated [Table S.8]. Collectively, the safety and tolerability data from the IV, LO, and PO groups demonstrated a pattern similar to the untreated controls (CO), suggesting that plain DOS administration has no impact on SKH1 mouse health and homeostasis. For reference, the precise DO amount, in milligrams, that each animal

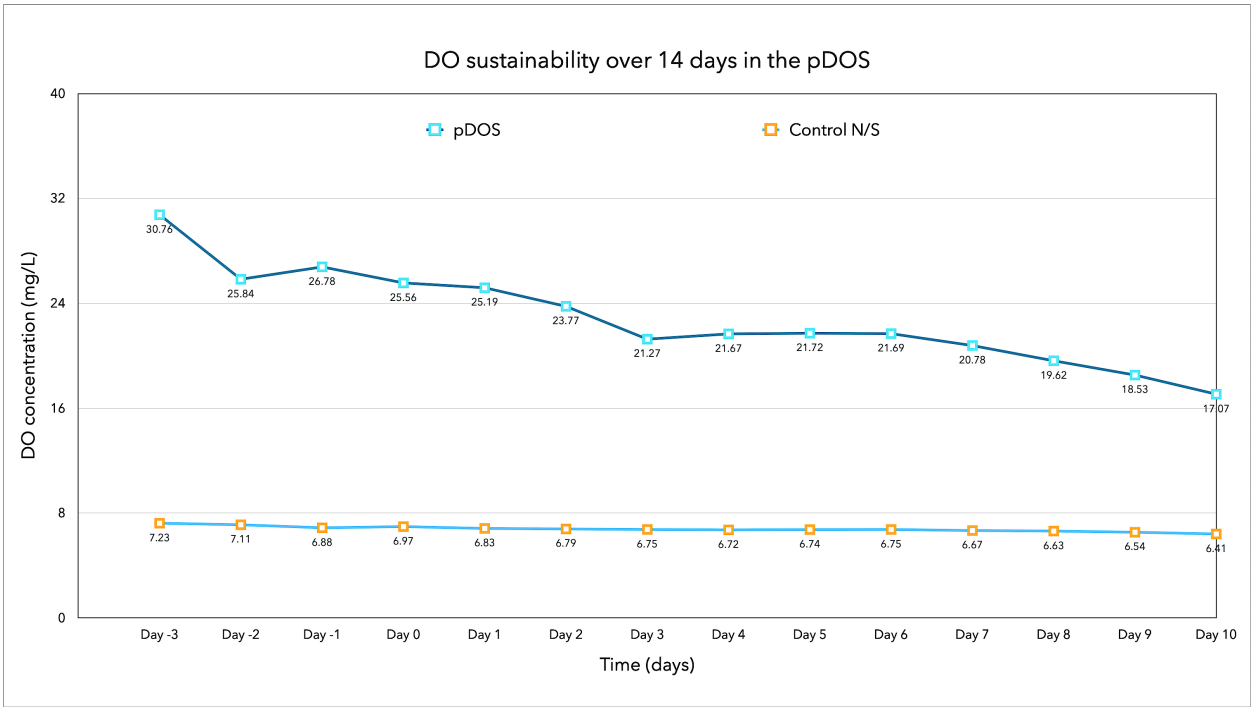

Figure 4.3: **Plain DOS demonstrates significant DO sustainability for at least 14 days, which can be consistent with real-life biomedical applications**. Daily [DO] measurements were recorded with a standardized DO sensor (HQ30d Portable Meter Kit; Hack, Düsseldorf, Germany), for 14 days, under identical physical parameters (median temperature, 25.8ºC (IQR, 0.7); atmospheric pressure), in both the plain DOS and a control N/S solution (0.9% NaCl) studied for comparisons. In the plain DOS, median [DO] was 21.71mg/L (IQR, 4.57; range, 17.07 – 30.76 mg/L). Also, [DO] measurements appeared to reach a plateau of 21.27mg/L, approximately at protocol day 3 corresponding to 7 days post-production, which was maintained for 4 days thereafter followed by a slowly-declining trend until the final time-point (protocol day 10). In the control N/S solution with no additional oxygen, [DO] levels were mostly stable as expected, with a median value of 6.75mg/L (IQR, 0.19) throughout the duration of Phase 1 experiments. Given the absence of chemical surfactants to prolong DO half-life, the recorded DO sustainability in the plain DOS is considered promising, and supports further *in vivo* testing in biomedical indications associated with hypoxia and

Figure 4.3 Caption (continued): ischemia, such as cutaneous wound healing as in this study. **Abbreviations**: DO, dissolved oxygen; DOS, dissolved oxygen solution; pDOS, plain dissolved oxygen solution; [DO], dissolved oxygen concentration in mg/L; IQR, interquartile range; N/S, normal saline (0.9% NaCl).

received in the IV and PO groups of plain DOS administration, are presented in Tables S.12 and S.13, respectively.

4.3.3 | Plain DOS treatment administered intravenously accelerates macroscopic wound closure in healthy SKH1 mice

Despite the presumed potential of DOS biotechnologies in wound-healing applications, dedicated data evaluating their healing efficacy *in vivo*, are scarce. Here, we measured three outcomes to evaluate the plain DOS' effect on the speed and the tissue-regenerating capacity of the healing response in healthy SKH1 mice: the macroscopic velocity of wound closure (VC, in mm^2/day), and the histopathological ratios of newly-formed cutaneous epithelium (ER) and collagen deposition (CR) versus the total size of each wound bed.

VC was calculated for all the timeframes among protocol days 0, 3, 7, and 10, from macroscopic wound photographs [Figure 4.4.A]. Mean VC was found significantly accelerated in the mice receiving the plain DOS IV versus the CO group, for the following timeframes: days 0 to 7 ($p=0.005$) [Figure 4.4.C], 3 to 7 ($p=0.022$) [Figure 4.4.E], 0 to 10 ($p=0.049$) [Figure 4.4.D], and 3 to 10 ($p=0.024$) [Figure 4.4.F]. Also, mean VC trended higher in the PO group compared to the CO for the majority of timeframes, with the largest difference recorded between days 3 and 7 still without reaching the statistical significance cutoff ($p=0.072$) [Figure 4.4.E]. In turn, LO administration demonstrated the least noticeable effect on VC, following a pattern similar to the PO group for the timeframes between days 3 and 7 ($p=0.373$) [Figure 4.4.E], and days 3 to 10 ($p=0.494$) [Figure 4.4.F], while approximating the mean values of the CO group between days 0 and 7 ($p=0.999$) [Figure 4.4.C], and from day 0 to day 10 ($p>0.999$) [Figure 4.4.D]. Meanwhile, no significant differences in mean VC were observed between any of the groups from day 0 to day 3 [Figure 4.4.B], or from day 7 to day 10

[Figure 4.4.G]. Detailed statistical data from the corresponding ANOVA and post-hoc tests are presented in Table S.9.

4.3.4 | Plain DOS treatment administered intravenously and *per os* enhances wound epithelialization and collagenation in healthy SKH1 mice

Subsequently, we investigated the restoration of cutaneous epithelium and the area of collagen deposition in each wound bed at two predetermined time-points, days 3 and 10. At day 3, mean ER was significantly elevated in the mice receiving the plain DOS IV compared to the CO ($p=0.012$), and in the PO group versus the CO ($p=0.026$) [Figures 4.5.A, 4.5.C]. Also, a trend increase in mean ER was observed with LO administration versus the CO group ($p=0.279$) [Figure 4.5.C].

At day 10, mean ER exceeded 0.98 (98.0%) in all experimental groups [Figure 4.5.D], in alignment with the corresponding macroscopic observations [Figure 4.4.A]. Concurrently, mean CR was found significantly increased with IV plain DOS administration compared to the CO group ($p=0.018$), and with PO plain DOS intake versus the CO ($p=0.011$) [Figures 4.5.B, 4.5.E], demonstrating a pattern analogous to the ER data from day 3 [Figure 4.5.C]. Meanwhile in the LO group, mean CR approximated the measurements of the CO group ($p>0.999$) [Figure 4.5.E]; a finding which aligns with the macroscopic VC data corresponding to the same timeframe [Figure 4.4.D], which spans the entire duration of *in vivo* experiments from day 0 to day 10. Additional numerical and statistical data are presented in Tables S.10 and S.11, for epithelialization and collagenation ratios, respectively.

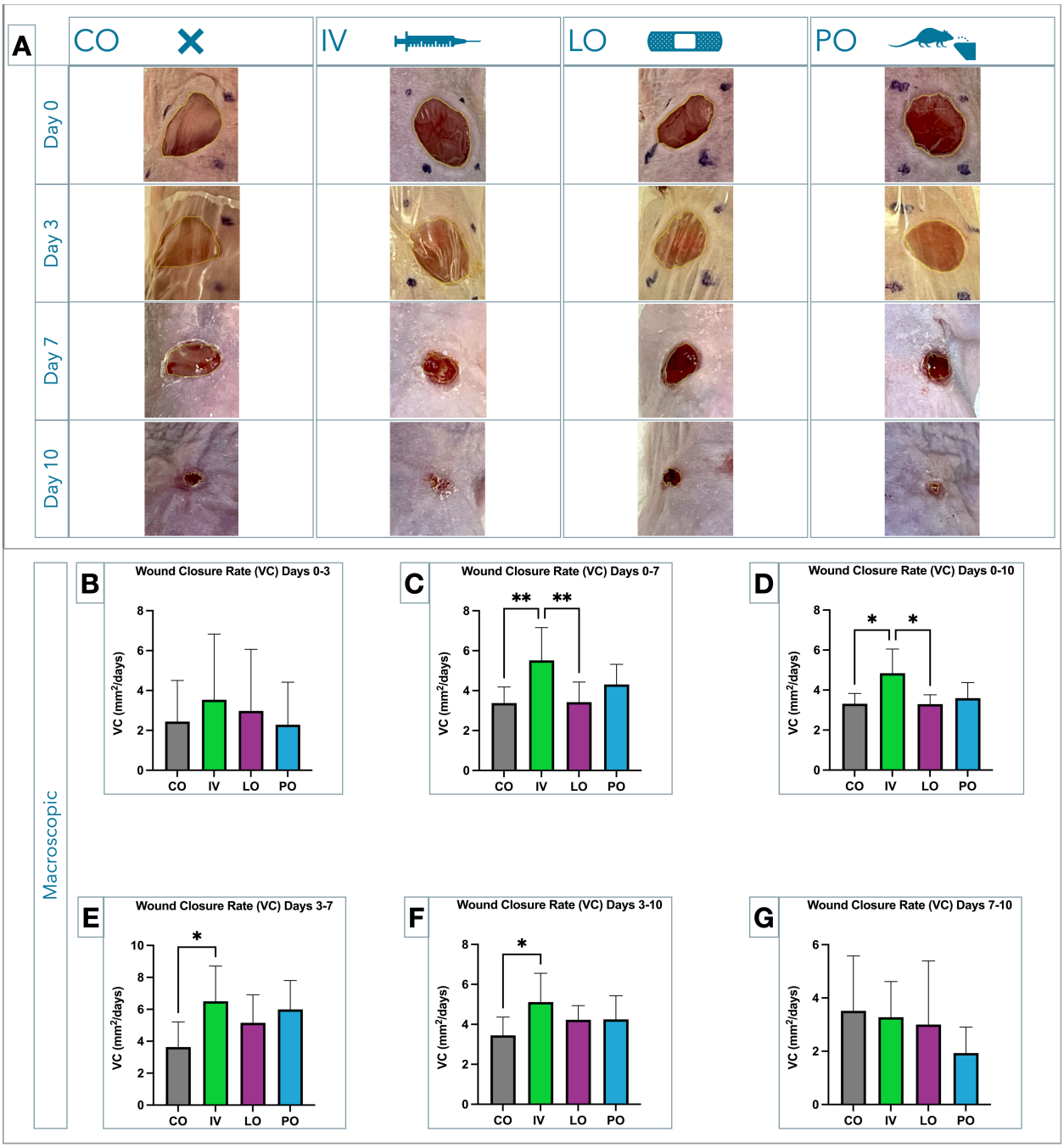

Figure 4.4: **Plain DOS treatment administered IV can accelerate wound closure macroscopically, in healthy SKH1 mice evaluated at pre-determined timeframes post-trauma, in Phase 1 experiments**. For reference, day 0 represents the time-point when two full-thickness wounds were simultaneously excised with an 8mm surgical punch per mouse dorsum, under general anesthesia with ketamine (100mg/kg) and xylazine (5mg/kg). At day 3, half of the mice from each group, sex-matched, were randomly selected to be sacrificed for tissue harvesting and histopathological studies, while day 10 was the final time-point for all *in vivo* experiments in our protocol design. (**A**) Representative macroscopic photographs depict healing progression in all experimental groups (CO, IV, LO, PO), captured at protocol days 0, 3, 7, and 10 under standardized conditions (iPhone 12 Pro Max, Wide 5.1mm lens [26mm

Figure 4.4 (continued): equivalent], f/1.6, 5.6x zoom). All photographs were analyzed with the open-source Fiji software [Schindelin et al., 2012], both manually and automatically using a custom Fiji macro (available upon request). (**B-G**) Macroscopic velocity of wound closure (VC), expressed in mm^2/day, was determined based on measurements of open wound surface at each protocol day x (OWS_x). The difference (ΔOWS_{x-y}) between days x and y represented wound closure area, which was then divided by the corresponding timeframe (Δt_{x-y}, days) to calculate VC (VC = ΔOWSx-y/Δtx-y, mm^2/day). Mean VC per experimental group (CO, IV, LO, PO) was calculated for all the timeframes among protocol days 0, 3, 7, and 10, and statistically compared among the groups per timeframe, as detailed in Table S.9; (**B**) from day 0 to day 3 (*n*=16 per group); (**C**) from day 0 to day 7 (*n*=8 per group); (**D**) from day 0 to day 10 (*n*=8 per group); (**E**) from day 3 to day 7 (*n*=8 per group); (**F**) from day 3 to day 10 (*n*=8 per group); (**G**) from day 7 to day 10 (*n*=8 per group). The data in the graphs represent mean VC values. Scale = 1mm. **Abbreviations**: CO, negative controls; IV, intravenous administration retro-orbitally; LO, local administration via irrigation on the wound surface with a syringe; PO, per os intake *ad libitum*; VC, macroscopic velocity of wound closure (in mm^2/day); *, $p<0.05$; **, $p<0.01$.

4.4 | Discussion

The work discussed in this Chapter contributes to the limited *in vivo* evidence evaluating DOS biotechnologies for healing applications, as a novel alternative to help alleviate the predicted growth in patient needs globally. Of note, our work supports that a DOS suitable for biomedical applications can be manufactured by a targeted mixture of high-purity (>99.9%) O_2 with sterile N/S under controlled temperature and pressure conditions; via a process that excludes *a priori* exogenous chemicals and surfactants while prioritizing the use of affordable equipment, and is easily reproducible. Of note, the plain DOS tested here contained no physical enhancements that could help sustain DO levels. Our findings demonstrate that the plain DOS can effectively deliver high DO levels consistently and effectively for at least 14 days; both the DO concentrations we recorded, and the corresponding timeframe of 14 days, are among the highest in the literature, encouraging further biomedical testing. Also, we verify that the proposed plain DOS is safe and well-tolerated *in vivo* via three routes of administration: IV, LO, and PO. Furthermore, by monitoring full-thickness excisional wounds on healthy SKH1 mice, we extend our observations to show that, independently, two IV injections and *ad libitum* PO intake of the DOS may accelerate wound closure macroscopically, and

improve epithelial regeneration and collagen deposition histopathologically. A detailed analysis of the findings presented in this Chapter, and their significance in association with the state-of-the-art knowledge and the results from relevant studies previously published in the field, is discussed in Chapter 6 of this dissertation. To our knowledge, our work represents one of the first studies to comprehensively evaluate the technical parameters, biological safety, and healing efficacy of a DOS with the aforementioned characteristics; paving the way for additional and targeted investigation towards the multifaceted potential of DOS biotechnologies in biomedical and clinical applications.

Figure 4.5: Plain DOS treatment administered IV and PO can enhance wound re-epithelialization and collagenation histopathologically, in healthy SKH1 mice evaluated at pre-determined time-points post-trauma, in Phase 1 experiments.

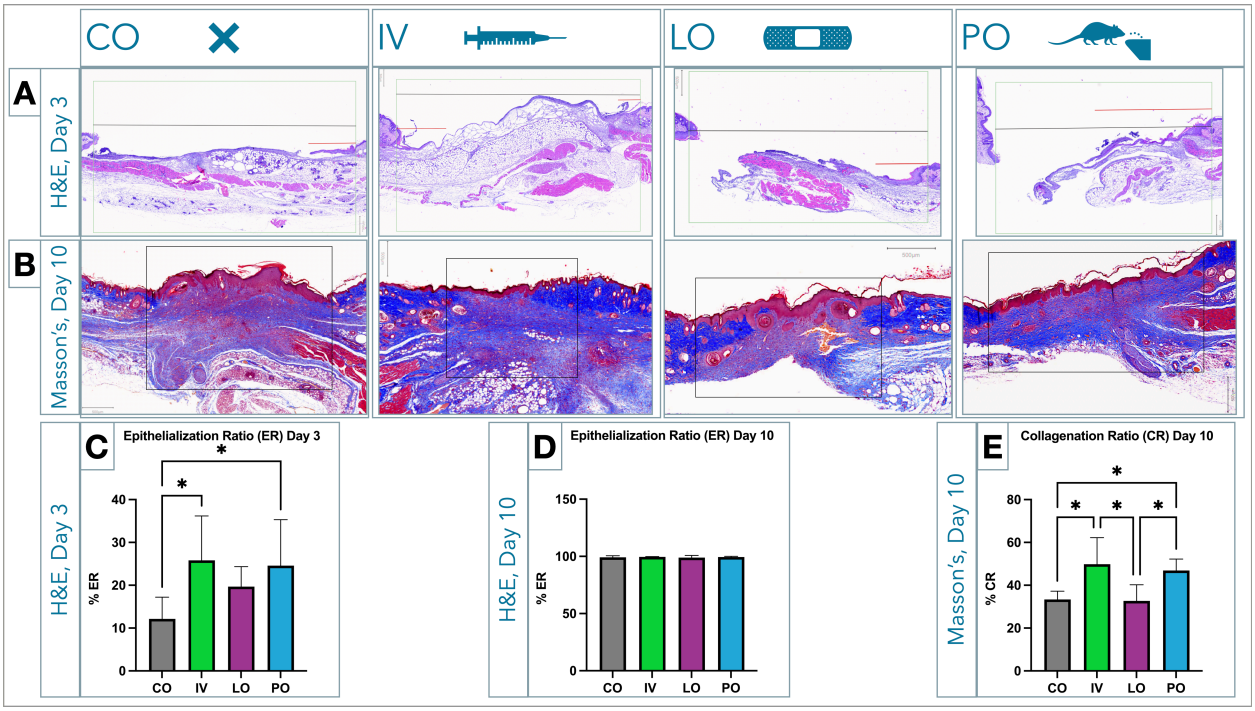

Figure 4.5 Caption: For reference, day 0 represents the time-point when two full-thickness wounds were simultaneously excised with an 8mm surgical punch per mouse dorsum, under general anesthesia with ketamine (100mg/kg) and xylazine (5mg/kg). At day 3, half of the mice from each group, sex-matched, were randomly selected to be sacrificed for tissue harvesting and histopathological studies, while day 10 was the final time-point for all *in vivo* experiments in our protocol design. (**A**) Representative histopathological slides stained with hematoxylin and eosin, illustrate wound epithelialization per experimental group (CO, IV, LO, PO) at day 3. The slides were prepared and digitalized with whole slide imaging by an external collaborator (iHisto, Inc., Salem, MA, USA), producing digital slides that integrated continuous optical magnification up to the equivalent of a 40x objective lens. These slides were studied using the open-source QuPath software [Bankhead et al., 2017]; high-resolution static images were captured under an identical magnification scale of 500μm, and were

Figure 4.5 (continued): exported for ER quantification to Fiji [Schindelin et al., 2012]. (**C**). At day 3, ER was calculated by dividing the length of the linear segment of the wound that was re-epithelialized, by the total linear length of the wound on the horizontal axis; the latter was identified based on the presence of cutaneous anatomical landmarks and organelles, microscopically. The resulting ER values were converted to percentages (% ER), and statistically analyzed as detailed in Table S.10. The data in the graphs represent mean values for each experimental group (CO, IV, LO, PO), at day 3. *n*=8 per group. (**D**) A similar analysis was conducted for the ER measurements recorded at day 10 [Table S.10]. (**B**) Representative histopathological slides stained with Masson's trichrome, illustrate collagen deposition in the wound beds per experimental group (CO, IV, LO, PO), at day 10. The slides were prepared and studied as described above for the H&E-stained sections illustrating wound epithelialization, at a 500μm scale. (**E**) CR was calculated by dividing the number of blue-stained pixels representing collagen deposition in the surface area of each wound bed, by the total number of pixels in the surface area spanning the entire wound bed; the latter was demarcated using the Fiji freehand tool, following microscopic identification of the original wound margins. The resulting CR values were converted to percentages (% CR), and were statistically analyzed as detailed in Table S.11. *n*=8 per group. The data in the graph represent mean values for each experimental group, at day 10. **Abbreviations**: CO, negative controls; IV, intravenous administration retro-orbitally; LO, local administration via irrigation on the wound surface with a syringe; PO, per os intake *ad libitum*; H&E, hematoxylin and eosin stain; ER, epithelialization ratio; Masson's, Masson's trichrome stain; CR, collagenation ratio; *, $p<0.05$; **, $p<0.01$.

5 | Oxygen nanobubble-enriched (ONBW) water biotechnology for excisional wounds *in vivo*

The contents of this chapter are also represented in the following submission to *Journal of the American College of Surgeons*:

Dimitrios Ntentakis, Anastasia Maria Ntentaki, Eleni Delavogia, Petroula Seridou, Zoi Kollia, Nikolaos Sfakianos, Victor San Martin Carvalho Corrêa, Patroklos Katafygiotis, Danae Venieri, Nikolaos Arkadopoulos, Nicolas Kalogerakis. Dissolved oxygen and O_2-nanobubble biotechnologies enhance physiologic wound healing and cutaneous regeneration *in vivo*. (2024) *Submitted at Journal of the American College of Surgeons*.

5.1 | Background information

Clinical administration of gaseous oxygen (O_2) has consistently demonstrated beneficial outcomes in cutaneous wounds, reflecting the pivotal contributions of O_2 to the physiological healing response [Tandara and Mustoe, 2004; Rodriguez et al., 2008]. The most characteristic example is hyperbaric O_2 therapy (HBOT), which has become an established management strategy for complicated wounds in patients with diabetes mellitus, alongside other clinical indications [Wang et al., 2003; de Smet et al., 2017]. Devices supplying topical O_2 therapy have also been successfully introduced, enabling continuous local application on wounds [Sayadi et al., 2018]. However, an important limitation lies in the short-lived efficacy of O_2 when administered in its gaseous form, as a result of passive diffusion within biological tissues in response to local O_2 pressure gradients. In the example of HBOT, this limitation necessitates frequent dosing sessions, typically on a daily basis, and lung ventilation under unnaturally-high pressures to establish a sustained elevation in blood oxygen content; which, in turn, requires the use of specialized equipment available exclusively in a hospitalized environment [Tibbles and Edelsberg, 1996]. Collectively, these factors can lead to substantial patient discomfort and non-adherence to treatment protocols, potentially compromising the anticipated healing benefits. Meanwhile, epidemiological interest in wound management is increasing on a global scale [Walmsley, 2002; Sen et al., 2009], due to a combination of the following factors: the rising prevalence in systemic vasculopathies predisposing to peripheral ischemia and suboptimal healing, such as diabetes [International Working Group on the Diabetic Foot, 2003; International Diabetes Federation, 2015], the aging world population [Wu et al., 1999; Gottrup, 2004], along with the questionable capacity of current management and prevention strategies to confront a potentially generalized surge in persisting wounds [Das and Baker, 2016].

Thereby, biotechnologies supplying dissolved oxygen (DO) within aqueous-based solutions, referred to as DO solutions (DOS), are being investigated as a novel approach to enhancing wound oxygenation. By enabling O_2 to become gradually bioavailable into the liquid medium, a DOS can theoretically supply high oxygen concentrations for longer periods, compared to both HBOT and topical O_2 therapies. However, sustaining DO levels without using artificial surfactants and complex

chemical additives, remains challenging. For instance, numerous DOS formulations currently developed for healing applications are manufactured on the basis of O_2 ultra-fine particles (OUPs) [Ntentakis et al., 2021]. OUPs are engineered with the incorporation of core-enhancing and coating chemicals, namely perfluorocarbons (PFCs), decafluoropentane (DFP), chitosan, and dextran, via high-speed centrifugation and sonication-driven emulsification processes [Bisazza et al., 2008; Cavalli et al., 2009a, Cavalli et al., 2009b; Magnetto et al., 2014; Khadjavi et al., 2015; Prato et al., 2015; Gulino et al., 2015; Basilico et al., 2015]. Although promising in terms of DO sustainability, the aforementioned chemicals have been associated with significant toxicities in human cell lines [Je et al., 2006; Wiegand et al., 2010], and dose-dependent complications in the human body upon repetitive exposure [Butenhoff et al., 2002; Nosé, 2004; Zhang et al., 2015]. Eliminating the risk of multifaceted and cumulative toxicities, while harnessing the potential benefits of DO in aqueous solutions, could introduce a potent therapeutic candidate for healing applications.

In this Chapter, we investigate the biomedical potential of another DO technology classified in the DOS category, manufactured without exogenous chemicals or surfactants; but instead, by leveraging the physics of the gas-liquid interphase and the cutting-edge technology of ultra-fine gas bubbles, namely an oxygen nanobubble-enriched water solution (ONBW). We describe the engineering background and quality-control steps for producing an ONBW suitable for biomedical applications. The latter include daily measurements of DO concentrations over 14 days, accompanied by recordings of the diameter, size distribution, and zeta potential of the O_2 ultra-fine bubbles (OUBs) in the ONBW, as markers of OUB physical stability, longevity, and their ensuing ability to supply high DO amounts with consistency and safety. Then, to further ascertain the biological safety of systemic ONBW administration in mice, we monitor a series of standardized tolerability endpoints and adverse events (AEs). Furthermore, we study macroscopic and histopathological markers of cutaneous restoration, to evaluate the ONBW's efficacy in healing full-thickness excisional wounds on healthy SKH1 mice. Our findings support a highly promising potential of ONBW biotechnology in healing applications, as it maintained substantially elevated DO concentrations throughout our 14-day evaluation period, while being safe for systemic administration *in vivo* and contributing to faster and effective restoration of rodent wounds.

5.2 | Methods

This section presents a synopsis of the experimental design and methodology followed while conducting this work, which corresponds to the experimental Phase 2 discussed in Chapter 3 of this dissertation. A detailed description of the manufacturing and quality control processes employed for producing the ONBW, the *in vivo* wound model, our endpoint selection for assessing safety and healing efficacy, along with our analytical methods and the academic rationale, per case, are included in Chapter 3 of this dissertation. A graphical timeline of the protocol design, showing all the endpoints assessed and the main time-points corresponding to each assessment, is illustrated in Figure 5.1. Key methodological parameters implicated in the experiments of Phase 2 are highlighted in Figure 5.2.

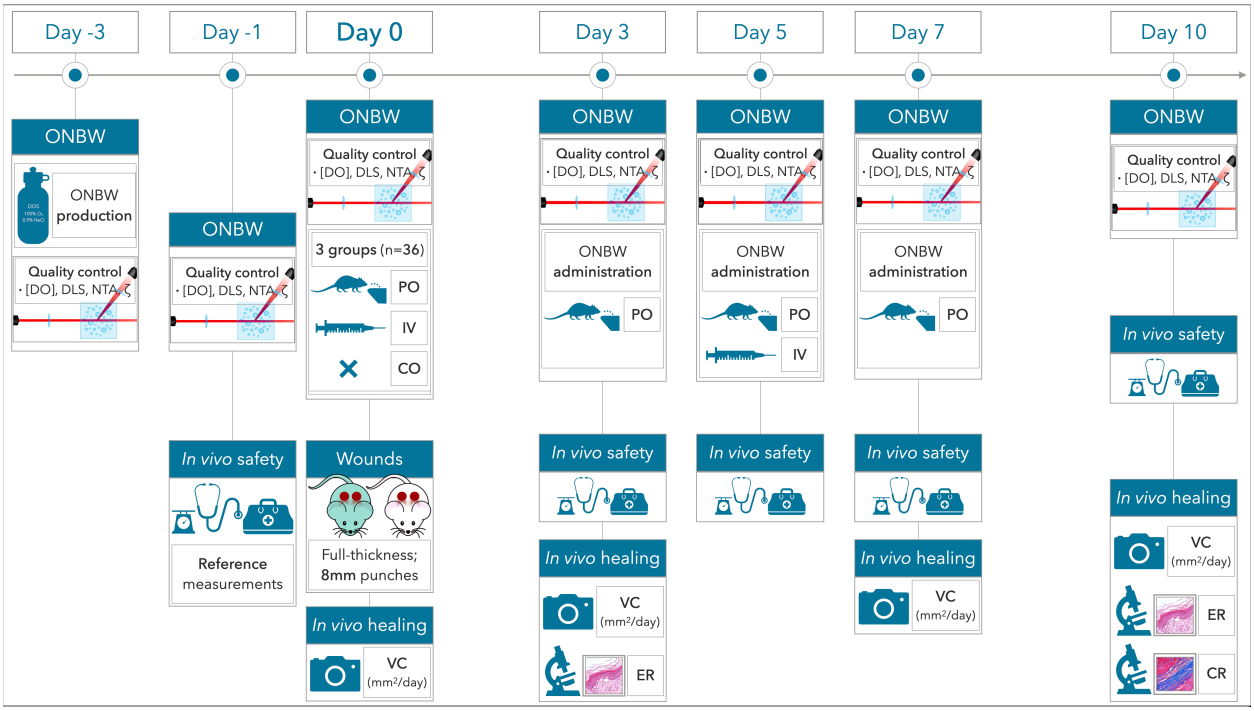

Figure 5.1: **Graphical synopsis of the protocol design of experimental Phase 2, illustrating the key timepoints corresponding to the production of ONBW biotechnology, the quality-control processes, and the *in vivo* assessments of biological safety and healing efficacy, on a chronological order**. ONBW was manufactured on day -3 of the protocol timeline, followed by quality-control processes which were conducted daily and prior to any *in vivo* use. The latter included daily [DO] measurements (in mg/L), DLS screening for the presence of large-diameter (≥28μm) bubbles; NTA to monitor the concentration and size distribution of OUBs, and ζ potential as a marker of electrostatic repulsion and physical stability of OUBs; detection of at least one bubble with diameter ≥28μm led to exclusion of the corresponding ONBW sample from all further experiments. At day 0, two full-thickness cutaneous wounds were simultaneously excised with an 8mm surgical punch per mouse dorsum, under general anesthesia with ketamine (100mg/kg) and xylazine (5mg/kg). Postoperatively, the SKH1 mice were randomly divided to 3 equally-populated, sex-matched experimental groups (PO, IV, CO), according to ONBW administration starting from day 0. IV administration was performed retro-orbitally, at days 0 and 5. Mice in the PO group consumed the ONBW *in lieu* of drinking water, *ad libitum*. The mice in the negative control (CO) group received no treatment, as there is no gold-standard treatment intervention for wound healing clinically. *In vivo* safety was monitored daily, based on severe adverse events and standardized safety and tolerability measures. VC (in mm^2/day) was calculated from macroscopic photographs for all the timeframes among days 0, 3, 7, and 10. ER (hematoxylin & eosin) was assessed on days 3 and 10, by dividing the length of re-epithelialization to the length of each wound bed on the horizontal axis. CR (Masson's trichrome) was evaluated on Day 10, by dividing the area of blue-stained collagen pixels to the total area corresponding to each wound bed. All pertinent methodological details are detailed in Chapter 3 of this dissertation, whereas key points are summarized in section 5.2 of this Chapter. **Abbreviations**: ONBW, oxygen nanobubble-enriched water; [DO], dissolved oxygen concentration in mg/L; DLS, dynamic light scattering; NTA, nanoparticle tracking analysis;

Figure 5.1 (continued): ζ (zeta), zeta potential; PO, per os intake; IV, intravenous administration; CO, negative controls; VC, macroscopic velocity of wound closure; ER, histopathologic epithelialization ratio; CR, histopathologic collagenation ratio; OUBs, oxygen ultra-fine bubbles.

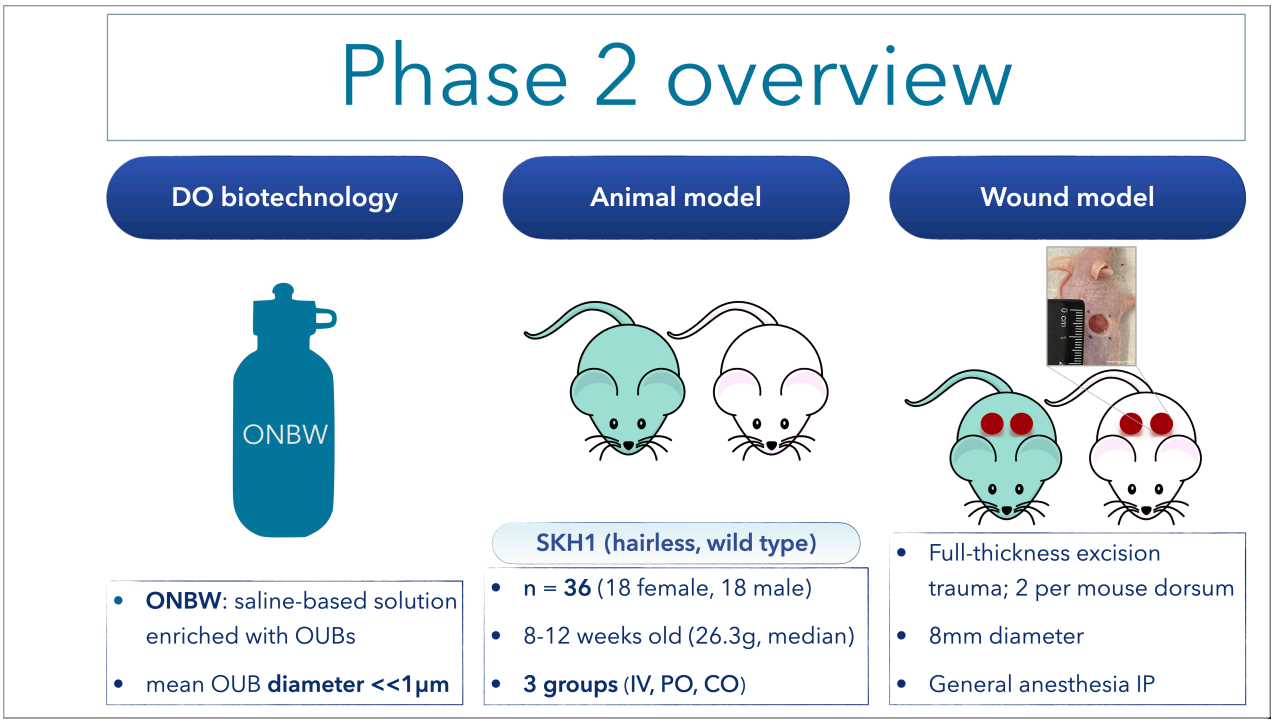

Figure 5.2: **Synoptic overview of the DOS biotechnology, the animal parameters, and the wound model used in experimental Phase 2. Abbreviations**: DO, dissolved oxygen; ONBW, oxygen nanobubble-enriched water; OUBs, oxygen ultra-fine bubbles; N/S, normal saline (0.9% NaCl); IV, intravenous administration; PO, per os intake; CO, negative controls; IP, intraperitoneally.

5.2.1 | Study approval

ONBW manufacturing and quality-control processes were approved by the Laboratory of Biochemical Engineering and Environmental Biotechnology of the School of Chemical and Environmental Engineering, at the Technical University of Crete (Technical University of Crete; Chania, Greece). Animal procedures and experiments were approved by the Institutional Animal Care and Use Committee of the National Center for Scientific Research (NCSR) Demokritos (NCSR Demokritos; Athens, Greece), and the Decentralized Administration of Attica, Greece, in accordance with the

Directive 2010/63/EU of the European Parliament on the Protection of Animals Used for Scientific Purposes [European Parliament, 2010].

5.2.2 | Manufacturing, storage, and monitoring of the ONBW

The DOS biotechnology studied in experimental Phase 2 employs the physics of the gas-liquid interphase and the cutting-edge technology of OUBs; it is referred to as ONBW throughout this Chapter. As in the case of the plain DOS studied in Chapter 4 of this dissertation, the use of exogenous chemicals and surfactants was excluded from ONBW manufacturing *a priori*. At protocol day -3 [Figure 5.1], the ONBW was aseptically produced using a commercially-available device (MK2 Nanobubbler; Fine Bubble Technologies Pty Ltd., Cape Town, South Africa). The latter generates OUBs by continuously recirculating 160 liters of sterile normal saline solution (N/S; 0.9% NaCl) with high-purity (>99.9%) O_2, infused from a different inlet at a flow rate of 22L/min, via a patented high-speed centrifugation device, for a period of 30 minutes.

Regarding quality control, the ONBW was packaged in tightly-sealed, autoclaved, 500mL, borosilicate glass bottles (IVYX Scientific, Seattle, WA, USA) to minimize oxygen losses from contact with atmospheric air, and stored at room temperature and pressure. DO concentrations, expressed in mg/L, were recorded daily for the ONBW and a regular N/S solution used for comparisons, under identical physical parameters, using standardized equipment (HQ30d Portable Meter Kit; Hack, Düsseldorf, Germany). Dynamic light scattering (DLS) analyses were also conducted daily (SALD-7500nano; Shimadzu Corporation, Columbia, MD, USA), to screen for larger-diameter bubbles (≥28μm) as a prognosticator of the potential risk of gas embolism from any naturally-forming bubbles. Additionally, mean OUB diameter and size distribution were validated via nanoparticle tracking analysis (NTA; Nanosight, Malvern, UK). Finally, zeta potential (ζ), an indicator of the unique electrostatic repulsion that OUBs demonstrate in the nanoscale, and thus, a marker of physical stability and sustainability of OUBs within the aqueous medium of the ONBW, was recorded using an electrophoresis instrument (Zetasizer Nano ZS90; Malvern, UK) [Tsuge, 2014].

5.2.3 | Animals and *in vivo* wound model

Thirty six SKH1 hairless mice (wild type, 1:1 female:male), with a median weight of 27.00g (8-12 weeks old), were randomly divided to three treatment groups according to ONBW administration: intravenous (IV), per os (PO), and negative controls (CO). At day 0, two full-thickness cutaneous wounds were simultaneously excised with an 8mm biopsy punch (Acu-Punch; Acuderm, Ft. Lauderdale, FL, USA) per mouse dorsum, under general anesthesia with ketamine (100 mg/kg) and xylazine (5 mg/kg), as previously described [Wang et al., 2013; Chen et al., 2015]. Postoperatively, the wounds were covered with a sterile transparent dressing (Tegaderm; 3M, St. Paul, MN, USA) to minimize the risk of infection, and each mouse was monitored until complete recovery from surgery and anesthesia. The ONBW was administered after successful recovery from surgery and anesthesia at day 0, and then prior to the daily assessments of biological safety until protocol day 10 [Figure 5.1]. All wounds were daily evaluated throughout the remaining duration of each *in vivo* experiment, until day 10 [Figure 5.1].

5.2.4 | Experimental groups and ONBW treatment administration

IV administration was performed in the retro-bulbar sinus, using a standardized technique [Yardeni et al., 2011]. Each mouse was injected 150μL of ONBW, twice in total during experimental Phase 2: once at day 0, and then at day 5, under general anesthesia. In the PO group, the ONBW was used *in lieu* of drinking water, which the mice consumed *ad libitum* throughout the duration of each experiment [Figure 5.1]. Mice in the CO groups received no treatment.

5.2.5 | *In vivo* safety and healing endpoints

All mice were monitored for their safety and well-being daily, based on standardized scoring systems characterizing tolerability and adverse events (AEs) [Arras et al., 2007; National Research Council, 2009; Hohlbaum et al., 2018; Supplement S.6]. Specifically, 13 well-being parameters were evaluated: body weight, food and water intake, burrowing behavior, spontaneous behavior, posture, breathing, behavior after provocation/weighing, movement after provocation/weighing, as well as the condition of the coat, body, eyes, and wounds [Deacon, 2006; Arras et al., 2007; National Research Council, 2009; Hohlbaum et al., 2018]. Additionally, the occurrence of the following 7 conditions, characterized as severe AEs, was cautiously monitored:

1) death, 2) local inflammation/infection persisting for more than 24 hours, 3) occurrence of non-healing cutaneous wounds/ulcers, 4) hemorrhage from any orifice that was unresponsive to treatment, 5) water consumption less than 5mL for more than 24 hours, 6) decrease in body mass equal or higher than 15% of the original measurement recorded at day 0, and 7) combination of abnormalities in physical appearance and behavior. The aforementioned endpoints used to assess animal safety, tolerability, and the incidence of AEs, alongside the criteria, timeline, and grading systems applied for evaluating each of them, are presented in Table 3.1 and Figure 3.4 of Chapter 3 of this dissertation.

Regarding healing efficacy, all wounds were photographed at days 0, 3, 7, and 10, under standardized conditions. The macroscopic velocity of wound closure (VC, in mm^2/days) was assessed from measurements of the wound surface area obtained from these photographs, in correlation with each of the timeframes among days 0, 3, 7, and 10, the key predetermined time-points of this protocol. Furthermore, wound specimens containing the mouse skin and subcutaneous in healthy margins were collected at days 3 and 10, for histopathological analyses of epithelialization (Hematoxylin/eosin; day 3, day 10) and collagenation (Masson's trichrome; day 10) ratios.

5.2.6 | Statistics

Statistical analyses and graphical illustrations were conducted using IBM SPSS Statistics (Version 27) and Prism (GraphPad 9.0, San Diego, CA, USA). DO concentrations were compared between the ONBW and regular N/S, using the Mann–Whitney U test. Route of administration of the ONBW served as the only independent variable in the analyses of *in vivo* data. Safety and tolerability data were qualitatively evaluated, based on standardized outcome measures and categorical scoring systems [Arras et al., 2007; National Research Council, 2009; Hohlbaum et al., 2018]. Investigators were blinded to experimental groups during the analyses of all data pertaining to healing outcomes. Of the two excisional wounds per mouse dorsum, one was randomly selected to be analyzed as a biological replicate. Data assessing healing outcomes (VC, ER, CR) were described as mean ± standard deviation (SD) or mean ranks, according to each sample's distribution; subsequently, they were analyzed using one-way analysis of variance (ANOVA) followed by Tukey's honest significant difference

(HSD) test, or the non-parametric version of one-way ANOVA on ranks (Kruskal-Wallis H test) followed by Dunn's multiple comparisons test, respectively. Each set of macroscopic VC comparisons referred to a specific timeframe between two of the predesignated timepoints in our experimental design, namely days 0, 3, 7, and 10 [Figure 5.1]. Histopathological comparisons were specific to each corresponding timepoint (day 3, day 10). The cutoff for statistical significance was defined as $p<0.05$.

5.3 | Results

5.3.1 | Enhanced DO concentrations are maintained in the ONBW consistently for 14 days

Based on the promising data from Phase 1 experiments testing the plain DOS, here in Phase 2 we focussed on a different DOS biotechnology, the ONBW. Although biochemically similar to plain DOS, since chemical surfactants were also excluded from its manufacturing, the ONBW was additionally enriched with OUBs; whose unique physical properties might contribute to enhanced DO levels, at least theoretically [Tsuge, 2014]. Upon daily measurements under identical conditions, median DO concentrations were 21.08mg/L in the ONBW, versus 7.89mg/L in the regular N/S solution used as comparator [Table 5.1]. Statistically, the corresponding mean-rank values were significantly higher in the ONBW compared to the regular N/S (21.50mg/L versus 7.50mg/L, $p<0.001$, Table 5.1). Furthermore, those significantly enhanced DO concentrations were maintained in the ONBW throughout the 14 consecutive days in our protocol, following an overall slowly-declining trend with time. As illustrated on the graph of Figure 5.3 in more detail, there were more prominent fluctuations in DO concentrations during the first 6 days post-production, though consistently above the median concentration of 21.08mg/L, followed by more stable DO measurements between 16.22mg/L and 20.28mg/L for the remaining days in our experimental design [Figure 5.3].

Meanwhile, serial measurements of zeta potential in the ONBW indicated a consistently present electrostatic repulsion among the OUBs [Supplement S.13]. The latter has been previously associated with increased physical stability and, thus, OUB

longevity and prolonged oxygen supply within OUB-enriched solutions [Tsuge, 2014]. Notably, the nature of the association between OUB stability as quantified via zeta potential, and the sustainability of DO concentrations in our 14-day experiments, could not be further clarified. Based on the available data, we could only hypothesize that the ONBW would be able to deliver enhanced DO amounts to tissues *in vivo*, and over a 14-day period conducive with biomedical applications; thus, making it a promising biotechnology for *in vivo* testing, particularly for indications that require adequate oxygen levels such as cutaneous wound healing [Tandara and Mustoe, 2004; Rodriguez et al., 2008].

Table 5.1: **Serial measurements of DO concentrations in the ONBW and the control saline solution per protocol day in Phase 2 experiments, along with the corresponding physical conditions of temperature and pressure, and an overview of the associated statistical analysis**.

Time-point	[DO] in ONBW (mg/L)	[DO] in control N/S (mg/L)	Temperature (°C)	Pressure
Day -3	31.47	8.18	23.40	Atmospheric
Day -2	27.86	8.05	21.50	Atmospheric
Day -1	26.60	8.15	21.10	Atmospheric
Day 0	27.29	8.03	21.10	Atmospheric
Day 1	23.06	8.05	21.80	Atmospheric
Day 2	26.55	8.10	23.50	Atmospheric
Day 3	21.87	7.87	23.70	Atmospheric
Day 4	20.28	7.90	24.70	Atmospheric
Day 5	18.99	7.70	25.20	Atmospheric
Day 6	18.27	7.85	24.50	Atmospheric
Day 7	19.43	7.50	22.40	Atmospheric
Day 8	18.78	7.30	22.50	Atmospheric
Day 9	17.45	7.10	22.90	Atmospheric
Day 10	16.22	6.95	22.80	Atmospheric
Median (IQR)	**21.08 (7.76)**	**7.89 (0.55)**	**22.85 (1.9)**	N/A
M RANK	**21.50**	**7.50**	N/A	N/A

Time-point	[DO] in ONBW (mg/L)	[DO] in control N/S (mg/L)	Temperature (°C)	Pressure
p value	**p<0.001**	N/A	N/A	N/A

Table 5.1 Notes: The ONBW was manufactured at protocol day -3. Day 0 represents the time-point when all excisional wounds were created *in vivo*. [DO] measurements were obtained for three days prior to any *in vivo* administration, to verify the ONBW's suitability for further biological testing, and subsequently throughout the duration of each *in vivo* experiment, on a daily basis. The M RANK values refer to the Mann-Whitney U test, and were calculated to compare the [DO] measurements between the ONBW (M Rank = 21.50mg/L, n=14) and the control N/S solution (M Rank = 7.50mg/L, n=14), which showed a statistically significant difference (U 0.00; z -4.50; p<0.001), with a large effect size (r=0.85). The [DO] measurements were recorded under temperature- and pressure-controlled conditions, consistently maintaining atmospheric pressure; meanwhile, median temperature was 22.85°C (IQR, 1.9). Detailed data from the statistical analyses are included in the Table S.14. **Abbreviations**: DO, dissolved oxygen; ONBW, oxygen nanobubble-enriched water; [DO], dissolved oxygen concentration in mg/L; N/S, normal saline solution 0.9% NaCl; N/A, not applicable; IQR, interquartile range.

5.3.2 | ONBW treatment is safe and well-tolerated in healthy SKH1 mice with intravenous and *per os* administration

The first step during the *in vivo* testing of the ONBW was a comprehensive evaluation of its biological safety and tolerability, via systemic administration in the IV and PO experimental groups. Safety assessments were conducted daily, following a protocol identical to the one described in Chapter 3 of this dissertation [Table 3.1]. Notably, before *in vivo* administrations, daily DLS and nanoparticle tracking analyses documented the absence of large-diameter (≥28μm) bubbles (data not shown, available upon request). Concurrently, zeta potential monitoring showed a sustained electrostatic repulsion among the OUBs, as mentioned in the previous subsection. Collectively, these data suggested that the occurrence of either preexisting large bubbles, or new ones generated via coalescence of smaller bubbles within the ONBW over time, would be extremely low; which, in turn, practically eliminated the risk of gas embolism [Figure S.1]. Throughout the duration of *in vivo* experiments, no severe AEs, safety concerns, or tolerability issues were recorded, regardless of IV or PO administration, similarly to the untreated mice in the CO group [Table S.15]. Thus, ONBW was considered safe and uneventful for systemic administration in SKH1 mice.

For reference, the precise DO amount, in milligrams, that each animal received in the IV and PO groups of ONBW administration, are presented in Tables S.19 and S.20, respectively.

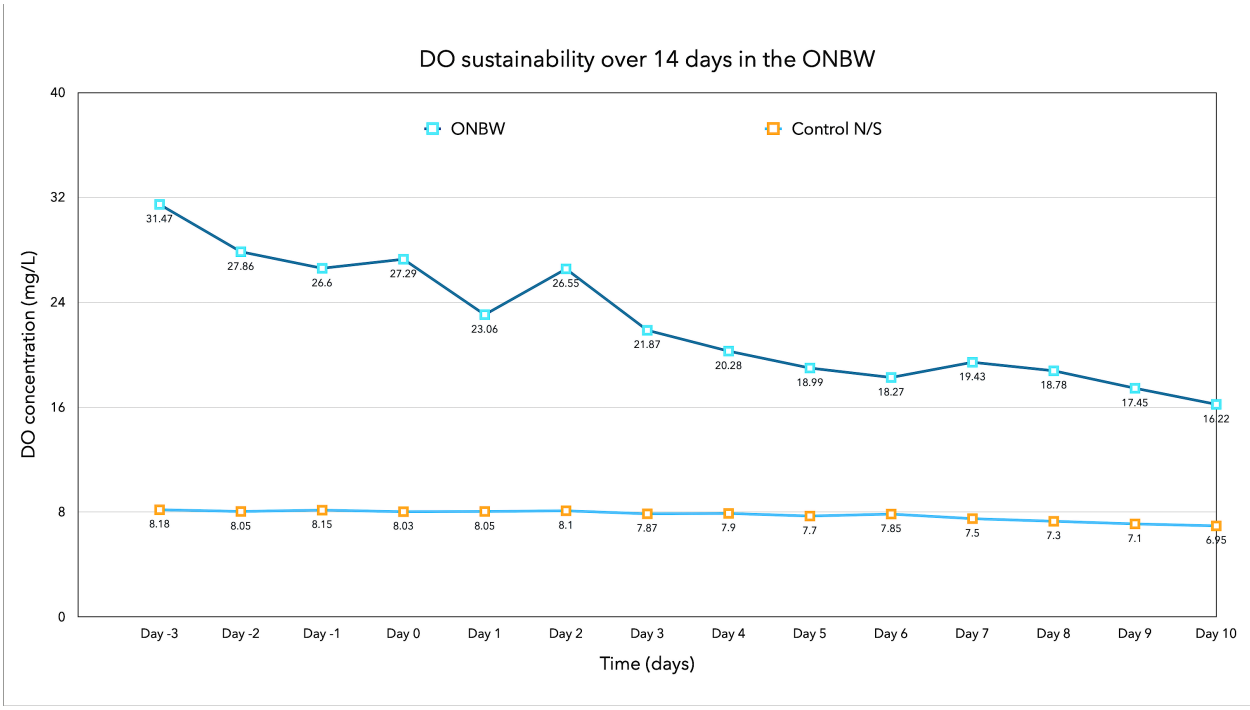

Figure 5.3: **The ONBW formulation demonstrates sustainability of enhanced DO concentrations [DO] for at least 14 days, a timeframe compatible with clinical translation in biomedical applications**. Daily [DO] measurements were recorded with a standardized DO sensor (HQ30d Portable Meter Kit; Hack, Düsseldorf, Germany) for 14 days under identical physical parameters (median temperature, 22.85°C (IQR, 1.9); atmospheric pressure), in both the ONBW and the control N/S solution (0.9% NaCl) studied for comparisons. In the ONBW, median [DO] was 21.08mg/L (IQR, 7.76; range, 16.22 – 31.47 mg/L). After the first 7 days post-production, [DO] measurements demonstrated only minor fluctuations, ranging from 16.22mg/L to 20.28mg/L, with a slowly declining trend until the final time-point (protocol day 10). In the control N/S solution with no additional oxygen, [DO] levels remained stable as originally expected, at a median value of 7.89mg/L (IQR, 0.55) throughout the duration of Phase 2 experiments. Given the absence of chemical surfactants to prolong DO half-life, the recorded DO sustainability in the ONBW is considered promising, and supports further *in vivo* testing in biomedical indications associated with hypoxia and ischemia, such as cutaneous wound healing as in this study. **Abbreviations**: DO, dissolved oxygen; ONBW, ONBW, oxygen nanobubble-enriched water; [DO], dissolved oxygen concentration in mg/L; IQR, interquartile range; N/S, normal saline (0.9% NaCl).

5.3.3 | ONBW treatment administered intravenously and *per os* accelerates macroscopic wound closure in healthy SKH1 mice

Similarly to Phase 1, macroscopic VC was determined from wound photographs taken on days 0, 3, 7, and 10 [Figure 5.4.A], and calculated based on wound closure for each timeframe between two of the aforementioned protocol days. Mean VC was significantly increased in the mice administered the ONBW IV, compared to the untreated CO group, during the following timeframes: days 0 to 3 ($p<0.0001$) [Figure 5.4.B], 0 to 7 ($p=0.002$) [Figure 5.4.C], and 0 to 10 ($p=0.015$) [Figure 5.4.D]. Also, mean VC was significantly higher in the mice receiving the ONBW PO versus the CO group, across the following timeframes: days 0 to 3 ($p=0.029$) [Figure 5.4.B], 0 to 7 ($p<0.0001$) [Figure 5.4.C], 0 to 10 ($p=0.001$) [Figure 5.4.D], 3 to 7 ($p=0.013$) [Figure 5.4.E], and 3 to 10 ($p=0.005$) [Figure 5.4.F]. Comparing the outcomes of the two routes of systemic ONBW administration over time, mean VC demonstrated a steeper acceleration with IV administration early, from day 0 to day 3, versus PO intake ($p<0.0001$, day 0 to day 3) [Figure 5.4.B], followed by a gradually attenuating effect towards day 10, when it became similar to the mean VC in the PO group ($p=0.590$, day 0 to day 10, Figure 5.4.D). Meanwhile, PO intake led to a more gradually-enhancing effect on VC when compared to IV administration, with their difference peaking between days 3 and 7 ($p<0.0001$) [Figure 5.4.E], and from day 3 to day 10 ($p<0.0001$) [Figure 5.4.F], ultimately culminating to a negligible difference from the IV group for the timeframe spanning the entire duration of *in vivo* experiments, from day 0 to day 10 ($p=0.590$, Figure 5.4.D). Furthermore, there were no differences in mean VC among the experimental groups for the timeframe from day 7 to day 10 [Figure 5.4.G], in accordance with the corresponding findings from Phase 1 experiments (Chapter 4). Detailed statistical data and analyses parameters for Phase 2 VC assessments are presented in Table S.16.

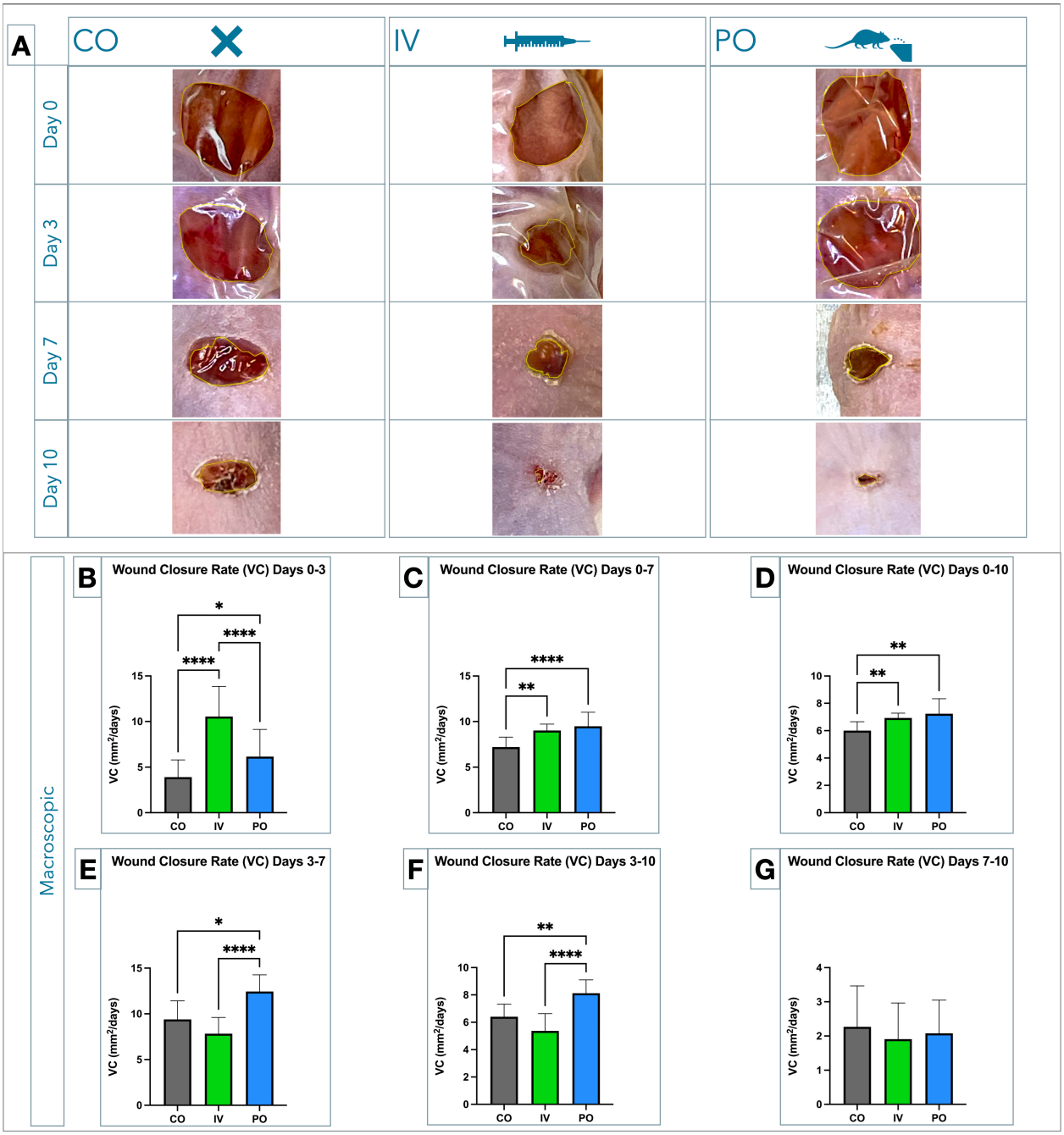

Figure 5.4: **ONBW treatment administered IV and PO can accelerate wound closure macroscopically, in healthy SKH1 mice evaluated at pre-determined timeframes post-trauma, in Phase 2 experiments**.: Day 0 represents the time-point when two full-thickness wounds were simultaneously excised with an 8mm surgical punch per mouse dorsum, under general anesthesia with ketamine (100mg/kg) and xylazine (5mg/kg). At day 3, half of the mice from each group, sex-matched, were randomly selected to be sacrificed for tissue harvesting and histopathological studies, while day 10 was the final time-point for all *in vivo* experiments in our protocol design. (**A**) Representative macroscopic photographs depict healing progression in all experimental groups (CO, IV, PO), captured at protocol days 0, 3, 7, and 10 under standardized conditions (iPhone 12 Pro Max, Wide 5.1mm lens [26mm equivalent], f/1.6, 5.6x zoom). All photographs were analyzed with the open-source Fiji

Figure 5.4 (continued): software [Schindelin et al., 2012], both manually and automatically using a custom Fiji macro (available upon request). (**B-G**) Macroscopic velocity of wound closure (VC), expressed in mm^2/day, was determined based on measurements of open wound surface at each protocol day x (OWS_x). The difference (ΔOWS_{x-y}) between days x and y represented wound closure area, which was then divided by the corresponding timeframe (Δt_{x-y}, days) to calculate VC (VC = ΔOWSx-y/Δtx-y, mm^2/days). Mean VC per experimental group (CO, IV, PO) was calculated for all the timeframes among protocol days 0, 3, 7, and 10, and statistically compared among the groups per timeframe, as detailed in Table S.16; (**B**) from day 0 to day 3 (*n*=21-24 per group, in the only timeframe preceding mouse sacrifice); (**C**) from day 0 to day 7 (*n*=12 per group); (**D**) from day 0 to day 10 (*n*=12 per group); (**E**) from day 3 to day 7 (*n*=12 per group); (**F**) from day 3 to day 10 (*n*=12 per group); (**G**) from day 7 to day 10 (*n*=12 per group). The data in the graphs represent mean VC values. Scale = 1mm. **Abbreviations**: ONBW, oxygen nanobubble-enriched water; CO, negative controls; IV, intravenous administration retro-orbitally; PO, per os intake *ad libitum*; VC, macroscopic velocity of wound closure (in mm^2/day); *, $p<0.05$; **, $p<0.01$; **** $p<0.0001$.

5.3.4 | ONBW treatment administered intravenously and *per os* enhances wound epithelialization and collagenation in healthy SKH1 mice

Analogously to Phase 1 experiments, our next step in the assessment of ONBW healing efficacy involved the histopathological quantification of epithelialization (ER) and collagenation (CR) ratios, from measurements in wound specimens harvested at protocol days 3 and 10 [Figures 5.5.A, 5.5.B]. At day 3, mean ER was significantly higher with IV administration of ONBW compared to the untreated CO ($p=0.003$), and with PO intake versus the CO ($p=0.028$) [Figure 5.5.C]. At day 10, mean ER measurements were above 0.99 in all experimental groups [Figure 5.5.D, Table S.17], corroborating the macroscopic observations indicating successful wound closure at the same time-point [Figure 5.4.A]. Furthermore, mean CR was found significantly enhanced in the mice receiving the ONBW IV compared to the CO group ($p<0.001$), and in the PO group versus the CO ($p=0.005$) [Figure 5.5.E]. The corresponding datasets, and details regarding the statistical analyses of ER and CR data, are presented in Tables S.17 and S.18, respectively.

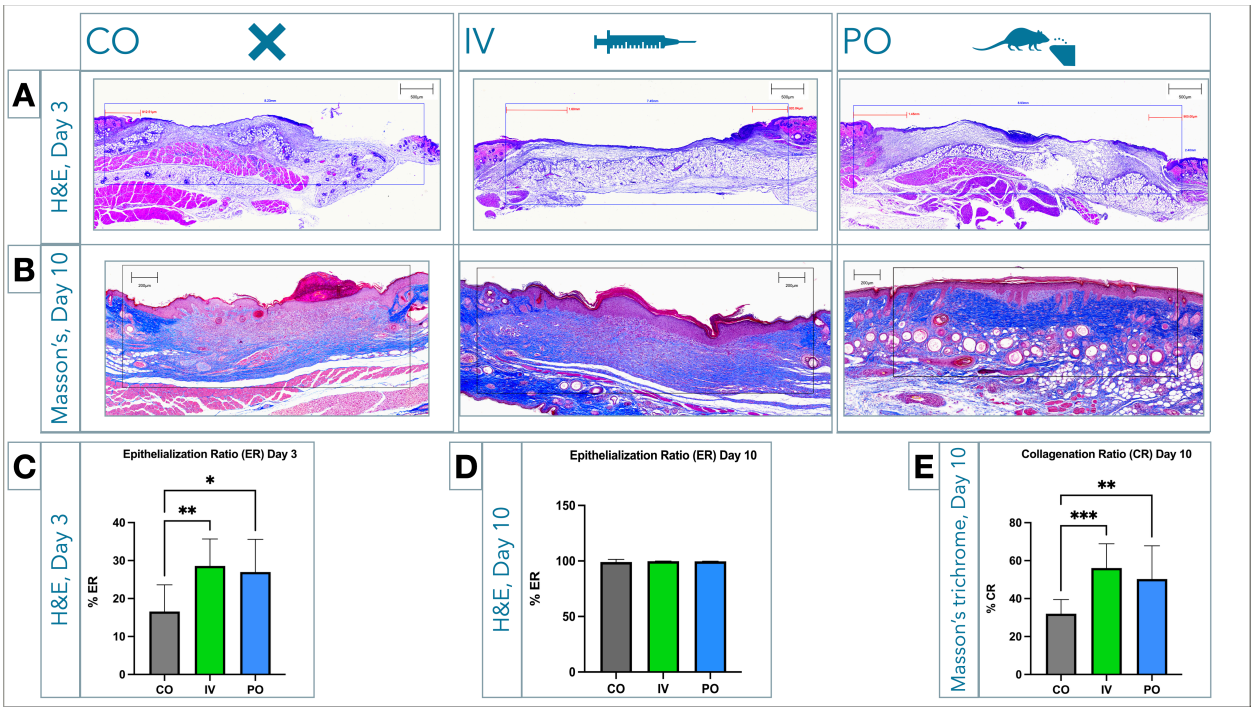

Figure 5.5: ONBW treatment administered IV and PO can enhance wound re-epithelialization and collagenation histopathologically, in healthy SKH1 mice evaluated at pre-determined time-points post-trauma, in Phase 2 experiments. (**A**) Representative histopathological slides stained with hematoxylin and eosin, illustrate wound epithelialization per experimental group (CO, IV, PO) at day 3. The slides were prepared and digitalized with whole slide imaging by an external collaborator (iHisto, Inc., Salem, MA, USA), producing digital slides that integrated continuous optical magnification up to the equivalent of a 40x objective lens. These slides were studied using the open-source QuPath software [Bankhead et al., 2017]; high-resolution static images were captured under an identical magnification scale of 500μm, and were exported for ER quantification to Fiji [Schindelin et al., 2012]. (**C**). At day 3, ER was calculated by dividing the length of the linear segment of the wound that was re-epithelialized, by the total linear length of the wound on the horizontal axis; the latter was identified based on the presence of cutaneous anatomical landmarks and organelles, microscopically. The resulting ER values were converted to percentages (% ER), and statistically analyzed as detailed in Table S.17. The data in the graphs represent mean values for each experimental group (CO, IV, PO), at day 3. *n*=12 per experimental group. (**D**) A similar analysis was conducted for the ER measurements recorded at day 10 [Table S.17]. (**B**) Representative histopathological slides stained with Masson's trichrome, illustrate collagen deposition in the wound beds per experimental group (CO, IV, PO), at day 10. The slides were prepared and studied as described above for the H&E-stained sections illustrating wound epithelialization, captured at a magnification scale of 200μm. (**E**) CR was calculated by dividing the number of blue-stained pixels representing collagen deposition in the surface area of each wound bed, by the total number of pixels in the surface area spanning the entire wound bed; the latter was demarcated using the Fiji freehand tool, following microscopic identification of the original wound margins, as described above. The resulting CR values were converted to percentages (% CR), and were statistically analyzed as detailed in Table S.18. The data in the graph represent mean values for each experimental group, at day 10.

Figure 5.5 (continued): *n*=12 per experimental group. **Abbreviations**: ONBW, oxygen nanobubble-enriched water; CO, negative controls; IV, intravenous administration retro-orbitally; PO, per os intake *ad libitum*; H&E, hematoxylin and eosin stain; ER, epithelialization ratio; Masson's, Masson's trichrome stain; CR, collagenation ratio; *, $p<0.05$; **, $p<0.01$; ***, $p<0.001$.

5.4 | Discussion

The findings presented in this Chapter add to the limited *in vivo* data evaluating the novel class of DOS formulations for healing applications, as a enabling technology to make wound-oxygenation therapies more efficient and accessible to the growing number of people affected by complicated wounds worldwide. Also, this is the first comprehensive analysis collectively evaluating the engineering principles, quality-control processes, biological safety, and healing efficacy of a DOS applying the cutting-edge technology of O_2 ultra-fine and nanobubbles *in vivo*, to our knowledge. Our data indicate that the proposed treatment factor using the aforementioned technology, the ONBW, can supply high DO amounts consistently and sustainably for at least 14 days. The DO concentrations recorded, ranging from 31.47 at protocol day -3 to 16.22mg/L at day 10, are equivalent to the highest comparable DO concentrations published in the literature. Combined with their sustainability for 14 consecutive days, the DO levels in the ONBW are highly promising for further biomedical exploration. This is strengthened by the remarkable biological safety of the ONBW *in vivo*, as our findings suggest that systemic ONBW administration, either IV or *per os*, has no impact on mouse health and homeostasis. Notably, these findings also mitigate the theoretical risk of gas embolism, which had been a key limitation for preceding technologies in the field, such as micro-bubble formulations, and the main reason why they could not be advanced into clinical development. Furthermore, our promising data on healing efficacy, achieved with both IV and *per os* administration of the ONBW, align with the outcomes of previous *in vivo* studies evaluating similar formulations though for different indications, ranging from physical development in healthy mice [Ebina et al., 2013], to sciatic nerve regeneration following complete crushing [Matsuoka et al., 2018], and preserved bone mass in a mouse osteoporosis model [Noguchi et al., 2017]. A detailed analysis of the findings presented in this Chapter, and their significance in association with the state-of-the-art knowledge and the results from relevant studies previously published in the field, is

discussed in Chapter 6 of this dissertation. Collectively, these data highlight the multifaceted potential of DOS biotechnologies in general, and of OUB-enriched formulations in particular, in a spectrum of biomedical indications implicating stages of the healing mechanism and/or tissue hypoxia.

6 | Discussion

The contents of this chapter are also represented in the following submission to *Journal of the American College of Surgeons*:

Dimitrios Ntentakis, Anastasia Maria Ntentaki, Eleni Delavogia, Petroula Seridou, Zoi Kollia, Nikolaos Sfakianos, Victor San Martin Carvalho Corrêa, Patroklos Katafygiotis, Danae Venieri, Nikolaos Arkadopoulos, Nicolas Kalogerakis. Dissolved oxygen and O_2-nanobubble biotechnologies enhance physiologic wound healing and cutaneous regeneration *in vivo*. (2024) *Submitted at Journal of the American College of Surgeons*.

6.1 | Synopsis of research findings

In this dissertation, we introduce the first systematic classification of the technologies enabling dissolved oxygen (DO) supplementation for wound healing and tissue-regenerating applications. Specifically, we identify four main technological categories: 1) dissolved oxygen solutions (DOS), 2) oxygenating dressings, 3) oxygenating hydrogels, and 4) oxygenating emulsions, each divided into subcategories based on their engineering fundamentals, manufacturing, and the biomechanics of DO supplementation. Following the systematic investigation of all these DO technologies, we focus on the category of aqueous-based DOS formulations containing no chemical surfactants or exogenous additives, which we consider the most promising approach for supplying DO to healing tissues. Subsequently, we propose a new *in vivo* protocol, designed to experimentally simulate a Phase 1 clinical trial while combining standardized methodologies from pre-existing protocols, as the initial step in the evaluation of novel biotechnologies targeted towards healing applications. Then, we successfully implement the proposed protocol to independently investigate the translational potential and biomedical suitability of two DOS biotechnologies, manufactured by exclusively leveraging the physics of the gas-liquid interphase while avoiding completely the use of chemical additives. Particularly, we discuss the technical and quality-control fundamentals required for the production and storage of two DOS biotechnologies with the aforementioned characteristics: a plain DOS, containing no physical enhancements to sustain DO levels, and an aqueous solution integrating the cutting-edge technology of ultra-fine gas bubbles, referred to as oxygen nanobubble-enriched water (ONBW). Then, we document their capacity to establish high DO concentrations consistently, for at least 14 days. Also, we verify that DOS administration is safe and well-tolerated *in vivo*, via three routes of administration: IV, LO, and PO. Furthermore, by monitoring full-thickness excisional wounds on the dorsal skin of healthy SKH1 mice, we extend our observations to show that, independently, two IV injections and *ad libitum* PO intake of either the plain DOS or the ONBW, may accelerate wound closure macroscopically, and improve epithelial regeneration and collagen deposition histopathologically.

6.2 | Current status of dissolved oxygen solutions studied for healing applications

In our proposed classification of DO technologies tested in the field of wound healing, presented in Chapter 2 of this dissertation, we identify three main engineering approaches for producing an aqueous-based DOS. The latest, and probably the most prevalent in the literature, yields solutions enriched with artificial oxygen (O_2) ultra-fine particles (OUPs) [Bisazza et al., 2008; Cavalli et al., 2009a, Cavalli et al., 2009b; Magnetto et al., 2014; Khadjavi et al., 2015; Prato et al., 2015; Gulino et al., 2015; Basilico et al., 2015]. OUPs are engineered through the incorporation of core-enhancing and coating chemicals, namely perfluorocarbons (PFCs), decafluoropentane (DFP), chitosan, and dextran. Such chemicals are added to augment the OUP O_2-carrying capacity and half-life, respectively, and thus the resulting DO concentrations in OUP-enriched solutions. The second engineering approach is based on O_2 ultra-fine bubbles (OUBs). With their nanoscale diameters, OUBs introduce an alternative strategy to sustain DO delivery, by leveraging the unique set of physical properties they exhibit within aqueous solutions [Tsuge, 2014]. Briefly, OUB-enriched solutions are generated by subjecting a mixture of pure O_2 and water to a sequence of high-speed centrifugations, employing Bernoulli's hydrodynamic principle, occasionally followed by brief sonication with specialized equipment to eliminate larger-diameter bubbles [Matsuki et al., 2012; Matsuki et al., 2014; Ebina et al., 2013; Tsuge, 2014; Noguchi et al., 2017; Matsuoka et al., 2018]. The third approach, and the simplest from a technical standpoint, entails the direct mixture of O_2 with water to produce an O_2-saturated DOS, upon equilibration of the two phases.

Naturally, at this early stage of research and biomedical development for the majority of technologies in the DOS category, their promising potential in would healing is mainly inferred from basic-science findings. However, it is prudent to acknowledge that only a fraction of these findings originates from *in vivo* experiments. For instance, only three articles studying OUB solutions contain *in vivo* data with potential correlation to the healing mechanism, with animal monitoring over a follow-up spectrum from 4 to 12 weeks [Ebina et al., 2013; Noguchi et al., 2017; Matsuoka et al., 2018]; these data are discussed in detail in the following sections of this Chapter. Similarly, in the field of OUP solutions, *in vivo* data are limited to the evaluation of sonophoresis-induced O_2 release by only two studies, and over a maximum timeframe of 15 minutes [Magnetto et al., 2014; Prato et al., 2015]. Instead, the majority of available evidence entails

isolated *in vitro* assessments of molecular pathways that correspond to different stages of the healing process [Bisazza et al., 2008; Cavalli et al., 2009a; Magnetto et al., 2014; Khadjavi et al., 2015; Prato et al., 2015; Gulino et al., 2015; Basilico et al., 2015]; these findings are discussed in detail in Chapter 2 of this dissertation. Yet, the inherent complexity of the healing physiology, which relies on the orchestrated interplay of multiple cellular types and signaling pathways, is quite challenging to simulate and accurately study *in vitro* [Boyko et al., 2017]; as presented in Chapter 1 of this dissertation. Thus, at this point, experimental data focussing on the *in vivo* properties, biological safety, and healing efficacy of DOS biotechnologies, as the ones presented in Chapters 4 and 5 of this dissertation, are important for advocating further biomedical testing and clinical translation.

Apart from the scarcity in data evaluating the outcomes of DOS administration *in vivo*, an additional factor that can decelerate, and even impede, the clinical translation of DOS biotechnologies in wound healing, is the huge methodological variability among the existing studies. A detailed list of the most significant among these methodological inconsistencies, is presented in the systematic analysis conducted in Chapter 2 of this dissertation. Regardless of the particular methodological inconsistencies though, it can be expected that, this variability dramatically impacts reproducibility, and thus, the validity of the ensuing research findings in the era of evidence-based medicine; which, in turn, can discourage not only researchers, but also potential investors to commit to such a project. Furthermore, it limits the ability to conduct rigorous comparisons among different DO-based interventions assessed for the same, or similar, indications in different studies; which, again, significantly hinders the decision-making processes preceding further investigation and development of a novel DOS biotechnology. In this setting, the comprehensive protocol discussed in Chapter 3 of this dissertation, and the rationale behind its design, can be regarded as a first step towards the direction of enhancing the comparability and reproducibility of pertinent *in vivo* data.

6.3 | Significance of measurements of DO concentrations

Verifying the capacity to establish significantly elevated DO levels, and sustainably over a period conducive to real-life clinical applications, is a pivotal step in the development of any biotechnology designed to enhance wound oxygenation. In

this study, DO concentrations were significantly higher in the plain DOS and the ONBW versus regular N/S, under identical pressure and temperature conditions. Of note, the majority of relevant DO measurements published in the literature have been obtained within the first 60 minutes upon production of each DOS formulation [Bisazza et al., 2008; Cavalli et al., 2009a; Ebina et al., 2013; Magnetto et al., 2014; Basilico et al., 2015; Gulino et al., 2015; Khadjavi et al., 2015; Prato et al., 2015; Noguchi et al., 2017; Matsuoka et al., 2018]. During this timeframe, our DO recordings of 30.76 mg/L and 31.47 mg/L in the plain DOS and the ONBW, respectively, stand at par with the highest DO concentrations from previous studies. The latter range from 8.50 to 30.00 mg/L (recorded at 25-37°C) in the OUP literature, including DO measurements from O_2-saturated solutions (OSS) similar to our plain DOS that have been used as control formulations in the OUP literature [Bisazza et al., 2008; Cavalli et al., 2009a; Khadjavi et al., 2015], and between 18.00 and 31.70 mg/L (recorded at 0.1 MPa, which is equivalent to atmospheric pressure, and at 25°C) in articles studying OUB solutions [Ebina et al., 2013; Noguchi et al., 2017; Matsuoka et al., 2018].

It is noteworthy that a subset of articles using different endpoints for DO quantification, have reported extremely variable DO measurements corresponding to the first hour post-production. Two characteristic examples are the data referring to oxygen-storing capacity, ranging from 400-420 mg/L in particular OUP and OSS formulations [Magnetto et al., 2014; Basilico et al., 2015; Gulino et al., 2015; Prato et al., 2015], as well as the measurements of DO release subsequently to OUP activation with ultrasound, recorded at 0.40-0.45 mg/L [Magnetto et al., 2014; Prato et al., 2015]. Apart from the distinct nature of each of those endpoints, such divergence from the values representing direct measurements of DO concentrations could also reflect differences in the duration of O_2 infusion whilst manufacturing each DOS formulation, the techniques and equipment applied to obtain these DO measurements, along with inconsistencies in temperature and pressure conditions. Concurrently, they could also be linked to the presence of additional chemical constituents, with or without surfactant properties; which, even in minute quantities, may alter the physicochemical dynamics and, thus, the accuracy of DO recordings within the solutions. Examples of such chemicals include ethanol, palmitic acid, and soya phosphatidylcholine, which have been used for the manufacturing of the OUP and OSS formulations discussed

herein [Magnetto et al., 2014; Khadjavi et al., 2015; Prato et al., 2015; Gulino et al., 2015; Basilico et al., 2015].

Along with the importance of adopting a universally-standardized methodology for monitoring DO levels, under identical physical and technical parameters, isolated DO measurements hold limited interpretative value by themselves. Especially in the field of DO-supplying biotechnologies designed for clinical applications, such measurements should not be evaluated as primary indicators of potential therapeutic efficacy. One characteristic example is presented by the ONBW assessed during our Phase 2 experiments. The DO concentrations recorded in an OUB-enriched formulation such as the ONBW, cannot integrate the amount of gaseous O_2 engulfed within the OUBs. Although impossible to quantify directly, the latter should be considered biomedically significant due to its superior bioavailability compared to DO. Indeed, the OUB-engulfed gaseous O_2 can be more readily available to be utilized by living tissues, as it can freely enter the cells via passive diffusion through their membranes; a spontaneous phenomenon that occurs more rapidly than the gradual O_2 dissolution within the aqueous microenvironment of tissues. Therefore, we believe it is preferable to contextualize DO concentrations in a broader framework, encompassing additional parameters specific to each corresponding DOS formulation and its intended applications. Such parameters include DO sustainability, biological safety, versatility regarding *in vivo* and clinical administration, alongside specific endpoints representing each therapeutic outcome tested. This rationale enables a more holistic appraisal of DOS biotechnologies, alongside a more accurate representation of their potential efficacy in clinical-grade scenarios.

6.4 | Biomedical significance of the recorded DO sustainability

Regarding DO sustainability, the elevated DO concentrations in our plain DOS and ONBW formulations demonstrated promising stability and consistency throughout the 14-day evaluation period. At 24 hours post-production, we observed an anticipated reduction from 30.76 mg/L to 25.84 mg/L in the plain DOS, and from 31.47 mg/L to 27.86 mg/L in the ONBW, representing a 15.9% and 11.4% decline, respectively. This was attributed to spontaneous macro-bubble formation in the pressurized microenvironment of each DOS formulation, naturally occurring upon exposure to

atmospheric pressures during *in vivo* administrations. Such macro-bubbles rapidly ascend towards the surface to release their O_2 content, with the tendency to equilibrate the solution's partial pressure of O_2 (PO_2) with ambient levels. Subsequently though, the recorded DO concentrations demonstrated a slowly-declining trend with gradually smoother fluctuations, almost stabilized at a narrow range between 17.07 and 21.07mg/L in the plain DOS, and from 16.22 to 20.28mg/L in the ONBW, during the second week post-production of each formulation. Notably, DO concentrations remained significantly higher in both the DOS formulations tested versus each corresponding N/S control, and consistently throughout the duration of our protocol design, for 14 days.

It should be noted that DO measurements extending beyond the first 60 minutes post-production are extremely scarce in the DOS literature [Ebina et al., 2013; Khadjavi et al., 2015]. Khadjavi and colleagues have described a declining trend in DO concentrations over the first 24 hours post-production, reaching approximately 10.75 mg/L in their OUP solution after 14 hours, and 8.75 mg/L in the corresponding OSS used as comparator after 17 hours [Khadjavi et al., 2015]. These values, recorded at room temperature as in our protocol, corresponded to a percent reduction of 15.4% and 18.6% from baseline, respectively; which align with our data for the same timeframe. Yet, a notable difference exists in the absolute DO values between the aforementioned OSS and our DOS formulations during the first 24 hours, measured at 8.75 mg/L in the OSS versus 25.84 mg/L in the plain DOS and 27.86 mg/L in the ONBW. Possibly, this divergence reflects the different duration of O_2 infusion while manufacturing each formulation. The latter ranged from 30 minutes during ONBW manufacturing and 10 minutes in our plain DOS protocol, to a substantially shorter 2-minute infusion in the OSS studied by Khadjavi's group [Khadjavi et al., 2015]. Yet, the extent to which this parameter may determine downstream DO concentrations and their long-term sustainability within the aqueous microenvironment of DOS biotechnologies, remains to be fully clarified.

In turn, Ebina and colleagues have reported a 72.6% decline in DO concentrations, from 31.7 mg/L during the first 45 minutes, to 8.7 mg/L at the 5-hour time-point post-production [Ebina et al., 2013]. These measurements were recorded in an OUB-enriched solution similar to our ONBW, stored at 4°C under atmospheric

pressure conditions. Beyond the 5-hour time-point though, DO levels remained constant at 8.7 mg/L, and persisted up to the 70th day of observation according to the authors [Ebina et al., 2013]. The etiology behind that steep reduction in DO concentrations during the first 5 hours, remains unclear. Assuming that the volume and pressure parameters were constant, it would be logical to consider a potential association with the substantially lower storage temperature of this formulation at 4°C, in contrast to the median temperatures of 22.85 and 25.80°C in our experiments. Yet, such an explanation would not align with the fact that O_2 dissolution is increased at lower temperatures. Instead, it is more likely that the lower storage temperature would lead to proportionately reduced levels of kinetic energy of the gas bubbles into an OUB-enriched formulation, thus enhancing OUB stability and enabling the extraordinary DO sustainability reported by Ebina and colleagues [Ebina et al., 2013].

6.5 | Validation of *in vivo* safety and tolerability

Thorough characterization of *in vivo* safety and tolerability is another pivotal step in the preliminary investigation of DOS biotechnologies developed for clinical applications. In this study, chemical surfactants were excluded from the manufacturing processes of both DOS formulations. Having eliminated the risk of surfactant-related toxicities *a priori*, our safety assessments were initially aimed towards the timely detection of potentially-harmful physical phenomena, arising from the interaction between the infused O_2 and the aqueous medium, prior to any *in vivo* use. Among the potential complications following systemic administration of DO, the most alarming would be the formation of gas bubbles, large enough to cause embolic sequelae in the circulation. In this study, the absence of larger-diameter bubbles (≥28μm), whose natural tendency to coalesce increases proportionately to their size, was confirmed upon daily DLS analyses in plain DOS and ONBW specimens. In the case of the ONBW, this was additionally verified with nanoparticle tracking analyses, while zeta-potential measurements documented the consistent electrostatic repulsion among the OUBs, further disfavoring coalescence into larger bubbles. Collectively, these steps effectively mitigated the theoretical risk of gas embolism. Also, the 28μm bubble-diameter threshold independently strengthened the safety profile of both DOS formulations, as it was adapted from the minimum acceptable size of the filter pores

used in clinical-grade extracorporeal membranous oxygenation (ECMO) devices [Barak and Katz, 2005]. Subsequently, during our *in vivo* experiments, the collection of detailed safety data verified that both DOS formulations entail no risk of eliciting severe adverse events (AEs) or alterations in murine well-being, regardless of local or systemic administration. These data align with the available, albeit limited, *in vivo* studies of relevant DOS biotechnologies manufactured without exogenous chemicals, where no safety issues have ever been reported [Ebina et al., 2013; Noguchi et al., 2017; Matsuoka et al., 2018].

Meanwhile, there are indications that our technological approach may encompass a more favorable safety profile, particularly when compared to formulations containing chemical surfactants whose complications in humans remain to be fully delineated. For instance, the possibility of AEs due to chitosan intake by humans, a popular OUP-coating hydrophobic carbohydrate [Bisazza et al., 2008; Cavalli et al., 2009a; Magnetto et al., 2014; Khadjavi et al., 2015], warrants careful consideration. There are reports of chitosan-induced cytotoxicity across three human cell lines of cutaneous, vascular, and respiratory histological origin [Je et al., 2006; Wiegand et al., 2010], whose translational significance is difficult to be addressed due to the unpredictable degree of chitosan de-acetylation *in vivo*. Furthermore, prolonged exposure to hydrophobic perfluorocarbons, the core-enhancing components most prevalent in the OUP literature [Bisazza et al., 2008; Cavalli et al., 2009a; Cavalli et al., 2009b; Magnetto et al., 2014; Khadjavi et al., 2015; Prato et al., 2015; Gulino et al., 2015; Basilico et al., 2015], has been linked to dose-dependent hepatotoxicity and gestational diabetes mellitus in humans [Butenhoff et al., 2002; Zhang et al., 2015]. Equally concerning is the risk of potential accumulation in the lungs, which may become significant as early as following a 12-month exposure [Nosé, 2004]. Thereby, it becomes evident that the risk of cumulative toxicity from the clinical use of fluorinated compounds can implicate multiple organs/systems in the human body, and thus, can be encountered by multiple specialties. Notably, many of the aforementioned chemicals are also frequently incorporated in other DO-supplying biotechnologies currently tested for healing applications, such as oxygenating hydrogels and emulsions [Davis et al., 2007; Wijekoon et al., 2013; Li et al., 2015; Patil et al., 2018; Ntentakis et al., 2021].

Collectively, any potential toxicity associated with cumulative dosing should be thoroughly considered during the development of novel healing factors. This becomes particularly relevant in the case of the epidemiologically-concerning chronic wounds [Walmsley, 2002; Sen et al., 2009], whose complicated natural history typically mandates prolonged treatment regimens with unpredictable duration and success rates. Thus, future studies should consider integrating an elaborate assessment of the risk-benefit ratio associated with the inclusion of chemical surfactants in DOS biotechnologies, and mathematically correlate any improvement in DO sustainability and clinically-translatable outcomes with the relative risk of biological AEs. Also, comparative studies could co-evaluate additional factors affecting this risk-benefit ratio, such as technical difficulties and equipment-related hazards, during both the production and the biomedical use of these biotechnologies. Prospectively, these data will be pivotal for documenting the most cost-effective and translatable approaches towards enhanced wound oxygenation via DO.

6.6 | Healing efficacy *in vivo* and biomedical potential

Regarding healing efficacy *in vivo*, IV and PO administration of either DOS biotechnology independently, was accompanied by very promising macroscopic and histopathological outcomes in this study. Macroscopically, a total of two IV injections of either DOS formulation, once every five days, enabled a significant increase in VC compared to the control mice. This significant acceleration of wound closure was documented during the majority of timeframes on our protocol timeline, all of which encompassed the timeframe between days 0 and 7 in both Phases 1 and 2. Yet, the IV administration of ONBW in Phase 2 was accompanied by an earlier significant increase in VC, recorded in the immediate post-operative period between days 0 and 3, versus the more gradual effect of plain DOS injections on VC during Phase 1 experiments. Also, with PO intake of plain DOS during Phase 1, VC showed only a trend elevation versus the CO group. However in Phase 2, PO intake of ONBW enabled a consistent VC acceleration compared to the CO mice in multiple protocol timeframes, with the most significant difference recorded between days 0 and 7. A potential explanation for these observations could be associated with two parameters. First, the superior bioavailability of the IV route of administration compared to PO intake, which applies to

the pharmacokinetics of any treatment factor. Our data on the specific DO amounts, in milligrams, that each mouse received in the IV and the PO groups of administration of either DOS we tested, point towards this conclusion [Tables S.12, S.13, S.19, S.20]. Interestingly, the aforementioned healing effects were achieved with two IV injections per mouse, where the absolute milligrams of DO where approximately 100 times lower than the DO amount received via PO intake. Secondly, it is the more readily available, and plausibly superior, total oxygen content within OUB-enriched solutions such as the ONBW, containing both DO and gaseous O_2; with the latter being able to freely enter the cells via passive diffusion, which is driven by local pressure and concentration gradients, and also more rapidly compared to the gradual dissolution of O_2 within the aqueous microenvironment.

Our histopathological data concurred with the aforementioned macroscopic findings, demonstrating a more consistent pattern of epithelialization and collagenation outcomes in Phases 1 and 2. At day 3, epithelialization (ER) was found significantly higher in the IV group compared to the CO, as well as in the PO group versus the CO, with both DOS formulations. Furthermore, exclusively in Phase 2, the magnitude of the differences in mean ER recorded with each route of administration, IV and PO, followed a pattern similar to the macroscopic measurements of VC corresponding to the same timeframe, between protocol days 0 and 3. Analogously, at day 10, collagenation (CR) was significantly enhanced with IV administration versus CO, and with PO intake versus CO, again with both plain DOS and ONBW treatments independently, mirroring the epithelialization outcomes from day 3.

Collectively, our *in vivo* data on healing efficacy are congruent with the literature describing the healing stages, their perceived duration, the sequence of molecular events defining each stage, and the documented relationship of key implicated enzymes with O_2 levels. For instance, the timeframe from day 0 to day 7 post-wounding, which was consistently associated with improved macroscopic outcomes in our healing assessments, entails enzymatic activities that primarily depend on adequate O_2 supply. An illustrative example is NADPH oxidase, a pivotal enzyme in the biochemical cascade leading to reactive O_2 species formation during the acute inflammation stage, which typically spans the initial three days post-wounding [Gurtner et al., 2008]. NADPH oxidase utilizes molecular O_2 as its substrate, and has been

shown to reach its half-maximal efficacy within a PO_2 range of 45–80 mmHg [Allen et al., 1997]. Theoretically, our findings from both Phases 1 and 2 may represent the downstream benefit from enhanced oxygen supply during acute inflammation, and thus, from the more efficient completion of the NADPH oxidase cascade, on the subsequent healing stages. Another pertinent example involves the activity of collagen hydroxylases during the proliferative stage of the healing mechanism, approximately from day 3 to day 10 post-wounding. These enzymes, which are crucial for collagen synthesis, have been found to reach their half-maximal velocity at a PO_2 of 25 mmHg [Myllylä et al., 1977]. Also, there are data suggesting that fibroblast-mediated collagen deposition necessitates a minimum PO_2 threshold of 30–40 mmHg [Hutton et al., 1967; Myllylä et al., 1977]. Of note, a dose-dependent correlation with PO_2 has been independently described for the functions of NADPH oxidase and collagen hydroxylases, achieving their peak efficacy at around 250 and 300 mmHg, respectively [Myllylä et al., 1977; Allen et al., 1997].

In the literature, macroscopic and histopathological data elucidating the healing efficacy of DOS biotechnologies *per se*, are scarce. Nevertheless, there are *in vivo* data from three studies that warrant acknowledgment [Ebina et al., 2013; Noguchi et al., 2017; Matsuoka et al., 2018], though they can only be extrapolated as presumed indications of a beneficial effect of DOS treatment on the healing mechanism. Macroscopically, Ebina and colleagues have demonstrated a statistically significant increase in body mass and length in healthy 5-week old DBA1/J mice [Ebina et al., 2013]. Those mice were drinking an OUB-enriched DOS *ad libitum*, similarly to the PO groups in our protocol, yet over a substantially longer period extending to 12 weeks [Ebina et al., 2013]. A connection between such anabolic outcomes and enhanced wound healing can be hypothesized, based on the hyper-metabolic state physiologically induced by trauma as a consequence of activation of the healing cascade [Matsuda et al., 1987; Gupta and Raghubir, 2005]. It has also been suggested that, the additional energy supply required to sustain the healing process primarily derives from oxidative metabolism, making the whole mechanism strongly dependent on adequate O_2 supply [Matsuda et al., 1987; Gupta and Raghubir, 2005].

Histopathologically, Noguchi and colleagues have documented reduced osteoclastic activation and preserved bone mass in a mouse model of glucocorticoid-induced osteoporosis, which was achieved via IP administration of an OUB-enriched solution similar to our ONBW, three times weekly, for eight weeks [Noguchi et al., 2017]. Furthermore, Matsuoka and colleagues have described a significant regeneration of myelinated axons in a rat sciatic nerve crush injury model, following IP injections of an OUB solution akin to the one administered by Noguchi's group, thrice weekly, over four weeks [Matsuoka et al., 2018]. Collectively, the aforementioned data suggest that systemic DOS administration may stimulate body metabolism, up-regulate tissue regeneration, and improve resistance to cellular injury and loss; all of which, could also be leveraged to physiologically enhance wound healing.

6.7 | Implications per route of administration

Healing efficacy per route of administration is another important parameter to consider during the translational investigation of DOS biotechnologies. In this study, our macroscopic and histopathological findings align in that, direct DOS application on wound surfaces may be accompanied by inferior healing outcomes compared to the IV and PO routes. Possibly, the explanation behind this observation lies in the technique we used for local administration, as described in the *Methods* section. Indeed, daily irrigations with plain DOS onto the wounds via a syringe needle through the dressing, may have washed away migrating cells and molecular signals whose presence is pivotal for the healing process; a phenomenon with potentially cumulative impact on the ultimate healing outcomes over time, according to our histopathological findings from Phase 1 experiments. Also, it may have caused significant DO losses, by establishing continuous PO_2 gradients through the punctured wound dressing. Concurrently, we should consider the additional stress for the mice from the daily physical manipulations during each irrigation, as opposed to the *ad libitum* PO intake and the IV injections performed once every five days. Still, this technique was preferred over the continuous application onto the wound surface, which requires a surgical gauge or dressing soaked with the DOS. The main reason was that, such materials may variably act as a scaffold for incoming cells and chemotactic molecules. Thereby, they might have introduced a substantial confounder to the findings of our Phase 1

experiments; particularly during the pairwise analyses of healing efficacy among the different experimental groups, which were defined by the different routes of administration in our protocol.

Given the implicated physics, and the natural dependance of DO concentrations on PO_2 gradients, it appears unlikely that local monotherapy with formulations similar to our plain DOS may be capable of improving wound healing as consistently as systemic administration; especially if applied via direct irrigation on wound surfaces. The healing outcomes recorded during our Phase 1 experiments also point towards this argument. Yet, before abandoning this route of administration completely, additional studies are encouraged to investigate local applications of DOS biotechnologies in more detail. For instance, comparative *in vivo* experiments could simultaneously examine all the alternative techniques of local administration, along with their corresponding safety and healing outcomes.

In turn, the promising efficacy of IV administration in this study, both macroscopically and histopathologically, prompts further exploration of systemic uses of DOS biotechnologies; even for indications that extend beyond the scope of wound healing and tissue regeneration. Combined with the sustained elevation in DO concentrations that we recorded in both the plain DOS and the ONBW, one such group of indications could be associated with systemic hypoxia. Interestingly, there are *in vivo* data from two previous studies demonstrating significantly improved survival rates and lung oxygenation in two different acute lung-trauma models in rats, following systemic (IP) administration of an OUP solution and an OSS, respectively [Feshitan et al., 2014; Fiala et al., 2020].

Analogously, we consider our findings with PO intake highly encouraging, given that the PO route stands as the most convenient and least invasive method for delivering any treatment factor. Specifically for DOS biotechnologies though, it warrants emphasis that, to thoroughly characterize their efficacy via PO intake, targeted research is required to precisely determine the optimal doses, dosing frequency, treatment duration, and minimum follow-up. Modifications in the aforementioned parameters will be indispensable, as a means to counterbalance for the inferior bioavailability of PO intake compared to the IV route.

6.8 | Clinical trials and biopharmaceutical industry

Notably, the biopharmaceutical industry is beginning to show increasing interest in the clinical translation of systemically-administered DO formulations that do not contain chemical surfactants. Since 2021, three early-stage clinical trials have been launched to specifically investigate the biomedical efficacy of OUB-enriched solutions, administered either PO [https://clinicaltrials.gov/. Identifiers NCT05777642 and NCT05711290] or IV [https://clinicaltrials.gov/. Identifier NCT03456882]. There is also an ongoing Phase 1 trial aiming to evaluate the outcomes of a locally-applied OUB-enriched solution on acute and chronic wounds [https://clinicaltrials.gov/. Identifier NCT05169814]; however, the technique used for local administration is different from the one tested in Chapter 4 of our work, as it involves the use of soaked sponges and negative-pressure therapy with instillation. A synoptic overview of these clinical trials is presented in Table 6.1.

Table 6.1: Overview of the ongoing early-stage clinical trials actively testing OUB-enriched DOS formulations, resembling the ONBW tested in our experiments.

Brief description	Clinical trial ID	Phase #	n	Intervention	Control	Route	Clinical indication	Follow -up	Results
ONBD impact on exercise in elite athletes	NCT05777642	1/2	42	"OUB drink (ONBD)"	Placebo *	PO	Healthy athletes, to enhance athletic performance	7 days	Not yet recruiting
ONBD impact on exercise in pulmonary fibrosis	NCT05711290	1/2	28	"OUB drink (ONBD)"	Placebo *	PO	Patients with Pulmonary Fibrosis	1 day	Completed, results pending
ONBW (N/S) "RNS60" on ALS biomarkers	NCT03456882	2	147	RNS60 + riluzole (N/S + OUBs); IV once weekly, then nebulization for next 6 days	N/S + riluzole (SoC)	IV + inhaled	Patients with ALS	24-48 weeks	Significant outcomes in FVC% & ALSAQ-40 (eating, drinking)

Brief description	Clinical trial ID	Phase #	n	Intervention	Control	Route	Clinical indication	Follow-up	Results
MNBs for treatment of acute & chronic wounds	NCT05169814	1	40	(a) MNB solution irrigation, daily (sponge replaced every 5 days); (b) MNB solution via NPWTi	N/S; (a) irrigation (b) NPWTi	(a) LO irrigation; b) NPWTi	Acute (daily) & chronic (NPWTi) wounds	2-4 weeks	Active recruiting

Table 6.1 Notes: Overview of key methodological parameters and endpoints assessed in ongoing early-stage clinical trials, testing OUB-enriched DOS formulations with variable degree of similarity to the ONBW in our work, for various clinical indications.* Placebo intervention was a mixture of natural flavorings (licorice, glycerol, and citric acid) with water. **Abbreviations**: OUBs, oxygen ultra-fine bubbles; DOS, dissolved oxygen solution; ONBW, oxygen nanobubble-enriched water; ONBD, oxygen nanobubble drink [oxygenated nanobubbles made from lecithin and natural flavorings (licorice, glycerol, and citric acid), mixed with water]; n, number of participants; IV, administered intravenously; PO, administered per os; LO, applied locally; N/S, normal saline solution 0.9% NaCl; ALS, Amyotrophic Lateral Sclerosis; SoC, standard of care; FVC%, Forced Vital Capacity percent value; ALSAQ-40, ALS Assessment Questionnaire with 40 items; MNBs; oxygen micro-/nano-bubbles; NPWTi, negative pressure wound therapy with instillation; N/A, not applicable.

While the aforementioned trials are currently in the recruitment stage or pending announcement of their results, it is important to note the broad spectrum of clinical indications being tested. The latter extend beyond wound healing [NCT05169814], and range from enhancement of physical performance in healthy athletes [NCT05777642] and in patients with idiopathic pulmonary fibrosis [NCT05711290], to adjunct therapy in cases of amyotrophic lateral sclerosis [NCT03456882]. In turn, the variability among the clinical indications tested may reflect the versatility in the potential biomedical applications of OUB-enriched solutions analogous to our ONBW. This argument is strengthened by the universality of the healing mechanism itself, which is not only evolutionally conserved across multiple different species [Boyko et al., 2017], but also encompasses pathologic responses such as inflammation, which are part of innate immunity; and are, thus, implicated in the pathophysiology of numerous human diseases.

6.9 | Future directions

Given the validation of biological safety of both the DOS biotechnologies tested, and their promising efficacy in wound healing, there are three research steps to be

considered in the immediate future. The two DOS formulations can be comparatively studied by conducting the same experimental protocol, as described in Chapter 3, with the aim to replicate the healing outcomes observed in our experiments, and to gather additional data on the superiority of one of the two formations versus the other, if any. In our experiments, the ONBW biotechnology demonstrated more promising healing outcomes, overall; therefore, if the concurrent testing of both DOS formulations is not experimentally feasible, we would encourage investigators to proceed with an OUB-enriched saline solution similar to the ONBW tested herein. In this scenario, the second research step would be to further investigate the biological safety and healing efficacy of the ONBW, this time in larger mammalian models with closer histologic similarities to human skin, such as swine models [Boyko et al., 2017], and otherwise similar specifications; young, healthy, sex-matched pigs would be the optimal starting point, so that the healing response would likely proceed physiologically as in the SKH1 mice in our experiments. Another research direction to consider, either concurrently or even prior to the aforementioned research steps, would be to evaluate the administration of ONBW in mouse models simulating human diseases, whose pathophysiology strongly implicates abnormalities in the healing mechanism, with or without tissue hypoxia. In this direction, one of the first protocols to consider would be diabetic mouse wounds, due to the epidemiological significance of type 2 diabetes along with the extremely high prevalence of non-healing wounds in this population.

Regarding further steps, the ONBW technology that utilizes ultra-fine bubbles, or nanobubbles, is considered highly promising to be implemented in multiple biomedical applications beyond the scope of wound healing. Historically, nanobubble technology became known for its impressive applications in Environmental Engineering, for the purification and disinfection of stagnant water [Agarwal et al., 2011; Etchepare et al., 2017]. Ever since, studying the unique physical properties of nanobubbles has brought out and highlighted their multifaceted biotechnological perspective, and the potential advantages from their applications into clinical practice. Thus, experimental nanobubble-enriched biotechnologies have gained increased attention by multidimensional research teams.

Interestingly, beyond their ability to deliver gas molecules, such as O_2, to tissues effectively and sustainably, nanobubble technology has also been studied for targeted

drug delivery [Cavalli et al., 2016]. Researchers have shown that doxorubicin-loaded nanobubbles with extracorporeal shock waves can increase intracellular drug content and cytotoxicity in cell lines from human anaplastic thyroid cancer [Marano et al., 2016]. *In vivo* experiments from the same group have also demonstrated superior accumulation of the chemotherapeutic drug in the same tumor type, accompanied by significant reduction in tumor volume and weight in a xenograft mouse model, [Marano et al., 2017]. In another study, an O_2-nanobubble drug-encapsulation system enabling ultrasound-guided delivery of mitomycin-C, led to significantly lower tumor progression while using a 50% lower concentration of chemotherapeutic drug, in a mouse model of urothelial carcinoma [Bhandari et al., 2018].

Furthermore, since hypoxia has been associated with higher rates of failure in tumor treatments with either radiotherapy, chemotherapy, or immunotherapy [Graham and Unger, 2018], OUB technologies are also being investigated as a means to reduce or even reverse tumor hypoxia [Jahanban-Esfahlan et al., 2018]. *In vitro*, OUBs have been reported to reverse the expression of hypoxia markers in breast cancer cell lines [Khan et al., 2018; Iijima et al., 2018], and to also increase their sensitivity to radiation therapy [Iijima et al., 2018]. *In vivo*, OUBs have been successfully tested for targeted O_2 delivery to tumors, via subcutaneous [Bhandari et al., 2017] and per os [Owen et al., 2016] administration. Collectively, the aforementioned evidence supports the multifaceted biomedical potential of OUB formulations, analogous to the ONBW tested in Chapter 5 of this dissertation, as an enabling technology with highly promising applications even in untreatable human diseases.

6.10 | Limitations

The findings of this study should be interpreted in the context of the challenges faced during the characterization of biological safety and efficacy for novel biotechnologies, before and during *in vivo* testing, and our experimental protocol *per se*. Thereby, we acknowledge the following limitations. First, we used a non-splitting approach in our wound model, unlike the historically-established protocol that recommends suturing the wound edges along the uninjured perimetry, towards healthy mouse skin [Wang et al., 2013]. The reproducibility and validity of non-splinting wound models, similar to the one we used, have been recently documented by independent

studies [Chen et al., 2015; Park et al., 2015; Yampolsky et al., 2024]. Currently, non-splinting models are frequently encountered in the healing literature [Tiganescu et al., 2014; Öri et al., 2017; Seo et al., 2021], as they can minimize physical stress, anesthesia requirements, and surgical time; all of which can benefit mouse well-being, without compromising the validity of healing assessments [Chen et al., 2015]. Nonetheless, to maximize the translational relevance of our findings, additional experiments using different protocols are highly recommended; starting with the established splinting model in mice, and followed by studies in swine wounds which bear the closest similarity to human skin [Sullivan et al., 2001].

Furthermore, the application of transparent adhesive dressings on the wound surfaces introduced additional variability in our macroscopic evaluations. Such dressings can mechanically interfere with the wound margins, as well as with the magnitude and direction of the naturally-occurring contraction of mouse skin towards the wound epicenter, both to an unpredictable degree [Yampolsky et al., 2024]. Yet, applying those dressings was deemed essential for the scope of our study, as they enabled a more precise assessment of *in vivo* safety. For instance, without a dressing sealing the wound surface, it would have been extremely hard to differentiate the etiology of any signs of systemic inflammation; which could have been caused by either a disseminated infection of the wound site unrelated to the treatment, or a large vessel embolized by gas bubbles from the administered plain DOS or ONBW.

To offset for any dressing-related variability, the following measures were taken during our experimental design. First, the optimal number of animals for each *in vivo* experiment was statistically determined, by applying the law of diminishing returns for Phase 1 experiments and conducting g*power analysis for Phase 2 experiments, based on calculations of the effect size from the Phase 1 dataset. Furthermore, one wound from each mouse was randomly selected to be analyzed as a biological replicate. Also, our protocol included the quantitative evaluation of two histopathological endpoints dedicated to healing efficacy, in addition to the macroscopic measurements. Collectively, the DO measurements we recorded prior to *in vivo* use, and the fact that the majority of our macroscopic and histopathological findings on wound closure are congruent, suggest that DOS biotechnologies containing no chemical surfactants should be further explored for healing applications. Nonetheless, additional *in vivo* and

clinical studies are required to validate the relationship between the statistical significance calculated experimentally, and the actual translational significance of DOS administration in the biomedical setting.

6.11 | Conclusions

This dissertation contributes to the limited body of *in vivo* evidence evaluating dissolved oxygen (DO) biotechnologies for wound healing, as an additional strategy to meet the anticipated growth in patient needs, globally. Our findings present novel and comprehensive insights into the biomedical leveraging of two aqueous-based DO biotechnologies classified in the category of DO solutions (DOS), manufactured without the use of potentially toxic chemicals: a plain DOS with no physical enhancements to sustain DO levels, and an aqueous solution integrating the cutting-edge technology of naturally-generated ultra-fine gas bubbles, referred to as oxygen nanobubble-enriched water (ONBW). Collectively, our data can be harnessed for further development of safe and effective DOS-based therapeutics, not only in wound healing but also in the broad spectrum of human pathologies whose etiopathology implicates tissue hypoxia.

Bibliography

Adamska M, Matus DQ, Adamski M, Green K, Rokhsar DS, Martindale MQ, Degnan BM. The evolutionary origin of hedgehog proteins. Curr Biol. 2007 Oct 9;17(19):R836-7.

Agarwal A, Ng WJ, Liu Y. Principle and applications of microbubble and nanobubble technology for water treatment. Chemosphere. 2011 Aug;84(9):1175-80.

Akula S, Brosch IK, Leipzig ND. Fluorinated Methacrylamide Chitosan Hydrogels Enhance Cellular Wound Healing Processes. Ann Biomed Eng. 2017 Nov;45(11):2693-2702.

Allen DB, Maguire JJ, Mahdavian M, Wicke C, Marcocci L, Scheuenstuhl H, Chang M, Le AX, Hopf HW, Hunt TK. Wound hypoxia and acidosis limit neutrophil bacterial killing mechanisms. Arch Surg. 1997 Sep;132(9):991-6.

Almeleh R. Spontaneous accelerated epithelialization in deep dermal burns using an oxygen-delivering hydrogel: a report of two cases. Wounds. 2013;25(10):E18-E25.

Androjna C, Gatica JE, Belovich JM, Derwin KA. Oxygen diffusion through natural extracellular matrices: implications for estimating "critical thickness" values in tendon tissue engineering. Tissue Eng Part A. 2008 Apr;14(4):559-69.

Arenas Gómez CM, Sabin KZ, Echeverri K. Wound healing across the animal kingdom: Crosstalk between the immune system and the extracellular matrix. Dev Dyn. 2020 Jul;249(7):834-846.

Arras M, Rettich A, Cinelli P, Kasermann HP, Burki K. Assessment of post-laparotomy pain in laboratory mice by telemetric recording of heart rate and heart rate variability. BMC Vet Res. 2007 Aug 2;3:16.

Ashcroft GS. Sex difference in wound healing. Adv Mol Cell Biol. 2004 Dec;34(12):321-8.

Babior BM. Oxygen-dependent microbial killing by phagocytes (first of two parts). N Engl J Med. 1978 Mar 23;298(12):659-68.

Bachmanov AA, Reed DR, Beauchamp GK, Tordoff MG. Food intake, water intake, and drinking spout side preference of 28 mouse strains. Behav Genet. 2002 Nov;32(6):435-43.

Bankhead P, Loughrey MB, Fernández JA, Dombrowski Y, McArt DG, Dunne PD, McQuaid S, Gray RT, Murray LJ, Coleman HG, James JA, Salto-Tellez M, Hamilton PW. QuPath: Open source software for digital pathology image analysis. Sci Rep. 2017 Dec 4;7(1):16878.

Barak M, Katz Y. Microbubbles: pathophysiology and clinical implications. Chest. 2005 Oct;128(4):2918-32.

Basilico N, Magnetto C, D'Alessandro S, Panariti A, Rivolta I, Genova T, Khadjavi A, Gulino GR, Argenziano M, Soster M, Cavalli R, Giribaldi G, Guiot C, Prato M. Dextran-shelled oxygen-loaded nanodroplets reestablish a normoxia-like pro-angiogenic phenotype and behavior in hypoxic human dermal microvascular endothelium. Toxicol Appl Pharmacol. 2015 Nov 1;288(3):330-8.

Belda FJ, Aguilera L, García de la Asunción J, Alberti J, Vicente R, Ferrándiz L, Rodríguez R, Company R, Sessler DI, Aguilar G, Botello SG, Ortí R; Spanish Reduccion de la Tasa de Infeccion Quirurgica Group. Supplemental perioperative oxygen and the risk of surgical wound infection: a randomized controlled trial. JAMA. 2005 Oct 26;294(16):2035-42.

Benavides F, Oberyszyn TM, VanBuskirk AM, Reeve VE, Kusewitt DF. The hairless mouse in skin research. J Dermatol Sci. 2009 Jan;53(1):10-8.

Bert P. La Pression Barometrique. Paris: Masson; 1878. Translated by Hitchcock M, Hitchcock A. Columbus (OH): College Book Company; 1943.

Berthod F, Germain L, Tremblay N, Auger FA. Extracellular matrix deposition by fibroblasts is necessary to promote capillary-like tube formation in vitro. J Cell Physiol. 2006 May;207(2):491-8.

Bhandari P, Novikova G, Goergen CJ, Irudayaraj J. Ultrasound beam steering of oxygen nanobubbles for enhanced bladder cancer therapy. Sci Rep. 2018 Feb 15;8(1):3112.

Bhandari PN, Cui Y, Elzey BD, Goergen CJ, Long CM, Irudayaraj J. Oxygen nanobubbles revert hypoxia by methylation programming. Sci Rep. 2017 Aug 24;7(1):9268.

Bisazza A, Giustetto P, Rolfo A, Caniggia I, Balbis S, Guiot C, Cavalli R. Microbubble-mediated oxygen delivery to hypoxic tissues as a new therapeutic device. Annu Int Conf IEEE Eng Med Biol Soc. 2008;2008:2067-70.

Boateng JS, Matthews KH, Stevens HN, Eccleston GM. Wound healing dressings and drug delivery systems: a review. J Pharm Sci. 2008 Aug;97(8):2892-923.

Boyko TV, Longaker MT, Yang GP. Laboratory Models for the Study of Normal and Pathologic Wound Healing. Plast Reconstr Surg. 2017 Mar;139(3):654-662.

Broussard CL. Hyperbaric oxygenation and wound healing. J Vasc Nurs. 2004 Jun;22(2):42-8.

Brucker MJ, Gruskin E, Farrell CL, Siddiqui A, Mustoe TA. Differential expression of platelet-derived growth factor receptor-beta in an aging model of wound repair. Wound Repair Regen. 1996 Apr-Jun;4(2):219-23.

Butenhoff J, Costa G, Elcombe C, Farrar D, Hansen K, Iwai H, Jung R, Kennedy G Jr, Lieder P, Olsen G, Thomford P. Toxicity of ammonium perfluorooctanoate in male cynomolgus monkeys after oral dosing for 6 months. Toxicol Sci. 2002 Sep;69(1):244-57.

Castro CI, Briceno JC. Perfluorocarbon-based oxygen carriers: review of products and trials. Artif Organs. 2010 Aug;34(8):622-34.

Cavalli R, Bisazza A, Rolfo A, Balbis S, Madonnaripa D, Caniggia I, Guiot C. Ultrasound-mediated oxygen delivery from chitosan nanobubbles. Int J Pharm. 2009 Aug 13;378(1-2):215-7. (a)

Cavalli R, Bisazza A, Giustetto P, Civra A, Lembo D, Trotta G, Guiot C, Trotta M. Preparation and characterization of dextran nanobubbles for oxygen delivery. Int J Pharm. 2009 Nov 3;381(2):160-5. (b)

Cavalli R, Soster M, Argenziano M. Nanobubbles: a promising efficient tool for therapeutic delivery. Ther Deliv. 2016;7(2):117-38.

Chandra PK, Ross CL, Smith LC, Jeong SS, Kim J, Yoo JJ, Harrison BS. Peroxide-based oxygen generating topical wound dressing for enhancing healing of dermal wounds. Wound Repair Regen. 2015 Nov-Dec;23(6):830-41.

Chang N, Goodson WH 3rd, Gottrup F, Hunt TK. Direct measurement of wound and tissue oxygen tension in postoperative patients. Ann Surg. 1983 Apr;197(4):470-8.

Chen H, Cheng Y, Tian J, Yang P, Zhang X, Chen Y, Hu Y, Wu J. Dissolved oxygen from microalgae-gel patch promotes chronic wound healing in diabetes. Sci Adv. 2020 May 15;6(20):eaba4311.

Chen L, Guo S, Ranzer MJ, DiPietro LA. Toll-like receptor 4 has an essential role in early skin wound healing. J Invest Dermatol. 2013 Jan;133(1):258-67.

Chen L, Mirza R, Kwon Y, DiPietro LA, Koh TJ. The murine excisional wound model: Contraction revisited. Wound Repair Regen. 2015 Nov-Dec;23(6):874-7.

Corral CJ, Siddiqui A, Wu L, Farrell CL, Lyons D, Mustoe TA. Vascular endothelial growth factor is more important than basic fibroblastic growth factor during ischemic wound healing. Arch Surg. 1999 Feb;134(2):200-5.

Dahlgren C, Karlsson A. Respiratory burst in human neutrophils. J Immunol Methods. 1999 Dec 17;232(1-2):3-14.

Das S, Baker AB. Biomaterials and Nanotherapeutics for Enhancing Skin Wound Healing. Front Bioeng Biotechnol. 2016 Oct 31;4:82.

Davis SC, Cazzaniga AL, Ricotti C, Zalesky P, Hsu LC, Creech J, Eaglstein WH, Mertz PM. Topical oxygen emulsion: a novel wound therapy. Arch Dermatol. 2007 Oct;143(10):1252-6.

de Smet GHJ, Kroese LF, Menon AG, Jeekel J, van Pelt AWJ, Kleinrensink GJ, Lange JF. Oxygen therapies and their effects on wound healing. Wound Repair Regen. 2017 Aug;25(4):591-608.

Deacon RM. Burrowing in rodents: a sensitive method for detecting behavioral dysfunction. Nat Protoc. 2006;1(1):118-21.

Dissemond J, Kröger K, Storck M, Risse A, Engels P. Topical oxygen wound therapies for chronic wounds: a review. J Wound Care. 2015 Feb;24(2):53-4, 56-60, 62-3.

Eaglstein WH, Mertz PM. “Inert” vehicles do affect wound healing. J Invest Dermatol. 1980;74(2):90-1.

Ebina K, Shi K, Hirao M, Hashimoto J, Kawato Y, Kaneshiro S, Morimoto T, Koizumi K, Yoshikawa H. Oxygen and air nanobubble water solution promote the growth of plants, fishes, and mice. PLoS One. 2013 Jun 5;8(6):e65339.

Edwards SW, Hallett MB, Campbell AK. Oxygen-radical production during inflammation may be limited by oxygen concentration. Biochem J. 1984 Feb 1;217(3):851-4.

Etchepare R, Azevedo A, Calgaroto S, Rubio J. Removal of ferric hydroxide by flotation with micro and nanobubbles. Sep Purif Technol. 2017;184:347–53.

European Parliament. Directive 2010/63/EU of the European Parliament and of the Council of 22 September 2010 on the protection of animals used for scientific purposes [Internet]. OJ L 276, 20.10.2010, p. 33–79. Available from: https://eur-lex.europa.eu/legal-content/EN/TXT/?uri=CELEX:32010L0063

Eyre DR, Paz MA, Gallop PM. Cross-linking in collagen and elastin. Annu Rev Biochem. 1984;53:717-48.

F-D-C Reports. Alpha Therapeutic's Fluosol oxygen transport fluid approved for use in angioplasty. 1990 Jan 8; p. 8.

Falabella AF. Debridement and wound bed preparation. Dermatol Ther. 2006 Nov-Dec;19(6):317-25.

Falanga V, Isseroff RR, Soulika AM, Romanelli M, Margolis D, Kapp S, Granick M, Harding K. Chronic wounds. Nat Rev Dis Primers. 2022 Jul 21;8(1):50.

Falanga V, Kirsner RS. Low oxygen stimulates proliferation of fibroblasts seeded as single cells. J Cell Physiol. 1993 Mar;154(3):506-10.

Falanga V, Martin TA, Takagi H, Kirsner RS, Helfman T, Pardes J, Ochoa MS. Low oxygen tension increases mRNA levels of alpha 1 (I) procollagen in human dermal fibroblasts. J Cell Physiol. 1993 Nov;157(2):408-12.

Falanga V, Qian SW, Danielpour D, Katz MH, Roberts AB, Sporn MB. Hypoxia upregulates the synthesis of TGF-beta 1 by human dermal fibroblasts. J Invest Dermatol. 1991 Oct;97(4):634-7.

Falanga V, Zhou L, Yufit T. Low oxygen tension stimulates collagen synthesis and COL1A1 transcription through the action of TGF-beta1. J Cell Physiol. 2002 Apr;191(1):42-50.

Feshitan JA, Legband ND, Borden MA, Terry BS. Systemic oxygen delivery by peritoneal perfusion of oxygen microbubbles. Biomaterials. 2014 Mar;35(9):2600-6.

Festing MF, Altman DG. Guidelines for the design and statistical analysis of experiments using laboratory animals. ILAR J. 2002;43(4):244-58.

Fiala A, Slagle C, Legband N, Aghabaglou F, Buesing K, Borden M, Harris S, Terry B. Treatment of a Rat Model of LPS-Induced ARDS via Peritoneal Perfusion of Oxygen Microbubbles. J Surg Res. 2020 Feb;246:450-456.

Fife CE, Carter MJ. Wound Care Outcomes and Associated Cost Among Patients Treated in US Outpatient Wound Centers: Data From the US Wound Registry. Wounds. 2012 Jan;24(1):10-7.

Fonder MA, Lazarus GS, Cowan DA, Aronson-Cook B, Kohli AR, Mamelak AJ. Treating the chronic wound: A practical approach to the care of nonhealing wounds and wound care dressings. J Am Acad Dermatol. 2008 Feb;58(2):185-206.

Fowler E. Chronic wounds: an overview. In: Krasner D, editor. Chronic wound care: a clinical source book for healthcare professionals. King of Prussia (PA): Health Management Publications Inc.; 1990. p. 12-8.

Gilliver SC, Ruckshanthi JP, Hardman MJ, Nakayama T, Ashcroft GS. Sex dimorphism in wound healing: the roles of sex steroids and macrophage migration inhibitory factor. Endocrinology. 2008 Nov;149(11):5747-57.

Goljan EF. Water, Electrolyte, Acid-Base, and Hemodynamic Disorders. In: Goljan EF, editor. Rapid Review Pathology. 4th ed. Philadelphia: Saunders; 2013. p. 93.

Gordillo GM, Sen CK. Revisiting the essential role of oxygen in wound healing. Am J Surg. 2003 Sep;186(3):259-63.

Görlach A, Brandes RP, Bassus S, Kronemann N, Kirchmaier CM, Busse R, Schini-Kerth VB. Oxidative stress and expression of p22phox are involved in the up-regulation of tissue factor in vascular smooth muscle cells in response to activated platelets. FASEB J. 2000 Aug;14(11):1518-28.

Gottrup F. A specialized wound-healing center concept: importance of a multidisciplinary department structure and surgical treatment facilities in the treatment of chronic wounds. Am J Surg. 2004 May;187(5A):38S-43S.

Grada A, Mervis J, Falanga V. Research Techniques Made Simple: Animal Models of Wound Healing. J Invest Dermatol. 2018 Oct;138(10):2095-2105.e1.

Graham K, Unger E. Overcoming tumor hypoxia as a barrier to radiotherapy, chemotherapy and immunotherapy in cancer treatment. Int J Nanomedicine. 2018 Oct 4;13:6049-6058.

Greif R, Akça O, Horn EP, Kurz A, Sessler DI; Outcomes Research Group. Supplemental perioperative oxygen to reduce the incidence of surgical-wound infection. N Engl J Med. 2000 Jan 20;342(3):161-7.

Gueldner J, Zhang F, Zechmann B, Bruce ED. Evaluating a novel oxygenating therapeutic for its potential use in the advancement of wound healing. Toxicol In Vitro. 2017 Sep;43:62-68.

Gulino GR, Magnetto C, Khadjavi A, Panariti A, Rivolta I, Soster M, Argenziano M, Cavalli R, Giribaldi G, Guiot C, Prato M. Oxygen-Loaded Nanodroplets Effectively Abrogate Hypoxia Dysregulating Effects on Secretion of MMP-9 and TIMP-1 by Human Monocytes. Mediators Inflamm. 2015;2015:964838.

Gupta A, Raghubir R. Energy metabolism in the granulation tissue of diabetic rats during cutaneous wound healing. Mol Cell Biochem. 2005 Feb;270(1-2):71-7.

Gurtner GC, Werner S, Barrandon Y, Longaker MT. Wound repair and regeneration. Nature. 2008 May 15;453(7193):314-21.

Harrison BS, Eberli D, Lee SJ, Atala A, Yoo JJ. Oxygen producing biomaterials for tissue regeneration. Biomaterials. 2007 Nov;28(31):4628-34.

Hinman CD, Maibach H. Effect of air exposure and occlusion on experimental human skin wounds. Nature. 1963 Oct 26;200:377-8.

Hohlbaum K, Bert B, Dietze S, Palme R, Fink H, Thöne-Reineke C. Systematic Assessment of Well-Being in Mice for Procedures Using General Anesthesia. J Vis Exp. 2018 Mar 20;(133):57046.

Hohn DC, MacKay RD, Halliday B, Hunt TK. Effect of O2 tension on microbicidal function of leukocytes in wounds and in vitro. Surg Forum. 1976;27(62):18-20.

Hopf HW, Gibson JJ, Angeles AP, Constant JS, Feng JJ, Rollins MD, Zamirul Hussain M, Hunt TK. Hyperoxia and angiogenesis. Wound Repair Regen. 2005 Nov-Dec;13(6):558-64.

Howick JCI, Glasziou P, Greenhalgh T, Heneghan C, Liberati A, et al. Oxford centre for evidence-based medicine. The Oxford 2011 Levels of Evidence. Available at https://www.cebm.ox.ac.uk/resources/levels-of-evidence/ocebm-levels-of-evidence (cited April 30, 2021).

Hutton JJ, Tappel AL, Undenfried S. Cofactor and substrate requirements of collagen proline hydroxylase. Arch Biochem Biophys. 1967;118:231-40.

Iijima M, Gombodorj N, Tachibana Y, Tachibana K, Yokobori T, Honma K, Nakano T, Asao T, Kuwahara R, Aoyama K, Yasuda H, Kelly M, Kuwano H, Yamanouchi D.

Development of single nanometer-sized ultrafine oxygen bubbles to overcome the hypoxia-induced resistance to radiation therapy via the suppression of hypoxia-inducible factor-1α. Int J Oncol. 2018 Mar;52(3):679-686.

International Diabetes Federation. IDF Diabetes Atlas. 7th ed. Brussels: International Diabetes Federation; 2015.

International Working Group on the Diabetic Foot. Epidemiology of diabetic foot infections in a population-based cohort. Paper presented at: International Consensus on the Diabetic Foot; 2003 May 22-24; Noordwijkerhout, the Netherlands.

Ivins N, Simmonds W, Turner A, Harding K. The use of an oxygenating hydrogel dressing in VLU. Wounds. 2007;3:1-5.

Jahanban-Esfahlan R, de la Guardia M, Ahmadi D, Yousefi B. Modulating tumor hypoxia by nanomedicine for effective cancer therapy. J Cell Physiol. 2018 Mar;233(3):2019-2031.

Je JY, Cho YS, Kim SK. Cytotoxic activities of water-soluble chitosan derivatives with different degree of deacetylation. Bioorg Med Chem Lett. 2006 Apr 15;16(8):2122-6.

Jonsson K, Hunt TK, Mathes SJ. Effect of environmental oxygen on bacterial induced tissue necrosis in flaps. Surg Forum. 1984;35:589-91.

Jönsson K, Hunt TK, Mathes SJ. Oxygen as an isolated variable influences resistance to infection. Ann Surg. 1988 Dec;208(6):783-7.

Jonsson K, Jensen JA, Goodson WH 3rd, Scheuenstuhl H, West J, Hopf HW, Hunt TK. Tissue oxygenation, anemia, and perfusion in relation to wound healing in surgical patients. Ann Surg. 1991 Nov;214(5):605-13.

Juffermans LJ, Dijkmans PA, Musters RJ, Visser CA, Kamp O. Transient permeabilization of cell membranes by ultrasound-exposed microbubbles is related to

formation of hydrogen peroxide. Am J Physiol Heart Circ Physiol. 2006 Oct;291(4):H1595-601.

Junker JP, Kamel RA, Caterson EJ, Eriksson E. Clinical Impact Upon Wound Healing and Inflammation in Moist, Wet, and Dry Environments. Adv Wound Care (New Rochelle). 2013 Sep;2(7):348-356.

Kellar RS, Audet RG, Roe DF, Rheins LA, Draelos ZD. Topically delivered dissolved oxygen reduces inflammation and positively influences structural proteins in healthy intact human skin. J Cosmet Dermatol. 2013 Jun;12(2):86-95.

Khadjavi A, Magnetto C, Panariti A, Argenziano M, Gulino GR, Rivolta I, Cavalli R, Giribaldi G, Guiot C, Prato M. Chitosan-shelled oxygen-loaded nanodroplets abrogate hypoxia dysregulation of human keratinocyte gelatinases and inhibitors: New insights for chronic wound healing. Toxicol Appl Pharmacol. 2015 Aug 1;286(3):198-206.

Khan MS, Hwang J, Seo Y, Shin K, Lee K, Park C, Choi Y, Hong JW, Choi J. Engineering oxygen nanobubbles for the effective reversal of hypoxia. Artif Cells Nanomed Biotechnol. 2018;46(sup3):S318-S327.

Kheir JN, Scharp LA, Borden MA, Swanson EJ, Loxley A, Reese JH, Black KJ, Velazquez LA, Thomson LM, Walsh BK, Mullen KE, Graham DA, Lawlor MW, Brugnara C, Bell DC, McGowan FX Jr. Oxygen gas-filled microparticles provide intravenous oxygen delivery. Sci Transl Med. 2012 Jun 27;4(140):140ra88.

Kindwall E. Contraindications and side effects to hyperbaric oxygen treatment. In: Kindwall EP, Whelan HT, editors. Hyperbaric medicine practice. 2nd ed. Flagstaff (AZ): Best Publishing Company; 1999. p. 83–97.

Kivisaari J, Vihersaari T, Renvall S, Niinikoski J. Energy metabolism of experimental wounds at various oxygen environments. Ann Surg. 1975 Jun;181(6):823-8.

Klapka N, Müller HW. Collagen matrix in spinal cord injury. J Neurotrauma. 2006 Mar-Apr;23(3-4):422-35.

Klyubin IV, Kirpichnikova KM, Gamaley IA. Hydrogen peroxide-induced chemotaxis of mouse peritoneal neutrophils. Eur J Cell Biol. 1996 Aug;70(4):347-51.

Knighton DR, Hunt TK, Scheuenstuhl H, Halliday BJ, Werb Z, Banda MJ. Oxygen tension regulates the expression of angiogenesis factor by macrophages. Science. 1983 Sep 23;221(4617):1283-5.

Knighton DR, Silver IA, Hunt TK. Regulation of wound-healing angiogenesis-effect of oxygen gradients and inspired oxygen concentration. Surgery. 1981 Aug;90(2):262-70.

Kourembanas S, Hannan RL, Faller DV. Oxygen tension regulates the expression of the platelet-derived growth factor-B chain gene in human endothelial cells. J Clin Invest. 1990 Aug;86(2):670-4.

Kumar A, Godwin JW, Gates PB, Garza-Garcia AA, Brockes JP. Molecular basis for the nerve dependence of limb regeneration in an adult vertebrate. Science. 2007 Nov 2;318(5851):772-7.

Kurahashi T, Fujii J. Roles of antioxidative enzymes in wound healing. J Dev Biol. 2015;3(2):57-70.

Lairet KF, Baer D, Leas ML, Renz EM, Cancio LC. Evaluation of an oxygen-diffusion dressing for accelerated healing of donor-site wounds. J Burn Care Res. 2014 May-Jun;35(3):214-8.

Leavitt T, Hu MS, Marshall CD, Barnes LA, Lorenz HP, Longaker MT. Scarless wound healing: finding the right cells and signals. Cell Tissue Res. 2016 Sep;365(3):483-93.

Legband N, Feshitan J, Borden M, Terry B. Peritoneal microbubble oxygenation: an extrapulmonary respiration treatment in rabbits. ASME J Med Devices. 2014;8(3):030944.

Li J, Ollague Sierra J, Zhu L, Tang L, Rahill K, El-Sabawi B, Liu-Mares W, Mertz PM, Davis SC. Effects of a topical aqueous oxygen emulsion on collagen deposition and angiogenesis in a porcine deep partial-thickness wound model. Exp Dermatol. 2013 Oct;22(10):674-6.

Li J, Zhang YP, Zarei M, Zhu L, Sierra JO, Mertz PM, Davis SC. A topical aqueous oxygen emulsion stimulates granulation tissue formation in a porcine second-degree burn wound. Burns. 2015 Aug;41(5):1049-57.

Lim Y, Phung AD, Corbacho AM, Aung HH, Maioli E, Reznick AZ, Cross CE, Davis PA, Valacchi G. Modulation of cutaneous wound healing by ozone: differences between young and aged mice. Toxicol Lett. 2006 Jan 5;160(2):127-34.

Lo JF, Brennan M, Merchant Z, Chen L, Guo S, Eddington DT, DiPietro LA. Microfluidic wound bandage: localized oxygen modulation of collagen maturation. Wound Repair Regen. 2013 Mar-Apr;21(2):226-34. doi: 10.1111/wrr.12021. Epub 2013 Feb 25.

Lovvorn HN 3rd, Cheung DT, Nimni ME, Perelman N, Estes JM, Adzick NS. Relative distribution and crosslinking of collagen distinguish fetal from adult sheep wound repair. J Pediatr Surg. 1999 Jan;34(1):218-23.

Lowe KC. Perfluorinated blood substitutes and artificial oxygen carriers. Blood Rev. 1999 Sep;13(3):171-84.

MacLeod AS, Mansbridge JN. The Innate Immune System in Acute and Chronic Wounds. Adv Wound Care (New Rochelle). 2016 Feb 1;5(2):65-78.

Magnetto C, Prato M, Khadjavi A, Giribaldi G, Fenoglio I, Jose J, Gulino GR, Cavallo F, Quaglino E, Benintende E, Varetto G, Troia A, Cavalli R, Guiot C. Ultrasound-activated

decafluoropentane-cored and chitosan-shelled nanodroplets for oxygen delivery to hypoxic cutaneous tissues. RSC Adv. 2014;4(72): 38433-41.

Marano F, Argenziano M, Frairia R, Adamini A, Bosco O, Rinella L, Fortunati N, Cavalli R, Catalano MG. Doxorubicin-Loaded Nanobubbles Combined with Extracorporeal Shock Waves: Basis for a New Drug Delivery Tool in Anaplastic Thyroid Cancer. Thyroid. 2016 May;26(5):705-16.

Marano F, Frairia R, Rinella L, Argenziano M, Bussolati B, Grange C, Mastrocola R, Castellano I, Berta L, Cavalli R, Catalano MG. Combining doxorubicin-nanobubbles and shockwaves for anaplastic thyroid cancer treatment: preclinical study in a xenograft mouse model. Endocr Relat Cancer. 2017 Jun;24(6):275-286.

Matsuda T, Clark N, Hariyani GD, Bryant RS, Hanumadass ML, Kagan RJ. The effect of burn wound size on resting energy expenditure. J Trauma. 1987 Feb;27(2):115-8.

Matsuki N, Ichiba S, Ishikawa T, Nagano O, Takeda M, Ujike Y, Yamaguchi T. Blood oxygenation using microbubble suspensions. Eur Biophys J. 2012 Jun;41(6):571-8.

Matsuki N, Ishikawa T, Ichiba S, Shiba N, Ujike Y, Yamaguchi T. Oxygen supersaturated fluid using fine micro/nanobubbles. Int J Nanomedicine. 2014 Sep 23;9:4495-505.

Matsuoka H, Ebina K, Tanaka H, Hirao M, Iwahashi T, Noguchi T, Suzuki K, Nishimoto S, Murase T, Yoshikawa H. Administration of Oxygen Ultra-Fine Bubbles Improves Nerve Dysfunction in a Rat Sciatic Nerve Crush Injury Model. Int J Mol Sci. 2018 May 7;19(5):1395.

Moen I, Ugland H, Strömberg N, Sjöström E, Karlson A, Ringstad L, Bysell H, Amiry-Moghaddam M, Haglerød C. Development of a novel in situ gelling skin dressing: Delivering high levels of dissolved oxygen at pH 5.5. Health Sci Rep. 2018 Jun 13;1(7):e57.

Moffatt CJ, Stanton J, Murray S, Doody V, Davis PJ, Franks PJ. A randomised trial to compare the performance of Oxyzyme® & Iodozyme® with standard care in the treatment of patients with venous and mixed venous/arterial ulceration. Wound Medicine. 2014;6:1-10.

Mogford JE, Tawil N, Chen A, Gies D, Xia Y, Mustoe TA. Effect of age and hypoxia on TGFbeta1 receptor expression and signal transduction in human dermal fibroblasts: impact on cell migration. J Cell Physiol. 2002 Feb;190(2):259-65.

Moher D, Liberati A, Tetzlaff J, Altman DG; PRISMA Group. Preferred reporting items for systematic reviews and meta-analyses: the PRISMA statement. BMJ. 2009 Jul 21;339:b2535.

Morgan DA. Wound management products in the drug tariff. Pharm J. 1999;263:820–5.

Myllylä R, Tuderman L, Kivirikko KI. Mechanism of the prolyl hydroxylase reaction. 2. Kinetic analysis of the reaction sequence. Eur J Biochem. 1977 Nov 1;80(2):349-57.

Narkowicz CK, Vial JH, McCartney PW. Hyperbaric oxygen therapy increases free radical levels in the blood of humans. Free Radic Res Commun. 1993;19(2):71-80.

National Research Council. Humane endpoints for animals in pain. In: National Research Council, editor. Recognition and alleviation of pain in laboratory animals. Washington (DC): The National Academies Press; 2009. p. 135-6.

Nichols SA, Dirks W, Pearse JS, King N. Early evolution of animal cell signaling and adhesion genes. Proc Natl Acad Sci U S A. 2006 Aug 15;103(33):12451-6.

Niethammer P, Grabher C, Look AT, Mitchison TJ. A tissue-scale gradient of hydrogen peroxide mediates rapid wound detection in zebrafish. Nature. 2009 Jun 18;459(7249):996-9.

Noguchi T, Ebina K, Hirao M, Morimoto T, Koizumi K, Kitaguchi K, Matsuoka H, Iwahashi T, Yoshikawa H. Oxygen ultra-fine bubbles water administration prevents bone loss of glucocorticoid-induced osteoporosis in mice by suppressing osteoclast differentiation. Osteoporos Int. 2017 Mar;28(3):1063-1075.

Nosé Y. Is there a role for blood substitutes in civilian medicine: a drug for emergency shock cases? Artif Organs. 2004 Sep;28(9):807-12.

Ntentakis DP, Ntentaki AM, Delavogia E, Kalomoiris L, Venieri D, Arkadopoulos N, Kalogerakis N. Dissolved oxygen technologies as a novel strategy for non-healing wounds: A critical review. Wound Repair Regen. 2021 Nov;29(6):1062-1079.

Nussbaum SR, Carter MJ, Fife CE, DaVanzo J, Haught R, Nusgart M, Cartwright D. An Economic Evaluation of the Impact, Cost, and Medicare Policy Implications of Chronic Nonhealing Wounds. Value Health. 2018 Jan;21(1):27-32.

O'Toole EA, Marinkovich MP, Peavey CL, Amieva MR, Furthmayr H, Mustoe TA, Woodley DT. Hypoxia increases human keratinocyte motility on connective tissue. J Clin Invest. 1997 Dec 1;100(11):2881-91.

Onouye T, Menaker G, Christian M, Moy R. Occlusive dressing versus oxygen mist therapy following CO2 laser resurfacing. Dermatol Surg. 2000 Jun;26(6):572-6.

Opalenik SR, Davidson JM. Fibroblast differentiation of bone marrow-derived cells during wound repair. FASEB J. 2005 Sep;19(11):1561-3.

Öri F, Dietrich R, Ganz C, Dau M, Wolter D, Kasten A, Gerber T, Frerich B. Silicon-dioxide-polyvinylpyrrolidone as a wound dressing for skin defects in a murine model. J Craniomaxillofac Surg. 2017 Jan;45(1):99-107.

Owen J, McEwan C, Nesbitt H, Bovornchutichai P, Averre R, Borden M, McHale AP, Callan JF, Stride E. Reducing Tumour Hypoxia via Oral Administration of Oxygen Nanobubbles. PLoS One. 2016 Dec 30;11(12):e0168088.Oxygen Nanobubble Drink

Impact on Exercise in Elite Athletes. ClinicalTrials.gov identifier NCT05777642. https://clinicaltrials.gov/study/NCT05777642?intr=nanobubble&rank=2.

Oxygen Nanobubble Drink Impact on Exercise in Pulmonary Fibrosis. ClinicalTrials.gov identifier NCT05711290. https://clinicaltrials.gov/study/NCT05711290?intr=nanobubble&rank=3.

Padberg FT, Back TL, Thompson PN, Hobson RW 2nd. Transcutaneous oxygen (TcPO2) estimates probability of healing in the ischemic extremity. J Surg Res. 1996 Feb 1;60(2):365-9.

Paola LD, Brocco E, Senesi A, Merico M, De Vido D, Assaloni R, DaRos R. Super-oxidized solution (SOS) therapy for infected diabetic foot ulcers. Wounds. 2006;18(9):262-70.

Park SA, Covert J, Teixeira L, Motta MJ, DeRemer SL, Abbott NL, Dubielzig R, Schurr M, Isseroff RR, McAnulty JF, Murphy CJ. Importance of defining experimental conditions in a mouse excisional wound model. Wound Repair Regen. 2015 Mar-Apr;23(2):251-61.

Patil PS, Evancho-Chapman MM, Li H, Huang H, George RL, Shriver LP, Leipzig ND. Fluorinated methacrylamide chitosan hydrogel dressings enhance healing in an acute porcine wound model. PLoS One. 2018 Sep 5;13(9):e0203371.

Patil PS, Fathollahipour S, Inmann A, Pant A, Amini R, Shriver LP, Leipzig ND. Fluorinated Methacrylamide Chitosan Hydrogel Dressings Improve Regenerated Wound Tissue Quality in Diabetic Wound Healing. Adv Wound Care (New Rochelle). 2019 Aug 1;8(8):374-385.

Patil PS, Fountas-Davis N, Huang H, Michelle Evancho-Chapman M, Fulton JA, Shriver LP, Leipzig ND. Fluorinated methacrylamide chitosan hydrogels enhance collagen synthesis in wound healing through increased oxygen availability. Acta Biomater. 2016 May;36:164-74.

Petticrew M, Roberts H. Systematic reviews in the social sciences: a practical guide. Malden (MA), Oxford: Blackwell Publishers; 2006. 336 p.

Prato M, Magnetto C, Jose J, Khadjavi A, Cavallo F, Quaglino E, Panariti A, Rivolta I, Benintende E, Varetto G, Argenziano M, Troia A, Cavalli R, Guiot C. 2H,3H-decafluoropentane-based nanodroplets: new perspectives for oxygen delivery to hypoxic cutaneous tissues. PLoS One. 2015 Mar 17;10(3):e0119769.

Purna SK, Babu M. Collagen based dressings--a review. Burns. 2000 Feb;26(1):54-62.

Queen D, Coutts P, Fierheller M, Sibbald RG. The use of a novel oxygenating hydrogel dressing in the treatment of different chronic wounds. Adv Skin Wound Care. 2007 Apr;20(4):200, 202, 204, 206.

Queen D, Orsted H, Sanada H, Sussman G. A dressing history. Int Wound J. 2004 Apr;1(1):59-77.

Riess JG, Le Blanc M. Solubility and transport phenomena in perfluorochemicals relevant to blood substitution and other biomedical applications. Pure appl. Chem. 1982;54(12):2383-406.

Rodrigues M, Kosaric N, Bonham CA, Gurtner GC. Wound Healing: A Cellular Perspective. Physiol Rev. 2019 Jan 1;99(1):665-706.

Rodriguez PG, Felix FN, Woodley DT, Shim EK. The role of oxygen in wound healing: a review of the literature. Dermatol Surg. 2008 Sep;34(9):1159-69.

Roe DF, Gibbins BL, Ladizinsky DA. Topical dissolved oxygen penetrates skin: model and method. J Surg Res. 2010 Mar;159(1):e29-36.

Roy S, Khanna S, Nallu K, Hunt TK, Sen CK. Dermal wound healing is subject to redox control. Mol Ther. 2006 Jan;13(1):211-20.

Russell WMS, Burch RL. The principles of humane experimental technique. Wheathampstead (UK): Universities Federation for Animal Welfare; 1959. Reprinted 1992.

Said HK, Hijjawi J, Roy N, Mogford J, Mustoe T. Transdermal sustained-delivery oxygen improves epithelial healing in a rabbit ear wound model. Arch Surg. 2005 Oct;140(10):998-1004.

Samakovlis C, Manning G, Steneberg P, Hacohen N, Cantera R, Krasnow MA. Genetic control of epithelial tube fusion during Drosophila tracheal development. Development. 1996 Nov;122(11):3531-6.

Sano H, Ichioka S. Influence of oxygen on wound healing dynamics in healing-impaired diabetic mice. J Plast Surg Hand Surg. 2015 Jun;49(3):135-40.

Sayadi LR, Banyard DA, Ziegler ME, Obagi Z, Prussak J, Klopfer MJ, Evans GR, Widgerow AD. Topical oxygen therapy & micro/nanobubbles: a new modality for tissue oxygen delivery. Int Wound J. 2018 Jun;15(3):363-374.

Schindelin J, Arganda-Carreras I, Frise E, Kaynig V, Longair M, Pietzsch T, Preibisch S, Rueden C, Saalfeld S, Schmid B, Tinevez JY, White DJ, Hartenstein V, Eliceiri K, Tomancak P, Cardona A. Fiji: an open-source platform for biological-image analysis. Nat Methods. 2012 Jun 28;9(7):676-82.

Schrementi ME, Ferreira AM, Zender C, DiPietro LA. Site-specific production of TGF-beta in oral mucosal and cutaneous wounds. Wound Repair Regen. 2008 Jan-Feb;16(1):80-6.

Sen CK, Gordillo GM, Roy S, Kirsner R, Lambert L, Hunt TK, Gottrup F, Gurtner GC, Longaker MT. Human skin wounds: a major and snowballing threat to public health and the economy. Wound Repair Regen. 2009 Nov-Dec;17(6):763-71.

Sen CK, Khanna S, Babior BM, Hunt TK, Ellison EC, Roy S. Oxidant-induced vascular endothelial growth factor expression in human keratinocytes and cutaneous wound healing. J Biol Chem. 2002 Sep 6;277(36):33284-90.

Seo Y, Heo Y, Jo S, Park SH, Lee C, Chang J, Jeon DK, Kim TG, Han G, Namkung W. Novel positive allosteric modulator of protease-activated receptor 1 promotes skin wound healing in hairless mice. Br J Pharmacol. 2021 Sep;178(17):3414-3427.

Serena TE. A Global Perspective on Wound Care. Adv Wound Care (New Rochelle). 2014 Aug 1;3(8):548-552.

Shah JB. Correction of Hypoxia, a Critical Element for Wound Bed Preparation Guidelines: TIMEO2 Principle of Wound Bed Preparation. J Am Col Certif Wound Spec. 2011 Oct 9;3(2):26-32.

Shandall A, Lowndes R, Young HL. Colonic anastomotic healing and oxygen tension. Br J Surg. 1985 Aug;72(8):606-9.

Sheffield PJ. Tissue oxygen measurements. In: Davis JC, Hunt TK, editors. Problem wounds: the role of oxygen. New York: Elsevier; 1988. p. 17-52.

Sheridan WG, Lowndes RH, Young HL. Tissue oxygen tension as a predictor of colonic anastomotic healing. Dis Colon Rectum. 1987 Nov;30(11):867-71.

Shweiki D, Itin A, Soffer D, Keshet E. Vascular endothelial growth factor induced by hypoxia may mediate hypoxia-initiated angiogenesis. Nature. 1992 Oct 29;359(6398):843-5.

Siddiqui A, Galiano RD, Connors D, Gruskin E, Wu L, Mustoe TA. Differential effects of oxygen on human dermal fibroblasts: acute versus chronic hypoxia. Wound Repair Regen. 1996 Apr-Jun;4(2):211-8.

Singer AJ, Clark RA. Cutaneous wound healing. N Engl J Med. 1999 Sep 2;341(10):738-46.

Singh A, Halder S, Menon GR, Chumber S, Misra MC, Sharma LK, Srivastava A. Meta-analysis of randomized controlled trials on hydrocolloid occlusive dressing versus conventional gauze dressing in the healing of chronic wounds. Asian J Surg. 2004 Oct;27(4):326-32.

Spears JR. Stabilized gas-enriched and gas supersaturated liquids. United States patent US 6,344,489. 2002.

Stephens FO, Hunt TK. Effect of changes in inspired oxygen and carbon dioxide tensions on wound tensile strength: an experimental study. Ann Surg. 1971 Apr;173(4):515-9.

Stichel CC, Müller HW. The CNS lesion scar: new vistas on an old regeneration barrier. Cell Tissue Res. 1998 Oct;294(1):1-9.

Sullivan TP, Eaglstein WH, Davis SC, Mertz P. The pig as a model for human wound healing. Wound Repair Regen. 2001 Mar-Apr;9(2):66-76.

Tandara AA, Mustoe TA. Oxygen in wound healing--more than a nutrient. World J Surg. 2004 Mar;28(3):294-300.

The Effect of RNS60 on ALS Biomarkers (RNS60). ClinicalTrials.gov identifier NCT03456882. https://clinicaltrials.gov/study/NCT03456882?intr=nanobubble&rank=5.

Tibbles PM, Edelsberg JS. Hyperbaric-oxygen therapy. N Engl J Med. 1996 Jun 20;334(25):1642-8.

Tiganescu A, Hupe M, Uchida Y, Mauro T, Elias PM, Holleran WM. Increased glucocorticoid activation during mouse skin wound healing. J Endocrinol. 2014 Mar 7;221(1):51-61.

Tsuge H. Micro- and Nanobubbles: Fundamentals and Applications. Singapore: Pan Stanford Publishing; 2014.

Tur E, Bolton L, Constantine BE. Topical hydrogen peroxide treatment of ischemic ulcers in the guinea pig: blood recruitment in multiple skin sites. J Am Acad Dermatol. 1995 Aug;33(2 Pt 1):217-21.

Valacchi G, Lim Y, Belmonte G, Miracco C, Zanardi I, Bocci V, Travagli V. Ozonated sesame oil enhances cutaneous wound healing in SKH1 mice. Wound Repair Regen. 2011 Jan-Feb;19(1):107-15.

van Rijswijk L. Ingredient-based wound dressing classification: a paradigm that is passé and in need of replacement. J Wound Care. 2006 Jan;15(1):11-4. doi: 10.12968/jowc.2006.15.1.26859. Erratum in: J Wound Care. 2006 Sep;15(8):371.

Vihersaari T, Kivisaari J, Ninikoski J. Effect of changes in inspired oxygen tension on wound metabolism. Ann Surg. 1974 Jun;179(6):889-95.

Walmsley S. Advances in wound management: executive summary. In: Clinical reports. London: PJB Publications, Ltd.; 2002.

Wang C, Sani ES, Shih CD, Lim CT, Wang J, Armstrong DG, Gao W. Wound management materials and technologies from bench to bedside and beyond. Nat Rev Mater. 2024 Jun;9:550–566.

Wang C, Schwaitzberg S, Berliner E, Zarin DA, Lau J. Hyperbaric oxygen for treating wounds: a systematic review of the literature. Arch Surg. 2003 Mar;138(3):272-9; discussion 280.

Wang X, Ge J, Tredget EE, Wu Y. The mouse excisional wound splinting model, including applications for stem cell transplantation. Nat Protoc. 2013 Feb;8(2):302-9.

Weavers H, Martin P. The cell biology of inflammation: From common traits to remarkable immunological adaptations. J Cell Biol. 2020 Jul 6;219(7):e202004003.

Werner S, Krieg T, Smola H. Keratinocyte-fibroblast interactions in wound healing. J Invest Dermatol. 2007 May;127(5):998-1008.

Wiegand C, Winter D, Hipler UC. Molecular-weight-dependent toxic effects of chitosans on the human keratinocyte cell line HaCaT. Skin Pharmacol Physiol. 2010;23(3):164-70.

Wijekoon A, Fountas-Davis N, Leipzig ND. Fluorinated methacrylamide chitosan hydrogel systems as adaptable oxygen carriers for wound healing. Acta Biomater. 2013 Mar;9(3):5653-64.

Wood W, Jacinto A, Grose R, Woolner S, Gale J, Wilson C, Martin P. Wound healing recapitulates morphogenesis in Drosophila embryos. Nat Cell Biol. 2002 Nov;4(11):907-12.

Woolner S, Jacinto A, Martin P. The small GTPase Rac plays multiple roles in epithelial sheet fusion: dynamic studies of Drosophila dorsal closure. Dev Biol. 2005;282(1):163-173.

Wright TE, Payne WG, Ko F, Ladizinsky D, Bowlby N, Neeley R, Mannari B, Robson MC. The effects of an oxygen-generating dressing on tissue infection and wound healing. J Appl Res. 2003;3(4):363–70.

Wu L, Xia YP, Roth SI, Gruskin E, Mustoe TA. Transforming growth factor-beta1 fails to stimulate wound healing and impairs its signal transduction in an aged ischemic ulcer model: importance of oxygen and age. Am J Pathol. 1999 Jan;154(1):301-9.

Xia YP, Zhao Y, Tyrone JW, Chen A, Mustoe TA. Differential activation of migration by hypoxia in keratinocytes isolated from donors of increasing age: implication for chronic wounds in the elderly. J Invest Dermatol. 2001 Jan;116(1):50-6.

Yampolsky M, Bachelet I, Fuchs Y. Reproducible strategy for excisional skin-wound-healing studies in mice. Nat Protoc. 2024 Jan;19(1):184-206.

Yardeni T, Eckhaus M, Morris HD, Huizing M, Hoogstraten-Miller S. Retro-orbital injections in mice. Lab Anim (NY). 2011 May;40(5):155-60.

Zellner S, Manabat R, Roe DF. A dissolved oxygen dressing: a pilot study in an ischemic skin flap model. J Int Med Res. 2015;43(1):93-103.

Zhang C, Sundaram R, Maisog J, Calafat AM, Barr DB, Buck Louis GM. A prospective study of prepregnancy serum concentrations of perfluorochemicals and the risk of gestational diabetes. Fertil Steril. 2015 Jan;103(1):184-9.

Zhao Y, Bao L, Chan LS, DiPietro LA, Chen L. Aberrant Wound Healing in an Epidermal Interleukin-4 Transgenic Mouse Model of Atopic Dermatitis. PLoS One. 2016 Jan 11;11(1):e0146451.

Supplement

Table S.1: Methodological details from available studies on DO technologies for wound healing and cutaneous regeneration, organized per category of DO technologies in the proposed classification system.

First author, year	LoE	Subject	Subjects ;wounds /subject (n)	Wound model (duration; etiology; thickness)	Treatment timeline (duration; frequency)	Follow-up duration	Treatment group(s)	Control group(s)
Dissolved O_2 solutions								
Magnetto et al. 2014	5	*in vitro*: HaCaT from an elderly; pig skin flap *in vivo*: mice (BALB/c, healthy)	N/A	N/A; N/A; *in vitro*: hypoxia (1% O_2) to mimic conditions in healing skin	*in vitro*: 135min; once in the beginning *in vivo*: 15min; once in the beginning	*in vitro*: 135min; checked every 45min *in vivo*: 15min; checked every 5min	OLNDs; tested before & after U/S	OLNBs, OFNDs, OFNBs, OSS; all formulas tested before & after U/S
Khadjavi et al. 2015	5	HaCaT from an elderly	N/A	N/A; N/A; all formulas tested in both normoxia (20% O_2) & hypoxia (1% O_2)	24h; once in the beginning	24h; tested every 2h	OLNDs in normoxia OLNDs in hypoxia	OFNDs in normoxia, OFNDs in hypoxia, OSS in normoxia,OSS in hypoxia
Pratto et al. 2015	5	*in vitro*: HaCaT from an elderly; pig skin flap *in vivo*: mice (BALB/c, healthy)	N/A	N/A; N/A; all approaches tested in both normoxia (20% O_2) & hypoxia (1% O_2); before & after U/S	*in vitro*: 135min; once in the beginning *in vivo*: 10min; once in the beginning	*in vitro*: 135min, checked every 45min; *in vivo*: 10min, checked before, during, & after a 10min interval	OLNDs	OLNBs, OFNDs, OFNBs, OSS
Gulino et al. 2015	5	human monocyte cell cultures	N/A	N/A; N/A; all formulas tested in both normoxia (20% O_2) & hypoxia (1% O_2)	incubation for 24h; once in the beginning	N/A	OLNDs	OFNDs, OSS
Basilico et al. 2015	5	HMEC-1 cell line	N/A	N/A; cell culture implants for healing assay	incubation for 24h; once in the beginning	N/A	OLNDs; tested in both normoxia (20% O_2) & hypoxia (1% O_2)	OFNDs, OSS; tested in both normoxia (20% O_2) & hypoxia (1% O_2)

First author, year	LoE	Subject	Subjects ;wounds /subject (n)	Wound model (duration; etiology; thickness)	Treatment timeline (duration; frequency)	Follow-up duration	Treatment group(s)	Control group(s)
Bisazza et al. 2008	5	non-fertilized chicken eggs; JEG-3 line human choriocarcinoma	N/A	N/A; N/A OMB N/S solution tested in normoxia (20% O_2) & hypoxia (3% O_2) conditions	10min; once in the beginning	10min; checked every 100s	OMB N/S solution; compared between normoxia & hypoxia	non-treated JEG-3 cells; only in HIF-1α studies
Cavalli et al. 2009 (a)	5	JEG-3 line human choriocarcinoma	N/A	N/A; N/A	once in the beginning	for DO studies: 60min; effects of U/S on DO: 10min; checked at 2, 5, 10min	N/A; 2 OUB formulas (**A, B**) mixed with hypoxic N/S (O_2 =0.4 mg/l)	N/A
Cavalli et al. 2009 (b)	5	N/A; study of 3 OUB N/S solutions	N/A	N/A; N/A	N/A	DO study: for 10min, in a total of 24h effects of U/S on DO: 10min; checked every 1min	N/A; 3 OUB formulas (A,B,C); each mixed with hypoxic N/S at 4 mg/l & 0.4 mg/l O_2	N/A
Feshitan et al. 2014	5	rats (Wistar, ~430g)	10; N/A	N/A; right pneumotho-rax (model for acute lung injury); N/A	2h; continuous at 40 mL/min for 1 min, then at 8 mL/min thereafter	2h; vital signs checked every 30s	IP phospholi-pid-coated OMBs, IP OSS; n=5	no treatment (n=5)
Fiala et al. 2020	5	rats (Wistar, 370-640g)	24 (12 treated); N/A	N/A; LPS-induced ARDS model for acute lung injury (24mg/kg, intra-tracheally)	48h; OMB solution at 12h, 24h, 36h	48h;	IP OMB solution (n=10)	IP N/S solution (n=7); no treatment (n=7)
Onouye et al. 2000	4	humans after CO_2 laser procedure in the face	3; 1	acute; postop healing after CO_2 laser resurfacing; partial	5 days; once daily	7-8 months	1/2 face with the lasered area: O_2 mist protocol (sterile water, O_2, nutrients)	other half of face; occlusive dressing (non-O_2 foam)
Paola et al. 2006	4	humans with DM type 1 or 2 & infected DFUs	218; 2-3 infected DFUs	chronic; DFU; N/A	till surgery for infection control; daily dressing changes	till surgery for infection control	daily dressing; gauzes soaked with 20ml SOS (n=110)	10% PVI (n=108)
Matsuki et al. 2012	5	hypoxic blood samples from healthy swine	N/A	N/A; N/A	N/A	N/A	Hypoxic swine blood gradually diluted with OMB N/S (10,20,30,50%)	N/A

First author, year	LoE	Subject	Subjects ;wounds /subject (n)	Wound model (duration; etiology; thickness)	Treatment timeline (duration; frequency)	Follow-up duration	Treatment group(s)	Control group(s)
Matsuki et al. 2014	5	hypoxic blood samples from healthy swine	N/A	N/A; N/A; 4 solutions commonly used in medical practice (N/S, dextran, albumin, lipid) enriched with OUBs	N/A	N/A	Hypoxic swine blood gradually diluted with 4 OUB-enriched solutions (10,20,30,50%)	N/A
Ebina et al. 2013	5	*in vivo*: DBA1/J mice (male, 5-week old)	N/A	N/A; N/A	12 weeks; free oral intake	12 weeks	distilled water solution enriched with OUBs	regular distilled water
Noguchi et al. 2017	5	*in vitro*: human PBMCs; *in vivo*: C57BL/6J mice (male, 6-mo old)	35; N/A	N/A; N/A; N/S solutions containing UFBs were diluted by the same non-UFB liquid to 75, 50, & 25%	8 weeks; 3 times per week	8 weeks	IP OUB-enriched N/S evaluated in GIO (n=11) mice	no GIO, N/S (n=8) GIO, N/S (n=8) GIO/NUB-enriched N/S (n=8)
Matsuoka et al. 2018	5	*in vitro*: DRG neurons & SC cultures; *in vivo*: Wistar rats (male,180–220g)	*in vitro*: N/A *in vivo*: 45; 1 SCI per rat	acute; SCI (peripheral nerve injury); full; N/S solutions with UFBs diluted by the same non-UFB liquid to 75,50,25%	4 weeks; 3 times per week	4 weeks	IP OUB-enriched N/S after SCI (n=11)	no SCI, N/S (n=11) SCI, N/S (n=15) SCI/NUB-enriched N/S (n=8)
O_2 dressings								
Tur et al. 1995	5	guinea pigs (500g); 2 experiments: 1st, 2nd	1st : 8;1 2nd : 18;1	chronic; ischemic ulcer (5cm transscapular incision, subcutaneous encircling with rubber band tourniquet to a 5cm^2 cycle); full	4 days; 1 day before ischemia, every 2 h during the 8h ischemic interval, & once daily for 2 more days	1st: 27 days 2nd: 14 days	1st: 2% H_2O_2 cream in the dressing 2nd: 1.5% H_2O_2 cream, 3% H_2O_2 cream	1st: two intact skin sites/animal at 1 & 3cm from ulcer, with placebo cream 2nd: 6/18 guinea pigs with placebo cream
Chandra et al. 2015	5	porcine (~30kg)	5; 4	chronic; excisional surgical (10 x 10cm); full	8 weeks; dressing change every 3-4 days	8 weeks	2 wounds/animal; treated with H_2O_2-generating dressing	2 wounds per animal; control dressing
Harrison et al. 2007	5	mice	16; 1	acute; ischemic skin flap (30 x 10mm); full	1 week; once in the beginning	1 week	group 1: PLGA-SPO dressing implanted	group 2: PLGA-only dressing (no O_2 production)

First author, year	LoE	Subject	Subjects ;wounds /subject (n)	Wound model (duration; etiology; thickness)	Treatment timeline (duration; frequency)	Follow-up duration	Treatment group(s)	Control group(s)
Wright et al. 2003	5	rats (Sprague-Dawley, male, ~350g); two experiments: 1st, 2nd	1st : 15; 1 2nd : 15; 1	chronic; granulated wound (2nd-degree burn + infection); full	10 days; every 12h control dressings were changed every 24h	10 days	hydrophilic colloid generating O_2 via breakdown of exogenous H_2O_2 by inorganic catalyst	1st: KGF-2 dressing, vehicle control 2nd: hydrogel colloid with and without inorganic catalyst
Lairet et al. 2014	2b	humans with burn wounds, 9.2% TBSA)	17; 2	acute; split-thickness skin grafts; partial	14 days; daily till day 4, then every 2 days till fully healed; not fixed	regularly for 14 days; after 30-45 days for cosmetic result	"OxyBand" dressing, releasing O_2 via a proprietary reservoir technology	Xeroform gauge dressing
Zellner et al. 2014	5	porcine (50-80kg)	4; 4	acute; skin flap; full	14 days; dressing change PRN	14 days; daily	8 wounds (2/animal) with OxyGenesys dressing	8 wounds (2/animal) with FlexiGel dressing (also a hydrogel)
Guelder et al. 2007	5	cultures of human keratinocytes & fibroblasts	N/A	N/A; toxicity & tissue recovery following chemical injury with 7% DMSO solution for 24h	24h	24h	Ox66™ dressing with oxygenated aluminum hydroxide	Positive controls in 1% Triton-X for 24hr, then in fresh media for another 24h; negative controls (untreated)
Kellar et al. 2013	2b	humans with intact skin	50; N/A	N/A; N/A	8 weeks; once daily	8 weeks	OxygeneSys dressing (O_2) on anterior tibia	Placebo dressing (Kling bandage) on each untreated tibia
Lo et al. 2013	5	*in vitro*: O_2 sensor coated with fluorescent dye *in vivo*: SKH1 mice (~25g)	15; 2	acute; excisional wound model (8mm); full	14 days; continuous O_2 supply 4 hours daily	14 days	5 diabetic mice treated with microfluidic O_2 bandage (100% gas O_2 by medical tank)	5 diabetic and 5 non-diabetic mice treated with microfluidic bandage (without O_2 supply)
O_2 hydrogels								
Patil et al. 2016	5	rats (Wistar 10 weeks old)	8; 1 (splinted in 5 locations)	acute; excisional wound model; full	8 days; dressing change every 2 days	8 days	1/5 wound surface/ rat; treated with MACF+O_2 hydrogel	2/5: MACF+air; 3/5: MAC+O_2; 4/5: MAC+air; 5/5: no treatment

First author, year	LoE	Subject	Subjects ;wounds /subject (n)	Wound model (duration; etiology; thickness)	Treatment timeline (duration; frequency)	Follow-up duration	Treatment group(s)	Control group(s)
Patil et al. 2018	5	porcine	3; 24	acute; square excisional wounds (2.5× 2.5cm); full	21 days; dressing changes on days 2, 4, 9, 11, 14, 17, & 21 postop	21 days	12 wounds per animal; treated with MACF+O_2 hydrogel	4 wounds: MACF-only hydrogel; 4 wounds: control dressing (no O_2, no chitosan); 4 wounds: no treatment
Patil et al. 2019	5	transgenic diabetic mice (8-12 weeks old)	N/A	acute; splinted (sutured) excisional wounds; full	14 days	14 days; dressing changes every 2-3 days	MACF+O_2 hydrogel	Control dressing (no O_2, no chitosan); no treatment (same animals)
Wijekoon et al. 2012	5	NIH-3T3 fibroblast cultures	N/A	N/A; N/A; cells studied at increased metabolic demands & 5% CO_2	4 days; every 24h, hydrogels saturated with O_2 for 4min	6 days	MACF +O_2 hydrogels with gradually increasing fluorine residues; (5, 10, 15)	MAC dressing (no O_2)
Akula et al. 2017	5	nHDFs & nHEK cell cultures	N/A	N/A; N/A; cultured in normoxia (21% O_2), hypoxia (5% CO_2, 1% O_2, & 94% N_2)	3 days; once in the beginning	3 days	MACF+O_2 hydrogel	MACF-only hydrogel (no O_2); no treatment
Almeleh et al.2013	4	humans with burn wounds	2; 1	acute; 2nd-degree burns, non-infected; partial	1 week - 1month; bid	1 month	O_2 hydrogel	N/A
Moen et al. 2018	5	HSF cells	N/A	N/A; N/A	N/A	N/A	Oxy Dressing	N/A; HSF cells grown at different DO levels (11,23,31,41,50 mg/l)
Queen et al. 2007	4	humans with chronic wounds	4; 1	chronic; variable; variable	4 weeks; 2-3 times per week	4 weeks	“Oxyzyme” dressing	N/A
Ivins et al. 2007	4	humans with chronic VLUs	5; 1	chronic; chronic VLUs; variable	6 weeks; variable	6 weeks	“Oxyzyme” dressing	N/A
Moffaat et al. 2014	2b	Humans with ulcer wounds	100; 1	chronic; VLUs/mixed AV ulcers; variable	12 weeks; weekly	24 weeks	Oxyzyme dressing/ Iodozyme dressing	Standard dressing

First author, year	LoE	Subject	Subjects ;wounds /subject (n)	Wound model (duration; etiology; thickness)	Treatment timeline (duration; frequency)	Follow-up duration	Treatment group(s)	Control group(s)
Chen et al. 2020	5	*in vitro*: HUVECs, HaCaTs, HSFs, mouse skin *in vivo*: Balb/C mice (high fat/ sugar diet, ~25g); healthy & diabetic	30; 1	both acute & chronic healing (diabetic mice); excisional wound model; full	until complete healing; daily for days 1 & 2, then every other day	until complete healing (up to 12 days postop)	AGP under light conditions (living microalgae & *S. elongatus*)	*in vitro*: TGO *in vivo*: AGP under dark; control hydrogel (no O_2); control film (no O_2); no treatment (air exposure)
O_2 emulsions								
Davis et al. 2007	5	porcine	16; 120	acute; 8 partial-thickness wounds, 8 2nd-degree burns; partial	variable; 2 times/day for first five days, then once a day until complete closure	partial-thickness wounds: maximum 9 days 2nd-degree burns: maximum 14 days	topical O_2 emulsion; 40 wounds (of the same type) per treatment group per animal	vehicle-only (proprietary oil): 40 wounds/animal; No treatment (air-exposed): 40/animal
Li et al. 2013	5	porcine (25-30kg, female)	6; 13	acute; partial thickness skin wounds; partial	3 weeks; 2 times/day for first five days, then once a day until complete closure	3 weeks	topical O_2 emulsion	vehicle-only (proprietary oil)
Li et al. 2015	5	porcine	6; 18	acute; 2nd-degree burn wounds; partial	3 weeks; 2 times/day for first five days, then once a day until complete closure	3 weeks	topical O_2 emulsion (200mg per wound)	vehicle-only (proprietary oil) no treatment (air-exposed)

Abbreviations: HaCaT, human keratinocyte cell cultures; O_2, oxygen; U/S, ultrasound; Min, minutes; OLNDs, oxygen-loaded nanodroplets; OFNDs, oxygen-free nanodroplets; OLNBs, oxygen-loaded nanobubbles; OFNBs, oxygen-free nanobubbles; OSS, oxygen-saturated solution; DO, dissolved oxygen concentration; HMEC-1, human dermal microvascular endothelium; DM, diabetes mellitus; DFU, diabetic foot ulcer; Grade 2 DFU, penetrates to tendon/capsule; Grade 3 DFU, penetrate to bone/ into the joint; SOS, super-oxidized solution; PVI, povidone iodide solution; HIF-1α, Hypoxia Inducible Factor 1α; OMBs, oxygen microbubbles; OUBs, oxygen ultra-fine bubbles; IP, intra-peritoneal; LPS, lipopolysaccharide; ARDS, acute respiratory distress syndrome; N/S, normal saline (0.9% NaCl); Air, atmospheric air (~21% O_2); GIO, glucocorticoid-induced osteoporosis; NUBs,

Abbreviations (continued): nitrogen ultra-fine bubbles; UFBs, ultra-fine bubbles; PBMCs, peripheral blood mononuclear cells; DRG, dorsal-root ganglion; SC, Schwann cells; SCI, sciatic nerve crush injury; H_2O_2, Hydrogen Peroxide; SPO, sodium percarbonate; PLGA, Poly(D,L-lactide–co–glycolide); KGF-2, Keratinocyte growth factor–2; TBSA, total body surface area; PRN, pro re nata (as needed); DMSO, dimethysulfoxide; CO_2, carbon dioxide; Postop, post-operative; MACF, fluorinated methacrylamide chitosan modified with perfluorocarbon chains; MAC, methacrylamide chitosan modified with perfluorocarbon chains; nHDFs, Neonatal human dermal fibroblasts; nHEK, Neonatal human epidermal keratinocytes; VLUs, venous leg ulcers; HUVECs, Human umbilical vein endothelial cells; HSFs, Human embryonic stem cells; AGP, algae gel patch; TGO, topical gas oxygen therapy; N/A, not available/applicable.

Table S.2: Technological subcategories, manufacturing, and technical details of the DO technologies studied in healing-related protocols.

First author, year	Manufacturing and application parameters	O_2 supply	Additional core materials	Additional coating materials	Additional solutes
OUPs					
Magnetto et al. 2014	OLNDs, OFNDs, OLNBs, OFNBs, OSS; Homogenization of core materials for 2min at 24.000 rpm; homogenization with coating materials for 2min at 13.000 rpm. liquid and gel formulations for each; tested before & after U/S application (*in vitro*: 2.5MHz, 5W; *in vivo*: 1MHz, 5W)	Each formulation saturated with 100% gas O_2 for 2min	DFP (OLNDs, OFNDs); PFP (OLNBs, OFNBs)	Chitosan (OLNDs, OFNDs, OLNBs, OFNBs)	Ethanol, palmitic acid, soya PC, PVP HEC (in gel formulations)
Khadjavi et al. 2015	As above; liquid formulations of OLNDs, OFNDs, OSS	As above	DFP (OLNDs, OFNDs)	Chitosan (OLNDs, OFNDs)	Ethanol, palmitic acid, soya PC, PVP
Pratto et al. 2015	As above: OLNDs, OFNDs, OLNBs, OFNBs, OSS; liquid and gel formulations; tested before & after U/S application (*in vitro*: 2.5MHz, 5W; *in vivo*: 1MHz, 5W)	As above	DFP (OLNDs, OFNDs); PFP (OLNBs, OFNBs)	Dextran (OLNDs, OFNDs, OLNBs, OFNBs)	Ethanol, palmitic acid, soy lecithin, PVP, NaCl, PBS HEC (in gel formulations)
Gulino et al. 2015	As above: OLNDs (~590nm); OFNDs (~240nm); OSS; ultra-pure water formulations	As above	DFP (OLNDs, OFNDs)	Dextran (OLNDs, OFNDs)	Ethanol, palmitic acid, soya PC, PVP
Basilico et al. 2015	As above: OLNDs (~nm); OFNDs (~nm); OSS; ultra-pure water formulations	As above;	OLNDs, OFNDs: DFP	OLNDs, OFNDs: dextran	ethanol, palmitic acid, soya PC, PVP
Bisazza et al. 2008	As above OMB N/S solution; mean diameter = 2.5µm	Before adding chitosan, N/S solution saturated with O_2 up to 35mg/l	PFP	chitosan	Ethanol, palmitic acid, soya PC, PVP, β-glycerol phosphate
Cavalli et al. 2009 (a)	OUB N/S solutions; formulation A (no PFP): mean diameter = 0.7µm; formulation B (PFP): mean diameter = 1.2µm; formulation A tested before & after U/S (45kHz, 260W)	As above	PFP (only in solution B)	Chitosan (~30nm shell)	ethanol, palmitic acid, soya PC, β-glycerol phosphate, NaOH

Cavalli et al. 2009 (b)	OUB N/S solutions; formulation A, C: mean diameter = 0.55μm; formulation B: mean diameter = 0.41μm; formulation A tested before & after U/S application (2.5MHz, 30W)	As above (before adding dextran)	PFP	dextran (~30nm shell); PVP in B	ethanol, palmitic acid, soya phosphatidylcho-line,
Feshitan et al. 2014	Phospholipid-coated OMBs (<14μm); all formulations manufactured as PBS solutions; lipid coating mixed with PBS (12mg/ml); O_2 is added to the mixture & then emulsified via sonication; OMBs collected after centrifuging (~70% O_2 volume concentrate)	Mixture of lipid coating with PBS combined with 100% O_2 at equal volumetric flow rates under U/S	N/A	DSPC, PEG-40S; ~13nm (1% OMB volume)	N/A
Fiala et al. 2020	As above	As above	N/A	As above	N/A
OSS/SOS					
Onouye et al. 2000	"O_2 mist protocol" applied postoperatively; combination of sterile water, O_2 (~93%), and additional solutes; followed by application of a cleaner and ointment 6-8 times per day (after O_2 mist protocol)	O_2 (~93%) was supplied continuously during the protocol for 15min; delivered at 15L/min	Chloride, sodium, potassium, lactate, acetate, glucose, urea, choline, aminoacids, and nucleic acid derivatives		Wheat germ oil, paraben derivatives, PEG-40
Paola et al. 2006	SOS (Dermacyn® Wound Care, Petaluma, Calif, USA); oxygenated saline solution enriched with oxygen and chloride free radicals via electrolysis; ORP >800mV; osmolality 13mOsm/Kg	Gauzes soaked in 20mL SOS per treatment; changed daily	N/A	N/A	Sodium hypochlo-rite, hypochlorous acid, NaCl
"Plain OUBs"					
Matsuki et al. 2012	OMB N/S solution; diameter ~ 20-30μm for the majority of OMBs; produced after hydrodynamic mixture of O_2 (1l/min) with 150ml N/S for 15min, at a peak pressure of 1–1.5MPa; after brief U/S for a few seconds, majority of OMBs were <10μm in diameter (classified as OUBs)	PO_2 resulting from hydrodynamic mixture: 1003.2mmHg	N/A	N/A	N/A
Matsuki et al. 2014	4 solutions commonly used in medical practice (N/S, dextran, albumin, lipid) were enriched with OUBs; OUBs produced as above; this time mixture of O_2 (1.5l/min) with 150ml of each solution for 15min after brief U/S for 30s, majority of OUB diameters in nanoscale <1.5μm	As above	N/A	N/A;	Constituents in each solution (N/S, dextran, albumin, lipid)

Ebina et al. 2013	Distilled water solution enriched with OUBs, produced in 3 steps; 1. hydrodynamic mixture of O_2 with distilled water to create OMB solution; 2. U/S for a few seconds (~30); 3. hydrodynamic mixture of O_2 (0.1MPa, 0.7L/min, 3600rpm) with OMB solution & water for 30min. Diameter: 70% of OUBs <2µm, immediately after production; ~60% of OUBs <2µm, 2.5 months after production	100% O_2 (0.1MPa, 0.7L/min) supplied for all mixtures	N/A	N/A	N/A
Noguchi et al. 2017	N/S solution enriched with OUBs or NUBs (negative control); produced in the 3 steps described above; diameter: filtered at <220nm, immediately after production	As above	N/A	N/A	N/A
Matsuoka et al. 2018	N/S solution enriched with OUBs or NUBs (negative control); produced in the 3 steps described above; diameter: filtered at <220nm, immediately after production	As above	N/A	N/A	N/A
H_2O_2 dressings					
Tur et al. 1995	H_2O_2 cream (Karin Herzog Ltd., Basel, Switzerland); covered by a gauge sponge & Bioclusive Transparent Dressing (Johnson & Johnson Products, New Brunswick, N.J.)	H_2O_2 pre-integrated in the cream product	Cream constituents non-significant to the oxygenating/healing outcomes		
Chandra et al. 2015	O_2-generating dressing; 4 layers (L1: gelatin-based for cushioning, contains $MnCl_2$, L2: O_2-generating layer, contains 10mg SPO and CPO, in a PVA and PCL polymer matrix; L3: silicone layer; L4: outermost layer, PVDC).	L1 absorbs exudate; in this aqueous environment, SPO and CPO from L2 degrade to release O_2 via a H_2O_2 intermediate	$MnCl_2$, SPO, CPO, PVA, PCL, PVDC		
Harrison et al. 2007	Polymeric O_2-generating films, manufactured via a solvent-casting process. Mixture of PLGA with SPO, left to dry for 72h	In a moist environment, SPO degrades to release O_2 via a H_2O_2 intermediate	Methylene chloride (5% w/v)		
Wright et al. 2003	O_2-generating hydrocolloid dressing (Kaltostat,® Convatec, Skillman N J); occlusive, consists of a hydrophilic colloid alginate and an embedded inorganic catalyst (manganese dioxide)	By adding a moist oxygenating substrate (3% H_2O_2), the inorganic catalyst degrades H_2O_2 to O_2 + H_2O	Inorganic catalyst (manganese dioxide powder 60 to 80 µg/cm^2)		
Dressings pre-loaded with O_2					
Lairet et al. 2014	"OxyBand" O_2-releasing hydrocolloid dressing (Oxyband Technologies, St. Louis, MO), non-adherent on wound bed; top layer is a barrier film to drive O_2 to the wound; bottom layer is porous, facilitating O_2 diffusion	"OxyBand" acts as an O_2 reservoir, supplying the wound based on local O_2 consumption rate; it comes pre-filled with O_2	N/A		

Zellner et al. 2014	"OxyGenesys" (OxyGenesys™; AcryMed Inc, Beaverton, OR, USA) closed-foam hydrogel dressing; consisting of a polyacrylamide polymer enriched with gaseous O_2 during the manufacturing process; dressing was pre-moisturized with 1mL N/S before application on wound	Gaseous O_2 is supplied in the closed cells of the polyacrylamide polymer during the manufacturing process	N/A
Guelder et al. 2007	Ox66™ (Hemotek, LLC, Plano, TX, USA) poly-oxygenated aluminum hydroxide consisting of 66.2% O_2; organized as a true clathrate with multiple openings to capture molecules; available in powder form, which can be dissolved in aqueous solutions at various concentrations	66.2% O_2 pre-packed in the clathrate structure of Ox66™ during manufacturing	Aluminum (poly-oxygenated aluminum hydroxide), chlorine
Kellar et al. 2013	OxygeneSys O_2 foam dressing (Active Group, OxygeneSys™ -Continuous, AcryMed, Inc., Beaverton, OR, USA); permeable dressing with an O_2 reservoir	>95% O_2 bubbles "stored" in this foam dressing	N/A
Microfluidics-based oxygenating bandage			
Lo et al. 2013	Microfluidic O_2 bandage, enabling fast equilibration (0-100% O_2 in 60s); fabricated from PDMS, consists of: 300 mm wide microfluidic channels, two O_2-filled chambers 10mm in diameter, and a 100mm thick gas-permeable PDMS membrane; connected to medical grade 100% O_2 tanks through the microchannels	Microfluidic O_2 bandage (100% O_2 supplied medical grade O_2 tanks)	PDMS
MACF-based hydrogels saturated with air/O_2			
Patil et al. 2016	MAC & MACF dissolved in ultra-pure water to produce hydrogels; then mixed with other chemicals at 3000rpm for 2min; washed with PBS; saturated with 100% O_2 before application; covered by Tegaderm™ surgical gauge; hydrogels are freeze-dried for storage	MAC & MACF hydrogels (~0.2g each) saturated with 100% O_2 for 10 min before application on wound; MACF can also sequester some O_2 from atmospheric air	MAC groups, fluorine (in MACF hydrogels), 1-hydroxycyclohexyl phenyl ketone, 1-vinyl-2-pyrrolidinone
Patil et al. 2018	MACF hydrogel, produced as above; only difference was in the duration of saturation with O_2 before application: increased to 30min	MACF hydrogel saturated with 100% O_2 for 30 min before application on wound	As above
Patil et al. 2019	Similar to previous study	As above	As above
Wijekoon et al. 2012	MAC & MACF produced by modifying medium molecular weight chitosan; addition of fluorine residues in acetic acid (2% w/w) water, fluorinated ligands, & methacrylic anhydride MACF hydrogels formed as described in previous studies	Cultures with MAC & MACF hydrogels were saturated with 100% O_2 for 4 min/24h, for 4 days in total	Acetic acid, fluorinated anhydrides, & methacrylic anhydride

Akula et al. 2017	MACF hydrogels formed as described in previous studies	Before saturation with 100% O_2 for 30min, MACF hydrogels equilibrated with culture media overnight (4°C)	1-hydroxycyclohexyl phenyl ketone, 1- vinyl-2-pyrrolidinone
Almeleh et al. 2013	Oxygenating hydrogel (under clinical investigation by Ozeion LLC, Wilmington, DE)	N/A	N/A
Moen et al. 2018	Oxy Dressing hydrogel; produced via mixture of Oxy Water (DO~65 mg/L) with 30% w/w poloxamer 407 powder (Lutrol F127, BASF, Ludwigshafen, Germany), at 0°C;	Oxy Water already saturated with 100% O_2 during manufacturing process	Poloxamer components, acetate buffer (20mM)
H_2O_2 hydrogels			
Queen et al. 2007	"Oxyzyme" (Oxyzyme™ Sterile Wound Dressing with Iodine; Insense Ltd, UK); sterile, occlusive, air-sealed, consists of 2 hydrogel sheets: the first contains glucose, and is placed directly upon the wound surface; the second contains glucose oxidase; upon opening and exposure to atmospheric O_2, H_2O_2 is produced locally; similarly, iodide is converted to molecular iodine for extra disinfection	When the air-sealed packaging is opened, O_2 from atmospheric air induces the oxidation of (beta)-D-glucose to D-gluconic acid and H_2O_2; H_2O_2 converted to O_2 & H_2O upon contact with wet/moist wound surface	Iodide (<0.04% w/w), Glucose
Ivins et al. 2007	"Oxyzyme" dressing	As above	As above
Moffaat et al. 2014	Oxyzyme dressing; Iodozyme dressing is manufactured similarly, yet with higher Iodide content (>0.04% w/w)	As above	As above
Microalgae hydrogels			
Chen et al. 2020	O_2-generating hydrogel (AGP); 1mm hydrogel beads containing living microalgae & active *S. elongatus*, which produce O_2 and CO_2 via respiration and photosynthesis; a hydrophilic PTFE membrane separates the hydrogel beads from the wound surface; the whole dressing is covered by an impermeable polyurethane film. O_2 release required light exposure (620-660nm NIR)	CO^{2-}_3 & HCO^-_3 are pre-supplied in the AGP dressing; these are converted by the living microalgae to O_2 and CO_2 via respiration & photosynthesis	PTFE, polyurethane, CO_2, HCO^-
O_2 emulsions			
Davis et al. 2007	O_2 emulsion in topical cream format (TherOx Inc. Irvine, CA, USA) PFC droplets encased in a continuous aqueous phase (20 times higher O_2 solubility than H_2O alone); O_2 is dissolved in the emulsion and stored under pressure; cream formed by the addition of emulsifying agents (surfactant oil), to stabilize the dispersed PFC droplets	O_2 dissolved in the PFC emulsion and stored under high pressure in small dispensing bottles; to prevent rapid de-saturation in atmospheric pressure	PFC, Proprietary surfactant oil (TherOx Inc. Irvine, CA, USA)

Li J et al. 2013	As above	As above	As above
Li J et al. 2015	As above	As above	As above

Abbreviations: DO, dissolved oxygen; OUPs, oxygen ultra-fine particles; OLNDs, oxygen-loaded nanodroplets; OFNDs, oxygen-free nanodroplets; OLNBs, oxygen-loaded nanobubbles; OFNBs, oxygen-free nanobubbles; OSS, oxygen-saturated solution; Min, minutes; U/S, ultrasound; O_2, oxygen; DFP, 2H,3H-decafluoropentane; PFP, perfluoropentane; PVP, polyvinylpyrrolidone; PC, phosphatidylcholine; HEC, hydroxyethylcellulose; UV, ultraviolet radiation; PBS, sodium phosphate biphasic/phosphate-buffered saline; OMBs, oxygen microbubbles; NaOH, sodium hydroxide; DSPC, 1,2-distearoyl-sn-glycero-3-phosphocholine (phospholipid); PEG-40S, polyoxyethylene-40 stearate; ORP, oxidation-reduction potential; OSS, oxygen-saturated solution (saline); SOS, super-oxidized solution (saline); NUBs, nitrogen ultra-fine bubbles; L1, layer 1; L2, layer 2; L3, layer 3; L4, layer 4; SPO, sodium percarbonate; CPO, calcium peroxide; PVA, polyvinyl alcohol; PCL, polycaprolactone; PVDC, polyvinylidene chloride; PLGA, Poly(D,L-lactide–co–glycolide); PDMS, polydimethylsiloxane; MACF, fluorinated methacrylamide chitosan modified with perfluorocarbon chains; MAC, methacrylamide chitosan modified with perfluorocarbon chains; AGP, algae gel patch; PTFE, polytetrafluoroethylene; NIR, near-infrared; PFC, perfluorocarbon; N/S, normal saline (0.9% NaCl); PO_2, oxygen partial pressure; OUBs, oxygen ultra-fine bubbles; H_2O_2, hydrogen peroxide; H2O, water; N/A, not available.

Table S.3: Oxygenating parameters, healing endpoints, and statistically significant outcomes of DO solutions in healing-related protocols.

First author, year	Resulting O_2 levels	Physical conditions	Healing Endpoints	Statistically significant healing outcomes
OUPs				
Magnetto et al. 2014	*in vitro*: Δ[O_2] induced with US-activated OLND formulation (within 2.25h): ~0.45 mg/L	N/A; most experiments performed at 37°C	*in vitro*: **1**. DO; **2**. O_2 penetration though pig skin; *in vivo*: **3**. $TcPO_2$, **4**. OxyHb	**1**, **2** (after U/S); **3**, **4** (after U/S, compared to untreated controls)
Khadjavi et al. 2015	O_2 release in cell culture medium (without U/S activation): OLNDs: ~10-16 mg/L (14h-plateau at ~11 mg/L); OSS: ~8.5-13 mg/L (17h-plateau at <9 mg/L); OFNDs: <9 mg/L (throughout the study)	N/A; most experiments performed at 37°C	expression of: **1**. MMP-2; **2**. MMP-9; **3**. TIMP-1; **4**. TIMP-2	**All** (restored to normoxic levels)
Pratto et al. 2015	*in vitro*: O_2 release after UV sterilization, before U/S application (within 6h): OLNDs (~12-19 mg/L), OLNBs (~8-18 mg/L), OSS (~8-14 mg/L); Δ[O_2] induced with US activation (within 2.25h): OLNDs (~0.43-0.57 mg/L), OLNBs (~0.34-0.38 mg/L), OSS (~0.16-0.35 mg/L)	N/A; most experiments performed at 37°C	*in vitro*: **1**. DO; **2**. O_2 penetration though pig skin *in vivo*: **3**. $TcPO_2$; **4**. OxyHb	**1** (in hypoxia for 6h); **2** (after U/S for 135min); *in vivo*: **3** (stable for 10min), **4** (only with U/S)
Gulino et al. 2015	Immediately after preparation & 20min after UV sterilization of OLND formulation: oxygen storing capacity= 400 mg/L (comparable levels in OSS)	N/A; most experiments performed at 37°C	**1**. DO; **2**. cell viability; **3**. MMP-9 expression; **4**. TIMP-1 expression; **5**. TIMP-2 expression	OLNDs safe *in vitro*; **3**, **4**
Basilico et al. 2015	Immediately after preparation & 20min after UV sterilization of OLND formulation: oxygen storing capacity= 400 mg/L (comparable levels in OSS)	N/A; most experiments performed at 37°C	**1**. DO; **2**. cell viability; **3**. MMP-2 expression; **4**. MMP-9 expression; **5**. TIMP-1 expression; **6**. TIMP-2 expression; **7**. healing parameters (migration, ECM invasion, new vessels)	**1**, **2**, **3**, **4**, **5**, **6** (after 24h after incubation, **7** (vs. OFNDs only)
Bisazza et al. 2008	DO~26 mg/L in OMB N/S solution before mixtures; 600% increase in [O_2] of hypoxic solution following mixture (within ~8 min)	Atmospheric pressure, 25°C	**1**. DO; **2**. O_2 diffusion coefficient; **3**. HIF-1α gene expression (in JEG-3 cell cultures)	**1**, **2**, **3** (in hypoxia)
Cavalli et al. 2009 (a)	DO~30 mg/L; in both OUB solutions before mixtures, without U/S; DO_A= 2.7 mg/L, DO_B= 4.6 mg/L; at 60min, after mixture with hypoxic N/S; ~20% increase of O_2 release to hypoxic N/S from formula A after 10 min of U/S application	Atmospheric pressure, 25°C	**1**. DO changes after mixture over 60min with both formulas; **2**. % increase in DO 10min after U/S in formulation A; **3**. HIF-1α gene expression (only with A, without U/S)	**1**, **2**, **3**

Cavalli et al. 2009 (b)	at 3h: after mixture with moderate-hypoxia N/S: formulation A ~5.7 mg/L; formulation B ~6.2 mg/L; after mixture with severe-hypoxia N/S: formulation A ~4.5 mg/L; formulation B ~3.8 mg/L; up to 133% increase in O_2 release to severe-hypoxia N/S with US-activated formulation A within 10 min	Atmospheric pressure, 25°C	**1**. DO after mixtures of A,B with hypoxic N/S solutions (5, 30, 60, & 180 min after OUB production); **2**. DO in A before and after U/S	**1** (more after mixture with severely- hypoxic N/S), **2** (higher, faster increase)
Feshitan et al. 2014	~107mL of OMB solution infused (70% O_2 volume) IP; stored at P=1atm, θ=4°C for 2-3 days	*in vivo* experiments at 37°C	**1**. 2h-survival following acute lung injury; **2**. HR, SaO_2	**1** (100%), **2** (normal in treatment group during 2h)
Fiala et al. 2020	As above	As above	**1**. 48h-survival following acute lung injury; **2**. SpO_2; **3**. post-mortem wet/dry ratio (edema); **4**. healing parameters on histology (hemorrhage, edema, inflammation scores)	**1**, **2**, **3**(only between IP OMB & no treatment groups), **4** (inflammation only)
OSS/SOS				
Onouye et al. 2000	N/A	Atmospheric pressure & room temperature	**1**. healing rate; **2**. healing effectiveness (observed tissue restoration) assessment based only on photographs; evaluated by 18 investigators	**1**, **2**; only during treatment (until day 5 postop)
Paola et al. 2006	N/A	Atmospheric pressure & room temperature	**1**. bacterial load (number of strains); **2**. healing time (days); **3**. type of surgical therapy; **4**. frequency of skin dehiscence post-infection; **5**. skin reaction	**1**, **2**, **5**
“Plain OUBs”				
Matsuki et al. 2012	PO_2 = 1003.2mmHg in ultra-pure water enriched with OMBs at 3min after dilution: PO_2= 81.9mmHg (10% dilution); PO_2 = 110.4mmHg (30% dilution); PO_2 = 166.7mmHg (50% dilution)	1–1.5MPa, 25°C	**1**. PO_2 in N/S solutions after OMB administration (pre-mixture PO_2 ~ 65mmHg); **2**. PO_2 after mixture of OMB N/S solution with hypoxic swine blood at 10,20,30, & 50% dilution ratios	**1**, **2** (dose-dependent PO_2 increase)
Matsuki et al. 2014	PO_2 = 1053.3mmHg in ultra-pure water enriched with OUBs 2min after dilution: PO_2 = 84.4mmHg (10% dilution); PO_2 = 115.8mmHg (30% dilution) PO_2 = 179mmHg (50% dilution)	1–1.5MPa, 25°C	**1**. PO_2 in solutions before mixtures with hypoxic swine blood; **2**. PO_2 after mixtures with hypoxic swine blood (pre-mixture PO_2 ~ 65mmHg)	**1**, **2** (dose-dependent increase in PO_2 in all mixtures)
Ebina et al. 2013	DO = 31.7 mg/L immediately after production; DO = 8.7 mg/L at 5h after production; maintained for 70 days	0.1 MPa, stable at 4°C for 70 days, given at 25°C	**1**. DO in OUB-enriched water over 70 days; **2**. changes in mouse body weight, length, & amounts of food intake	**1**, **2**

Noguchi et al. 2017	DO = 18.0 mg/L; 30min after production in OUB N/S	0.1 MPa, stable at 4°C for 70 days, given at 25°C	*in vitro*: **1**.osteoclast number; **2**. bone resorption by osteoclasts; *in vivo*: **3**. DO in each solution; **4**. bone preservation (bone mass/bone resorption); **5**. decrease in osteoclast number	**1** & **2** (dose-dependent); **3**, **4**, **5**
Matsuoka et al. 2018	DO = 18.0mg/L 30min after production in OUB N/S	0.1 MPa, stable at 4°C for 70 days, given at 25°C	*in vitro*: **1**. DRG neurite outgrowth; **2**. SC differentiation, proliferation, growth-factor expression, proliferation & apoptosis under hypoxia (1% O_2); *in vivo*: **3**. motor & sensory recovery, **4**. NCV, **5**. re-myelination	**1**, **2** (dose dependent), **3**, **4**, **5**

Abbreviations: DO, dissolved oxygen; DO, dissolved oxygen; $\Delta[O_2]$, change in oxygen levels; OUPs, oxygen ultra-fine particles; OLNDs, oxygen-loaded nanodroplets; OFNDs, oxygen-free nanodroplets; OLNBs, oxygen-loaded nanobubbles; OFNBs, oxygen-free nanobubbles; OSS, oxygen-saturated solution; $TcPO_2$, transcutaneous oxygen partial pressure; U/S, ultrasound; OxyHb, oxyhemoglobin; MMP, matrix metalloproteinases; TIMP, tissue inhibitors of metalloproteinases; ECM, extracellular matrix; OMBs, oxygen microbubbles; $[O_2]$, oxygen concentraction; HIF-1α, Hypoxia Inducible Factor 1α; IP, intraperitoneal administration; HR, heart rate; SaO_2, hemoglobin O_2 saturation; SpO_2, hemoglobin O_2 saturation in the peripheral blood; DRG, dorsal-root ganglion; SC, Schwann cells; NCV, nerve conduction velocity; UV, ultraviolet radiation; SOS, super-oxidized solution (saline); N/S, normal saline (0.9% NaCl); O_2, oxygen; PO_2, oxygen partial pressure; OUBs, oxygen ultra-fine bubbles; N/A, not available; Min, minutes..

Table S.4: Oxygenating parameters, healing endpoints, and statistically significant outcomes of O2 dressings in healing-related protocols.

First author, year	Resulting O_2 levels	Physical parameters	Healing Endpoints	Statistically significant healing outcomes
H_2O_2 dressings				
Tur et al. 1995	N/A; study evaluated changes in vascular perfusion	Atmospheric pressure, room temperature	**1**. wound surface area (% of non-necrotic wound surface); **2**. vascular perfusion (blood flow) in wound area	1st : **2** ; 2nd : **2** (dose-dependent)
Chandra et al. 2015	N/A; dressing replaced every 3-4 days to "renew" O_2 supply	Room temperature	**1**. % wound closure; **2**. re-epithelialization; **3**. dermis collagen content; **4**. epidermal thickness; **5**. neovascularization	**1**, **2**, **3**, **4**
Harrison et al. 2007	Sigmoidal curve towards a maximum of 121ml of O_2 per gram of SPO (*in vitro*)	Atmospheric pressure, 37°C	**1**. re-epithelialization; **2**. flap survival/necrosis; **3**. preserved skin architecture; **4**. local inflammation; **5**. wound breaking strength	**2** (only at days 2 & 3) **3** (days 3 & 7)
Wright et al. 2003	Intermittent increase in PO_2; depending on substrate consumption rate	Atmospheric pressure, room temperature	**1**. wound surface area; **2**. bacterial load (quantification)	**1**, **2**
Dressings pre-loaded with O_2				
Lairet et al. 2014	N/A	Applied at atmospheric pressure & room temperature	**1**. time to healing (90% or more re-epithelialization); **2**. pain score; **3**. cosmetic result	**1**, **2**
Zellner et al. 2014	N/A	Applied at atmospheric pressure & room temperature	**1**. clinical assessment of healing (drainage volume, flap erythema, skin sloughing, drainage on previous dressings) **2**. histological evaluation of healing (inflammation, ischemia, necrosis, bacterial load, fibrosis)	**1**, **2** (except for SC necrosis & SC fibrosis in the most ischemic flap zones)
Guelder et al. 2007	Depends on Ox66™ concentration in each solution	Applied at atmospheric pressure & room temperature	**1**. toxicity; **2**. recovery (cell viability & proliferation); **3**. cell migration rate upon scratch test	No toxicity; **2** (at specific concentration ranges), **3**
Kellar et al. 2013	N/A	Atmospheric pressure & room temperature	**1**. clinical assessment of skin (hydration, desquamation, roughness, texture); **2**. histology/gene expression to evaluate inflammation, structural skin proteins (collagen I, elastin, filaggrin), safety (p53 protein)	**1**, **2** No toxicity (safe)
Microfluidics-based oxygenating bandage				

Lo et al. 2013	Equilibration of multiple concentrations (10-100%) via the PDMS membrane within 60s	Atmospheric pressure & room temperature	*in vitro*: (**1**) local O_2 delivery in 60s; *in vivo*: (**2**) collagen maturation in wound bed; (**3**) total collagen amount (measurement of hydroxyproline); (**4**) microvasculature (CD31 staining); (**5**) wound surface area; (**6**) wound oxygenation	**2** (compared to untreated diabetics), **6** (at days 3 & 14)

Abbreviations: O_2, oxygen; H_2O_2, hydrogen peroxide; L1, layer 1; L2, layer 2; SPO, sodium percarbonate; L3, layer 3; L4, layer 4; N/S, normal saline (0.9% NaCl); PEG-40, Polyethylene Glycol; PDMS, polydimethylsiloxane; SC, subcutaneous; PO_2, oxygen partial pressure; N/A, not available/applicable.

Table S.5: Oxygenating parameters, healing endpoints, and statistically significant outcomes of O2 hydrogels in healing-related protocols.

First author, year	Resulting O_2 levels	Physical parameters	Healing Endpoints	Statistically significant healing outcomes
MACF-based hydrogels saturated with air/O_2				
Patil et al. 2016	Right after saturation of 0.2g hydrogel: PO_2 with MACF: 265.0 ± 9.5 mmHg; O_2 delivery significantly more efficient with MACF	PO_2 measured at atmospheric pressure, 37°C	**1**. re-epithelialization; **2**. collagen synthesis	**1** (no difference between 1/5 and 2/5), **2**
Patil et al. 2018	N/A	Applied at room temperature & pressure	**1**. re-epithelialization; **2**. collagen synthesis; **3**. angiogenesis; **4**. collagen maturation; **5**. hydroxyproline synthesis; **6**. keratinocyte maturation	**1**, **5** (only compared to control dressing); **4** (only compared to MACF-only hydrogel)
Patil et al. 2019	N/A	As above	**1**. re-epithelialization; **2**. collagen synthesis; **3**. angiogenesis; **4**. regenerated skin maturation; **5**. accumulation of MACF degradation products in vital organs over 14 days	**2**, **4** 5: not detected
Wijekoon et al. 2012	Highest with the most fluorine residues (15): PO_2 = 134.20 ± 3.73 mmHg; gradually increasing PO_2, reached the above value at day 5; equilibrium for 1 more day	Cells cultured at 37°C, atmospheric pressure	**1**. time to maximum O_2 uptake; **2**. duration of O_2 release; **3**. PO_2 achieved via O_2 release; **4**. cellularity (number of cells); **5**. Cells metabolism	all higher with the highest number of fluorine residues added (15)
Akula et al. 2017	Highest PO_2 at 2h: 233.8± 9.9 mmHg; gradually decreased to a plateau at 20h; maintained for 48h	Cells cultured at 37°C, atmospheric pressure	**1**. PO_2; **2**. cell metabolism; **3**. cell migration; **4**. cellularity (number of cells); **5**. protein synthesis; **6**. DNA synthesis; **7**. ATP synthesis	**1**, **2**, **3**, **4**, **5 7**
Almeleh et al. 2013	N/A	Applied at room temperature & pressure	**1**. time to complete healing	3-7 days
Moen et al. 2018	DO >22mg/L for at least 30 hours (upon *in vitro* testing, at 35°C); DO >30mg/L; stable for 3 months when stored at 5 & 23°C)	Atmospheric pressure	**1**. intracellular ATP; **2**. reactive oxygen species formation; **3**. HSF proliferation rate; 4. HSF viability	**1**; **2**, **3**, **4** remained stable
H_2O_2 hydrogels				
Queen et al. 2007	N/A	Applied at room temperature & pressure	**1**. wound closure	all fully healed at 4 weeks

Ivins et al. 2007	N/A	As above	**1**. wound closure	4/6 fully healed at 6 weeks
Moffaat et al. 2014	N/A	As above	**1**. healing outcomes; **2**. quality of life; **3**. adverse events; **4**. High MMP & protease activity; **5**. cost-effectiveness	**4** (improved & faster healing), **5**
Microalgae hydrogels				
Chen et al. 2020	***in vitro***: DO~600μM, measured at 37°C after 30min of NIR exposure; DO~1000μM, measured after storage at 4°C under NIR conditions; remained stable for 15 days; absence of *S. elongatus* did not significantly affect DO	Room temperature & pressure *in vivo* NIR light exposure of applied AGP for 30-60min	*in vitro*: **1**. DO penetration through mouse skin samples; **2**. HIF-1α expression; **3**. cell migration; **4**. tube formation; **5**. immune reactivity; **6**. cell proliferation. *in vivo*: **7**. re-epithelialization; **8**. collagen synthesis; **9**. angiogenesis (CD31, CD68, & HIF-1α expression); **10**. immune reactivity (iNOS, GSK); **11**: cell migration (β-catenin)	**All**

Abbreviations: MACF, fluorinated methacrylamide chitosan modified with perfluorocarbon chains; O_2, oxygen; PO_2, oxygen partial pressure; H_2O_2, hydrogen peroxide; DO, dissolved oxygen concentration; HSF, Human embryonic stem cells; MMP, matrix metalloproteinases; NIR, near-infrared; AGP, alga-gel patch; HIF-1α, Hypoxia Inducible Factor 1α; iNOS, Nitric oxide synthase; GSK, Glycogen synthase kinase 3 beta; N/A, not available/applicable.

Table S.6: Oxygenating parameters, healing endpoints, and statistically significant outcomes of O2 emulsions in healing-related protocols.

First author, year	Resulting O_2 levels	Physical parameters	Healing Endpoints	Statistically significant healing outcomes
O_2 emulsions				
Davis et al. 2007	Immediately before dispensation, DO = 2ml O_2 per ml of emulsion (standard temperature & pressure)	Stored under pressure in small bottles before dispensing, room temperature	**1**. re-epithelialization rate (time to complete closure)	**1**
Li J et al. 2013	As above	As above	**1**. quantification of type I collagen, type III collagen, & VEGF; **2**. histology for granulation tissue formation, re-epithelialization, angiogenesis	**1** (peaked at day 7), **2** (highest difference until day 4)
Li J et al. 2015	As above; $TcPO_2$ = 25 mmHg (at day 4), 22 mmHg at day 7	As above	**1**. quantification of type I collagen, type III collagen, & VEGF; **2**. histology for granulation tissue formation, re-epithelialization, angiogenesis**3**. $TcPO_2$ at wound sites	**All**; except collagen type I

Abbreviations: O_2, oxygen; DO, dissolved oxygen; VEGF, vascular endothelial growth factor; $TcPO_2$, transcutaneous oxygen partial pressure.

Table S.7: Statistical analysis of DO concentrations in the plain DOS versus the N/S solution in Phase 1 experiments.

Descriptive statistics

		[DO]_PDOS	[DO]_NS
N	Valid	14	14
	Missing	0	0
Mean		22.875	6.787
Median		21.705	6.750
Std. Deviation		3.658	0.214
Variance		13.378	0.046
Range		13.690	0.820
Minimum		17.070	6.410
Maximum		30.760	7.230

Group Statistics

	GROUP	N	Mean	Std. Deviation	Std. Error Mean
TIMES	[DO]_PDOS	14	22.875	3.658	0.978
	[DO]_NS	14	6.787	0.214	0.057

Independent Samples Test

		Levene's Test for Equality of Variances		t-test for Equality of Means						
		F	Sig.	t	df	Sig. (2-tailed)	Mean Difference	Std. Error Difference	95% Confidence Interval of the Difference	
									Lower	Upper
TIMES	Equal variances assumed	27.162	0.000	16.430	26.000	0.000	16.088	0.979	14.075	18.101

	Equal variances not assumed			16.430	13.089	0.000	16.088	0.979	13.974	18.202

Independent Samples Effect Sizes

		Standardizer[a]	Point Estimate	95% Confidence Interval	
				Lower	Upper
TIMES	Cohen's d	2.591	6.210	4.365	8.033
	Hedges' correction	2.669	6.029	4.237	7.799
	Glass's delta	0.214	75.168	46.647	103.696

a. The denominator used in estimating the effect sizes.
Cohen's d uses the pooled standard deviation.
Hedges' correction uses the pooled standard deviation, plus a correction factor.
Glass's delta uses the sample standard deviation of the control group.

Table S.7 Notes: An independent-samples t-test was conducted to compare the DO concentrations between the plain DOS formulation and the control N/S solution. The test results showed a significant difference in the mean DO concentrations between the plain DOS group (M = 22.87, SD = 3.66), and the regular N/S control group (M = 6.79, SD = 0.21), with Cohen's d= 6.2, which indicates a large effect size. Details regarding the corresponding descriptive statistics, and the parameters of the independent-samples t-test are included in the tables above. **Abbreviations:** DO, dissolved oxygen; pDOS, plain dissolved oxygen solution; N/S, normal saline solution 0.9% NaCl; [DO], dissolved oxygen concentration in mg/L; N, statistical sample size; M, mean; SD, standard deviation.

Table S.8: Detailed in vivo safety, tolerability, and adverse-event data per experimental group, in the IV, LO, PO, and CO groups during Phase 1 experiments.

Safety/tolerability endpoint		Day -2	Day -1	Day 0	Day 2	Day 3	Day 7	Day 9	Day 10
Well-being & tolerability parameters									
Body weight (median; IQR)									
	IV			26,00; 5,00		26,00; 6,50			26,00; 3,00
	LO			24,00; 5,00		25,00; 5,00			25,00; 4,00
	PO			25,00; 5,00		26,00; 5,00			26,00; 2,50
	CO			25,00; 7,00		25,00; 5,00			24,00; 6,00
Food intake [1] (mean ± SD)									
	IV		4,95 ± 0,24		4,94 ± 0,18			5,01 ± 0,16	
	LO		5,03 ± 0,21		5,07 ± 0,22			5,09 ± 0,20	
	PO		5,10 ± 0,20		4,99 ± 0,22			4,94 ± 0,11	
	CO		5,00 ± 0,21		5,04 ± 0,20			5,12 ± 0,16	
Water intake [1] (mean ± SD)									
	IV		8,99 ± 0,94		8,80 ± 1,10			8,53 ± 0,92	
	LO		11,14 ± 1,76		10,94 ± 1,48			10,45 ± 1,17	
	PO		11,02 ± 1,87		11,37 ± 1,12			10,51 ± 2,26	
	CO		13,20 ± 2,47		13,00 ± 2,21			13,28 ± 3,12	
Burrowing behavior [2] (median; IQR)									
	IV	26,25%; 2,50%		26,75%; 1,75%		27,00%; 2,50%	27,50%; 1,75%		
	LO	26,75%; 2,75%		27,25%; 2,50%		27,50%; 2,25%	27,25%; 2,25%		

Safety/tolerability endpoint		Day -2	Day -1	Day 0	Day 2	Day 3	Day 7	Day 9	Day 10
	PO	28,75%; 1,75%		28,00%; 1,50%		28,00%; 2,25%	28,25%; 1,00%		
	CO	25,25%; 2,50%		25,50%; 1,75%		26,25%; 1,75%	26,25%; 1,25%		
Spontaneous behavior [3] (mean ± SD)									
	IV	1,00 ± 0,00	1,00 ± 0,00	1,00 ± 0,00	1,00 ± 0,00	1,00 ± 0,00	1,00 ± 0,00	1,00 ± 0,00	1,00 ± 0,00
	LO	1,00 ± 0,00	1,00 ± 0,00	1,00 ± 0,00	1,00 ± 0,00	1,00 ± 0,00	1,00 ± 0,00	1,00 ± 0,00	1,00 ± 0,00
	PO	1,00 ± 0,00	1,00 ± 0,00	1,00 ± 0,00	1,00 ± 0,00	1,00 ± 0,00	1,00 ± 0,00	1,00 ± 0,00	1,00 ± 0,00
	CO	1,00 ± 0,00	1,00 ± 0,00	1,00 ± 0,00	1,00 ± 0,00	1,00 ± 0,00	1,00 ± 0,00	1,00 ± 0,00	1,00 ± 0,00
Posture [3] (mean ± SD)									
	IV	1,00 ± 0,00	1,00 ± 0,00	1,00 ± 0,00	1,00 ± 0,00	1,00 ± 0,00	1,00 ± 0,00	1,00 ± 0,00	1,00 ± 0,00
	LO	1,00 ± 0,00	1,00 ± 0,00	1,00 ± 0,00	1,00 ± 0,00	1,00 ± 0,00	1,00 ± 0,00	1,00 ± 0,00	1,00 ± 0,00
	PO	1,00 ± 0,00	1,00 ± 0,00	1,00 ± 0,00	1,00 ± 0,00	1,00 ± 0,00	1,00 ± 0,00	1,00 ± 0,00	1,00 ± 0,00
	CO	1,00 ± 0,00	1,00 ± 0,00	1,00 ± 0,00	1,00 ± 0,00	1,00 ± 0,00	1,00 ± 0,00	1,00 ± 0,00	1,00 ± 0,00
Breathing [3] (mean ± SD)									
	IV	1,00 ± 0,00	1,00 ± 0,00	1,00 ± 0,00	1,00 ± 0,00	1,00 ± 0,00	1,00 ± 0,00	1,00 ± 0,00	1,00 ± 0,00
	LO	1,00 ± 0,00	1,00 ± 0,00	1,00 ± 0,00	1,00 ± 0,00	1,00 ± 0,00	1,00 ± 0,00	1,00 ± 0,00	1,00 ± 0,00
	PO	1,00 ± 0,00	1,00 ± 0,00	1,00 ± 0,00	1,00 ± 0,00	1,00 ± 0,00	1,00 ± 0,00	1,00 ± 0,00	1,00 ± 0,00

Safety/tolerability endpoint		Day -2	Day -1	Day 0	Day 2	Day 3	Day 7	Day 9	Day 10
	CO	1,00 ± 0,00	1,00 ± 0,00	1,00 ± 0,00	1,00 ± 0,00	1,00 ± 0,00	1,00 ± 0,00	1,00 ± 0,00	1,00 ± 0,00
Behavior after provocation/ weighing [3] (mean ± SD)									
	IV	1,00 ± 0,00	1,00 ± 0,00	1,00 ± 0,00	1,00 ± 0,00	1,00 ± 0,00	1,00 ± 0,00	1,00 ± 0,00	1,00 ± 0,00
	LO	1,00 ± 0,00	1,00 ± 0,00	1,00 ± 0,00	1,00 ± 0,00	1,00 ± 0,00	1,00 ± 0,00	1,00 ± 0,00	1,00 ± 0,00
	PO	1,00 ± 0,00	1,00 ± 0,00	1,00 ± 0,00	1,00 ± 0,00	1,00 ± 0,00	1,00 ± 0,00	1,00 ± 0,00	1,00 ± 0,00
	CO	1,00 ± 0,00	1,00 ± 0,00	1,00 ± 0,00	1,00 ± 0,00	1,00 ± 0,00	1,00 ± 0,00	1,00 ± 0,00	1,00 ± 0,00
Movement after provocation/ weighing [3] (mean ± SD)									
	IV	1,00 ± 0,00	1,00 ± 0,00	1,00 ± 0,00	1,00 ± 0,00	1,00 ± 0,00	1,00 ± 0,00	1,00 ± 0,00	1,00 ± 0,00
	LO	1,00 ± 0,00	1,00 ± 0,00	1,00 ± 0,00	1,00 ± 0,00	1,00 ± 0,00	1,00 ± 0,00	1,00 ± 0,00	1,00 ± 0,00
	PO	1,00 ± 0,00	1,00 ± 0,00	1,00 ± 0,00	1,00 ± 0,00	1,00 ± 0,00	1,00 ± 0,00	1,00 ± 0,00	1,00 ± 0,00
	CO	1,00 ± 0,00	1,00 ± 0,00	1,00 ± 0,00	1,00 ± 0,00	1,00 ± 0,00	1,00 ± 0,00	1,00 ± 0,00	1,00 ± 0,00
Coat condition [3] (mean ± SD)									
	IV	1,00 ± 0,00	1,00 ± 0,00	1,00 ± 0,00	1,00 ± 0,00	1,00 ± 0,00	1,00 ± 0,00	1,00 ± 0,00	1,00 ± 0,00
	LO	1,00 ± 0,00	1,00 ± 0,00	1,00 ± 0,00	1,00 ± 0,00	1,00 ± 0,00	1,00 ± 0,00	1,00 ± 0,00	1,00 ± 0,00
	PO	1,00 ± 0,00	1,00 ± 0,00	1,00 ± 0,00	1,00 ± 0,00	1,00 ± 0,00	1,00 ± 0,00	1,00 ± 0,00	1,00 ± 0,00

Safety/tolerability endpoint		Day -2	Day -1	Day 0	Day 2	Day 3	Day 7	Day 9	Day 10
	CO	1,00 ± 0,00	1,00 ± 0,00	1,00 ± 0,00	1,00 ± 0,00	1,00 ± 0,00	1,00 ± 0,00	1,00 ± 0,00	1,00 ± 0,00
Body condition [3] (mean ± SD)									
	IV	1,00 ± 0,00	1,00 ± 0,00	1,00 ± 0,00	1,00 ± 0,00	1,00 ± 0,00	1,00 ± 0,00	1,00 ± 0,00	1,00 ± 0,00
	LO	1,00 ± 0,00	1,00 ± 0,00	1,00 ± 0,00	1,00 ± 0,00	1,00 ± 0,00	1,00 ± 0,00	1,00 ± 0,00	1,00 ± 0,00
	PO	1,00 ± 0,00	1,00 ± 0,00	1,00 ± 0,00	1,00 ± 0,00	1,00 ± 0,00	1,00 ± 0,00	1,00 ± 0,00	1,00 ± 0,00
	CO	1,00 ± 0,00	1,00 ± 0,00	1,00 ± 0,00	1,00 ± 0,00	1,00 ± 0,00	1,00 ± 0,00	1,00 ± 0,00	1,00 ± 0,00
Eye condition [3] (mean ± SD)									
	IV	1,00 ± 0,00	1,00 ± 0,00	1,00 ± 0,00	1,00 ± 0,00	1,00 ± 0,00	1,00 ± 0,00	1,00 ± 0,00	1,00 ± 0,00
	LO	1,00 ± 0,00	1,00 ± 0,00	1,00 ± 0,00	1,00 ± 0,00	1,00 ± 0,00	1,00 ± 0,00	1,00 ± 0,00	1,00 ± 0,00
	PO	1,00 ± 0,00	1,00 ± 0,00	1,00 ± 0,00	1,00 ± 0,00	1,00 ± 0,00	1,00 ± 0,00	1,00 ± 0,00	1,00 ± 0,00
	CO	1,00 ± 0,00	1,00 ± 0,00	1,00 ± 0,00	1,00 ± 0,00	1,00 ± 0,00	1,00 ± 0,00	1,00 ± 0,00	1,00 ± 0,00
Wound condition [3] (mean ± SD)									
	IV	1,00 ± 0,00	1,00 ± 0,00	1,00 ± 0,00	1,00 ± 0,00	1,00 ± 0,00	1,00 ± 0,00	1,00 ± 0,00	1,00 ± 0,00
	LO	1,00 ± 0,00	1,00 ± 0,00	1,00 ± 0,00	1,00 ± 0,00	1,00 ± 0,00	1,00 ± 0,00	1,00 ± 0,00	1,00 ± 0,00
	PO	1,00 ± 0,00	1,00 ± 0,00	1,00 ± 0,00	1,00 ± 0,00	1,00 ± 0,00	1,00 ± 0,00	1,00 ± 0,00	1,00 ± 0,00

Safety/tolerability endpoint		Day -2	Day -1	Day 0	Day 2	Day 3	Day 7	Day 9	Day 10
	CO	1,00 ± 0,00	1,00 ± 0,00	1,00 ± 0,00	1,00 ± 0,00	1,00 ± 0,00	1,00 ± 0,00	1,00 ± 0,00	1,00 ± 0,00
Serious adverse events									
Death [4] (number of events)									
	IV	N/A	N/A	0	0	0	0	0	0
	LO	N/A	N/A	0	0	0	0	0	0
	PO	N/A	N/A	0	0	0	0	0	0
	CO	N/A	N/A	0	0	0	0	0	0
Local inflammation/ infection persisting for >24h [4] (number of events)									
	IV	N/A	N/A	0	0	0	0	0	0
	LO	N/A	N/A	0	0	0	0	0	0
	PO	N/A	N/A	0	0	0	0	0	0
	CO	N/A	N/A	0	0	0	0	0	0
Non-healing cutaneous wounds/ ulcers [4] (number of events)									
	IV	N/A	N/A	0	0	0	0	0	0
	LO	N/A	N/A	0	0	0	0	0	0
	PO	N/A	N/A	0	0	0	0	0	0
	CO	N/A	N/A	0	0	0	0	0	0
Hemorrhage from any orifice, not responding to treatment [4] (number of events)									
	IV	N/A	N/A	0	0	0	0	0	0
	LO	N/A	N/A	0	0	0	0	0	0
	PO	N/A	N/A	0	0	0	0	0	0
	CO	N/A	N/A	0	0	0	0	0	0
Water consumption <5mL for >24h									
	IV	N/A	N/A	0	0	0	0	0	0

Safety/tolerability endpoint		Day -2	Day -1	Day 0	Day 2	Day 3	Day 7	Day 9	Day 10
(number of events)	LO	N/A	N/A	0	0	0	0	0	0
	PO	N/A	N/A	0	0	0	0	0	0
	CO	N/A	N/A	0	0	0	0	0	0
Decrease in body mass ≥15% of Day 0 value [4] (number of events)									
	IV	N/A	N/A	0	0	0	0	0	0
	LO	N/A	N/A	0	0	0	0	0	0
	PO	N/A	N/A	0	0	0	0	0	0
	CO	N/A	N/A	0	0	0	0	0	0
Abnormal physique & behavior [4] (number of events)									
	IV	N/A	N/A	0	0	0	0	0	0
	LO	N/A	N/A	0	0	0	0	0	0
	PO	N/A	N/A	0	0	0	0	0	0
	CO	N/A	N/A	0	0	0	0	0	0

Table S.8 Notes: To enhance visibility, the mean ± SD/median with IQR/absolute number of events are presented per experimental group in Phase 1. The recorded data for each individual mouse from each group at each corresponding time-point, are available upon request. The following safety and tolerability endpoints were monitored for each mouse on a daily basis: spontaneous behavior, posture, breathing, behavior after provocation/weighing, movement after provocation/weighing, along with the condition of the coat, body, eyes, and wounds. Day 0 represents the day when the excisional wounds were created on each mouse's dorsum, and thus, the starting point the *in vivo* experiment. [1], evaluation methods, time-points, and grading/scoring systems adapted from *Hohlbaum et al., 2018*; [2], evaluation methods, time-points, and grading/scoring systems adapted from *Deacon, 2006*; [3], evaluation methods, time-points, and grading/scoring systems adapted from *Arras et al., 2007*; [4], evaluation methods, time-points, and grading/scoring systems adapted from the *National Research Council, Humane Endpoints for Animals in Pain, 2009*. **Abbreviations**: SD, standard deviation; IQR, interquartile range; IV, intravenous administration retro-orbitally; PO, per os intake *ad libitum*; LO, local administration by washing the wound surface with a syringe; CO, negative controls; N/A, not applicable.

Table S.9: Overview of descriptive statistics, one-way ANOVA tests, and post hoc tests applied to evaluate the effects of plain DOS treatment on macroscopic VC (in mm2/days).

VC	IV		LO		PO		CO		ANOVA	Post Hoc
	M	SD	M	SD	M	SD	M	SD		
Days 0-7 [1]	5.51	1.64	3.42	1.01	4.31	1.01	3.37	0.81	Ordinary one-way ANOVA (F(3, 28) = 5.99, p = 0.003)	Tukey's HSD test
Days 0-10 [2]	4.84	1.21	3.30	0.47	3.60	0.78	3.32	0.51	Brown-Forsythe (F^*(3.00, 17.38) = 6.69, p = 0.003); Welch (W(3.00,14.98) = 3.74, p = 0.035)	Dunnett's T3 multiple comparisons test
Days 3-7 [1]	6.50	2.21	5.15	1.76	6.00	1.81	3.64	1.58	Ordinary one-way ANOVA (F(3, 28) = 3.65, p = 0.024)	Tukey's HSD test
Days 3-10 [1]	5.12	1.44	4.23	0.71	4.25	1.17	3.45	0.92	Ordinary one-way ANOVA (F(3, 28) = 3.10, p = 0.043)	Tukey's HSD test
Days 7-10 [1]	3.28	1.34	3.00	2.39	1.93	0.97	3.52	2.06	Ordinary one-way ANOVA (F(3, 28) = 1.23, p = 0.319)	Tukey's HSD test
	M Rank		M Rank		M Rank		M Rank			
Days 0-3 [3]	35.75		33.72		30.13		30.41		Kruskal-Wallis H test (Kruskal-Wallis statistic (x^2) = 1.02; p = 0.797)	Dunn's multiple comparisons test (CO vs. IV, MR diff. = -5.34, p > 0.999; CO vs. PO, MR diff. = 0.28, p > 0.999; CO vs. LO, MR diff. = -3.31, p > 0.999)

Table S.9 Notes: The mean values or mean rank values are presented for each timeframe. The mean values were incorporated in the calculations of the corresponding mean ranks illustrated. Day 0 represents the time-point when all excisional wounds were created *in vivo*. Between day 0 and day 7, a Tukey's HSD test showed that the mean VC of the IV group was significantly higher that the one in the CO group (p = 0.005); meanwhile, there were no significant differences between the mean VCs of the PO and CO groups (p = 0.388), or between the LO and the CO groups (p > 0.999). From day 0 to 10, a Dunnett's T3 multiple comparisons test indicated that the mean VC of the IV group was significantly higher that the one of the CO group (p = 0.049); meanwhile, no significant differences were found between the mean VCs of the PO and CO groups (p = 0.945), or between the LO and the CO

Table S.9 Notes (continued): groups ($p > 0.999$). From day 3 to 7, a Tukey's HSD test showed that the mean VC of the IV group was significantly higher that the one in the CO group ($p = 0.022$); meanwhile, there was a non-significant trend elevation in the mean VC of the PO versus the CO group ($p = 0.075$), and a non-significant difference in the VCs of the LO and the CO groups ($p = 0.377$). From day 3 to day 10, a Tukey's HSD test showed that the mean VC of the IV group was significantly higher that the one in the CO group ($p = 0.024$); meanwhile, there were no significant differences between the mean VCs of the PO and CO groups ($p = 0.468$), or between the LO and the CO groups ($p = 0.494$). No significant differences in VC were observed between any of the groups from day 0 to day 3, or from day 7 to day 10. [1] post hoc analyses performed with Tukey's HSD test, as the corresponding data followed a normal distribution with homogenous variance. [2], dataset analyzed using Brown-Forsythe and Welch ANOVA tests followed by post hoc analyses with Dunnett's T3 multiple comparisons test, as the values followed a normal distribution with non-homogenous variance. [3], the corresponding data were analyzed using the non-parametric Kruskal-Wallis H test, as it did not fulfill the normality and homogeneity of variance criteria required to apply a parametric test. **Abbreviations**: ANOVA, analysis of variance; DOS, dissolved oxygen solution; IV, intravenous administration retro-orbitally; LO, local administration by washing the wound surface with a syringe; PO, per os intake *ad libitum*; CO, negative controls; VC, velocity of wound closure (in mm^2/days); M, mean; SD, standard deviation; HSD, honest significant difference; M Rank, mean rank; MR diff., mean rank difference.

Table S.10: Overview of descriptive statistics, one-way ANOVA tests, and post hoc tests used to evaluate the effects of plain DOS treatment on wound re-epithelialization (% epithelialization ratio, % ER) histopathologically.

% ER	IV		LO		PO		CO		ANOVA	Post Hoc
	M	SD	M	SD	M	SD	M	SD		
Day 3	25.83	10.36	19.68	4.67	24.58	10.75	12.14	5.08	Ordinary one-way ANOVA ($F(3, 28) = 4.56$, $p = 0.010$)	Tukey's HSD test
	M Rank		M Rank		M Rank		M Rank			
Day 10	17.00		15.38		17.13		16.50		Kruskal-Wallis H test (Kruskal-Wallis statistic (x^2) = 0.17; $p = 0.982$)	Dunn's multiple comparisons test (CO vs. IV, MR diff. = -0.50, $p > 0.999$; CO vs. PO, MR diff. = -0.63, $p > 0.999$; CO vs. LO, MR diff. = 1.13, $p > 0.999$)

Table S.10 Notes: The mean values or mean rank values are presented for each time-point. The mean values were incorporated in the calculations of the corresponding mean ranks illustrated. The time-point when all excisional wounds were created *in vivo*, is day 0. At day 3, a Tukey's HSD test showed that the mean % ER of the IV group was significantly higher than the one in the CO group ($p = 0.012$), and that the mean % ER of the PO group was significantly higher than the one in the CO group ($p = 0.026$). Meanwhile, there was no significant difference between the mean % ERs of the LO and CO groups ($p = 0.280$). At day 10, a Dunn's multiple comparisons test showed that there is no significant difference in % ER among the different routes of plain DOS administration (experimental groups), $x^2 = 0.17$, $p = 0.982$, with a mean rank % ER of 17.00 for IV administration, 15.38 for LO administration, 17.13 for PO intake, and 16.50 for the untreated CO. These data from day 10, demonstrating the successful re-epithelialization of the wounds in all experimental groups, indicate that plain DOS administration has no negative effect on the normal progression of the healing mechanism. **Abbreviations**: ANOVA, analysis of variance; DOS, dissolved oxygen solution; IV, intravenous administration retro-orbitally; LO, local administration by washing the wound surface with a syringe; PO, per os intake *ad libitum*; CO, negative controls; % ER, percentage epithelialization ratio; M, mean; SD, standard deviation; HSD, honest significant difference; M Rank, mean rank; MR diff., mean rank difference.

Table S.11: Overview of descriptive statistics, one-way ANOVA on ranks (Kruskal-Wallis H test), and post hoc tests used to evaluate the effect of plain DOS treatment on collagen deposition (% collagenation ratio, % CR), histopathologically.

% CR	IV	LO	PO	CO	ANOVA (Kruskal-Wallis)	Post Hoc
	M Rank	M Rank	M Rank	M Rank		
Day 10	23.31	9.38	23.94	9.38	Kruskal-Wallis H test (Kruskal-Wallis statistic (x^2) = 18.48; p = 0.0003)	Dunn's multiple comparisons test (CO vs. IV, MR diff. = -13.94, p = 0.018; CO vs. PO, MR diff. = -14.56, p = 0.011; CO vs. LO, MR diff. = 0.00, p > 0.999)

Table S.11 Notes: The mean values were incorporated in the calculations of the corresponding mean ranks illustrated. The time-point when all excisional wounds were created *in vivo*, is day 0. At day 10, a Kruskal-Wallis H test indicated a significant difference in % CR among the different routes of plain DOS administration (experimental groups), x^2 = 18.48, p = 0.0003, with a mean rank % CR of 23.31 for IV administration, 9.38 for LO administration, 23.94 for PO intake, and 9.38 for the untreated CO. Subsequently, a post-hoc Dunn's multiple comparisons test showed that the mean rank % CR of the IV group was significantly higher than that of the CO group (p = 0.018), and that the mean rank % CR of the PO group was significantly higher than that of the CO group (p = 0.011). Meanwhile, there was no significant difference between the mean rank % CR of the LO group compared to that of the CO group (p > 0.999). **Abbreviations**: ANOVA, analysis of variance; DOS, dissolved oxygen solution; IV, intravenous administration retro-orbitally; LO, local administration by washing the wound surface with a syringe; PO, per os intake *ad libitum*; CO, negative controls; % CR, percentage collagenation ratio; M Rank, mean rank; MR diff., mean rank difference.

Table S.12: DO dosage (mg) delivered via plain DOS administration in the IV group during Phase 1 experiments.

Mouse	DO concentration (mg/dL); Day 0	Volume injected (dL); Day 0	DO amount (mg); Day 0		DO concentration (mg/dL); Day 5	Volume injected (dL); Day 5	DO amount (mg); Day 5		TOTAL DO amount (mg) in Phase 1
IVF1	2,556	0,0015	0,004		2,172	0,0015	**0,003**		0,0071
IVF2	2,556	0,0015	0,004		2,172	0,0015	**0,003**		0,0071
IVF3	2,556	0,0015	0,004		2,172	0,0015	**0,003**		0,0071
IVF4	2,556	0,0015	0,004		2,172	0,0015	**0,003**		0,0071
									0,0000
IVM1	2,556	0,0015	0,004		2,172	0,0015	**0,003**		0,0071
IVM2	2,556	0,0015	0,004		2,172	0,0015	**0,003**		0,0071
IVM3	2,556	0,0015	0,004		2,172	0,0015	**0,003**		0,0071
IVM4	2,556	0,0015	0,004		2,172	0,0015	**0,003**		0,0071

Abbreviations: DO, dissolved oxygen; DOS, dissolved oxygen solution; IV, intravenous administration retro-orbitally.

Table S.13: DO dosage (mg) delivered via plain DOS intake in the PO group during Phase 1 experiments.

Mouse	DO concentration (mg/dL); Day 0	Volume consumed (mL); Day 0	Volume consumed (dL); Day 0	DO amount (mg); Day 0	DO concentration (mg/dL); Day 1	Volume consumed (mL); Day 1	Volume consumed (dL); Day 1	DO amount (mg); Day 1	DO concentration (mg/dL); Day 2	Volume consumed (mL); Day 2	Volume consumed (dL); Day 2	DO amount (mg); Day 2	DO concentration (mg/dL); Day 3	Volume consumed (mL); Day 3	Volume consumed (dL); Day 3	DO amount (mg); Day 3
POF1	2,556	9,20	0,09	0,24	2,519	10,40	0,10	0,26	2,377	10,20	0,10	0,24	2,127			
POF2	2,556	8,10	0,08	0,21	2,519	9,70	0,10	0,24	2,377	9,70	0,10	0,23	2,127	12,60	0,13	0,27
POF3	2,556	8,40	0,08	0,21	2,519	11,20	0,11	0,28	2,377	9,90	0,10	0,24	2,127	10,10	0,10	0,21
POF4	2,556	7,90	0,08	0,20	2,519	9,90	0,10	0,25	2,377	9,50	0,10	0,23	2,127			
POM1	2,556	9,30	0,09	0,24	2,519	9,70	0,10	0,24	2,377	9,80	0,10	0,23	2,127	10,00	0,10	0,21
POM2	2,556	10,40	0,10	0,27	2,519	12,80	0,13	0,32	2,377	10,10	0,10	0,24	2,127			
POM3	2,556	9,60	0,10	0,25	2,519	10,20	0,10	0,26	2,377	9,60	0,10	0,23	2,127			
POM4	2,556	12,10	0,12	0,31	2,519	9,50	0,10	0,24	2,377	10,50	0,11	0,25	2,127	13,80	0,14	0,29

Mouse	DO concentration (mg/dL); Day 4	Volume consumed (mL); Day 4	Volume consumed (dL); Day 4	DO amount (mg); Day 4	DO concentration (mg/dL); Day 5	Volume consumed (mL); Day 5	Volume consumed (dL); Day 5	DO amount (mg); Day 5	DO concentration (mg/dL); Day 6	Volume consumed (mL); Day 6	Volume consumed (dL); Day 6	DO amount (mg); Day 6
POF1	2,167				2,172				2,169			
POF2	2,167	18,50	0,19	0,40	2,172	17,10	0,17	0,37	2,169	14,20	0,14	0,31
POF3	2,167	16,70	0,17	0,36	2,172	19,50	0,20	0,42	2,169	12,10	0,12	0,26
POF4	2,167				2,172				2,169			
POM1	2,167	17,90	0,18	0,39	2,172	14,40	0,14	0,31	2,169	14,00	0,14	0,30
POM2	2,167				2,172				2,169			
POM3	2,167				2,172				2,169			
POM4	2,167	14,20	0,14	0,31	2,172	16,70	0,17	0,36	2,169	12,20	0,12	0,26

Mouse	DO concentration (mg/dL); Day 7	Volume consumed (mL); Day 7	Volume consumed (dL); Day 7	DO amount (mg); Day 7	DO concentration (mg/dL); Day 8	Volume consumed (mL); Day 8	Volume consumed (dL); Day 8	DO amount (mg); Day 8	DO concentration (mg/dL); Day 9	Volume consumed (mL); Day 9	Volume consumed (dL); Day 9	DO amount (mg); Day 9	TOTAL DO amount (mg) in Phase 1
POF1	2,078				1,962				1,853				0,740
POF2	2,078	11,40	0,11	0,24	1,962	13,80	0,14	0,27	1,853	10,30	0,10	0,19	2,729
POF3	2,078	15,30	0,15	0,32	1,962	12,40	0,12	0,24	1,853	9,80	0,10	0,18	2,738
POF4	2,078				1,962				1,853				0,677
POM1	2,078	13,60	0,14	0,28	1,962	14,50	0,15	0,28	1,853	10,00	0,10	0,19	2,684
POM2	2,078				1,962				1,853				0,828
POM3	2,078				1,962				1,853				0,731
POM4	2,078	14,10	0,14	0,29	1,962	10,20	0,10	0,20	1,853	6,50	0,07	0,12	2,640

Abbreviations: DO, dissolved oxygen; DOS, dissolved oxygen solution; PO, per os intake *ad libitum*.

Table S.14: Statistical analyses of DO concentrations in the ONBW versus the N/S solution used as control comparator, in Phase 2 experiments.

Tests of Normality

		Kolmogorov-Smirnov[a]			Shapiro-Wilk		
	GROUPS	Statistic	df	Sig.	Statistic	df	Sig.
TIMES	[DO] in ONBW	0.176	14	.200*	0.922	14	0.232
	[DO] in control	0.225	14	0.052	0.865	14	.036

*. This is a lower bound of the true significance.

a. Lilliefors Significance Correction

Descriptive statistics

		[DO]_ONBW	[DO]_NS
N	Valid	14	14
	Missing	0	0
Mean		22.4371	7.7664
Median		21.0750	7.8850
Std. Deviation		4.71779	0.40182
Variance		22.258	0.161
Maximum		31.47	8.18

Independent-Samples Mann-Whitney U Test Summary

Total N	28

Mann-Whitney U	0.000
Wilcoxon W	105.000
Test Statistic	0.000
Standard Error	21.761
Standardized Test Statistic	-4.503
Asymptotic Sig.(2-sided test)	0.000
Exact Sig.(2-sided test)	0.000

Table S.14 Notes: Based on the sample size (n<50), normality was assessed using the Shapiro-Wilk test. Since the measurements in the N/S (control) group did not follow a normal distribution, the Mann-Whitney U test was selected to evaluate whether DO concentrations differed between the ONBW formulation and the control N/S solution. The test results showed a significant difference in DO concentrations between the ONBW (M Rank= 21.5) and the N/S solution (M Rank=7.5). The tables above present detailed data on normality testing, descriptive statistics, and the parameters of the Mann-Whitney U test. **Abbreviations**: DO, dissolved oxygen; ONBW, oxygen nanobubble-enriched water; N/S, normal saline solution 0.9% NaCl; [DO], dissolved oxygen concentration in mg/L; N, statistical sample size.

Table S.15: Detailed in vivo safety, tolerability, and adverse-event data per experimental group, in the IV, PO, and CO groups during Phase 2 experiments.

Safety/tolerability endpoint		Day -2	Day -1	Day 0	Day 2	Day 3	Day 7	Day 9	Day 10
Well-being & tolerability parameters									
Body weight (median; IQR)									
	IV			28,00; 6,00		27,00; 7,00			27,00; 6,00
	PO			26,00; 6,00		25,00; 8,00			27,00; 6,00
	CO			25,00; 6,00		25,00; 6,00			26,00; 8,00
Food intake [1] (mean ± SD)									
	IV		5,07 ± 0,21		5,10 ± 0,22			5,17 ± 0,11	
	PO		5,05 ± 0,23		5,03 ± 0,23			5,19 ± 0,17	
	CO		5,01 ± 0,26		5,05 ± 0,21			5,17 ± 0,24	
Water intake [1] (mean ± SD)									
	IV		9,14 ± 1,03		9,81 ± 1,02			10,68 ± 1,44	
	PO		9,60 ± 1,72		9,79 ± 2,09			10,83 ± 1,33	
	CO		9,75 ± 2,27		10,33 ± 2,52			10,94 ± 2,45	
Burrowing behavior [2] (median; IQR)									
	IV	24,25%; 2,00%		24,00%; 1,50%		24,75%; 1,75%	26,25%; 2,50%		
	PO	24,00%; 1,50%		24,00%; 1,00%		25,00%; 1,50%	26,50%; 1,00%		
	CO	24,00%; 1,75%		23,50%; 1,25%		24,75%; 1,50%	26,50%; 1,50%		
Spontaneous									

Safety/tolerability endpoint		Day -2	Day -1	Day 0	Day 2	Day 3	Day 7	Day 9	Day 10
behavior [3] (mean ± SD)	IV	1,00 ± 0,00	1,00 ± 0,00	1,00 ± 0,00	1,00 ± 0,00	1,00 ± 0,00	1,00 ± 0,00	1,00 ± 0,00	1,00 ± 0,00
	PO	1,00 ± 0,00	1,00 ± 0,00	1,00 ± 0,00	1,00 ± 0,00	1,00 ± 0,00	1,00 ± 0,00	1,00 ± 0,00	1,00 ± 0,00
	CO	1,00 ± 0,00	1,00 ± 0,00	1,00 ± 0,00	1,00 ± 0,00	1,00 ± 0,00	1,00 ± 0,00	1,00 ± 0,00	1,00 ± 0,00
Posture [3] (mean ± SD)									
	IV	1,00 ± 0,00	1,00 ± 0,00	1,00 ± 0,00	1,00 ± 0,00	1,00 ± 0,00	1,00 ± 0,00	1,00 ± 0,00	1,00 ± 0,00
	PO	1,00 ± 0,00	1,00 ± 0,00	1,00 ± 0,00	1,00 ± 0,00	1,00 ± 0,00	1,00 ± 0,00	1,00 ± 0,00	1,00 ± 0,00
	CO	1,00 ± 0,00	1,00 ± 0,00	1,00 ± 0,00	1,00 ± 0,00	1,00 ± 0,00	1,00 ± 0,00	1,00 ± 0,00	1,00 ± 0,00
Breathing [3] (mean ± SD)									
	IV	1,00 ± 0,00	1,00 ± 0,00	1,00 ± 0,00	1,00 ± 0,00	1,00 ± 0,00	1,00 ± 0,00	1,00 ± 0,00	1,00 ± 0,00
	PO	1,00 ± 0,00	1,00 ± 0,00	1,00 ± 0,00	1,00 ± 0,00	1,00 ± 0,00	1,00 ± 0,00	1,00 ± 0,00	1,00 ± 0,00
	CO	1,00 ± 0,00	1,00 ± 0,00	1,00 ± 0,00	1,00 ± 0,00	1,00 ± 0,00	1,00 ± 0,00	1,00 ± 0,00	1,00 ± 0,00
Behavior after provocation/ weighing [3] (mean ± SD)									
	IV	1,00 ± 0,00	1,00 ± 0,00	1,00 ± 0,00	1,00 ± 0,00	1,00 ± 0,00	1,00 ± 0,00	1,00 ± 0,00	1,00 ± 0,00
	PO	1,00 ± 0,00	1,00 ± 0,00	1,00 ± 0,00	1,00 ± 0,00	1,00 ± 0,00	1,00 ± 0,00	1,00 ± 0,00	1,00 ± 0,00
	CO	1,00 ± 0,00	1,00 ± 0,00	1,00 ± 0,00	1,00 ± 0,00	1,00 ± 0,00	1,00 ± 0,00	1,00 ± 0,00	1,00 ± 0,00
Movement after									

Safety/tolerability endpoint		Day -2	Day -1	Day 0	Day 2	Day 3	Day 7	Day 9	Day 10
provocation/ weighing [3] (mean ± SD)	IV	1,00 ± 0,00	1,00 ± 0,00	1,00 ± 0,00	1,00 ± 0,00	1,00 ± 0,00	1,00 ± 0,00	1,00 ± 0,00	1,00 ± 0,00
	PO	1,00 ± 0,00	1,00 ± 0,00	1,00 ± 0,00	1,00 ± 0,00	1,00 ± 0,00	1,00 ± 0,00	1,00 ± 0,00	1,00 ± 0,00
	CO	1,00 ± 0,00	1,00 ± 0,00	1,00 ± 0,00	1,00 ± 0,00	1,00 ± 0,00	1,00 ± 0,00	1,00 ± 0,00	1,00 ± 0,00
Coat condition [3] (mean ± SD)									
	IV	1,00 ± 0,00	1,00 ± 0,00	1,00 ± 0,00	1,00 ± 0,00	1,00 ± 0,00	1,00 ± 0,00	1,00 ± 0,00	1,00 ± 0,00
	PO	1,00 ± 0,00	1,00 ± 0,00	1,00 ± 0,00	1,00 ± 0,00	1,00 ± 0,00	1,00 ± 0,00	1,00 ± 0,00	1,00 ± 0,00
	CO	1,00 ± 0,00	1,00 ± 0,00	1,00 ± 0,00	1,00 ± 0,00	1,00 ± 0,00	1,00 ± 0,00	1,00 ± 0,00	1,00 ± 0,00
Body condition [3] (mean ± SD)									
	IV	1,00 ± 0,00	1,00 ± 0,00	1,00 ± 0,00	1,00 ± 0,00	1,00 ± 0,00	1,00 ± 0,00	1,00 ± 0,00	1,00 ± 0,00
	PO	1,00 ± 0,00	1,00 ± 0,00	1,00 ± 0,00	1,00 ± 0,00	1,00 ± 0,00	1,00 ± 0,00	1,00 ± 0,00	1,00 ± 0,00
	CO	1,00 ± 0,00	1,00 ± 0,00	1,00 ± 0,00	1,00 ± 0,00	1,00 ± 0,00	1,00 ± 0,00	1,00 ± 0,00	1,00 ± 0,00
Eye condition [3] (mean ± SD)									
	IV	1,00 ± 0,00	1,00 ± 0,00	1,00 ± 0,00	1,00 ± 0,00	1,00 ± 0,00	1,00 ± 0,00	1,00 ± 0,00	1,00 ± 0,00
	PO	1,00 ± 0,00	1,00 ± 0,00	1,00 ± 0,00	1,00 ± 0,00	1,00 ± 0,00	1,00 ± 0,00	1,00 ± 0,00	1,00 ± 0,00
	CO	1,00 ± 0,00	1,00 ± 0,00	1,00 ± 0,00	1,00 ± 0,00	1,00 ± 0,00	1,00 ± 0,00	1,00 ± 0,00	1,00 ± 0,00
Wound condition [3]									

Safety/tolerability endpoint		Day -2	Day -1	Day 0	Day 2	Day 3	Day 7	Day 9	Day 10
(mean ± SD)	IV	1,00 ± 0,00	1,00 ± 0,00	1,00 ± 0,00	1,00 ± 0,00	1,00 ± 0,00	1,00 ± 0,00	1,00 ± 0,00	1,00 ± 0,00
	PO	1,00 ± 0,00	1,00 ± 0,00	1,00 ± 0,00	1,00 ± 0,00	1,00 ± 0,00	1,00 ± 0,00	1,00 ± 0,00	1,00 ± 0,00
	CO	1,00 ± 0,00	1,00 ± 0,00	1,00 ± 0,00	1,00 ± 0,00	1,00 ± 0,00	1,00 ± 0,00	1,00 ± 0,00	1,00 ± 0,00
Serious adverse events									
Death [4] (number of events)									
	IV	N/A	N/A	0	0	0	0	0	0
	PO	N/A	N/A	0	0	0	0	0	0
	CO	N/A	N/A	0	0	0	0	0	0
Local inflammation/ infection persisting for >24h [4] (number of events)									
	IV	N/A	N/A	0	0	0	0	0	0
	PO	N/A	N/A	0	0	0	0	0	0
	CO	N/A	N/A	0	0	0	0	0	0
Non-healing cutaneous wounds/ ulcers [4] (number of events)									
	IV	N/A	N/A	0	0	0	0	0	0
	PO	N/A	N/A	0	0	0	0	0	0
	CO	N/A	N/A	0	0	0	0	0	0
Hemorrhage from any orifice, not responding to treatment [4] (number of events)									
	IV	N/A	N/A	0	0	0	0	0	0
	PO	N/A	N/A	0	0	0	0	0	0
	CO	N/A	N/A	0	0	0	0	0	0
Water consumption <5mL for >24h									
	IV	N/A	N/A	0	0	0	0	0	0

Safety/tolerability endpoint		Day -2	Day -1	Day 0	Day 2	Day 3	Day 7	Day 9	Day 10
(number of events)	PO	N/A	N/A	0	0	0	0	0	0
	CO	N/A	N/A	0	0	0	0	0	0
Decrease in body mass ≥15% of Day 0 value [4] (number of events)									
	IV	N/A	N/A	0	0	0	0	0	0
	PO	N/A	N/A	0	0	0	0	0	0
	CO	N/A	N/A	0	0	0	0	0	0
Abnormal physique & behavior [4] (number of events)									
	IV	N/A	N/A	0	0	0	0	0	0
	PO	N/A	N/A	0	0	0	0	0	0
	CO	N/A	N/A	0	0	0	0	0	0

Table S.15 Notes: To enhance visibility, the mean ± SD/median ± IQR/absolute number of events are presented per experimental group in Phase 2. The recorded data for each individual mouse from each group at each corresponding time-point, are available upon request. The following safety and tolerability endpoints were monitored for each mouse on a daily basis: spontaneous behavior, posture, breathing, behavior after provocation/weighing, movement after provocation/weighing, along with the condition of the coat, body, eyes, and wounds. Day 0 represents the day when the excisional wounds were created on each mouse's dorsum, and thus, the starting point of each *in vivo* experiment. [1], evaluation methods, time-points, and grading/scoring systems adapted from *Hohlbaum et al., 2018*; [2], evaluation methods, time-points, and grading/scoring systems adapted from *Deacon, 2006*; [3], evaluation methods, time-points, and grading/scoring systems adapted from *Arras et al., 2007*; [4], evaluation methods, time-points, and grading/scoring systems adapted from the *National Research Council, Humane Endpoints for Animals in Pain, 2009*. **Abbreviations**: SD, standard deviation; IQR, interquartile range; IV, intravenous administration retro-orbitally; PO, per os intake *ad libitum*; CO, negative controls; N/A, not applicable.

Table S.16: Overview of descriptive statistics, one-way ANOVA tests, and post hoc tests applied to evaluate the effects of ONBW treatment on macroscopic VC (in mm2/days).

VC	IV		PO		CO		ANOVA	Post Hoc
	M	SD	M	SD	M	SD		
Days 0-3 [1]	10.55	3.30	6.14	2.98	3.91	1.89	Ordinary one-way ANOVA ($F(2, 64) = 33.64$, $p < 0.0001$)	Tukey's HSD test
Days 0-7 [1]	9.02	0.71	9.48	1.54	7.20	1.10	Ordinary one-way ANOVA ($F(2, 33) = 12.90$, $p < 0.0001$)	Tukey's HSD test
Days 0-10 [1]	6.93	0.35	7.24	1.10	6.00	0.65	Ordinary one-way ANOVA ($F(2, 33) = 8.44$, $p = 0.001$)	Tukey's HSD test
Days 7-10 [1]	1.91	1.06	2.08	0.97	2.27	1.20	Ordinary one-way ANOVA ($F(2, 33) = 0.33$, $p = 0.718$)	Tukey's HSD test
	M Rank		M Rank		M Rank			
Days 3-7 [2]	9.75		29.00		16.75		Kruskal-Wallis H test (Kruskal-Wallis statistic (x^2) = 20.53; $p < 0.0001$)	Dunn's multiple comparisons test (CO vs. IV, MR diff. = 7.00, p = 0.311; CO vs. PO, MR diff. = -12.25, p = 0.013; IV vs. PO, MR diff. = -19.25, p < 0.0001)
Days 3-10 [2]	10.08		29.50		15.92		Kruskal-Wallis H test (Kruskal-Wallis statistic (x^2) = 21.47; $p < 0.0001$)	Dunn's multiple comparisons test (CO vs. IV, MR diff. = 5.83, p = 0.525; CO vs. PO, MR diff. = -13.58, p = 0.005; IV vs. PO, MR diff. = -19.42, p < 0.0001)

Table S.16 Notes: The mean values or mean rank values are presented for each timeframe. The mean values were incorporated in the calculations of the corresponding mean ranks illustrated. Day 0 represents the time-point when all excisional wounds were created *in vivo*. Between day 0 and day 3, a Tukey's HSD test showed that the mean VC of the IV group was significantly higher than the one in the CO group ($p < 0.0001$), and that the mean VC of the PO group was significantly higher than the one in the CO group ($p = 0.029$). From day 0 to 7, a Tukey's HSD test demonstrated that the mean VC of the IV group was significantly higher than the one in the CO group ($p = 0.002$), and that the mean VC of the PO group was significantly higher than the one in the CO group ($p < 0.0001$). From day 0 to 10, a Tukey's HSD test showed that the mean VC of the IV group was significantly higher than the one in the CO group ($p = 0.015$), and that the mean VC of the PO group was significantly higher than the one in the CO group

Table S.16 Notes (continued): ($p = 0.001$). From day 3 to 7, a Kruskal-Wallis H test indicated a significant difference in VC among the different routes of ONBW administration (experimental groups), $x^2 = 20.53$, $p < 0.0001$, with a mean rank VC of 9.75 for IV administration, 29.00 for PO intake, and 16.75 for the untreated CO. Subsequently, a post-hoc Dunn's multiple comparisons test showed that the mean rank VC of the PO group was significantly higher than that of the CO group ($p = 0.013$), and that the mean rank VC of the PO group was significantly higher than that of the IV group ($p < 0.0001$). From day 3 to 10, a Kruskal-Wallis H test indicated a significant difference in VC among the different routes of ONBW administration (experimental groups), $x^2 = 21.47$, $p < 0.0001$, with a mean rank VC of 10.08 for IV administration, 29.50 for PO intake, and 15.92 for the untreated CO. Subsequently, a post-hoc Dunn's multiple comparisons test showed that the mean rank VC of the PO group was significantly higher than that of the CO group ($p = 0.005$), and that the mean rank VC of the PO group was significantly higher than that of the IV group ($p < 0.0001$). No significant differences in VC were observed between any of the groups from day 7 to day 10. **[1]** post hoc analyses performed with Tukey's HSD test, as the corresponding data followed a normal distribution with homogenous variance. **[2]**, the corresponding data were analyzed using the non-parametric Kruskal-Wallis H test, as it did not fulfill the normality and homogeneity of variance criteria required to apply a parametric test. **Abbreviations**: ANOVA, analysis of variance; ONBW, oxygen nanobubble-enriched water; IV, intravenous administration retro-orbitally; PO, per os intake *ad libitum*; CO, negative controls; VC, velocity of wound closure (in mm^2/days); M, mean; SD, standard deviation; HSD, honest significant difference; M Rank, mean rank; MR diff., mean rank difference.

Table S.17: Overview of descriptive statistics, one-way ANOVA on ranks (Kruskal-Wallis H test), and post hoc tests used to evaluate the effects of ONBW treatment on wound re-epithelialization (% epithelialization ratio, % ER) histopathologically.

% ER	IV	PO	CO	ANOVA (Kruskal-Wallis)	Post Hoc
	M Rank	M Rank	M Rank		
Day 3	24.33	21.17	10.00	Kruskal-Wallis H test (Kruskal-Wallis statistic (x^2) = 12.26; p = 0.002)	Dunn's multiple comparisons test (CO vs. IV, MR diff. = -14.33, p = 0.003; CO vs. PO, MR diff. = -11.17, p = 0.028; IV vs. PO, MR diff. = 3.17, p > 0.999)
Day 10	22.13	15.92	17.46	Kruskal-Wallis H test (Kruskal-Wallis statistic (x^2) = 2.35; p = 0.310)	Dunn's multiple comparisons test (CO vs. IV, MR diff. = -4.67, p = 0.807; CO vs. PO, MR diff. = 1.54, p > 0.999; IV vs. PO, MR diff. = 6.21, p = 0.424)

Table S.17 Notes: The mean values were incorporated in the calculations of the corresponding mean ranks illustrated for each time-point. The time-point when all excisional wounds were created *in vivo*, is day 0. At day 3, a Kruskal-Wallis H test indicated a significant difference in % ER among the different routes of ONBW administration (experimental groups), $x^2 = 12.26$, $p = 0.002$, with a mean rank % ER of 24.33 for IV administration, 21.17 for PO intake, and 10.00 for the untreated CO. Subsequently, a post-hoc Dunn's multiple comparisons test showed that the mean rank % ER of the IV group was significantly higher than that of the CO group ($p = 0.003$), and that the mean rank % ER of the PO group was significantly higher than that of the CO group ($p = 0.028$). At day 10, a Kruskal-Wallis H test followed by a Dunn's multiple comparisons test showed that there is no significant difference in % ER among the different routes of ONBW administration (experimental groups), $x^2 = 2.35$, $p = 0.310$, with a mean rank % ER of 22.13 for IV administration, 15.92 for PO intake, and 17.46 for the untreated CO. These data from day 10, demonstrating the successful re-epithelialization of the wounds in all experimental groups, indicate that ONBW administration has no negative effect on the normal progression of the healing mechanism. **Abbreviations**: ANOVA, analysis of variance; ONBW, oxygen nanobubble-enriched water; IV, intravenous administration retro-orbitally; PO, per os intake *ad libitum*; CO, negative controls; % ER, percentage epithelialization ratio; M Rank, mean rank; MR diff., mean rank difference.

Table S.18: Overview of descriptive statistics, one-way ANOVA and post hoc tests used to evaluate the effects of ONBW treatment on collagen deposition (% collagenation ratio, % CR), histopathologically.

% CR	IV		PO		CO		ANOVA	Post Hoc
	M	SD	M	SD	M	SD		
Day 10	56.13	12.78	50.33	17.50	32.06	7.45	Ordinary one-way ANOVA ($F(2, 33) = 10.82$, $p = 0.0002$)	Tukey's HSD test

Table S.18 Notes: The mean values of each experimental group are presented. The time-point when all excisional wounds were created *in vivo*, is day 0. At day 10, a Tukey's HSD test showed that the mean % CR of the IV group was significantly higher than the one in the CO group ($p = 0.0003$), and that the mean % CR of the PO group was significantly higher than the one in the CO group ($p = 0.005$). **Abbreviations**: ANOVA, analysis of variance; ONBW, oxygen nanobubble-enriched water; IV, intravenous administration retro-orbitally; PO, per os intake *ad libitum*; CO, negative controls; % CR, percentage collagenation ratio; M, mean; SD, standard deviation; HSD, honest significant difference.

Table S.19: DO dosage (mg) delivered via ONBW administration in the IV group during Phase 2 experiments.

Mouse	DO concentration (mg/dL); Day 0	Volume injected (dL); Day 0	DO amount (mg); Day 0		DO concentration (mg/dL); Day 5	Volume injected (dL); Day 5	DO amount (mg); Day 5		TOTAL DO amount (mg) in Phase 2
IVF1	2,729	0,0015	0,004		1,90	0,0015	**0,003**		0,0069
IVF2	2,729	0,0015	0,004		1,90	0,0015	**0,003**		0,0069
IVF3	2,729	0,0015	0,004		1,90	0,0015	**0,003**		0,0069
IVF4	2,729	0,0015	0,004		1,90	0,0015	**0,003**		0,0069
IVF5	2,729	0,0015	0,004		1,90	0,0015	**0,003**		0,0069
IVF6	2,729	0,0015	0,004		1,90	0,0015	**0,003**		0,0069
IVM1	2,729	0,0015	0,004		1,90	0,0015	**0,003**		0,0069
IVM2	2,729	0,0015	0,004		1,90	0,0015	**0,003**		0,0069
IVM3	2,729	0,0015	0,004		1,90	0,0015	**0,003**		0,0069
IVM4	2,729	0,0015	0,004		1,90	0,0015	**0,003**		0,0069
IVM5	2,729	0,0015	0,004		1,90	0,0015	**0,003**		0,0069
IVM6	2,729	0,0015	0,004		1,90	0,0015	**0,003**		0,0069

Abbreviations: DO, dissolved oxygen; ONBW, oxygen nanobubble-enriched water; IV, intravenous administration retro-orbitally.

Table S.20: DO dosage (mg) delivered via ONBW intake in the PO group during Phase 2 experiments.

Mouse	DO concentration (mg/dL); Day 0	Volume consumed (mL); Day 0	Volume consumed (dL); Day 0	DO amount (mg); Day 0	DO concentration (mg/dL); Day 1	Volume consumed (mL); Day 1	Volume consumed (dL); Day 1	DO amount (mg); Day 1	DO concentration (mg/dL); Day 2	Volume consumed (mL); Day 2	Volume consumed (dL); Day 2	DO amount (mg); Day 2	DO concentration (mg/dL); Day 3	Volume consumed (mL); Day 3	Volume consumed (dL); Day 3	DO amount (mg); Day 3
POF1	2,73	8,31	0,08	0,23	2,31	9,28	0,09	0,21	2,66	7,46	0,07	0,20	2,19	6,89	0,07	0,15
POF2	2,73	8,58	0,09	0,23	2,31	8,16	0,08	0,19	2,66	7,74	0,08	0,21	2,19	8,37	0,08	0,18
POF3	2,73	7,49	0,07	0,20	2,31	6,44	0,06	0,15	2,66	8,29	0,08	0,22	2,19	7,58	0,08	0,17
POF4	2,73	9,67	0,10	0,26	2,31	10,38	0,10	0,24	2,66	7,52	0,08	0,20	2,19	8,24	0,08	0,18
POF5	2,73	8,26	0,08	0,23	2,31	7,30	0,07	0,17	2,66	8,55	0,09	0,23	2,19	6,41	0,06	0,14
POF6	2,73	10,84	0,11	0,30	2,31	9,51	0,10	0,22	2,66	10,36	0,10	0,28	2,19	8,83	0,09	0,19
POM1	2,73	9,43	0,09	0,26	2,31	10,64	0,11	0,25	2,66	7,94	0,08	0,21	2,19	8,16	0,08	0,18
POM2	2,73	7,25	0,07	0,20	2,31	9,37	0,09	0,22	2,66	8,63	0,09	0,23	2,19	7,25	0,07	0,16
POM3	2,73	10,72	0,11	0,29	2,31	9,35	0,09	0,22	2,66	6,84	0,07	0,18	2,19	6,30	0,06	0,14
POM4	2,73	9,74	0,10	0,27	2,31	9,48	0,09	0,22	2,66	9,79	0,10	0,26	2,19	8,69	0,09	0,19
POM5	2,73	10,87	0,11	0,30	2,31	8,94	0,09	0,21	2,66	9,47	0,09	0,25	2,19	8,22	0,08	0,18
POM6	2,73	6,26	0,06	0,17	2,31	7,36	0,07	0,17	2,66	6,73	0,07	0,18	2,19	7,14	0,07	0,16

Mouse	DO concentration (mg/dL); Day 4	Volume consumed (mL); Day 4	Volume consumed (dL); Day 4	DO amount (mg); Day 4	DO concentration (mg/dL); Day 5	Volume consumed (mL); Day 5	Volume consumed (dL); Day 5	DO amount (mg); Day 5	DO concentration (mg/dL); Day 6	Volume consumed (mL); Day 6	Volume consumed (dL); Day 6	DO amount (mg); Day 6
POF1	2,03				1,90				1,83			
POF2	2,03	7,48	0,07	0,15	1,90	6,92	0,07	0,13	1,83	7,60	0,08	0,14
POF3	2,03	6,92	0,07	0,14	1,90	6,55	0,07	0,12	1,83	8,46	0,08	0,15
POF4	2,03				1,90				1,83			
POF5	2,03	7,57	0,08	0,15	1,90	7,48	0,07	0,14	1,83	8,34	0,08	0,15
POF6	2,03				1,90				1,83			
POM1	2,03				1,90				1,83			
POM2	2,03				1,90				1,83			
POM3	2,03	7,29	0,07	0,15	1,90	6,83	0,07	0,13	1,83	8,75	0,09	0,16
POM4	2,03	8,18	0,08	0,17	1,90	7,52	0,08	0,14	1,83	9,94	0,10	0,18
POM5	2,03	7,74	0,08	0,16	1,90	7,19	0,07	0,14	1,83	8,67	0,09	0,16
POM6	2,03				1,90				1,83			

Mouse	DO concentration (mg/dL); Day 7	Volume consumed (mL); Day 7	Volume consumed (dL); Day 7	DO amount (mg); Day 7	DO concentration (mg/dL); Day 8	Volume consumed (mL); Day 8	Volume consumed (dL); Day 8	DO amount (mg); Day 8	DO concentration (mg/dL); Day 9	Volume consumed (mL); Day 9	Volume consumed (dL); Day 9	DO amount (mg); Day 9	TOTAL DO amount (mg) in Phase 2
POF1	1,94				1,88				1,75				0,79
POF2	1,94	9,72	0,10	0,19	1,88	10,17	0,10	0,19	1,75	8,38	0,08	0,15	1,76
POF3	1,94	10,61	0,11	0,21	1,88	11,48	0,11	0,22	1,75	7,64	0,08	0,13	1,71
POF4	1,94				1,88				1,75				0,88
POF5	1,94	10,93	0,11	0,21	1,88	9,74	0,10	0,18	1,75	10,57	0,11	0,18	1,79
POF6	1,94				1,88				1,75				0,98
													0,00
POM1	1,94				1,88				1,75				0,89
POM2	1,94				1,88				1,75				0,80
POM3	1,94	10,88	0,11	0,21	1,88	10,95	0,11	0,21	1,75	9,96	0,10	0,17	1,86
POM4	1,94	12,46	0,12	0,24	1,88	11,56	0,12	0,22	1,75	11,48	0,11	0,20	2,08
POM5	1,94	11,23	0,11	0,22	1,88	10,29	0,10	0,19	1,75	10,31	0,10	0,18	1,98
POM6	1,94				1,88				1,75				0,68

Abbreviations: DO, dissolved oxygen; ONBW, oxygen nanobubble-enriched water; PO, per os intake *ad libitum*.

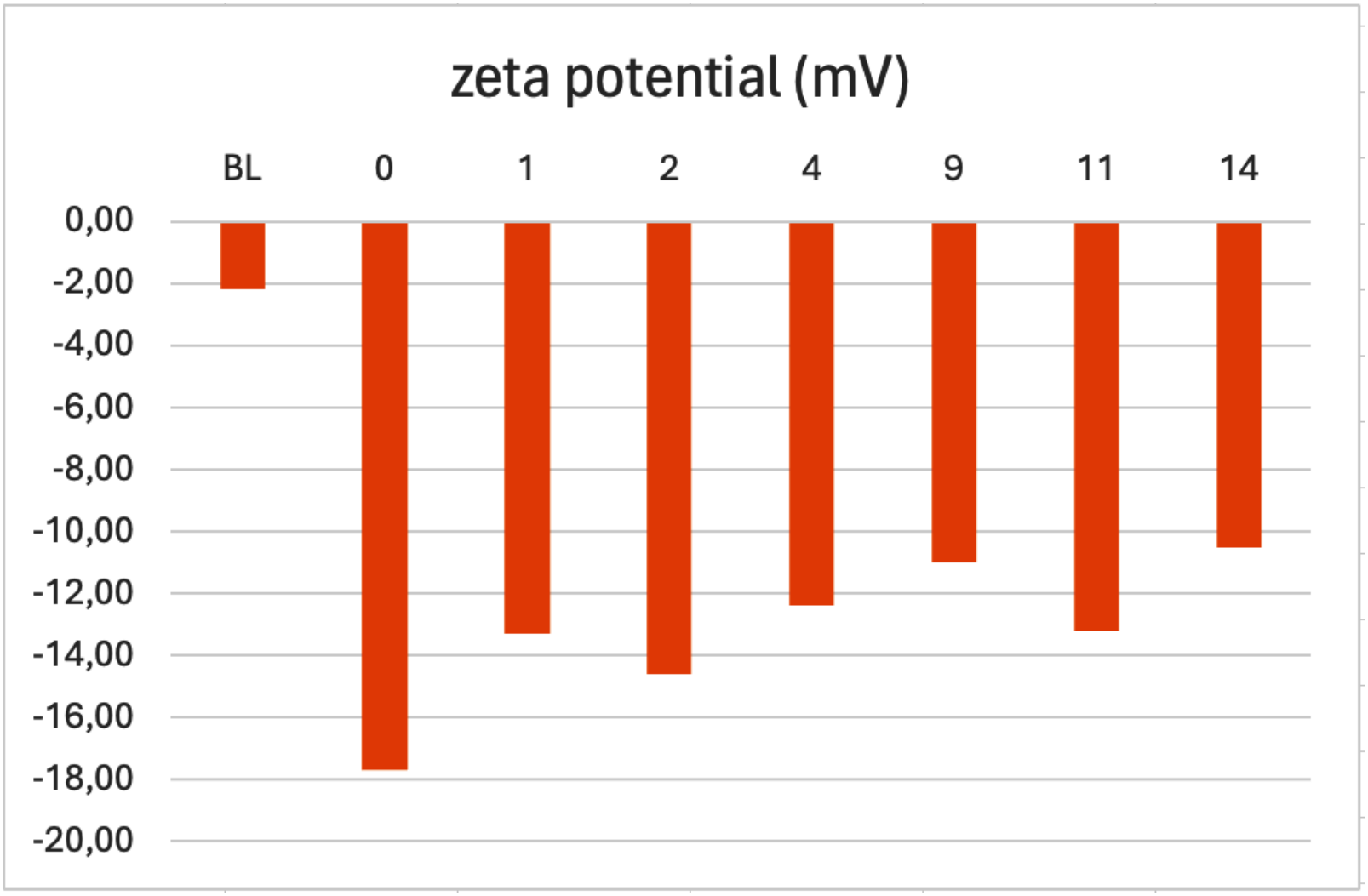

Figure S.1: Zeta potential values recorded in the ONBW solution during Phase 2 experiments.: The zeta potential values shown above contribute to the exceptional physical and biological stability exhibited by nanobubbles at the nanoscale. Our measurements are consistent with the prolonged sustainability of DO concentrations recorded during our Phase 2 experiments, and presented in Chapter 5 of this dissertation, thus encouraging further exploration of the ONBW in biomedical applications. **Abbreviations**: ONBW, oxygen nanobubble-enriched water; DO, dissolved oxygen.

About the author

Dr. Dimitrios Ntentakis graduated from the Medical School of the National and Kapodistrian University of Athens, Greece, where he was accepted after ranking third among 102.049 candidates. Dr. Ntentakis graduated *Summa Cum Laude*, and emerged as the valedictorian of his class. His academic performance as a medical student was recognized through numerous scholarships and awards. Furthermore, he was accepted for sub-internships in cardiovascular surgery and trauma surgery at Johns Hopkins University School of Medicine in Baltimore, Maryland and at Harvard Medical School in Boston, Massachusetts, respectively; where he received honors evaluations for his clinical performance. The main objective of his PhD research at the School of Chemical and Environmental Engineering of the Technical University of Crete, has been to apply the cutting-edge technology of O_2 nanobubbles to enhance physiologic wound healing and cutaneous regeneration; being one of the first to comprehensively explore this biomedical indication. For this project, he was awarded a scholarship by the Hellenic Foundation for Research and Innovation. The main *in vivo* findings of his PhD research have been accepted as oral presentations at the Clinical Congress of the American College of Surgeons, for two consecutive years in 2023 and 2024. Also, Dr. Ntentakis has worked at Mass Eye and Ear, a teaching hospital for the Department of Ophthalmology of Harvard Medical School in Boston, Massachusetts, primarily focussing on neuroprotection, photoreceptor regeneration, and macular degeneration. He has made pioneering contributions towards deciphering the pathophysiology of two enigmatic diseases of the human retina; namely macular telangiectasia type 2 (MacTel), and the maculopathy associated with the chronic use of pentosan polysulfate sodium. Also, Dr. Ntentakis is an academic affiliate and visiting scientist at the BROAD Institute of MIT and Harvard in Cambridge, Massachusetts, where he studies the potential translation of BRD7635, a novel treatment factor with documented efficacy in kidney proteinopathies, to the management of retinal diseases with a similar pathophysiology. For his research in the field of ophthalmology, Dr. Ntentakis has been recognized with four international awards: from the Association for Research in Vision and Ophthalmology (ARVO) in 2020, the American Macular Degeneration Foundation (AMDF) in 2021, the New England Ophthalmological Society (NEOS) in 2023, and the New England Hellenic Medical and Dental Society (NEHMDS) in 2024. Beyond academia, Dr. Ntentakis has established a national voluntary program called "Summer Medical Landing", which provides critical healthcare assistance to refugees, locals, and visitors in Greece's most inaccessible islands—a program that remains operational after 12 years. He has also launched local initiatives to address healthcare disparities among medically underserved children.

PhD publications

Ntentakis DP, Ntentaki AM, Delavogia E, Kalomoiris L, Venieri D, Arkadopoulos N, Kalogerakis N. Dissolved oxygen technologies as a novel strategy for non-healing wounds: a critical review. *Wound Rep Reg.* 2021; 1- 18. doi:10.1111/wrr.12972.

Ntentakis DP, Ntentaki AM, Delavogia E, Seridou P, Kollia Z, Sfakianos N, Correa VSMC, Katafygiotis P, Venieri D, Arkadopoulos N, Kalogerakis N. Dissolved oxygen and O_2-nanobubble biotechnologies enhance physiologic wound healing and cutaneous regeneration *in vivo*. Manuscript under review in *Journal of the American College of Surgeons (JACS)*. Submitted. September;2024.

PhD congress presentations

Kalogerakis N, Kalogerakis GC, Seridou P, **Ntentakis DP**, Komnitsas KA, Botha QP, Kolliopoulos G. Tackling environmental problems with nanobubble technology. Presented at: CCEC 2021; 71st Canadian Chemical Engineering Conference; Montreal, Canada; Oct 2021.

Ntentakis DP, Ntentaki AM, Delavogia E, Kalomoiris L, Venieri D, Arkadopoulos N, Kalogerakis N. Nanoparticle technologies to enrich aqueous solutions with oxygen for healing applications. Presented at: 77th Congress of the Hellenic Society of Orthopaedic Surgery and Traumatology; Athens, Greece; October 2021.

Ntentakis DP, Ntentaki AM, Seridou P, Venieri D, Arkadopoulos N, Kalogerakis N. Introducing a methodology for evaluating the biological safety and efficacy of aqueous-based nanobubble solutions in excisional wound models *in vivo*. Third Annual Congress for PhD Candidates; School of Chemical and Environmental Engineering, Chania, Crete, Greece; Apr 2022.

Ntentakis DP, Ntentaki AM, Seridou P, Venieri D, Arkadopoulos N, Kalogerakis N. Applying the Laws of Physics to Engineer an Original Dissolved-Oxygen Biotechnology for Biomedical Applications. Presented at: Forth Annual Congress for PhD Candidates; School of Chemical and Environmental Engineering, Chania, Crete, Greece; Apr 2023.

Ntentakis DP, Ntentaki AM, Delavogia E, Seridou P, Sfakianos N, Correa VSMC, Katafygiotis P, Venieri D, Arkadopoulos N, Kalogerakis N. Enhancing In Vivo Wound Healing Using an Original Dissolved-Oxygen Biotechnology. Oral Presentation Presented at: American College of

Surgeons Clinical Congress 2023; Boston Convention and Exhibition Center, Boston, Massachusetts, USA; Oct 2023.

Ntentakis DP, Ntentaki AM, Seridou P, Venieri D, Arkadopoulos N, Kalogerakis N. Applying Oxygen-Nanobubble Biotechnology to Enhance Physiologic Wound Healing *In Vivo*. Presented at: Fifth Annual Congress for PhD Candidates; School of Chemical and Environmental Engineering, Chania, Crete, Greece; Apr 2024.

Ntentakis DP, Ntentaki AM, Delavogia E, Seridou P, Sfakianos N, Correa VSMC, Katafygiotis P, Venieri D, Arkadopoulos N, Kalogerakis N. Applying Oxygen-Nanobubble Biotechnology to Enhance Physiologic Wound Healing *In Vivo*. Oral Presentation Accepted at: American College of Surgeons Clinical Congress 2024; Moscone Center, San Francisco, California, USA; Oct 2024.

Complete list of publications

1. Chen Y, Wei W, Zhang F, She H, Zhou H, Li L, Huang Y, **Ntentakis DP**, Shi X. Incidence of Endophthalmitis After Intravitreal Anti-Vascular Endothelial Growth Factor Injections in an Operating Room in China. *Journal of Ophthalmology*, vol. 2020, ArticleID 5163484, 6 pages, 2020. https://doi.org/10.1155/2020/5163484.
2. **Dimitrios Ntentakis**, Saghar Bagheri, Mark P. McGarrey, Lakshmi Nayak, Lucia Sobrin, Ivana K Kim, Dean Eliott, Mary E Aronow; Vitreoretinal lymphoma: clinical features, treatment, and outcomes. *Invest. Ophthalmol. Vis. Sci.* 2021;62(8):41.
3. Itika Garg, Raviv Katz, Ying Cui, Rongrong Le, Ying Zhu, Jade Y. Moon, Chibuike Uwakwe, Edward S. Lu, **Dimitrios Ntentakis**, David M. Wu, Leo A. Kim, Dean Eliott, Deeba Husain, Demetrios G. Vavvas, Joan W. Miller, John B. Miller; Retinal Vascular Changes in Macular Telangiectasia Type 2 (MacTel2) using Wide-Field Swept-Source Optical Coherence Tomography Angiography (WF SS-OCTA). *Invest. Ophthalmol. Vis. Sci.* 2021;62(11):10.
4. **Ntentakis DP**, Ntentaki AM, Delavogia E, Kalomoiris L, Venieri D, Arkadopoulos N, Kalogerakis N. Dissolved oxygen technologies as a novel strategy for non-healing wounds: a critical review. *Wound Rep Reg.* 2021; 1- 18. doi:10.1111/wrr.12972.
5. Yu, Z., Efstathiou, N.E., Correa, V.S.M.C., Chen, X., Ishihara, K., Iesato, Y., Narimatsu, T., **Ntentakis, D.P.**, Chen, Y., Vavvas, D.G.. Receptor interacting protein 3 kinase, not 1 kinase, through MLKL-mediated necroptosis is involved in UVA-induced corneal endothelium cell death. *Cell Death Discov.* 7, 366 (2021). https://doi.org/10.1038/s41420-021-00757-w.

6 Yeung, V.; Boychev, N.; Farhat, W.; **Ntentakis, D.P.**; Hutcheon, A.E.K.; Ross, A.E.; Ciolino, J.B. Extracellular Vesicles in Corneal Fibrosis/Scarring. *Int. J. Mol. Sci.* 2022,*23*,5921. https://doi.org/ 10.3390/ijms23115921.

7 Delavogia E, **Ntentakis DP**, Cortinas JA, Fernandez-Gonzalez A, Mitsialis SA, Kourembanas S. Mesenchymal stromal/stem cell extracellular vesicles and perinatal injury: one formula for many diseases. *Stem Cells*. 2022 Aug 31:sxac062. doi: 10.1093/stmcls/sxac062.

8 Yu, Z., Correa, V.S.M.C., Efstathiou, N.E., Albertos-Arranz, H., Chen, X., Ishihara, K., Iesato, Y., Narimatsu, T., **Ntentakis, D.P.**, Vavvas, D.G.. UVA induces retinal photoreceptor cell death via receptor interacting protein 3 kinase mediated necroptosis. *Cell Death Discov.* 8, 489 (2022). https://doi.org/10.1038/s41420-022-01273-1.

9 Efstathiou, N.E., Correa, V.S.M.C., Narimatsu, T., **Ntentakis, D.P.**, Vavvas, D.G. Peripherin 2 (PRPH2) is expressed in retinal pigment epithelium (RPE) cells: Implications for PRPH2 associated diseases. Manuscript under review in *Ophthalmology Science.* Submitted. May;2024.

10 Correa VSMC, Efstathiou NE, **Ntentakis DP**, Yu Z, Narimatsu T, Gragoudas E, Kim IK, Vavvas DG. The NLRP3 inflammasome - interleukin 1β axis in uveal melanoma. FEBS Open Bio. 2023 Mar;13(3):545-555. doi: 10.1002/2211-5463.13566.

11 Correa VSMC, **Ntentakis DP**, Narimatsu T, Adibnia Y, Yan B, Liu J, Loscertales M, Vavvas DG, Efstathiou NE. Transcriptomic analysis of pentosan polysulfate sodium (PPS) on ARPE-19 cells – new insights into PPS maculopathy. Manuscript under review in *Ophthalmology Science*. Submitted. August;2024.

12 **Ntentakis DP**, Correa VSMC, Ntentaki AM, Delavogia E, Narimatsu T, Efstathiou NE, Vavvas DG. Effects of Newer-Generation Anti-Diabetics on Diabetic Retinopathy: a Critical Review. Graefes Arch Clin Exp Ophthalmol. 2023 Sep 20. doi: 10.1007/s00417-023-06236-5. Epub ahead of print. PMID: 37728754.

13 Liu Y, Du Y, Wang X, Zhao X, Zhang S, Yu Z, Wu Z, **Ntentakis DP**, Tian R, Chen Y, Wang C, Yao X, Li R, Heng PA, Zhang G. An Artificial Intelligence System for Screening and Recommending the Treatment Modalities for Retinopathy of Prematurity. Asia Pac J Ophthalmol (Phila). 2023 Sep-Oct 01;12(5):468-476. doi: 10.1097/APO.0000000000000638. Epub 2023 Sep 22. PMID: 37851564.

14 Yaling Liu; Hai Xie; Xinyu Zhao; Sifan Zhang; Jiannan Tang; Zhen Yu; Zhenquan Wu; Ruyin Tian; Yi Chen; Miaohong Chen; **Dimitrios P. Ntentakis**; Yueshanyi Du; Tingyi Chen; Yarou Hu; Baiying Lei; Guoming Zhang. Automated Detection of Nine Infantile Fundus Diseases and Conditions in Retinal Images Using a Deep Learning System. EPMA J. 2024 Feb 15;15(1):39-51. doi: 10.1007/s13167-024-00350-y. PMID: 38463622; PMCID: PMC10923762.

15 **Ntentakis DP**, Corrêa VSMC, Ntentaki AM, Vavvas DG. Differences in effects of some newer-generation anti-diabetics on diabetic retinopathy versus nephropathy. *Graefes Arch Clin Exp Ophthalmol* (2024). https://doi.org/10.1007/s00417-023-06353-1.

16 Matthew Finn,Francesco Romano, Isabella Stettler, **Dimitrios Ntentakis**, Mauricio Garcia, Hanna Choi, Filippos Vingopoulos, Grace Baldwin, Itika Garg, Peyman Razavi, Hannah Wescott, Cade Bennett, Augustine Bannerman, Katherine Overbey, Ioanna Ploumi, Raviv Katz, Nimesh A. Patel, Leo A. Kim, David M. Wu, Demetrios G. Vavvas, Deeba Husain, Joan W. Miller, John B. Miller. Contrast Sensitivity Function Correlates with Optical Coherence Tomography (OCT) Findings in Macular Telangiectasia Type 2. Manuscript under review in *RETINA*. Submitted. May;2023.

17 **Ntentakis DP**, Ntentaki AM, Delavogia E, Correa VSMC, Efstathiou N, Aronow ME, Chew EY, Miller JW, Vavvas DG. Clinical Histopathology and Pathogenesis of Macular Telangiectasia Type 2. Manuscript under review in *Progress in Retinal and Eye Research (PRER)*. Submitted. August;2024.

18 **Ntentakis DP**, Ntentaki AM, Delavogia E, Seridou P, Kollia Z, Sfakianos N, Correa VSMC, Katafygiotis P, Venieri D, Arkadopoulos N, Kalogerakis N. Dissolved oxygen and O_2-nanobubble biotechnologies enhance physiologic wound healing and cutaneous regeneration *in vivo*. Manuscript under review in *Journal of the American College of Surgeons (JACS)*. Submitted. September;2024.